$$I_{os} = 57.0 \frac{m_\ell v_o^2 v_{ge} Q_{on}}{e r_{sn} \omega k_b L^3} \qquad (36)$$

$$\doteq 28.5 \frac{m_\ell v_o^2}{e r_{sn} k_b L^2}$$

If we use $v_o = 0.5\,c$, $L = 3$m, $\omega = 2\pi \times 800$ Mc, and $r_{sn} = 20$ MΩ/m, we obtain about 5.5 A for the starting current for the TM_{01} mode.* This current is considerably smaller than that estimated for the deflecting mode,[10] though it is sufficiently high compared with the present design. The build-up time, T_b, for this effect is also given by using (19) as

$$T_b = \frac{1}{\mathrm{Re}\, j(\omega - \omega_n)} \approx \frac{1}{\mathrm{Re}(v_{ge}\delta_1)} \approx \frac{Q_{on}}{\omega} \sim 4\,\mu\mathrm{sec}\,.$$

Certainly, a similar longitudinal blow-up having a lower starting current may be expected for the excitation of other modes as TM_{01n} $(n > 0)$ rather than TM_{010}. Also, there may be another mechanism of blow-up as a resonant or a coherent interaction suggested by Leiss,[11] which should be a quite nonlinear phenomenon and beyond this study; however, it might be strongly dependent on circuit conditions as discussed by Gluckstern.[10]

At any rate, before such a beam blow-up would appear, one can assume that the actual accelerator should become a decelerator as a TWT amplifier. In the first approximation, the critical current is given by (16b) when the value of Q_b becomes negative. Using (17) and taking the values of parameters used in the paragraph four, one will find about 0.2 A for the critical value. Although this value increases as the field strength due to the external source increases, the actual limiting current of a high energy proton linac will be determined by such a condition.

The author wishes to offer his sincere thanks to Dr. J. P. Blewett for his stimulating interest in this work and for the hospitality of the

---

* At the MURA Linac Conference, we had neglected the effect of the wall loss in (35) and obtained a much smaller value.

Brookhaven National Laboratory. It is a great pleasure to acknowledge the invaluable information about his experimental studies and the helpful discussion of Mr. S. Giordano, who contributed especially to the analysis in the Appendix. The author also thanks Dr. R. L. Gluckstern and Dr. H. Hirakawa for their useful discussions.

APPENDIX

Wave Propagation in a π-Mode Accelerator

As is well known, in the ideal π-mode section, we have essentially zero group velocity from the dispersion curve. On the other hand, in the actual guide with losses, to maintain the field distribution constant along the guide, we need continuous power flow from the external source to the guide, or a finite group velocity in the steady state. Such a condition is only fulfilled with phase shifts and shifts of resonant frequencies which are different for each cell in one section. This has been examined and verified experimentally by Giordano who obtained the dependence of these shifts on cell numbers and Q_o values[12] (Fig. 1 and Fig. 2). We have considered such effects from a simple power relation and a dispersion-equation, giving an idea of the group velocity in the π-mode.*

The energy flow along the guide is denoted by S(z) (J/sec) and the equation of continuity for the energy flow can be written as

$$\frac{\partial U}{\partial t} + \frac{\partial S}{\partial z} + R = 0 \qquad \text{(A-1)}$$

with the linear density of stored energy U(z) (J/m) and the loss per unit length R(z) (J/sec, m). In the steady state the time derivative is zero so that the first term of (A-1) is eliminated. The energy flow S is expressed quite generally by using the group velocity, v_g, which is also a function of z in the present case, by[13]

$$S(z) = v_g(z)\ U(z) \qquad \text{(A-2)}$$

Using this expression, (A-1) becomes

$$v_g(z) \frac{\partial U(z)}{\partial z} + \frac{\partial v_g(z)}{\partial z} U(z) = - R(z) \qquad \text{(A-3)}$$

As is shown in paragraph 2, the peak axial field $E_o(z)$ is related to U(z) through the shunt impedance and the Q-value by means of

---

* A somewhat similar analysis had been done by Nagle and Knapp using an equivalent circuit model (D. E. Nagle and E. A. Knapp, Minutes of the Conference on P. L. A. at Yale University, Oct. 1963, p. 171, E. A. Knapp, LASL Tech Memo P-11/EAK-3, Oct. 1963, unpublished).

$$\frac{E_o^2(z)}{R(z)} = r_s \qquad \text{and} \qquad \frac{\omega\, U(z)}{R(z)} = Q_o \quad . \tag{A-4}$$

Thus, so far as we consider the nearly uniform structure of cells, the constant field-distribution (i.e. E(z) is constant) corresponds to constant loss and stored energy density (i.e. both R(z) and U(z) are constant). Using the second expression of (A-4), (A-3) becomes

$$\frac{\partial v_g(z)}{\partial z} = -\frac{\omega}{Q_o} \quad . \tag{A-5}$$

By integration,

$$v_g(z) = -\frac{\omega}{Q_o}\ (z + \text{const.}) \ .$$

If the power is fed from z = o (single feed), it could be assumed to be completely reflected at the end-wall, or $v_g = 0$ at z = L. Then,

$$v_g(z) = \frac{\omega}{Q_o}\ (L - z) \tag{A-6}$$

Now, we assume a simple dispersion equation between the frequency and the propagation constant k like

$$\omega \doteq \omega_o - \frac{\delta\omega}{2} \cos k L_o \ , \tag{A-7}$$

taking the center frequency of the passband, ω_o, the bandwidth, $\delta\omega$, and the unit cell length, L_o. The group velocity is calculated from

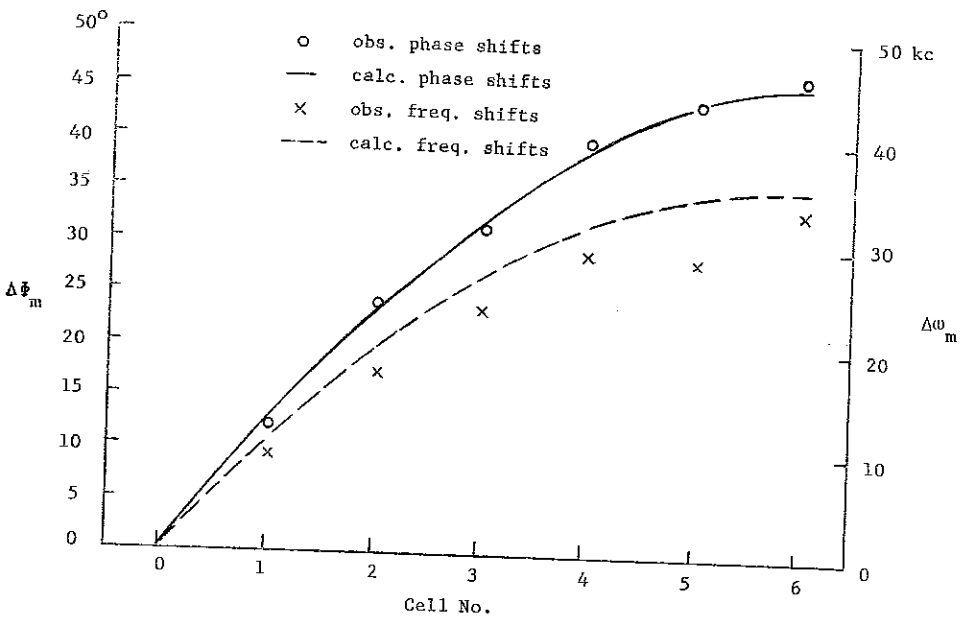

Fig. 1

Dependence of Phase and Frequency Shifts on Cell Numbers

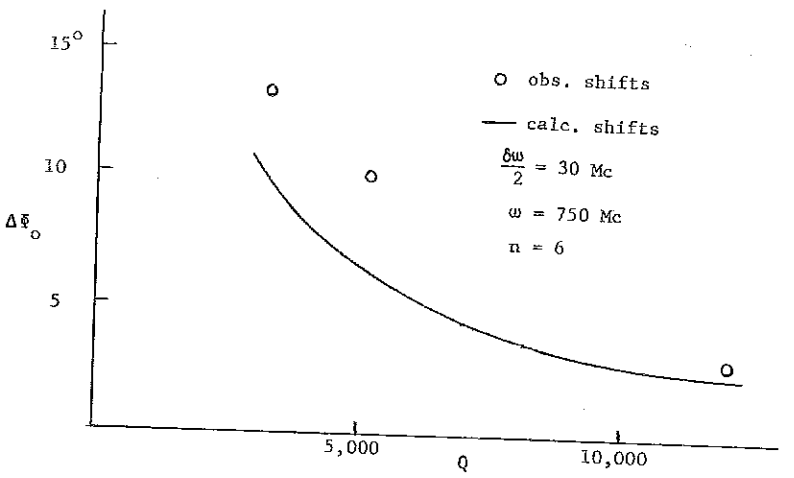

Fig. 2

Dependence of the Total Phase Shift on Q-Value
(Experimental Condition is Different from Fig. 1)

this equation as,

$$v_g = \frac{d\omega}{dk} = \frac{\delta\omega L_o}{2} \sin kL_o \qquad \text{(A-8)}$$

Combining (A-4) and (A-6), the necessary phase shift for the m^{th} cell in a π-mode guide is

$$\Delta\phi_m = \Delta(kL_o)_m = \frac{2v_g}{\delta\omega L_o} = \frac{2}{Q_o} \frac{\omega}{\delta\omega} (N-m) , \qquad \text{(A-9)}$$

where z is replaced by mL_o considering end half-cells (m = 0, 1, 2, ... N for an N-cell section). The phase shifts are accumulated and the total shift is given by

$$\Delta\Phi_o = \sum_{m=o}^{N} \Delta\phi_m = \frac{\omega}{Q_o\delta\omega} N(N+1) \qquad \text{(A-10)}$$

The observed phase shift is the accumulated phase shift at the center of each cell. Referring to the first cell (m = o), they are

$$\Delta\Phi_m = \Delta\Phi_o - \sum_{n=m}^{N} \Delta\phi_n = \frac{\omega}{Q_o\delta\omega} m(2N - m + 1) . \qquad \text{(A-11)}$$

Corresponding frequency shifts are also obtained by a Taylor expansion of (A-7) around the π-mode propagation constant, or

$$\omega'_\pi \doteq \omega_\pi + \frac{1}{2}\left(\frac{d^2\omega}{dk^2}\right) (\Delta\phi)^2 . \qquad \text{(A-12)}$$

Taking $\Delta\omega_m = \omega'_{\pi m} - \omega_\pi$, we have

$$\Delta\omega_m = \frac{1}{4}\delta\omega\ (\Delta\phi_m)^2 = \frac{\omega^2}{Q_{on}^2}\ \frac{1}{\delta\omega}\ (N - m)^2 \ . \qquad (A-13)$$

One can compare these formulae with the experiments. Taking $\omega = 2\pi$ x 880 Mc, $\delta\omega = 2\pi$ x 2.7 Mc, $Q_o = 1.7 \times 10^4$, * and N = 6, the total phase shift and the maximum frequency shift calculated are 46° and 36 kc, respectively. Corresponding experimental values are 47° and 34 kc which are surprisingly close to the calculated values. Also their dependence on cell-numbers gives good agreement between calculations and experiments as shown in Fig. 1, and Fig. 2 gives results of another experiment showing the $1/Q_o$ dependence of the total phase shift, which is also expected by the above analysis, while the calculated absolute values are about 30% smaller than observed, probably because of the very wide band structure.

Now, we have an idea of the group velocity, which varies along the guide. In the present approximation of this article, which is based on a uniform-cell structure, we have no reason to use velocity other than its average value of $\langle v_g \rangle = \omega L/2Q_o$. This velocity also corresponds to the value obtained by the well known dispersion-relation between the phase change and the frequency change of a resonant circuit, in which we consider the whole π-mode section as one cavity. ** In a transient phenomenon such as a pulse build-up, one may find another velocity for v_{ge}, which is the velocity of beats between the π-mode and other modes excited by disturbances. The slowest velocity is the velocity of the beat between the fundamental and the next modes, and should be most important. Fortunately, this slowest beat velocity is also of the same order and slightly slower than the above average group velocity in the steady state, in the present designed accelerator.

---

* Observed Q_o-value is 1.5×10^4, whereas a slightly high value is used by taking into account the effect of end-walls.

** The dispersion relation is $\Delta\Psi = -\frac{\Delta\omega}{2\omega_o} Q_o$, and considering

$$\frac{\Delta\lambda_g}{\lambda_g} = \frac{\Delta\Psi}{\pi N} \ , \quad v_g = \frac{\Delta\omega}{\Delta k} = \frac{\omega_o}{Q}\ \frac{L}{2} \ .$$

REFERENCES

1. A Proposal for Increasing the Intensity of the Alternating-Gradient Synchrotron at the Brookhaven National Laboratory, BNL 7956, (May 1964).

2. J.C. Slater, Microwave Electronics, (Van Nostrand, 1950), Chap. IV.

3. A.J. Lichtenberg, Rev. Sci. Instr. 33, 395, (1962), J.E. Leiss, NBS Int. Rept. (1958, unpublished).

4. J.R. Pierce, Traveling Wave Tubes, (Van Nostrand, 1950).

5. L. Brillouin, J. App. Phys. 20, 1196 (1949).

6. A. Nordsieck, Proc. IRE 41, 630 (1953), P.K. Tien, et al., Bell System Tech. J. 35, 349 (1956).

7. J.R. Pierce, ibid, Chap. XII.

8. P.B. Wilson, HELPL Rept. No. 297, (June 1963) Stanford University.

9. H. Hirakawa, Jap. J. App. Phys. 3, 27 (1964).

10. R.L. Gluckstern, AADD-38 (July, 1964) Brookhaven National Laboratory Internal Report.

11. J.E. Leiss, ibid and NBS Int. Rept. (Oct. 1962, unpublished).

12. S. Giordano, private communications. The author expresses his thanks for permission to quote here some of the unpublished experimental results.

13. J.C. Slater, ibid, Chap. III and App.

THE CERN-PS LINAC - BEAM LOADING AND RF STUDIES

C. S. Taylor and Y. Dupuis
CERN

ABSTRACT

The CERN-PS linac is at present accelerating currents of the order of 60 mA and partial compensation of the beam loading is being provided by "bumps" on the rf pulses. The evolution of this type of compensation is described and the results of energy spread and emittance measurements with and without compensation are presented.

An alternative method of supplying beam power from a supplementary power source is considered and preliminary tests are described.

Measurements of the phasing between tanks and the velocity of propagation of fields along the walls of the cavities are also reported.

I. INTRODUCTION

Beam loading in the accelerating cavities first became detectable in the rf envelopes with beam currents around 15 mA, and in 1961 attempts were made to compensate the fall in field during the beam pulse by moving the beam to the rising edge of the tank field and increasing the level. At that period, however, there was a 20 μs jitter in the initial rise of field in the 10 MeV tank, attributed to multipactor effect, and this jitter resulted in wide variation in accelerating field level and consequently in linac beam quality and PS intensity. The increased level also encouraged sparking although that could have been overcome by shortening the rf pulse.

Efforts were then directed towards supplying more power to the cavities during the beam pulse with the beam restored to its normal position near the end of the rf build-up.

II. EVOLUTION OF PRESENT METHOD OF COMPENSATION

In July 1962, attempts were made to increase the plate voltage of the TH 470 power amplifiers at the moment of beam injection. It was found that, with some sacrifice of pulse length, we could produce a useful "bump" on the anode pulse by increasing the terminal capacitor of the modulator delay line as shown in Fig. 1.

This method was applied first to the modulator of the three final amplifiers (see Fig. 8 for a general schematic of the rf system), and then extended to the drive modulator, both to increase the tank bumps and to suppress the over-voltages which appeared as a result of pulse length disparities.

The next step was to decrease the cathode bias voltage simultaneously with the anode bump by firing a hydrogen thyratron connected in parallel with part of the cathode resistor (Fig. 2). Careful adjustment of this combination of anode voltage and cathode current bumps led to the present situation, where a beam of 30-35 mA can be fully compensated in each of the three tanks.

It has been found convenient to assess these effects by displaying the time derivative of the tank field rather than the field itself. Both signals are shown in Fig. 3. Knowing the beam current we can immediately calibrate our signal and derive the percentage compensation for any given rf adjustment.

III. BEAM QUALITY WITH PRESENT METHOD

For the case of a beam pulse short by comparison with the cavity time constant, it can be shown by approximate solution[1] that the beam produces a change of accelerating field

$$\frac{\Delta V}{V_o} = -\frac{P_b}{2 W_o} t$$

where P_b is the instantaneous power delivered to the beam and W_o is the cavity stored energy at $t = 0$, and a change of phase

$$\Delta\varphi = -\frac{P_b \tan \varphi_s}{2 W_o} t$$

where φ_s is the synchronous phase angle.

Since this phase term is roughly the same for each of the three tanks (about 2.5^o for 50 mA), the original phase relations between the tanks will be preserved during the passage of beam, although not necessarily between the last tank and the debuncher.

The more significant effect of field change we should expect to be equivalent to a change of synchronous phase angle during the pulse and in our case on uncompensated 50 mA should produce an 8% change in $\cos \varphi_s$, for example from $\varphi_s = 30^o$ to $\varphi_s = 21^o$, and detectable changes in energy spread and emittance.

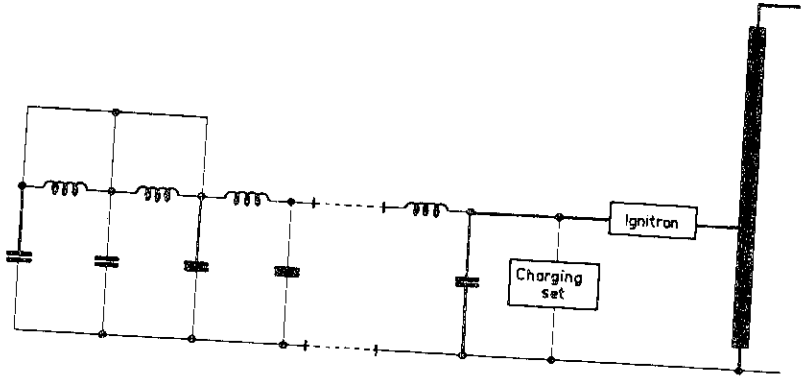

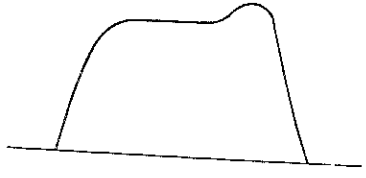

Resulting anode pulse

Fig. 1

Modified delay - line

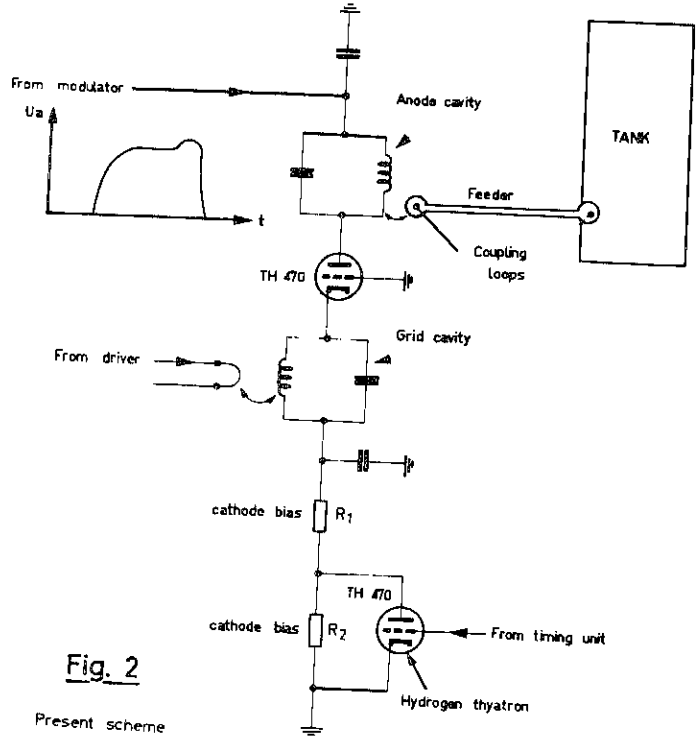

Fig. 2

Present scheme

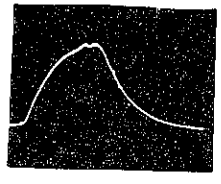

Accelerating voltage : V

Fig. 3

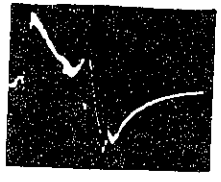

derivative : $\frac{dV}{dt}$

In Fig. 4a we see the measured energy spectra for an uncompensated 55 mA beam and for a beam compensated to an average value of 50% in the three tanks, with and without debuncher. It is evident that the debuncher is doing all the real work but that changes during the pulse are reduced by the compensation. The uncompensated beam is in fact not very satisfactory since particles are lost at the end of the pulse in the linear accelerator itself, the end of the pulse being only one-half the height at the beginning.

The experimental arrangement comprised a 0.5 mm object slit, approximately unity magnification, a 1 mm resolving slit equivalent to $\pm$ 30 kV, and about 6 mA of total beam current, with this reduced current passing through the debuncher. This resolution is not adequate for small energy spreads and the energy spread may be less than that measured. However, from the point of view of what the synchrotron actually sees with 60 mA, this error may be countered by the deterioration of the energy spread due to the reactive beam loading in the debuncher which we estimate to change the phase by some 10° and to add 80 kV to the energy spread.

In Figs. 4b and 4b' we see the emittance plots for the same condition of no compensation and 50% compensation. The horizontal plane (emittance Y) appears to be subjected to a clockwise rotation with time whereas this effect in the vertical plane (emittance Z) is much less marked. The distorted envelope for the end of the pulse in "emittance Y without compensation" probably indicates aperture limitations in the linear accelerator.

Care was taken during these measurements to keep the rf field constant in the middle of the pulse. However, the emittances with and without compensation in the middle of the pulse are not identical and this requires further investigation.

IV. SUPPLEMENTARY POWER SOURCE

In order to drive a 50 mA beam through the 30-50 MeV tank, we need 1 MW of rf power, and since this tank dissipates 1.5 MW, the total instantaneous power requirements are already beyond the capacity of our 2 MW amplifiers. If, however, we separate the functions of feeding losses and feeding beam power , we should be able to approach 100 mA beam currents with our present amplifiers.

Our present proposal is to drive the tank up to operating level by means of the existing delay line modulator, and then to supply the beam power by means of a second coupling loop and power amplifier for the

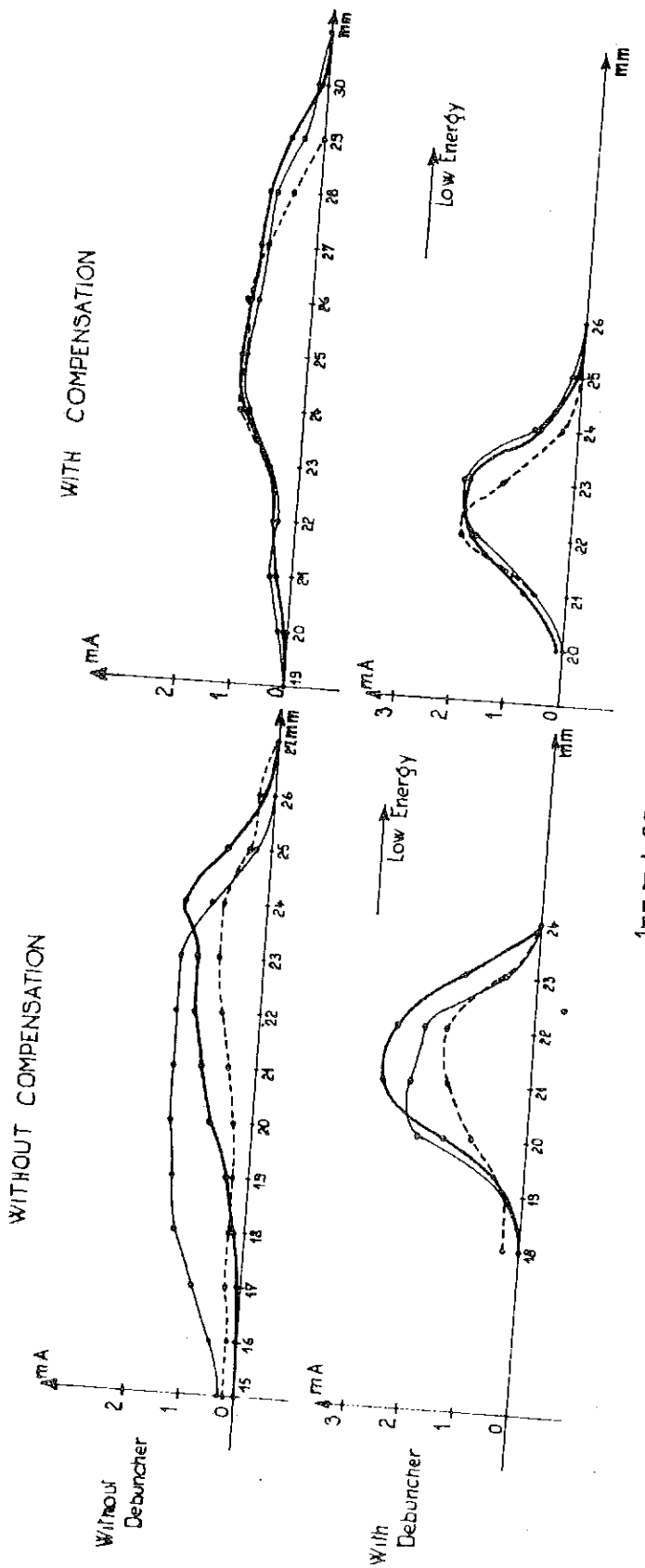

50 MeV ENERGY SPECTRA

Fig. 4A

duration of the beam pulse. We propose a hard-tube modulator for the beam power pulse, with the possibility of servo control from the beam current. One advantage of this system is that the phase of the beam power source can be varied with respect to that of the main source, i.e., power can be fed to the beam with the accelerating voltage in phase with the beam current Fourier fundamental φ_s from the crest.

The proposed scheme is shown in Fig. 5.

Preliminary tests of such a system have been made on the 30-50 MeV tank. The beam power amplifier was excited by rf power taken capacitively from the main loop feeder, and a modulator was modified to provide a short anode pulse (Fig. 6). Using the normal 200 μs pulse transformer, we could not obtain a very satisfactory rise time. Nevertheless full compensation of a 60 mA beam was obtained (Fig. 7). Unfortunately beam quality checks could not be made in the time available, apart from a quick measurement of energy spread which appeared to be normal.

V. PHASING BETWEEN TANKS

The three accelerating cavities are each held at a fixed phase by means of a phase servo loop. Line lengtheners in the final amplifier grid circuits are coupled mechanically to line lengtheners in the phase reference lines and this arrangement permits relative movement of the tank phases (see Fig. 8: Schematic of complete rf system).

A good beam can be obtained by a purely empirical adjustment of relative phases. Alternatively, one can employ a criterion based on the 3 φ_s trapping width. In the early experiments it was accepted a priori that the correct adjustment was the "in-phase" condition although some attempts to measure relative phases with hybrid ring bridges gave conflicting results. With, however, the installation of accurately adjusted cables and a lissajous figure type of phase comparison (Fig. 9), it has become fairly certain that the beam likes best to find the 10 and 50 MeV tanks in phase but the 30 MeV tank advanced by some 25°, that is, this dephasing produces the best energy spread.

There is as yet no satisfactory explanation of this effect. One possible contribution comes from the two-cell drift distance between the first and second tanks, combined with the fact that we normally inject our bunched beam into the first tank well above the center of the rf bucket in order to profit from the higher trapping. However, our step-by-step computations using the program developed at Harwell by Taylor and Carne show that the energy error resulting at 10 MeV is only about

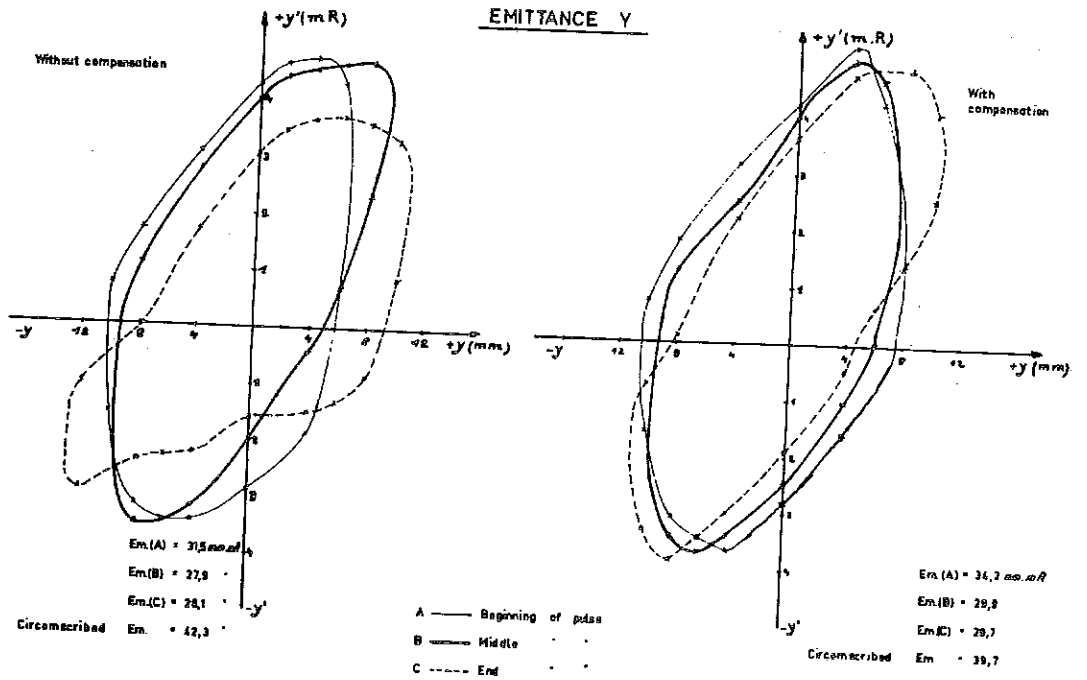
EMITTANCE Y
Without compensation
+y'(m.R)
+y (mm)
-y
-y'
Em.(A) = 31,5 mm.mR
Em.(B) = 27,9 "
Em.(C) = 28,1 "
Circumscribed Em. = 42,3 "
With compensation
Em.(A) = 34,2 mm.mR
Em.(B) = 29,8 "
Em.(C) = 29,7 "
Circumscribed Em = 39,7 "
A —— Beginning of pulse
B —— Middle " "
C ----- End " "

Fig. 4b

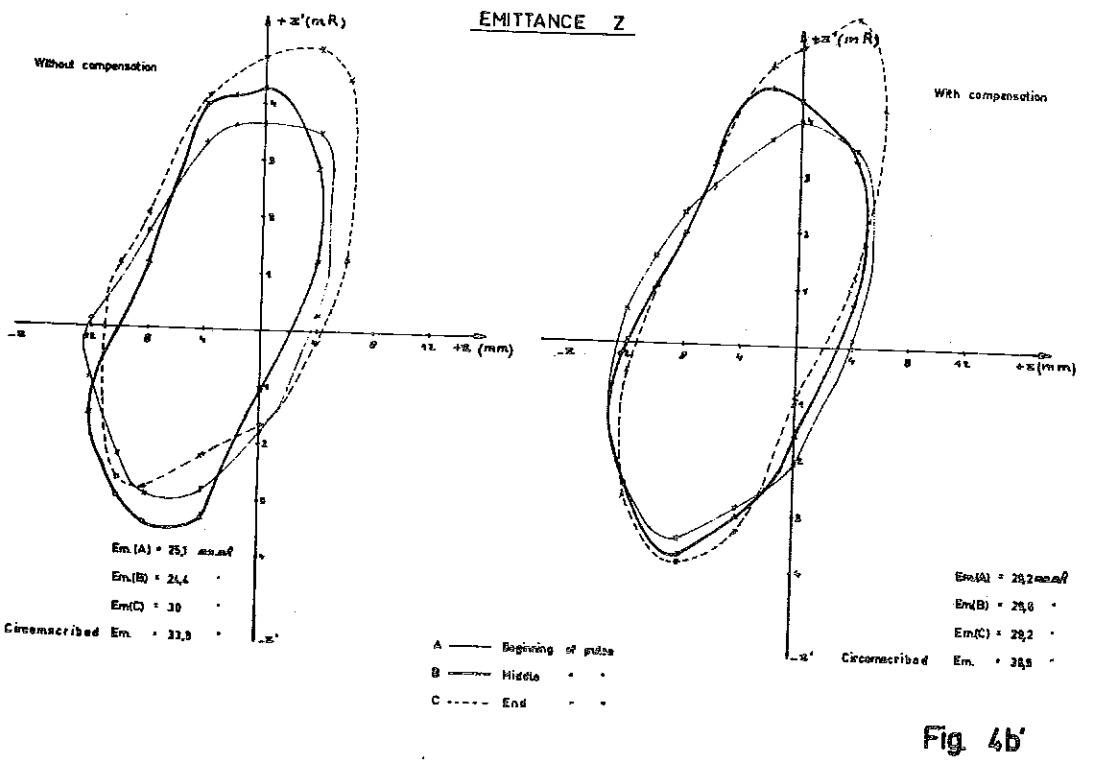
EMITTANCE Z
Without compensation
+x'(m.R)
+x (mm)
-x
-x'
Em.(A) = 25,1 mm.mR
Em.(B) = 24,4 "
Em(C) = 30 "
Circumscribed Em. = 33,9 "
With compensation
Em.(A) = 28,2 mm.mR
Em(B) = 28,6 "
Em.(C) = 29,2 "
Circumscribed Em. = 38,9 "
A —— Beginning of pulse
B —— Middle " "
C ----- End " "

Fig. 4b'

100 kV, and produces a phase error due to the drift distance of only 3 or 4 degrees.

Another possibility, which came out of a discussion with Teng and Lapostolle, is that we are exploiting the nonlinear region of the Tank II bucket to spread the bunch out, and then rotating this elongated bunch around to the position of minimum 50 MeV energy spread by adjustment at Tank II and III levels, thereby varying the number of phase oscillations in these tanks. This mechanism would require an integral number of wavelengths in Tank II and an odd number of quarter wavelengths in Tank III.

VI. PROPAGATION

Recent discussions of group velocities[2] have led us to compare the build-up of tank fields at the extremities of the 30-50 MeV tank (with power fed in at one end). Using the phase measurement loops and cables we have employed the chopped beam facility of an oscilloscope to superimpose the detected signals from both loops. In Fig. 10, we see the field signals and the initial build-up on a shorter time base. From these oscillograms one can put an upper limit of a microsecond on the delay and a lower limit of 10^7 m/sec on the corresponding velocity for field propagation along the cavity walls.

ACKNOWLEDGEMENTS

It is a pleasure to acknowledge the excellent contributions of Messrs. Block, Marti, Têtu and Weiss to the experimental work and computations.

TURNER: Could you repeat the specifications for the new FTH 515 tube you mentioned?

TAYLOR: 4 MW peak power; heater, 12 kW; anode dissipation, 11 kW. I think the drive power is 700 kW.

VAN STEENBERGEN: Do you have to make a modification to the tube cavity?

TAYLOR: No, the specification calls for a tube which is a mechanical plug-in replacement for the FTH-470. It will have the same anode volts but double the current. We will probably have to modify the loop and the coupling.

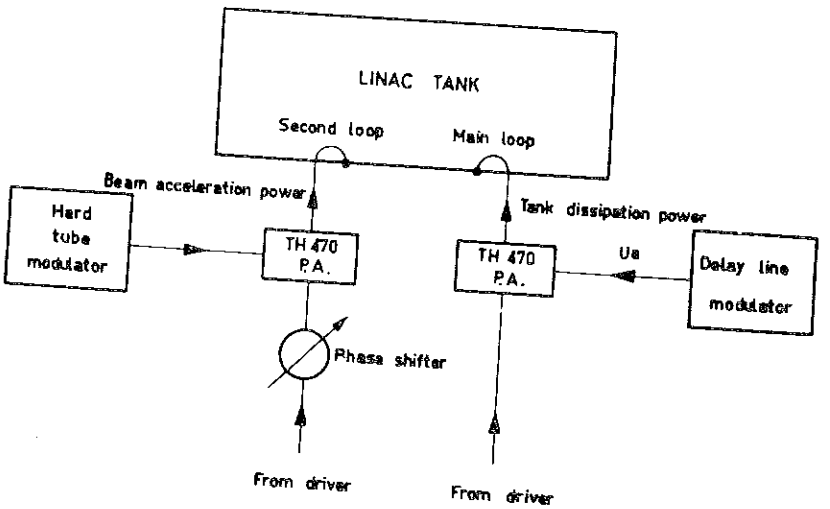

Fig. 5

Proposed scheme

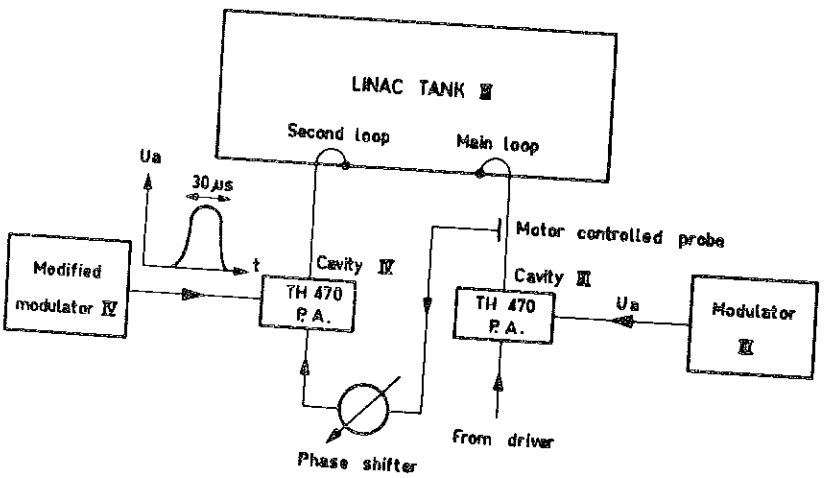

Fig. 6

Tested scheme

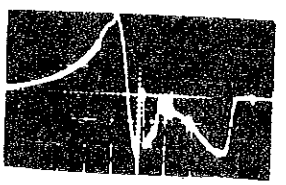

$\frac{dV}{dt}$ for a 50mA beam.

Fig. 7

VAN STEENBERGEN: What is the promised delivery date on this tube?

TAYLOR: I think we should get a tube within about six months.

QUESTION: Have you watched some of the modeling on this tube?

TAYLOR: It is only just started. I might mention that the cost is something like $6,500 per tube.

PERRY: I didn't understand the phase shift from 30^{o} to 21^{o}.

TAYLOR: This is simply the field going up and then dropping due to the presence of beam. This is equivalent to a change in the synchronous phase from 30^{o} to 21^{o}.

PERRY: When you have 50 mA beam loading and 8% droop, was the 30^{o} to 21^{o} the phase shift due to beam loading?

TAYLOR: The difference in cos φ_s was 8%.

KEANE: You mentioned that you had no phase or time delay in the field propagation along the tank. I have noted on Brookhaven's linac that we have at least 1-1/2 microsecond delay from the center drive point to both ends of the tank.

TAYLOR: In our measurement, the difference in path length is about 10 m. In your case it is 15 - 16 m.

MARTIN, J. H.: You used the term "compensated" and "uncompensated." Did that consist of anything besides just an additional bump at the end?

TAYLOR: No, that was simply a bump.

MARTIN: It had influence on the energy distribution and phase-space accommodation and so forth; did it have anything to do with the phase relations between the tanks?

TAYLOR: That occurs with a small beam. If we stop the beam down, we still have this effect.

MARTIN: So this effect is independent of beam loading?

TAYLOR: Yes.

KEANE: You mentioned that you used a separate amplifier for beam compensation. Did you have any trouble with power coupling between the loops of the two driving sources?

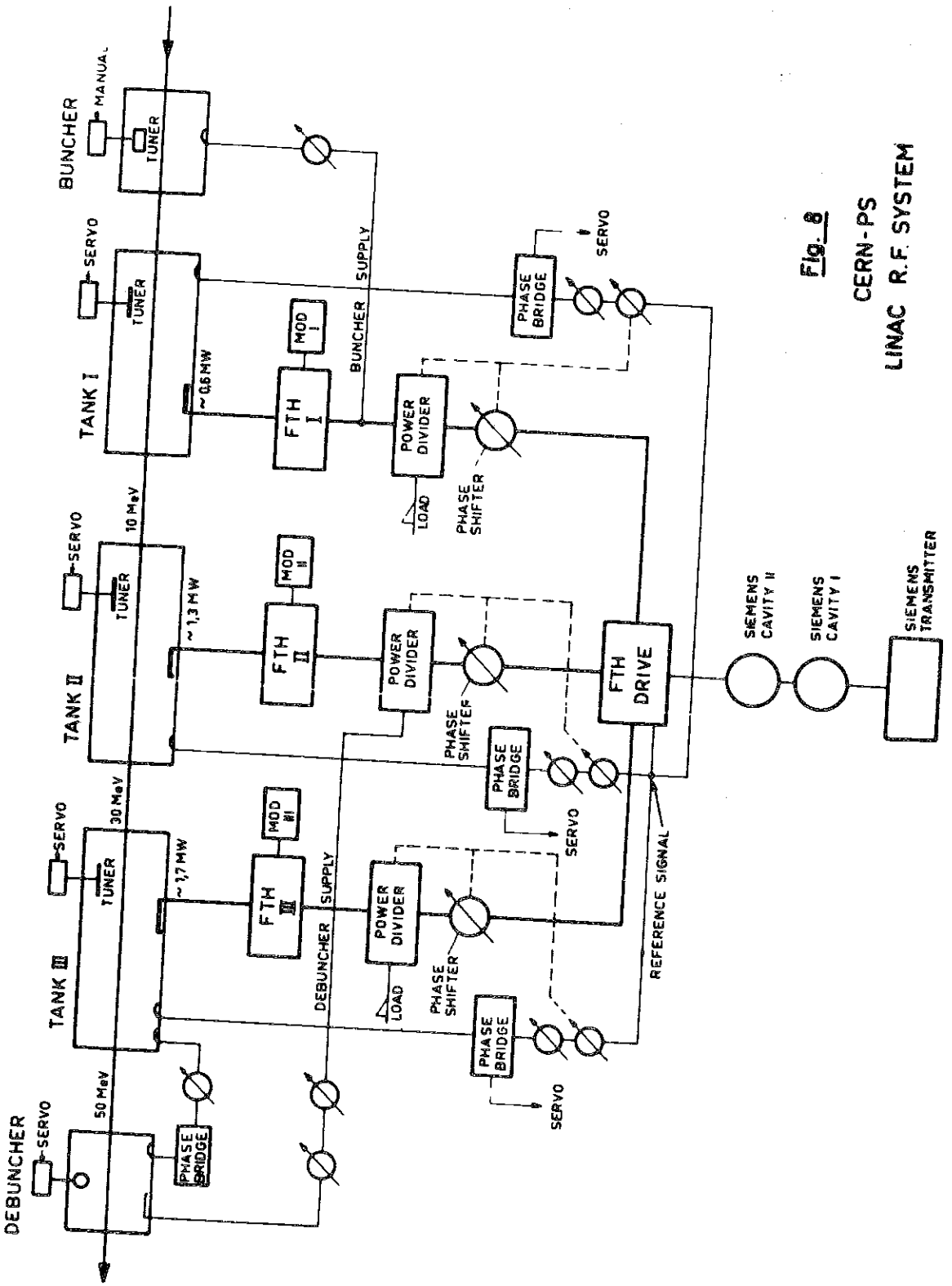

Fig. 8

CERN-PS
LINAC R.F. SYSTEM

TAYLOR: We were a little worried about this and our first move was to put a short circuit piston on the auxiliary loop. We made it as close to a short circuit in a tank as we could. Then we found that by moving this up and down, it made no difference. It is surprising. Then when we connected a FTH amplifier cavity in place of the short circuit, there was a tendency for it to "diode", and we found ourselves in a little bit of trouble getting enough power from the main amplifier.

KEANE: Were the loops the same?

TAYLOR: Exactly the same loop. It probably makes a terrible bump on the flattening, but so far we have not noticed it.

DICKSON: Going back to the phase changing in Tank 2, how do you find running all tanks in phase and adjusting the wave lengths of Tanks 2 and 3 together to get an integral half-wave length?

TAYLOR: We have tried to run them in phase and adjust the levels of all tanks together, but we went through a fair range and we could not find an energy spread as good as the energy spread which we get with the normal adjustment of the phasing.

REFERENCES

1. Y. Dupuis, Etude de la charge introduite par le faisceau dans les cavités H.F. du Linac du CPS. Internal report MPS/Int. LIN 36-8.

2. J. M. Dickson, Private communication.

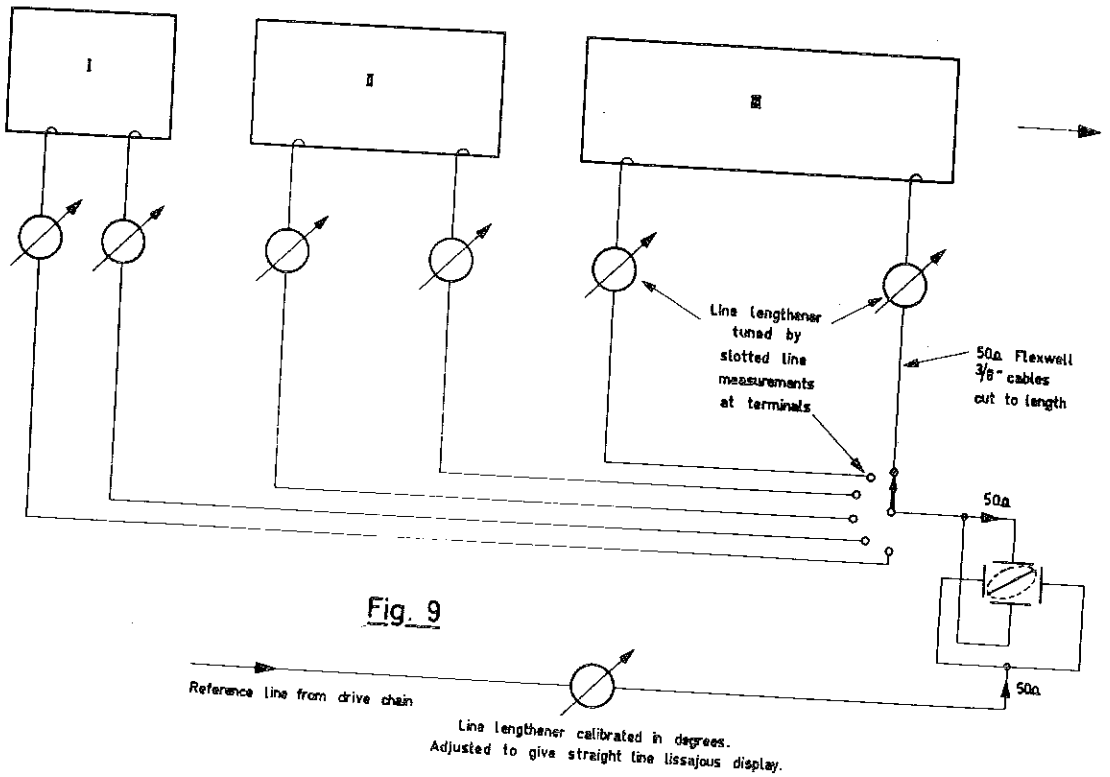

Fig. 9

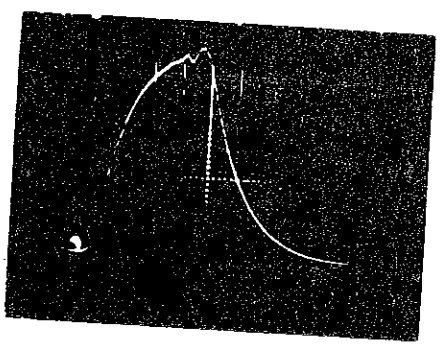

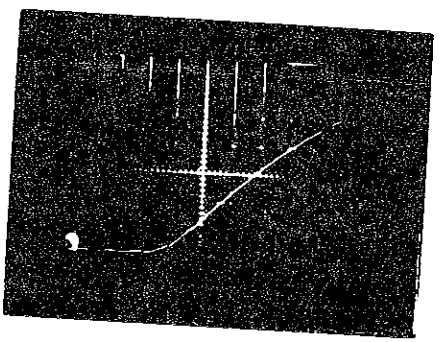

0.5 V/cm 50 μs/cm
Chopped beam.
Equalisation of detector outputs.

A

As Fig. 10 A but 10 μs/cm

B

Fig. 10

MODEL MEASUREMENTS AND CORRECTION OF BEAM LOADING EFFECTS IN PROTON LINACS

S. Giordano
Brookhaven National Laboratory

When a proton beam is being accelerated in a linac, there is an interaction with the fields in the accelerator cavity. The effect of the beam on the cavity is referred to as beam loading. Beam loading affects the cavity in two ways: there is a real part which absorbs energy from the cavity, and a reactive part that detunes the cavity. Some estimates of the relative magnitude of these effects have been considered by a number of people, using an equivalent R, L, C circuit. It is the purpose of this paper to measure the effects of beam loading in a multiple-cell linac structure, and to determine the relative magnitude of these effects for two structures of different bandwidths.

It was first necessary to devise some method which would duplicate beam loading in a model cavity. It should be pointed out that the method to be described considers only the steady-state beam-loading effects, and is based on the premise that the beam-loading effects are uniformly distributed along the length of a cavity.

If all the cells of a cavity were detuned by a fixed amount, and the drive was kept at the original resonant frequency, then the effect upon the cavity would be the same as a uniformly distributed reactive component of beam loading. The same results can be obtained by detuning the frequency of the rf drive by a fixed amount. It should be emphasized that the above method results in simulating only the reactive component of beam loading.

The real component of beam loading can be duplicated in a cavity by increasing the losses (decreasing the Q) of all the cells uniformly. The Q is decreased by placing a strand of cotton thread that has been loaded with graphite,* down the axis of a cavity. The cotton thread has a very small reactive effect, which only slightly detunes the cavity. Since the reactive detuning of the loaded cotton thread is uniformly distributed along the cavity, its effects can be eliminated by adjusting the

---

*A piece of cotton thread is soaked in a graphite alcohol suspension. The thread is then squeezed to eliminate excess liquid and hung to dry. By varying the concentration of graphite and alcohol, the losses introduced by the thread can be varied.

perturbation tunes in each cell. Rather than adjusting the tuners, the same results are achieved by changing the frequency of the rf drive to the new resonant frequency of the loaded cavity. It should be pointed out that this simulates only the real component of beam loading.

We now see that it is possible to separate the effects of both the reactive part and the real part of beam loading. It is also possible to combine both of these effects, by simultaneously introducing the loaded string and detuning the drive frequency.

Measurements were made on two different cavities shown in Figs. 1 and 2. Figure 1 shows a shaped iris cavity having a center frequency ($\pi/2$ mode) of 880 Mc and a bandwidth of 2.7 Mc (bandwidth is defined as the difference in frequency between the "0" mode and the π mode). Figure 2 shows a slotted iris cavity (reported by this author in these minutes) having a center frequency of 824 Mc and a bandwidth of 72 Mc. Both the above cavities had pickup loops and perturbation tuners in each cell.

All measurements reported in this paper were made in the "π" mode at $\beta \approx 0.5$. Of interest is the phase and amplitude variations of the electric and magnetic fields along the cavity, as a function of beam loading. In all the measurements to be discussed, the cavity was first tuned to have a flat field (no amplitude variation). The Q and frequency of the drive were then varied in steps, representing different magnitudes of beam loading. Measurements were also made with two different drive conditions:

(1) A single drive at one end of the cavity.
(2) Two separate drives, both in phase, one at each end of the cavity.

Figures 4, 5, 6 and 7 show the results of the measurements made on the shaped iris cavity. These measurements were made for the unloaded Q. Because of the very narrow bandwidth of the shaped iris structure, any attempts to reduce the Q resulted in the overlapping of adjacent modes. Figures 4 and 6 show the amplitude variations along the cavity at three different frequencies for the one-drive and two-drive case. Figures 5 and 7 show the phase variations along the cavity at three different frequencies for both the one-drive and two-drive case. (All phase measurements were made by measuring the phase of each cell relative to one of the end cells.) For the two-drive case we see a considerable reduction of the relative phase change along the cavity, as compared to the single-drive case.

Figures 8 through 21 are the results of the measurement of phase and amplitude variations for the slotted iris structure. Figures 8, 10 and 12 are for Q values of 12,000, 5,000 and 3,000, with a single drive,

and show the variations of the field amplitude for different frequencies. In the above-mentioned figures, it is interesting to note that changes in the amplitude of the field are very sensitive to changes in frequency. It should be pointed out that changing the Q from 12,000 to 5,000 and to 3,000, had only a small effect on the variations of the amplitude.

Figures 9, 11 and 13 are for Q values of 12,000, 5,000 and 3,000, with a single drive, and show the relative phase variations along the cavity. It is interesting to note the relative insensitivity of the phase to changes in frequency, as compared to the large changes in phase due to the changes in Q. In Figs. 9, 11 and 13, when the Q is varied from 12,000 to 5,000 and to 3,000, the relative phase difference between the ends of the cavity varies from 3^{o}, 10^{o} and 14^{o} respectively.

Figures 14, 16 and 18 are for Q values of 12,000, 5,000 and 3,000, with two drives, and show variations of field amplitude for different frequencies. Figures 15, 17 and 19 show the relative phase variations along the cavity, for the same conditions mentioned above.

It is interesting to compare the relative phase and amplitude variations for both the single and double-drive cases. Figure 20 is a plot of the over-all phase difference between the ends of the cavity vs Q, at f_o, $f_o + 150$ kc, and $f_o - 150$ kc, for both the single and double drive cases. For the same above-mentioned conditions, Fig. 21 is a plot of $\frac{\Delta E}{E_{av}}$ vs Q. ($\frac{\Delta E}{E_{av}} = \frac{E_{max} - E_{min}}{2\,E_{av}}$, where E_{max} is the maximum field in the cavity, E_{min} is the minimum field, and E_{av} is the average field.) Figures 20 and 21 closely show that there is a considerable reduction in both the amplitude and the relative phase changes with respect to beam loading changes.

In comparing the narrow band-shaped iris cavity to the wider band-slotted iris cavity, we see that the narrow band structure is considerably more sensitive to beam-loading effects.

Figure 3 shows a hollow cylinder which is to be operated in the TM_{010} mode. Work was recently started on this structure, and measurements are to be made in the near future.

VAN STEENBERGEN: In that diagram you showed a tilt in the tank amplitude. Could you not correct this tilt in the amplitude by changing the frequency?

GIORDANO: There are two reasons that could cause a tilt: (1) a change in the drive frequency as you have indicated, (2) a local detuning of the cavity which can be caused by a change in the thermal gradient along the cavity.

VAN STEENBERGEN: Don't these two effects amount to the same thing?

GIORDANO: No.

LEISS: Your resistive string represents only the beam loading which is 180^{o} out of phase with the field in the tank. A beam of particles is at the equilibrium phase and not at the peak of the radio-frequency voltage, and so there is an additional phase shift due to this.

GIORDANO: We are only considering the steady-state condition and assuming that the beam-loading effects are uniformly distributed along the cavity. The resistive string represents the real component of beam loading, and the reactive component is obtained by changing the frequency of the drive.

LEISS: When you speak of reactive part, what you really mean is that the beam is not running at the peak of the wave, and as such we have an in-phase component and out-of-phase component, so that it is not really right to represent this by a frequency shift.

GIORDANO: What you call an out-of-phase component, I call the reactive part. This reactive component actually causes a detuning of the cavity, which I have duplicated by shifting the frequency of the drive. In Fig. 20, I have shown the effect by varying the frequency from f_o + 150 kc to f_o - 150 kc, and we see that the effect is small. It should be pointed out that this frequency variation is considerably greater than one would expect from a beam of 50 mA.

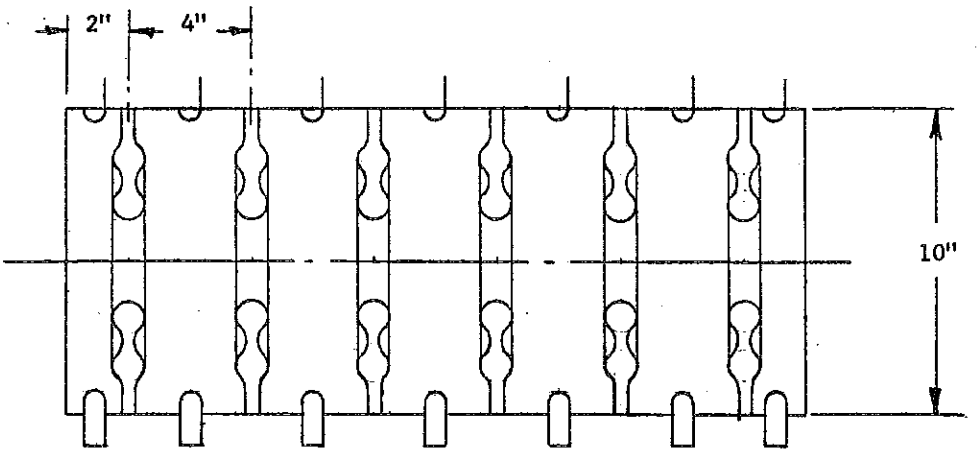

Fig. 1 Shaped Iris

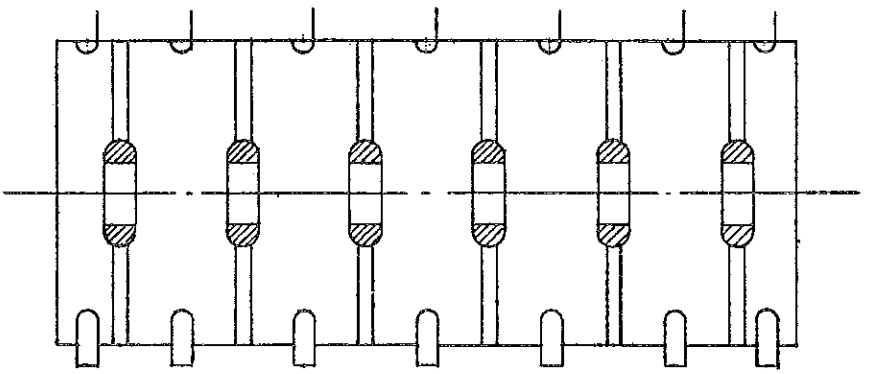

Fig. 2 Slotted Iris

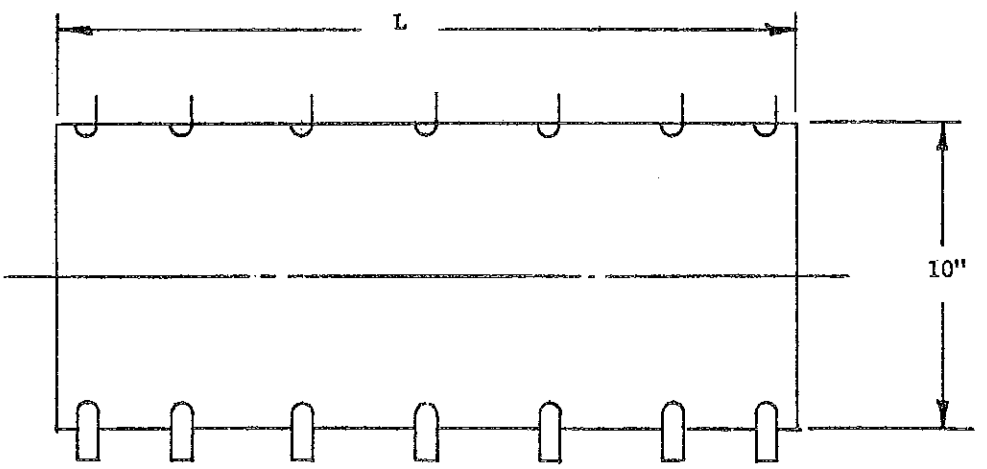

Fig. 3 Hollow Structure

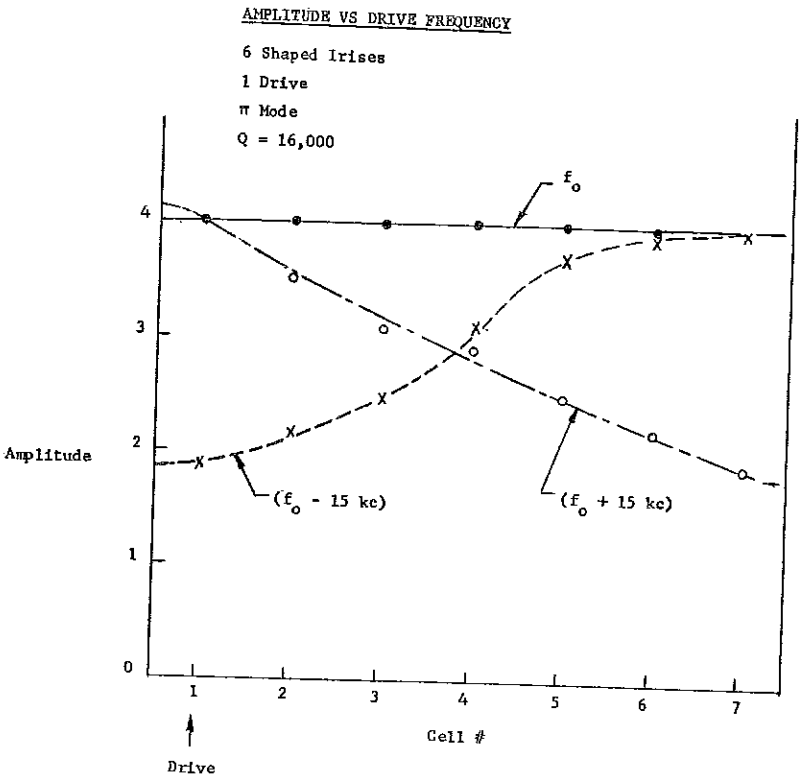
AMPLITUDE VS DRIVE FREQUENCY
6 Shaped Irises
1 Drive
π Mode
Q = 16,000
f_o
$(f_o - 15\ kc)$
$(f_o + 15\ kc)$
Amplitude
Cell #
Drive

Fig. 4

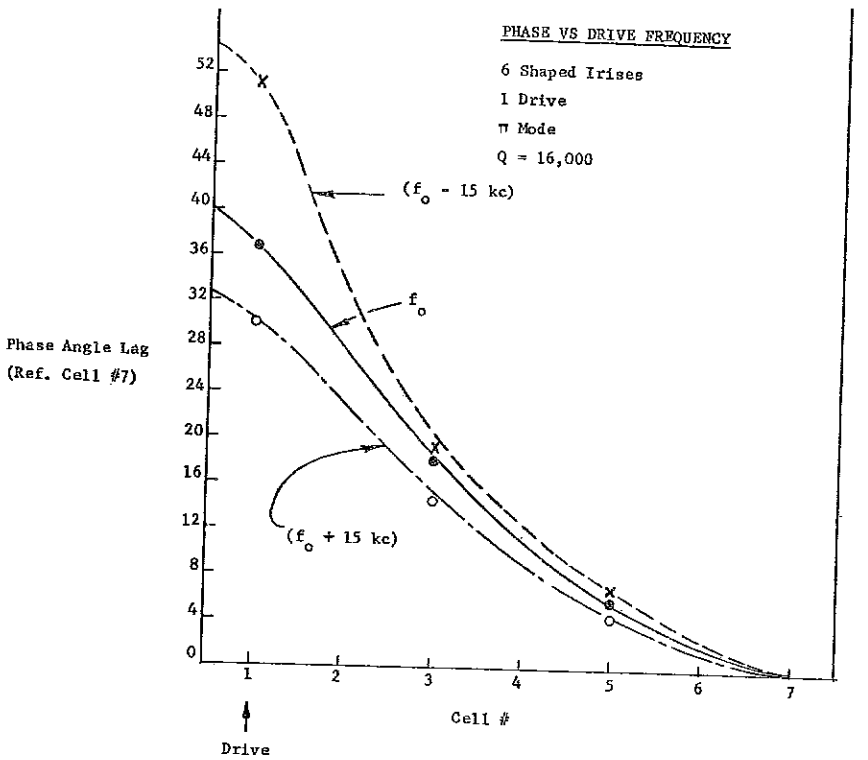
PHASE VS DRIVE FREQUENCY
6 Shaped Irises
1 Drive
π Mode
Q = 16,000
$(f_o - 15\ kc)$
f_o
$(f_o + 15\ kc)$
Phase Angle Lag
(Ref. Cell #7)
Cell #
Drive

Fig. 5

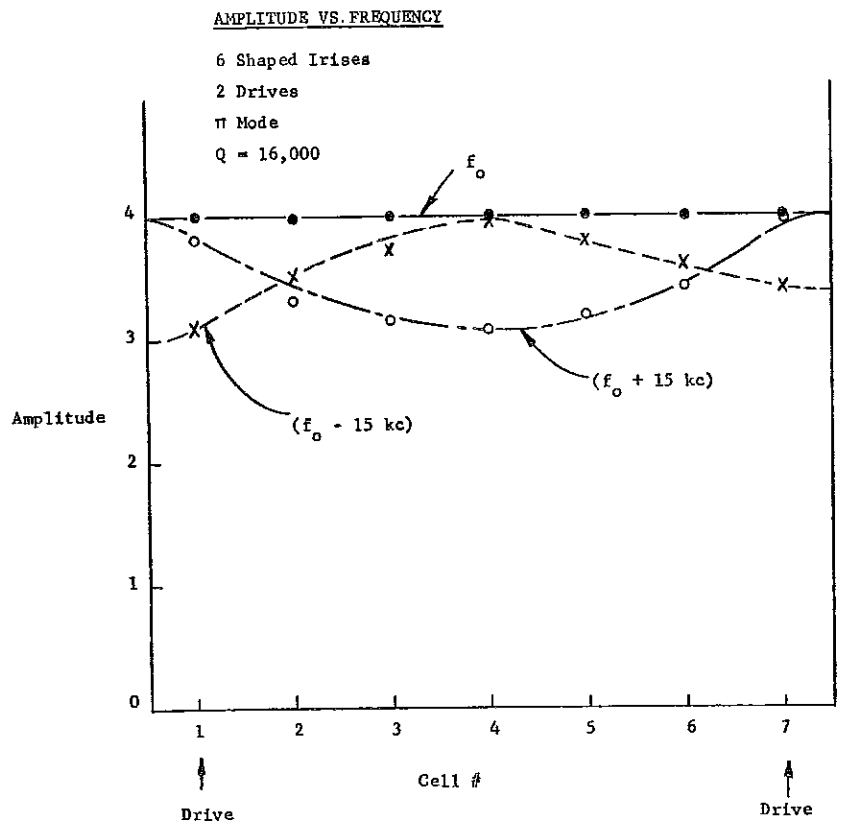
AMPLITUDE VS. FREQUENCY
6 Shaped Irises
2 Drives
π Mode
Q = 16,000
f_o
$(f_o + 15\ kc)$
$(f_o - 15\ kc)$
Amplitude
0
1
2
3
4
1
2
3
4
5
6
7
Cell #
Drive
Drive

Fig. 6

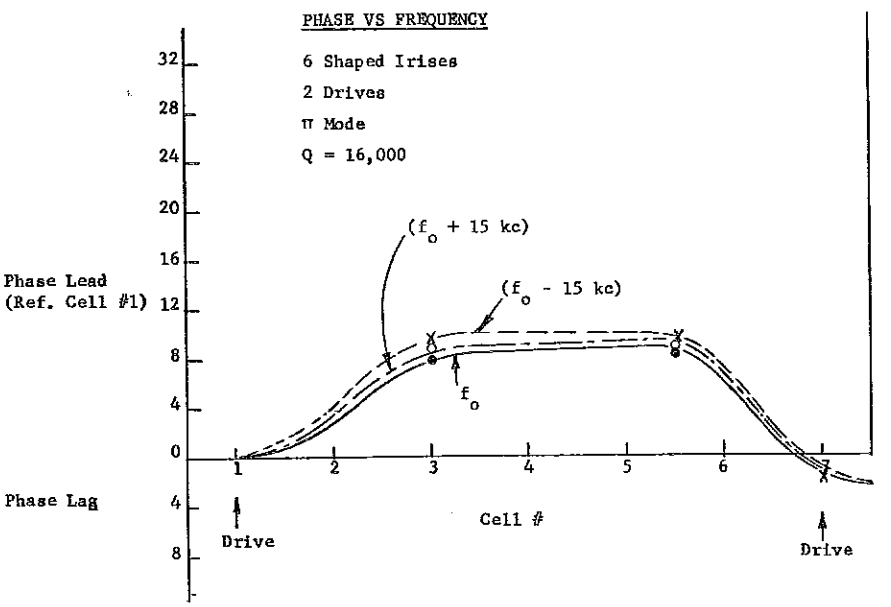
PHASE VS FREQUENCY
6 Shaped Irises
2 Drives
π Mode
Q = 16,000
$(f_o + 15\ kc)$
$(f_o - 15\ kc)$
f_o
Phase Lead
(Ref. Cell #1)
Phase Lag
32
28
24
20
16
12
8
4
0
4
8
1
2
3
4
5
6
7
Cell #
Drive
Drive

Fig. 7

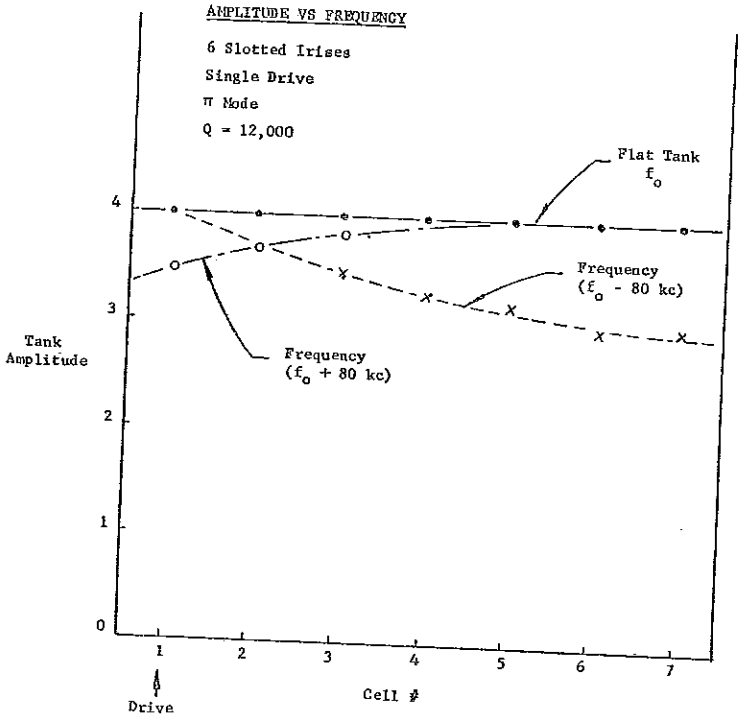
AMPLITUDE VS FREQUENCY
6 Slotted Irises
Single Drive
π Mode
Q = 12,000
Flat Tank
f_o
Frequency
(f_o - 80 kc)
Frequency
(f_o + 80 kc)
Tank
Amplitude
0
1
2
3
4
1
2
3
4
5
6
7
Drive
Cell #

Fig. 8

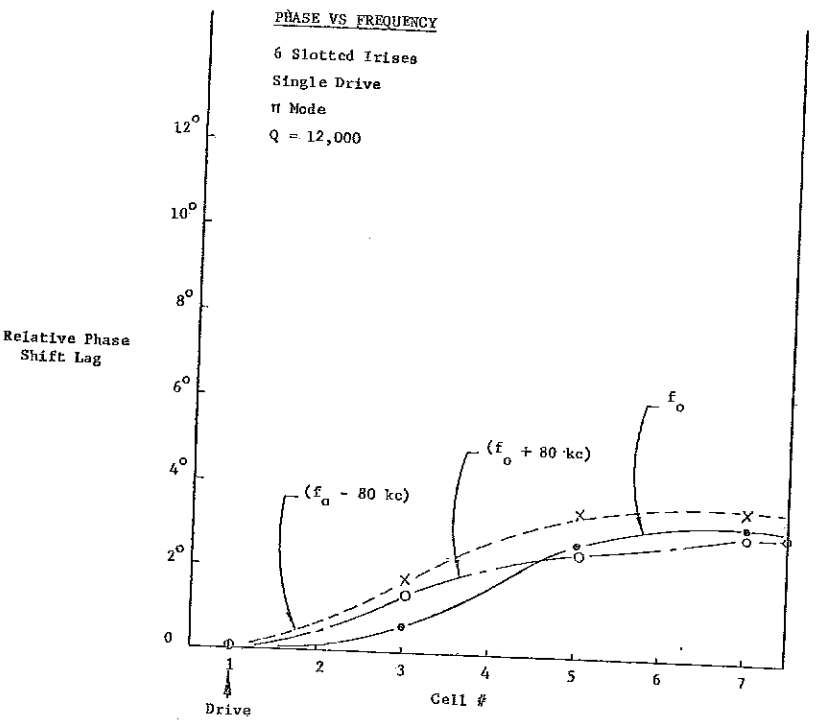
PHASE VS FREQUENCY
6 Slotted Irises
Single Drive
π Mode
Q = 12,000
Relative Phase
Shift Lag
0
2°
4°
6°
8°
10°
12°
(f_o - 80 kc)
(f_o + 80 kc)
f_o
1
2
3
4
5
6
7
Drive
Cell #

Fig. 9

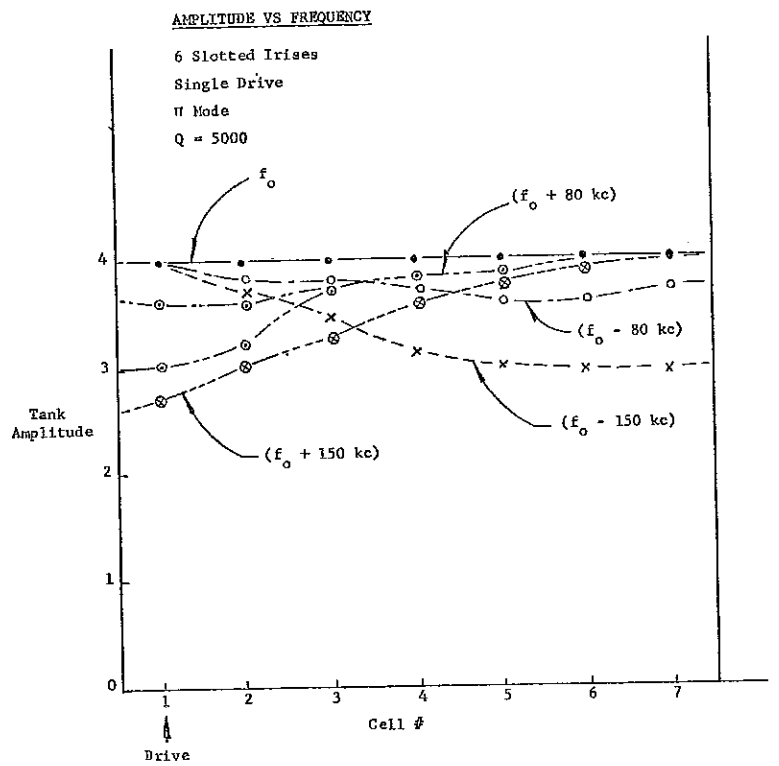
AMPLITUDE VS FREQUENCY
6 Slotted Irises
Single Drive
π Mode
Q = 5000
f_o
$(f_o + 80\ kc)$
$(f_o - 80\ kc)$
$(f_o - 150\ kc)$
$(f_o + 150\ kc)$
Tank Amplitude
0
1
2
3
4
1
2
3
4
5
6
7
Cell #
Drive

Fig. 10

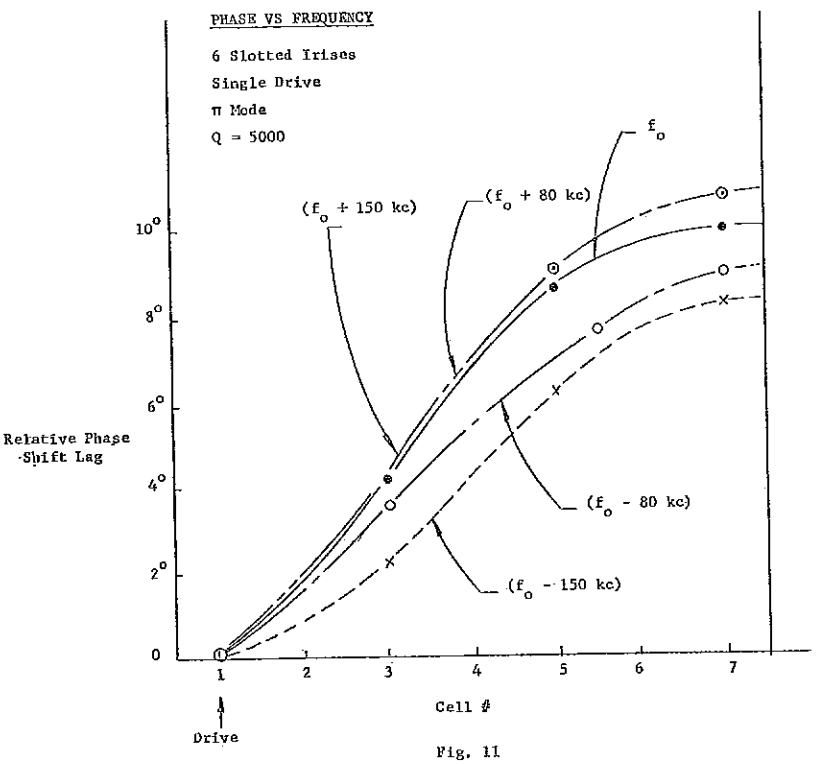
PHASE VS FREQUENCY
6 Slotted Irises
Single Drive
π Mode
Q = 5000
f_o
$(f_o + 150\ kc)$
$(f_o + 80\ kc)$
$(f_o - 80\ kc)$
$(f_o - 150\ kc)$
Relative Phase Shift Lag
0
2°
4°
6°
8°
10°
1
2
3
4
5
6
7
Cell #
Drive

Fig. 11

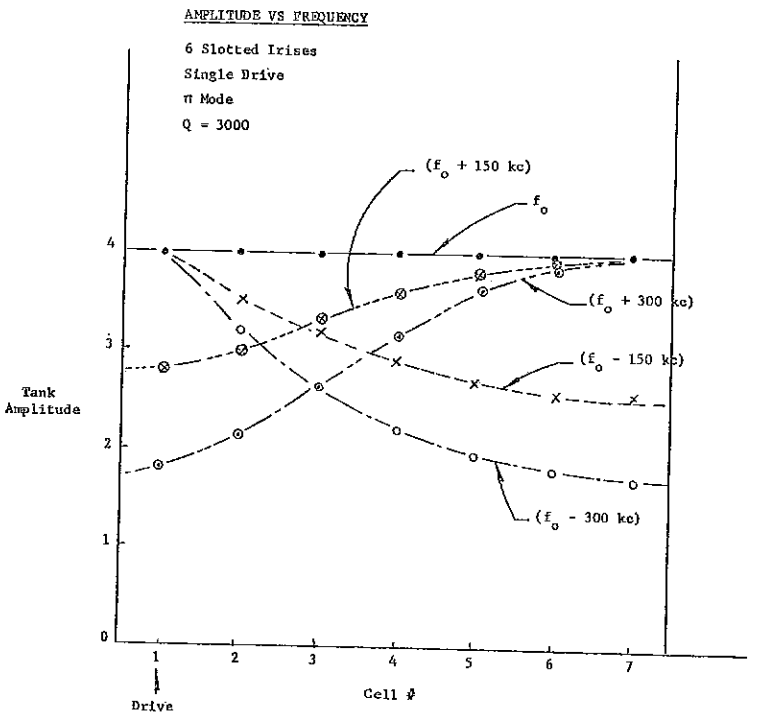
AMPLITUDE VS FREQUENCY
6 Slotted Irises
Single Drive
π Mode
Q = 3000
(f_o + 150 kc)
f_o
(f_o + 300 kc)
(f_o - 150 kc)
(f_o - 300 kc)
Tank Amplitude
0
1
2
3
4
1
2
3
4
5
6
7
Drive
Cell #

Fig. 12

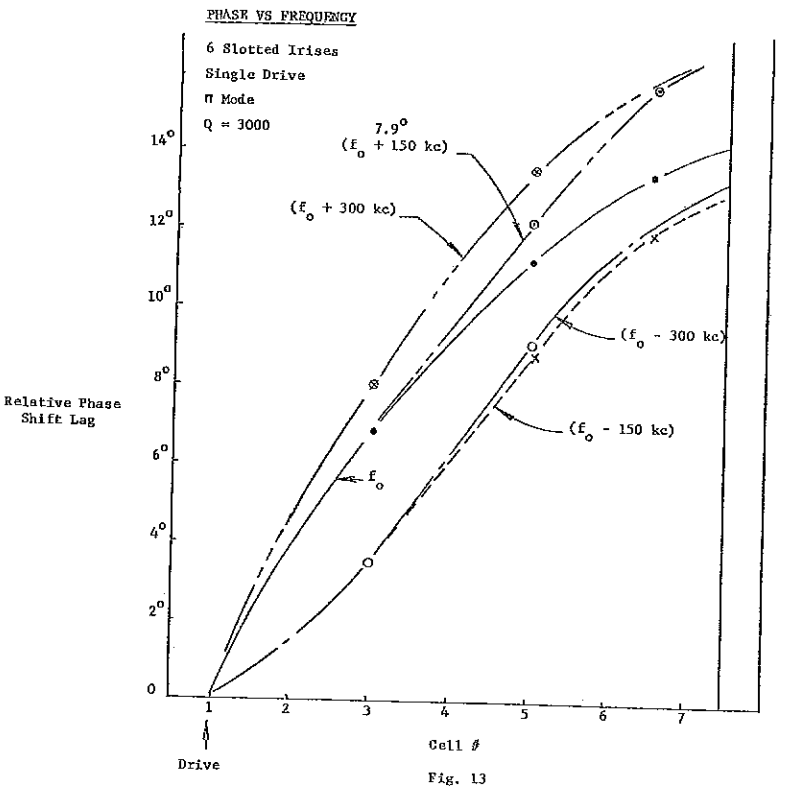
PHASE VS FREQUENCY
6 Slotted Irises
Single Drive
π Mode
Q = 3000
7.9°
(f_o + 150 kc)
(f_o + 300 kc)
(f_o - 300 kc)
(f_o - 150 kc)
f_o
Relative Phase Shift Lag
0
2°
4°
6°
8°
10°
12°
14°
1
2
3
4
5
6
7
Drive
Cell #

Fig. 13

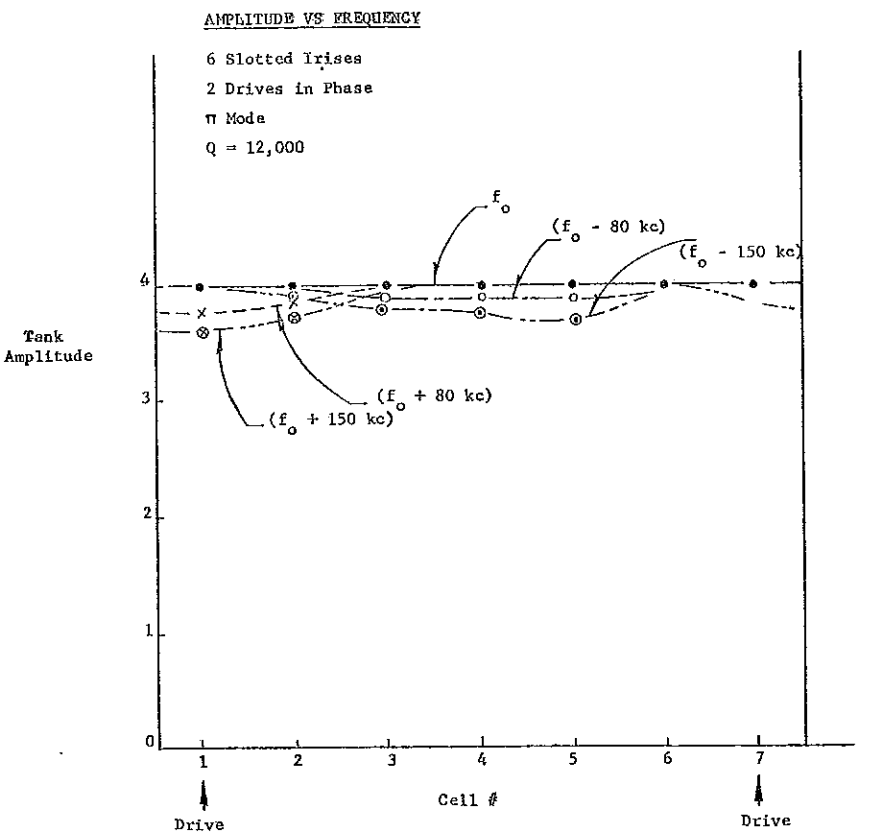
AMPLITUDE VS FREQUENCY
6 Slotted Irises
2 Drives in Phase
π Mode
Q = 12,000
f_o
(f_o - 80 kc)
(f_o - 150 kc)
(f_o + 80 kc)
(f_o + 150 kc)
Tank Amplitude
0
1
2
3
4
1
2
3
4
5
6
7
Cell #
Drive
Drive

Fig. 14

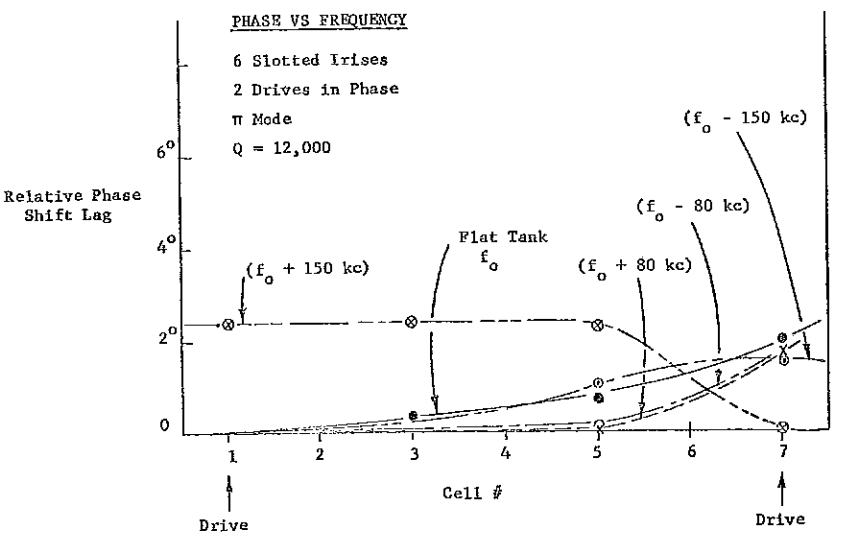
PHASE VS FREQUENCY
6 Slotted Irises
2 Drives in Phase
π Mode
Q = 12,000
(f_o - 150 kc)
(f_o - 80 kc)
Flat Tank f_o
(f_o + 150 kc)
(f_o + 80 kc)
Relative Phase Shift Lag
0
2°
4°
6°
1
2
3
4
5
6
7
Cell #
Drive
Drive

Fig. 15

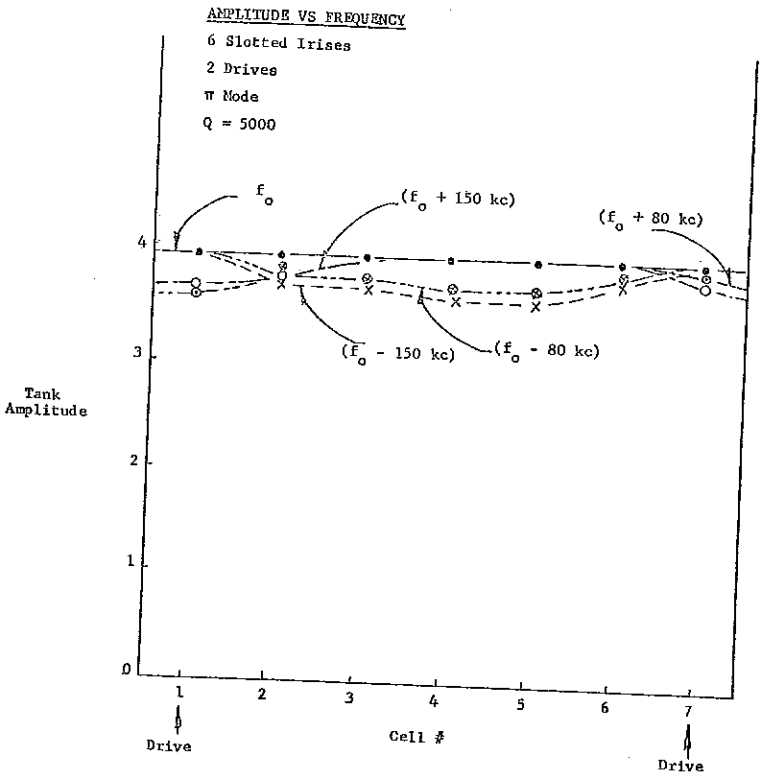
AMPLITUDE VS FREQUENCY
6 Slotted Irises
2 Drives
π Mode
Q = 5000
f_o
$(f_o + 150\ kc)$
$(f_o + 80\ kc)$
$(f_o - 150\ kc)$
$(f_o - 80\ kc)$
Tank Amplitude
0
1
2
3
4
1
2
3
4
5
6
7
Drive
Cell #
Drive

Fig. 16

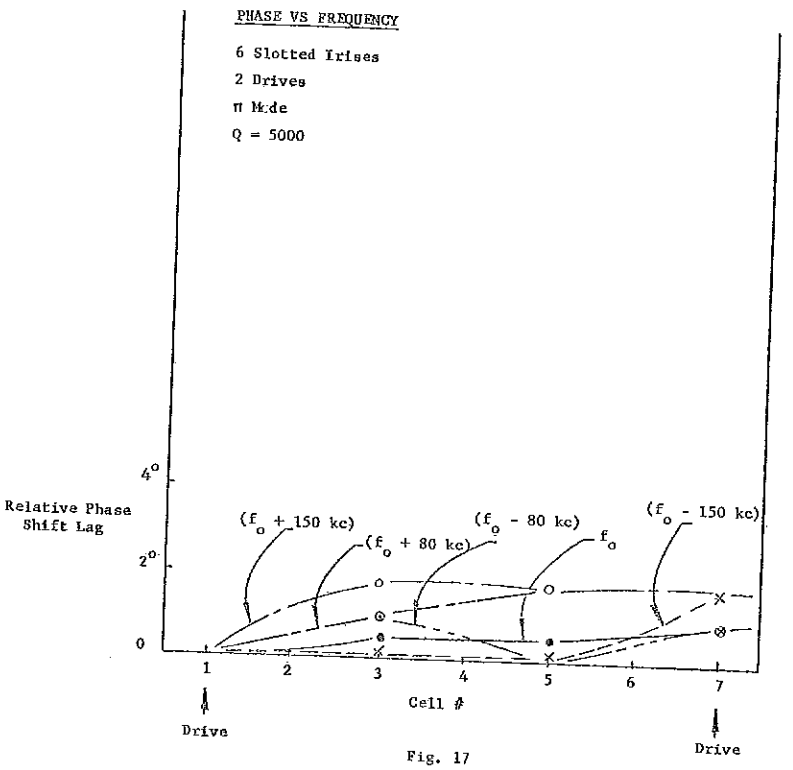
PHASE VS FREQUENCY
6 Slotted Irises
2 Drives
π Mode
Q = 5000
Relative Phase Shift Lag
0
2^o
4^o
$(f_o + 150\ kc)$
$(f_o + 80\ kc)$
$(f_o - 80\ kc)$
f_o
$(f_o - 150\ kc)$
1
2
3
4
5
6
7
Drive
Cell #
Drive

Fig. 17

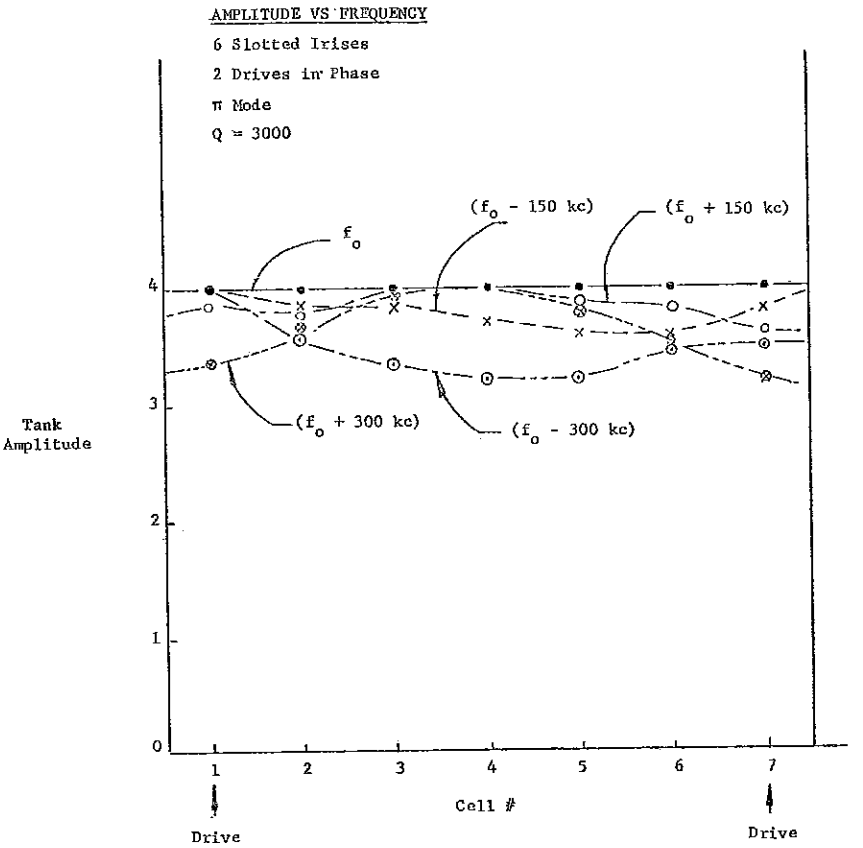
AMPLITUDE VS FREQUENCY
6 Slotted Irises
2 Drives in Phase
π Mode
Q = 3000
f_o
$(f_o - 150\ kc)$
$(f_o + 150\ kc)$
$(f_o + 300\ kc)$
$(f_o - 300\ kc)$
Tank Amplitude
0
1
2
3
4
1
2
3
4
5
6
7
Cell #
Drive
Drive

Fig. 18

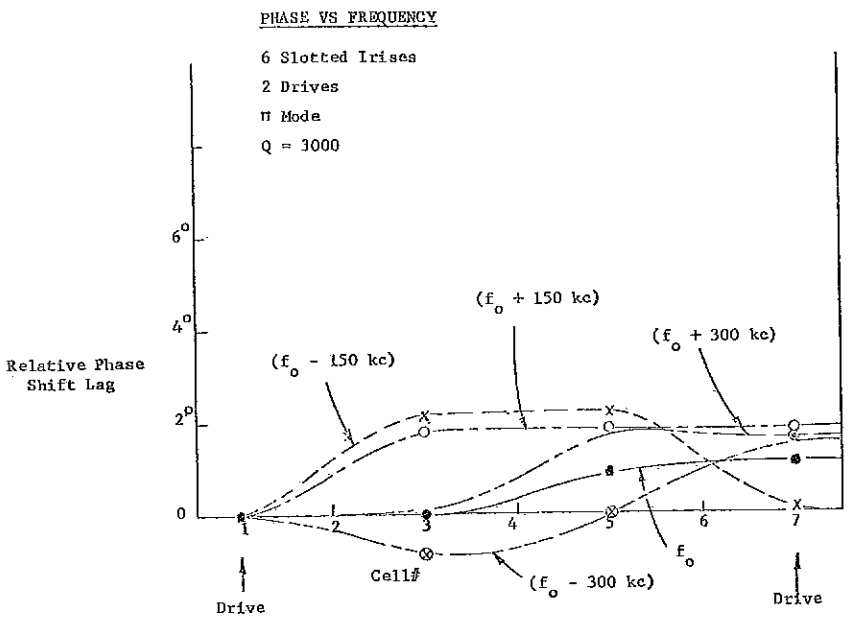
PHASE VS FREQUENCY
6 Slotted Irises
2 Drives
π Mode
Q = 3000
6^o
4^o
2^o
0
Relative Phase Shift Lag
$(f_o + 150\ kc)$
$(f_o + 300\ kc)$
$(f_o - 150\ kc)$
f_o
$(f_o - 300\ kc)$
1
2
3
4
5
6
7
Cell#
Drive
Drive

Fig. 19

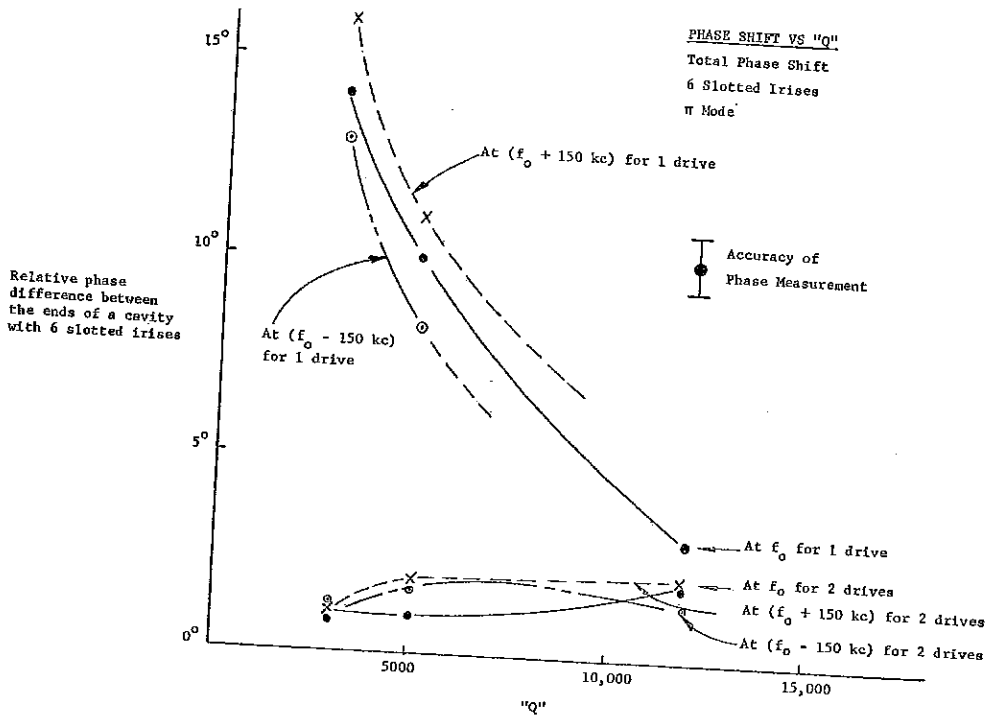
PHASE SHIFT VS "Q"
Total Phase Shift
6 Slotted Irises
π Mode
15°
10°
5°
0°
Relative phase difference between the ends of a cavity with 6 slotted irises
At (f_o + 150 kc) for 1 drive
Accuracy of Phase Measurement
At (f_o - 150 kc) for 1 drive
At f_o for 1 drive
At f_o for 2 drives
At (f_o + 150 kc) for 2 drives
At (f_o - 150 kc) for 2 drives
5000
10,000
15,000
"Q"

Fig. 20

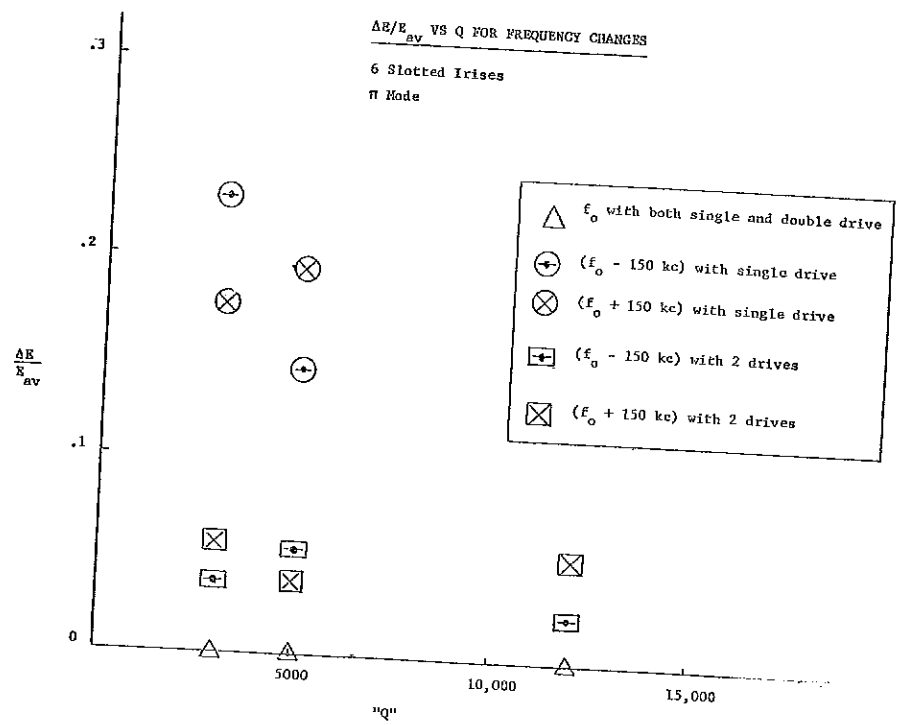
$\Delta E/E_{av}$ VS Q FOR FREQUENCY CHANGES
6 Slotted Irises
π Mode
.3
.2
.1
0
$\frac{\Delta E}{E_{av}}$
f_o with both single and double drive
(f_o - 150 kc) with single drive
(f_o + 150 kc) with single drive
(f_o - 150 kc) with 2 drives
(f_o + 150 kc) with 2 drives
5000
10,000
15,000
"Q"

Fig. 21

PARTICLE MOTIONS AND THE FOCUSING SYSTEM IN PROTON LINACS*

S. Ohnuma
Yale University

Introduction

Last year, at the conference on proton linacs, computer programs developed at Yale for particle motions and some of their preliminary results were presented.[1] Since then, there have been a number of modifications in our design parameters, particularly in the iris-loaded section. The results here are mostly based on the design parameters of the proposed 500 MeV injector for the AGS in Brookhaven which was presented by G. W. Wheeler. The computer programs are essentially the same as the one discussed in Ref. (1).

Buncher

No change has been made to the buncher which was presented last year.[2] The essential requirement here is that the beam must be tightly bunched near the synchronous point ($\Delta\varphi = \Delta\gamma = 0$). The distribution of particles from a double buncher is shown in Fig. 1. If the ion source can produce 100 mA, about 79 mA will be confined to within $\Delta\varphi = \pm 14^{o}$ and $\Delta W = \pm 20$ keV. On the other hand, there are still particles near the boundary ($\sim .5$ mA) which come out of the drift tube section with relatively large values of ($\Delta\varphi, \Delta\gamma$). For a linac of higher intensity, a bunching scheme that gives very small fraction of beams near the boundary would become important.

Drift Tube Section

Phase and transverse oscillations of particles 1 and 2 in Fig. 1 are given in Figs. 2-3 together with those of the synchronous particle. The focusing system used here is shown in Fig. 4. Two different doublet arrangements, (A) and (B), have been tried in the last two tanks to see the change in the emittance shape. In Tanks No. 1 and No. 2, the strengths of quadrupole magnets are chosen such that they correspond to optimum values for the synchronous particle. For non-synchronous particles, the optimum condition is different and the amplitude of the transverse oscillation may increase instead of damping down. (see Fig. 3.) Since the

---

* The work reported here has been done by R. Bakeman, T. W. Ludlam, J. N. Vitale and S. Ohnuma.

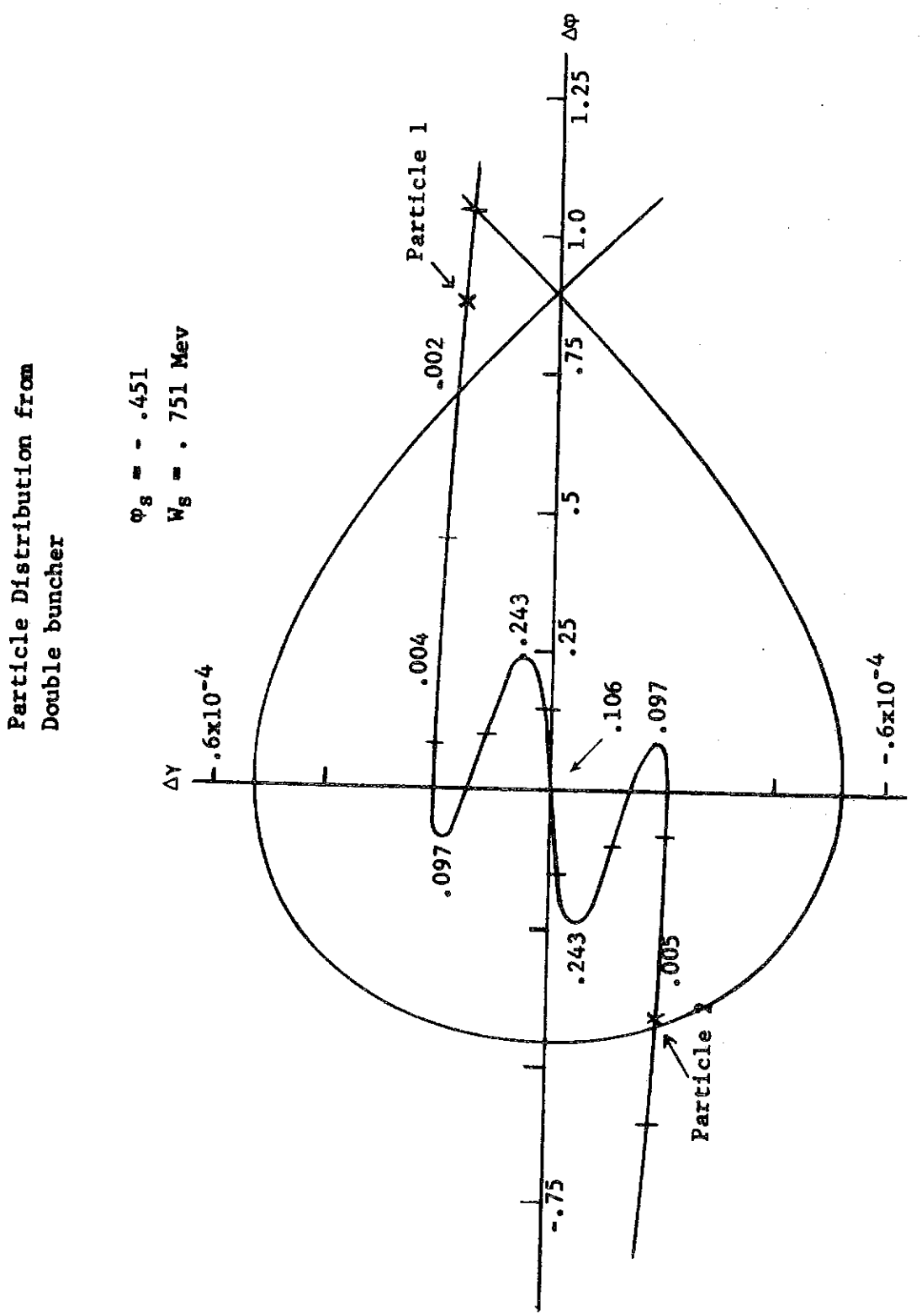
Particle Distribution from
Double buncher
φ_s = - .451
W_s = . 751 Mev
Δγ
.6x10⁻⁴
-.6x10⁻⁴
Δφ
1.25
1.0
.75
.5
.25
-.75
Particle 1
Particle 2
.002
.004
.097
.243
.106
.097
.243
.005

FIG. 1

focusing system is continuous from Tank No. 1 to Tank No. 2 with a very short drift space, no matching magnet is required. This, however, is not true between Tank No. 3 and No. 4 where the system suddenly changes. At least one set of triplet is necessary in order to achieve a near perfect matching in x- as well as y-direction. After that, the system is continuous (i.e., the change is "adiabatic") and the matching system can be eliminated entirely.

The acceptance in x - x' space of the drift tube section for the synchronous particle is shown in Fig. 5. When the smallest bore radius is .75 cm, the area is 17π cm-mrad. For most of the non-synchronous particles, the acceptance area remains fairly close to the 17π cm-mrad. but the shapes are quite different. Thus, if the input beam is matched to the shape given in Fig. 5, the effective acceptance value for particles in ($\Delta\varphi = \pm 14^{\circ}$, $\Delta\gamma = \pm 20$ keV) region is reduced to $\sim 16\pi$ cm-mrad. For particles 1 and 2, the shaded area in Fig. 5 is not acceptable and the area is less than 15π cm-mrad. It is, of course, possible to get a larger acceptance by simply taking a larger bore radius. This, however, will give a larger output bunch in ($\Delta\varphi$) - ($\Delta\gamma$) space and may cause particle loss when the frequency is increased in the high energy section. If (NNSS) configuration is used instead of (NSNS) type, the acceptance for the synchronous particle is 14π cm-mrad. The change of the acceptance shape for non-synchronous particle from that of the synchronous particle is more serious than (NSNS) configuration.

The maximum radial excursion of the beam in Tanks No. 3 - No. 7 will be substantially smaller than shown in Fig. 3 if the focusing system is (NSNS) throughout instead of doublets with gradually increasing repeat lengths taken here. The particular advantage of the doublet system will be discussed later.

It would be useful for the purpose of shielding designs to see where particles are lost radially. The location depends on the initial position of particles in x - x', y - y' and ($\Delta\varphi$) - ($\Delta\gamma$) spaces. For example, most of the particle 1 in the shaded area in Fig. 5 are lost at drift tubes No. 7, No. 9, and No. 13 of the first tank and at drift tubes No. 2 and No. 6 of the second tank, whereas the particle 2 are lost at drift tubes No. 5 and No. 7 of the first tank and No. 2 of the second tank. By assuming a particle distribution, one can calculate the distribution of lost particles along the drift tube section. However, extensive study of this problem has not been made so far. The results we have accumulated clearly indicate that the loss will be entirely in the first two tanks and most likely below $\sim$ 20 MeV.

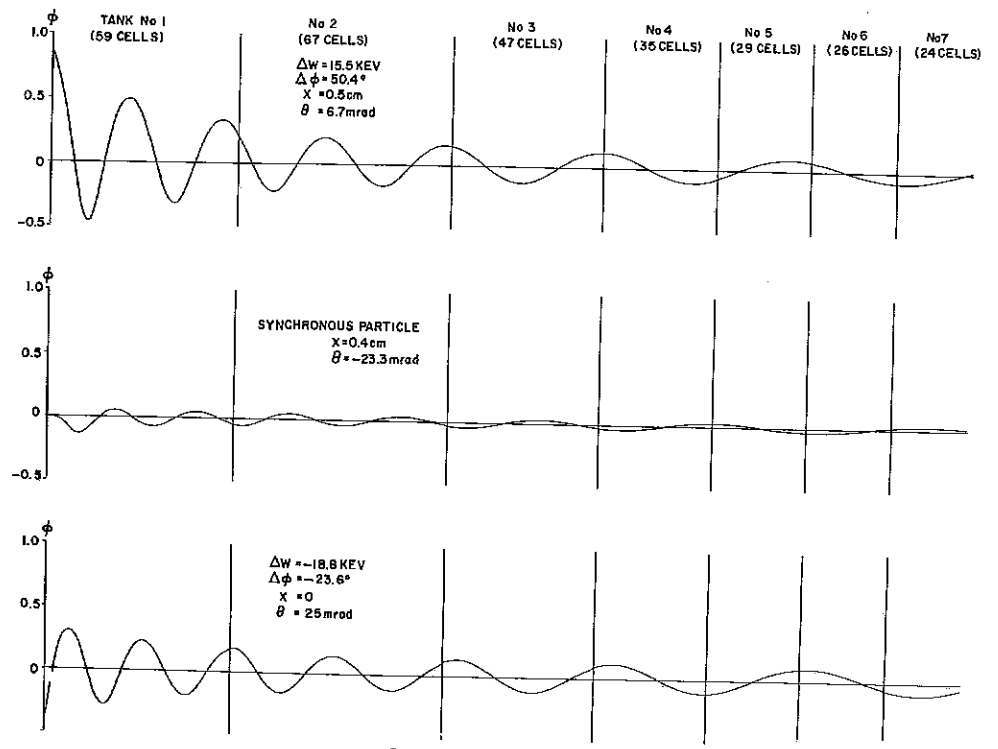
φ
TANK No 1
(59 CELLS)
No 2
(67 CELLS)
ΔW = 15.5 KEV
Δφ = 50.4°
X = 0.5 cm
θ = 6.7 mrad
No 3
(47 CELLS)
No 4
(35 CELLS)
No 5
(29 CELLS)
No 6
(26 CELLS)
No 7
(24 CELLS)
1.0
0.5
0
-0.5
SYNCHRONOUS PARTICLE
X = 0.4 cm
θ = -23.3 mrad
ΔW = -18.8 KEV
Δφ = -23.6°
X = 0
θ = 25 mrad

FIG. 2

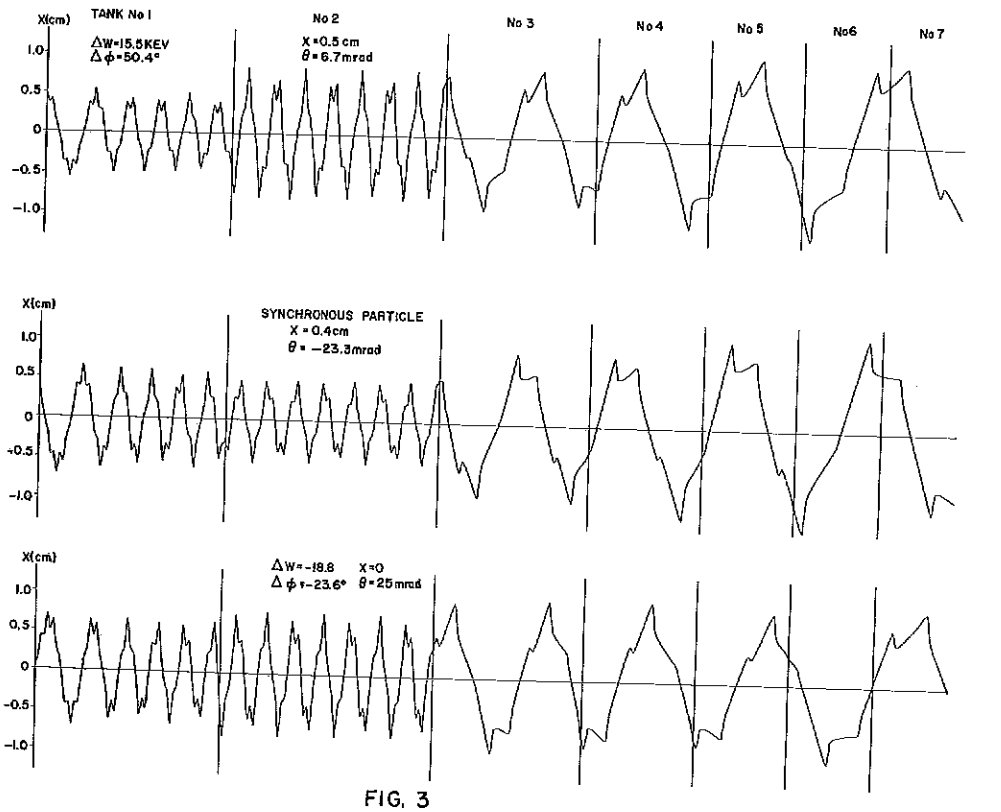
X(cm)
TANK No 1
ΔW = 15.5 KEV
Δφ = 50.4°
No 2
X = 0.5 cm
θ = 6.7 mrad
No 3
No 4
No 5
No 6
No 7
1.0
0.5
0
-0.5
-1.0
SYNCHRONOUS PARTICLE
X = 0.4 cm
θ = -23.3 mrad
ΔW = -18.8 X = 0
Δφ = -23.6° θ = 25 mrad

FIG. 3

In the $(\Delta\varphi)$ - $(\Delta\gamma)$ space, particles coming out of the drift tube section with the final energy of 187 MeV are all contained in the tilted ellipse shown in Fig. 6. Several dots are those particles with $(\Delta\varphi) \gtrsim 1.0$ or $(\Delta\varphi) \lesssim -.6$ at the injection. Since their "effective" transverse acceptance is very small ($0 - 3\pi$ cm-mrad), the total intensity of these stray particles is less than 5×10^{-5} of the main output current (i.e., the ellipse in Fig. 6). The other ellipse in Fig. 6 is the particle bunch assumed in calculating particle motions in the iris section.

Fig. 7 shows the emittance from the drift tube section in x - x' space. The area is very close to π cm-mrad. (A) and (B) correspond, respectively, to the doublet configuration (A) and (B) shown in Fig. 4.

In the low energy region ($\beta \lesssim .2$) where the rate of the change of β is large, the accuracy of the calculation is not too good. As has been already suggested previously[3], it may be necessary to integrate the equations of motion point by point. This, however, requires a detailed information on electric and magnetic fields at every point. When there is no bore hole, the fields of the shaped drift tube[4] are accurately known but the effect of the bore is difficult to evaluate. It is hoped that the calculation at MURA and at Los Alamos ("MESSY MESH")[5] will eventually give the fields with the desired accuracy.

Matching between Drift Tube and Iris Sections

It is clear from Fig. 6 that a long drift space between the two sections must be avoided in order to keep the resulting phase spread as small as possible. Although β here is large (.55), the spread could be as large as $\pm 2.6^{\circ}$/m (for $\Delta\gamma = \pm .8 \times 10^{-3}$) so that a drift space longer than $\sim$ 4m will definitely cause trouble. This is particularly serious for a linac injector of a large synchrotron where a small momentum spread ($\Delta p/p$) is essential in getting a high capture efficiency. On the other hand, it is highly desirable to have a bending magnet (to guide the beam for the energy measurement), one or two slit boxes (for measuring the beam shape in x and y-space), and one or two current transformers. If, in addition to these, two or three sets of quadrupole triplet are required to match the beam shape in both x and y-direction simultaneously, a 4m long space does not seem to be sufficient. Two schemes have been tried to solve this problem.

The first is to employ a matching scheme in the longitudinal phase space that is based on the principle of the strong focusing[6]. A tank operated at the stable synchronous phase $\varphi = \varphi_s$ acts as a "focusing lens" and a tank operated at $\varphi = -\varphi_s$ as a "defocusing lens". The drift space

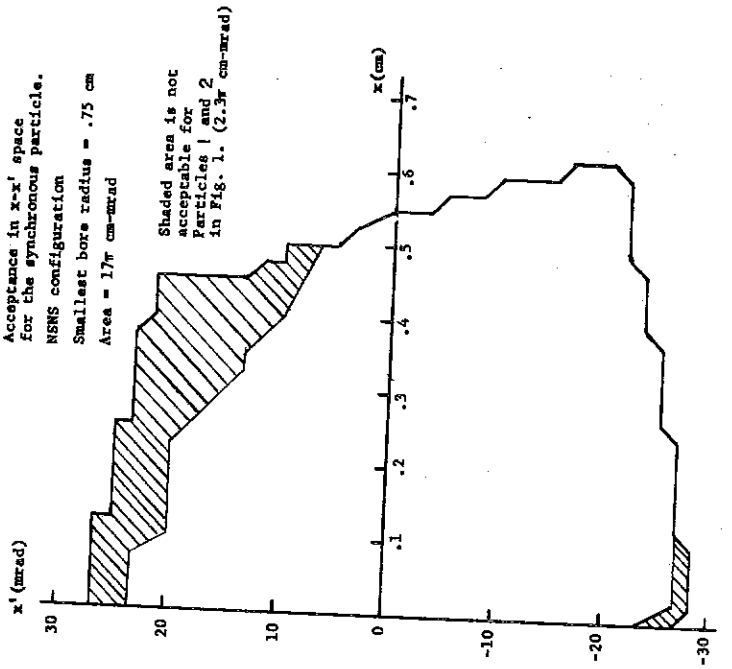
Acceptance in x-x' space
for the synchronous particle.
NSNS configuration
Smallest bore radius = .75 cm
Area = 17π cm-mrad
Shaded area is not
acceptable for
Particles 1 and 2
in Fig. 1. (2.3π cm-mrad)
x'(mrad)
x(cm)

FIG. 5

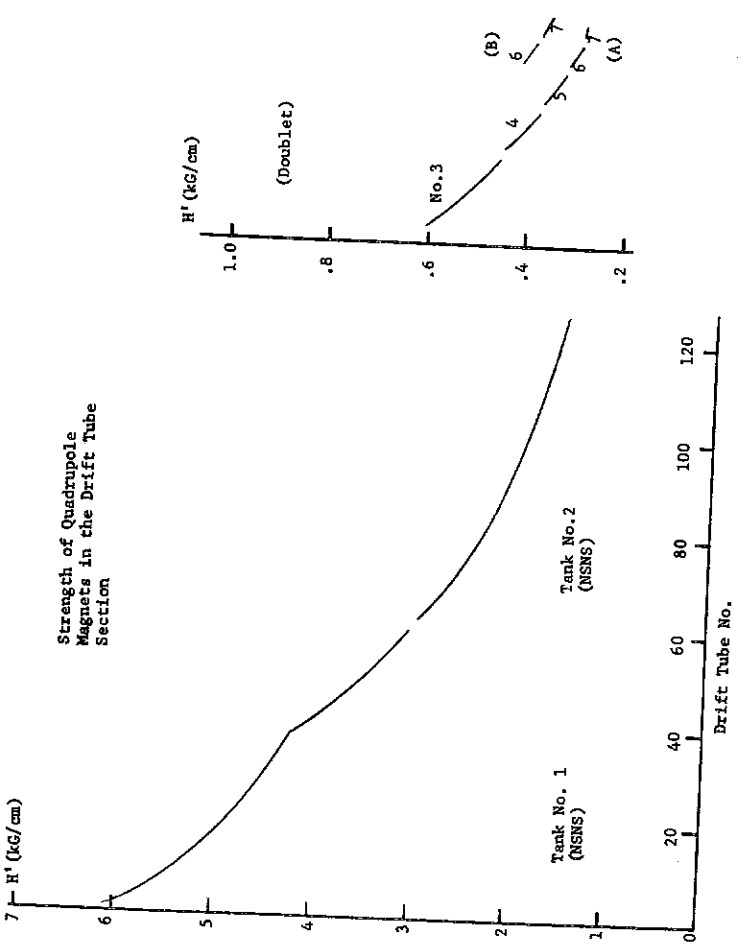
Strength of Quadrupole
Magnets in the Drift Tube
Section
H' (kG/cm)
Drift Tube No.
Tank No. 1
(NSNS)
Tank No.2
(NSNS)
(Doublet)
No.3
(A)
(B)

FIG. 4

then will be an element of the matching optical system and does not necessarily have to be short. The system will be composed of 10 – 15 regular tanks with reasonable values of rf level. Based on the linear theory, we found that we can achieve an almost 100% matching even with a 10 m drift space. However, numerical calculation has shown that the non-linear effects are so serious as to make the scheme rather impractical. It may be possible to design an elaborate system composed of very special tanks just for the matching purpose but this does not seem too easy.

The second choice is to eliminate the matching magnets for two transverse directions entirely, or use only one doublet. This means that the focusing system in the drift tube section (at least in the last two tanks or so) must be joined continuously to that in the iris section. Otherwise, one doublet or triplet cannot give a perfect matching in the both directions simultaneously. Since a doublet is used after each even-numbered tank in the iris section, one doublet just before the first tank together with a properly spaced doublet system in Tanks No. 6 and No. 7 will achieve the desirable matching. With 3.5 m space between two sections, we have found that the matching efficiency could be as large as 95% in both directions. It will be even better if two or three auxiliary magnets are placed in the last few drift tubes to make adjustments.

Iris Section

Various systems of quadrupole doublets and triplets to be used for the focusing in the high-energy section have been investigated in order to get the necessary information for the choice of multiplet type[7]. The doublet system used in the calculation and its acceptance shape are shown in Fig. 8 while the strength of magnets and the maximum (theoretical) excursions are given in Fig. 9. If the transverse phase space area is 10π cm-mrad at the injection (.75 MeV), the area at 187 MeV is $.6\pi$ cm-mrad. One advantage of doublet system is the relatively large space available between two magnets for a given drift space (1 m in this design). The maximum x or y excursion at 500 MeV is 68% of the excursion at 187 MeV. This is due to the increase of the momentum and the decrease of (Courant-Snyder) β_{max}[8]. It is, of course, possible to take longer magnet repeat lengths gradually as the energy increases. This, however, will increase the value of β_{max} and, for β_{max} (500 MeV)/ β_{max} (187 MeV) = 1.75, the maximum excursion stays constant. If, on the other hand, the focusing system is changed at some points, some kind of matching device will be required.

A good matching at the entrance is essential in achieving the smallest possible x_{max} or y_{max}. Different systems require different acceptance shapes so that a particular point in x-x' space leads to an entirely different maximum excursion. In connection with the matching, a device that can

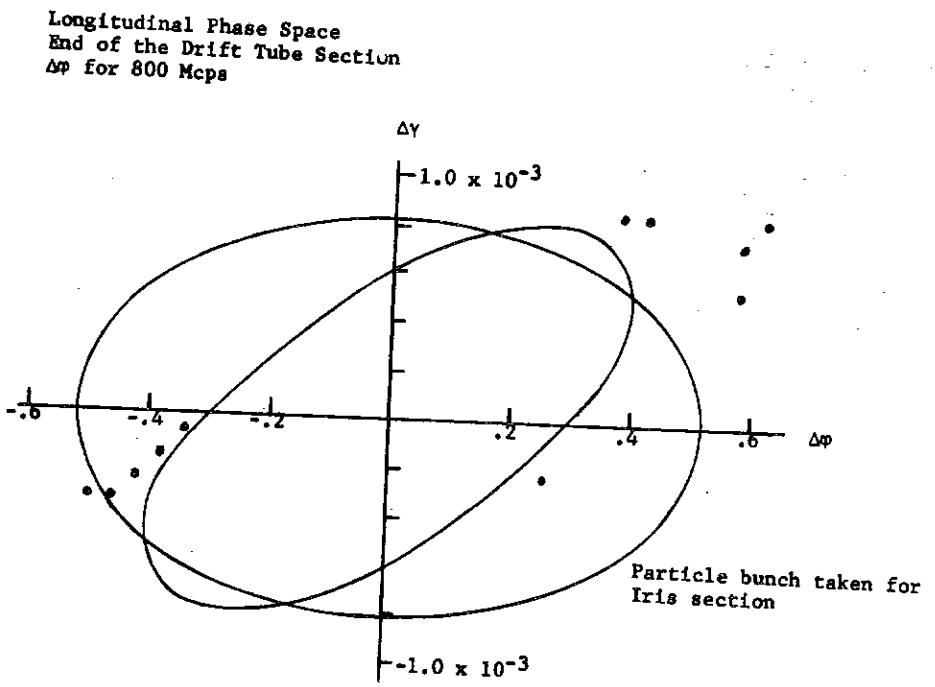
Longitudinal Phase Space
End of the Drift Tube Section
Δφ for 800 Mcps
Δγ
1.0 x 10⁻³
-1.0 x 10⁻³
-.6
-.4
-.2
.2
.4
.6
Δφ
Particle bunch taken for
Iris section

FIG. 6

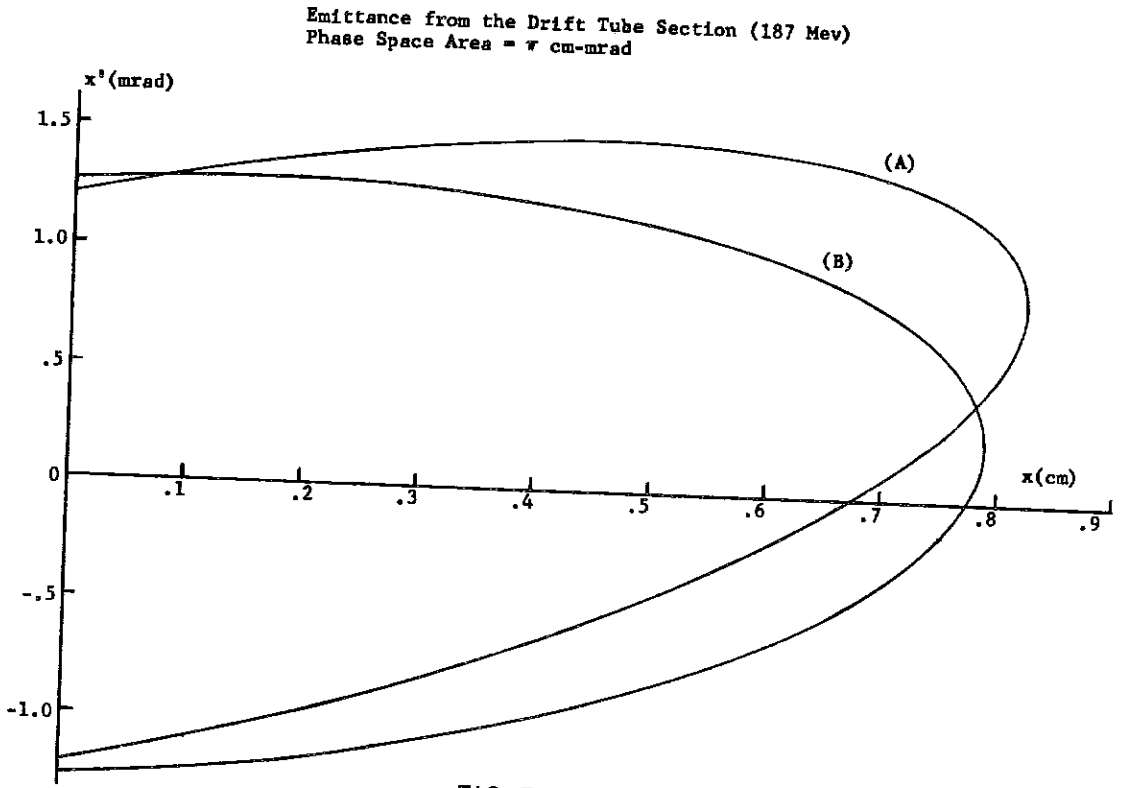
Emittance from the Drift Tube Section (187 Mev)
Phase Space Area = π cm-mrad
x'(mrad)
1.5
1.0
.5
0
-.5
-1.0
(A)
(B)
.1
.2
.3
.4
.5
.6
.7
.8
.9
x(cm)

FIG. 7

accurately measure the beam shape in x-x' and y-y' space will be extremely useful.

The theoretical maximum excursions in Fig. 9 are computed for synchronous particles. For non-synchronous particles, the acceptance shape is slightly different from those given in Fig. 8. This slight mismatching would, in general, give larger excursions for non-synchronous particles. The largest deviation recorded from the theoretical value is .25 cm. Of course, only those particles which are near the boundary of the acceptance ellipse in Fig. 8 deviate from the theoretical maximum excursion. For example, particles within an ellipse of size $.63\pi$ cm-mrad in x-x' space are not lost if, in $(\Delta \varphi) - (\Delta \gamma)$ space, they are inside of the (larger) ellipse in Fig. 6. On the other hand, it seems very difficult to keep the iris aperture smaller than 1 cm (radius) and still not lose particles. One obvious solution would be shorter tanks at the beginning to reduce the magnet repeat length. Since a smaller iris aperture gives a smaller power loss for the same structure, further studies of this point may be called for in the future.

The choice of the doublet arrangement instead of a triplet was made because of the better over-all quality in focusing the high energy beam.[7] Triplet arrangements (+) (-) (+) (rf tanks) (+) (-) (+) are not symmetric in x and y directions so that the best operating point in one direction is very close to the stability boundary in another direction. This situation is shown in Fig. 10(*) where g_s is related to H' by

$$H' \text{ (kG/cm)} = .313\ (\gamma\beta)\ g_s^2$$

and the parameter Ω for each curve is

$$\Omega = \left[\frac{\pi\, eE_o \sin|\varphi|}{m_p c^2 \lambda\ (\gamma\beta)^3} \right]^{1/2} \quad ; \quad \frac{d\gamma}{dz} = \frac{eE_o}{m_p c^2} \cos\varphi$$

Symmetric arrangements (+) (-) (+) (rf tanks) (-) (+) (-) give a very narrow stability range with large values of β_{max} as can be seen from Fig. 11(*). There is a possibility of using an upper stability region

---

(*) Figs. 10 and 11 are taken from Ref. (7). Tank length is 2.5 m instead of 3 m here and β_{max} is slightly smaller than for 3 m tanks.

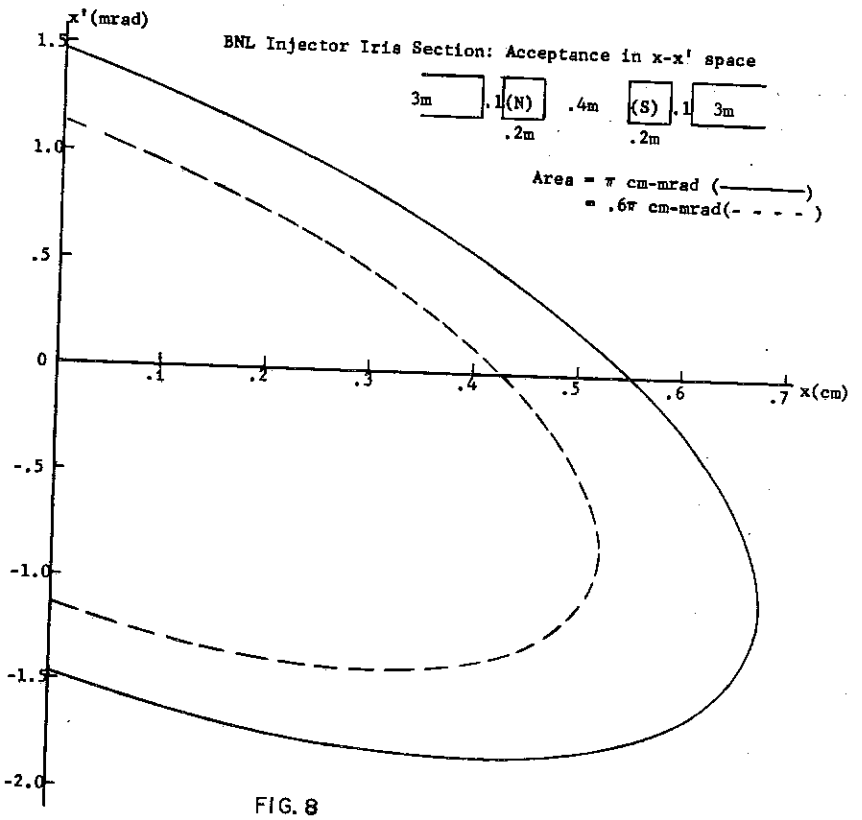
x'(mrad)
BNL Injector Iris Section: Acceptance in x-x' space
3m
.1
(N)
.2m
.4m
(S)
.2m
.1
3m
Area = π cm-mrad (———)
= .6π cm-mrad(- - - -)
1.5
1.0
.5
0
-.5
-1.0
-1.5
-2.0
.1
.2
.3
.4
.5
.6
.7
x(cm)

FIG. 8

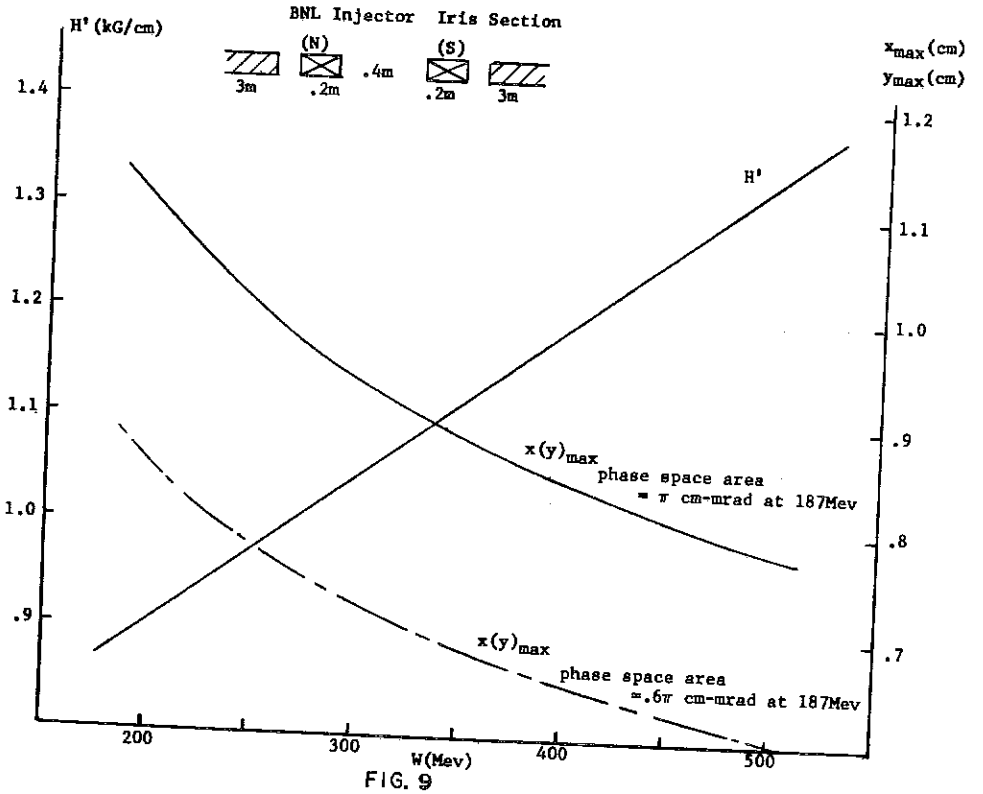
H'(kG/cm)
BNL Injector Iris Section
3m
(N)
.2m
.4m
(S)
.2m
3m
x_{max}(cm)
y_{max}(cm)
1.4
1.3
1.2
1.1
1.0
.9
1.2
1.1
1.0
.9
.8
.7
H'
$x(y)_{max}$
phase space area
= π cm-mrad at 187Mev
$x(y)_{max}$
phase space area
=.6π cm-mrad at 187Mev
200
300
400
500
W(Mev)

FIG. 9

where β_{max} are much smaller. However, aside from large magnetic fields required in the high energy region, non-synchronous particles may spend some time near the stability boundary or even cross the boundary into the stopband and get a large radial excursion. Unless an extensive numerical calculation is done, it does not seem safe to design the focusing system operating in upper stability regions.

The only remaining question is whether tolerance requirements for doublets are too difficult to achieve in the proton linac, as they appear to be in the Stanford two-mile electron linac[9], so that one is forced to take triplets. This has also been investigated in a semi-analytic fashion in Ref. (7). The method used there is outlined by R. L. Gluckstern.[10] As has been discussed in Ref. (9) and Ref. (10), the advantage of triplets is the possibility of "bench alignment" which makes the effect of magnet displacements entirely negligible (maximum tolerances are order of 100 mils). For doublets, bench alignment offers no improvement as far as the tolerance of "skew" (rotation about transverse axes) is concerned. On the other hand, it does not seem at all difficult to achieve the required tolerances for doublets (as well as for triplets) with the help of aligning monuments.[10] [11] A computer program has also been used to check the validity of the semi-analytic results. All together 50 random sets of misaligned doublets have been investigated at 400 MeV, 580 MeV, and 750 MeV. The displacements in x and y direction (individually) are larger than the analytic results in 5 cases at 400 MeV, 7 cases at 580 MeV, and 2 cases at 750 MeV. However, the radial displacements

$$(\sqrt{x^2 + y^2})$$

are always smaller than the expected values. Since these 50 runs are performed for a particular particle, we will have to repeat the similar calculation for many different particles. Nevertheless, we feel that the tolerance requirements for doublets are not too stringent to achieve.

Loss of Particles due to Failures of rf Tanks and Focusing Magnets[12]

The computer program for particle motions in the iris section can be used to find out whether the loss of particles is, in general, localized or extended over a long distance when certain tanks or a pair of focusing magnets fail.

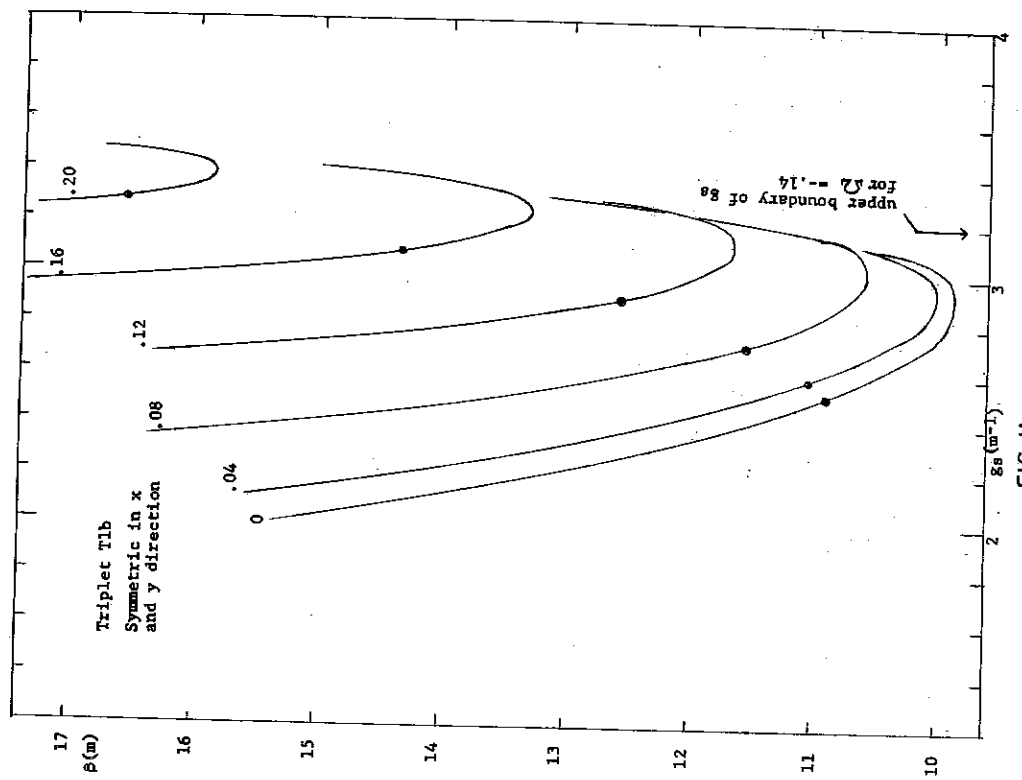
Triplet T1b
Symmetric in x
and y direction
upper boundary of β_s
for Δ_2 = -.14
0
.04
.08
.12
.16
.20
β(m)
g_s(m^{-1})

FIG. 11

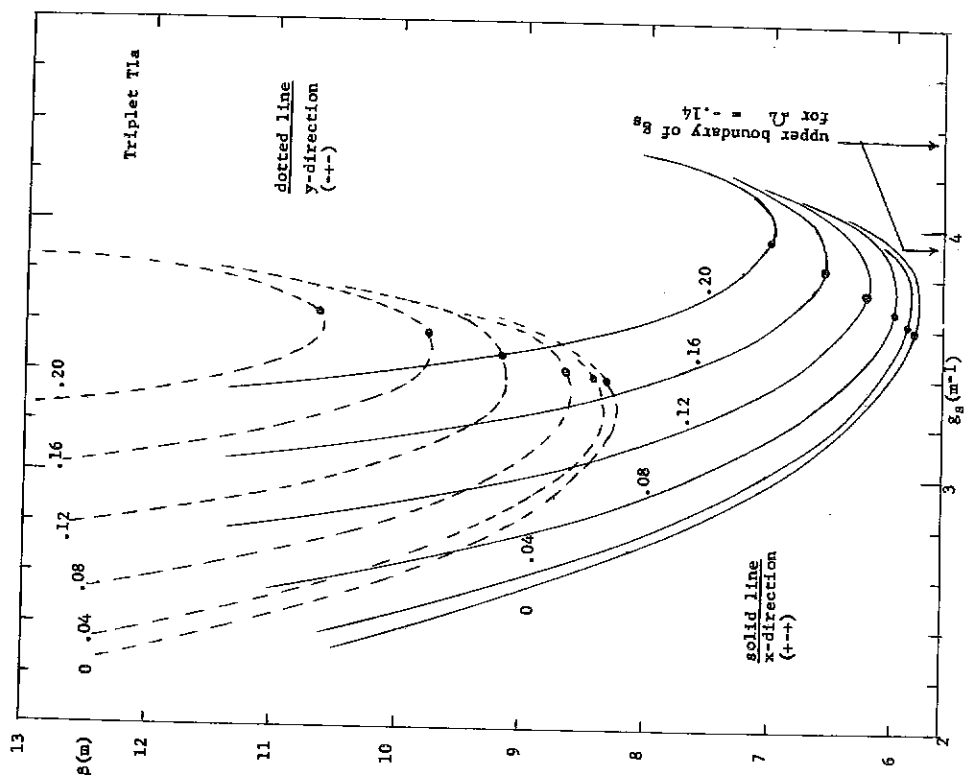
Triplet T1a
dotted line
y-direction
(+-)
upper boundary of β_s
for Δ_2 = -.14
solid line
x-direction
(+-+)
0
.04
.08
.12
.16
.20
β(m)
g_s(m^{-1})

FIG. 10

If an amplifier tube fails, two consecutive tanks will be de-excited and there will be no increase in particle energy. The energy gain through two tanks are, in general, greater than the size of the "fish" (in $\Delta\gamma$ direction) so that all particles will become longitudinally unstable after passing de-excited tanks. The energy of such particles fluctuates around a certain value that is very close to what they had just before becoming unstable. For all practical purposes, the problem is then reduced to the transportation of particles with a constant momentum (in z direction) through a focusing system that is optimized for particles with increasing momenta. This means that we can predict where particles will be lost from the stability diagram of the focusing system. A detailed numerical calculation has confirmed this but it has also shown that particles are lost in a relatively long area ($\sim$ 100 m). Particles with 400 MeV or more energy are not expected to be lost at all. It is not possible to retain the bunch inside the longitudinal stability region by simply increasing the rf level in nearby tanks[13].

Since two quadrupole magnets will be getting power from the same source, the problem in case of magnet failures is to find the increase of the transverse amplitudes (A_x, A_y) when one pair of doublet is missing. At the "optical" centers, (x, x') and (y, y') will satisfy

$$x^2 + \beta_{max}\, x'^2 = A_x^2 \; ; \; y^2 + \beta_{max}^2\, y'^2 = A_y^2$$

with $\quad A_x \leq \sqrt{\beta_{max} W_x} \quad , \quad A_y \leq \sqrt{\beta_{max} W_y}$.

W_x and W_y are the phase space area divided by π in x and y direction, respectively. Because of the missing pair, these ellipses will be distorted to other forms (without changing the size):

$$ax^2 + bx'^2 + 2hxx' = 1 \quad , \quad a'y^2 + b'y'^2 + 2h'yy' = 1$$

where $1/\sqrt{ab-h^2} = A_x^2/\beta_{max}$ and $1/\sqrt{a'b' - h'^2} = A_y^2/\beta_{max}$.

If these distorted ellipses are entirely inside the ellipse

$$x^2 + \beta_{max}\, x'^2 = R^2 \text{ or } y^2 + \beta_{max}^2\, y'^2 = R^2$$

with R = quadrupole aperture, there will be no loss of particles. For R = 2 cm and $A_x = A_y = 1.5$ cm, the fractional loss in both x and y directions changes from 30% at 200 MeV to 20% at 500 – 700 MeV. For R = 1.5 cm and $A_x = A_y = 1.0$ cm, corresponding figures are 40% and 30%, respectively. The important feature here is that most of these particles are lost in a relatively localized region ($\sim$ 15 m) because they can travel the distance which is at most one-half of the transverse wave length (29m) before getting the maximum excursions. Again it is not possible to adjust the strength of adjacent doublets (*) such that the loss would be decreased substantially. Preliminary results of numerical calculations show the recovery of only 5% or less at all energies.

VISSCHER: What is the radius of the aperture in your iris section calculations?

OHNUMA: The aperture radius really does not affect the calculation. It simply gives a criterion when you are concerned about the beam loss. Theoretically, the size of the beam would be about 1.5 cm or less. In calculating the misalignment effects, we used 2 cm radius.

VISSCHER: The value π cm-mrad of the transverse phase-space area you are using must have been based on some aperture radius.

OHNUMA: No. That is what we get out of the drift tube section independent of the iris section. The acceptance of the iris section is of course much larger. The calculation is a continuous one for both sections.

LAPOSTOLLE: About the possibility of a correction of the missing gap and drift spaces between tanks, especially in the Alvarez section, I think that, for transverse motions, it is possible to compensate with a slight correction of the quadrupole magnets. I wonder whether, for the longitudinal motion, it would not be possible also to compensate by a slight displacement of the accelerating gaps in order to change the phase when the bunch crosses the gap and modify the phase-focusing condition. Did you think about the idea of trying to compensate for any disturbance due to spaces between tanks, possibly by some modification at the end of the tank?

(*) Here it is assumed that the strength of two magnets of a doublet can be changed only simultaneously.

OHNUMA: We have not studied this problem in any detail in the Alvarez section. I believe that in the actual operation one must always make fine adjustments of the focusing magnets. As to the compensation for the longitudinal motion, it seems very difficult to adjust unless we can accurately measure the position of the bunch relative to the rf field in tanks. In the iris section, unless you change the strength of each magnet independently, even the transverse adjustment is not easy. You must remember that each doublet is 7 m apart. If one tank is out of operation, the bunch is completely out of the longitudinal stability region and there is no way of recovering it into the bucket. Of course, the focusing system still could transport this low energy beam down to the end without any beam loss. It depends on the energy acceptance of your focusing system.

KNAPP: You have two drift tubes close to one another that have magnets in them and then you have a large series of drift tubes with no magnet in them. Could you describe the distribution of magnets in the last four tanks of the Alvarez section?

OHNUMA: In Tank No. 3, there are 14 pairs for 46 full drift tubes; in No. 4, 6 pairs for 34; in No. 5, 4 pairs for 28; in No. 6, 3 pairs for 25; in No. 7, 3 pairs for 23 full drift tubes. The distance between the center of a focusing magnet to the next one, the magnet repeat length, ranges from 0.89 m to 7.3 m. The value of β_{max} changes gradually from 1.45 m to 12.5 m.

TENG: About the longitudinal phase space matching between the drift tube section and the iris section, have you considered the use of dispersive magnets? The distortion of the bunch in the longitudinal phase space due to the drift space can be compensated by such magnets.

OHNUMA: No, we have not thought about it. I don't know how wise it is to construct a special section or system just for this particular purpose. If we can use some regular sections as an option, it will be all right. Besides, such a system would require additional transverse matching systems and might not be desirable to have for the overall matching purpose.

TENG: You might have to bend the beam so that the drift tube section and the iris section are at an angle to one another. As far as the transverse phase space matching is concerned, you can always do that by a number of quadrupole magnets.

WHEELER: The figure of 10 m, which we have been using, was a somewhat arbitrary number which would allow us to have ample space between the sections. We have not looked carefully at how far down we can bring

this distance. I expect that it can be brought down quite a lot further, far enough so that it will satisfy beam dynamics requirements.

LEISS: Isn't it true of course that the reason for a short distance is removed if you do put a phase compression system such as Teng was talking about?

WHEELER: Yes, but I would rather try for a shorter distance than to try to put in a major magnet system which would be expensive, because of a longer tunnel length and require additional complex equipment and be consuming in manpower.

WALKINSHAW: Have you looked at the possible advantages of coming down in frequency to 600 Mc or even to 400 Mc where, I think, this problem would be less serious?

WHEELER: It would be nice to come down to 600 or 400 Mc for the purpose of solving this problem but the cost is going up proportionately. I think we are caught here in an attempt to keep the cost down but still meet the dynamics requirements. Based on our numerical calculations, we feel that we can operate at 800 Mc.

REFERENCES

1. Ohnuma, S., Minutes of the Conference on Proton Linear Accelerators at Yale University, October 1963, p. 14.

2. Ohnuma, S., ibid., p. 273.

3. Comment by R. Beringer in Ref. 1 above.

4. Gluckstern, R. L., Internal Reports Y-1 and Y-4, April and September, 1961, Yale University.

5. For example, see Edwards, T. W., MURA Report No. 622, June 15, 1961.

6. Teng, L. C., 1961 International Conference on High Energy Accelerators, Brookhaven National Laboratory, September 6-12, 1961, p. 212.

7. Ohnuma, S., Internal Report Y-10, March 1964, Yale University.

8. Courant, E. D., and Snyder, H. S., Annals of Physics, 3, 1 (1958).

9. Helm, R. H., Technical Report SLAC-15, March 1963, Stanford Linear Accelerator Center.

10. Gluckstern, R. L., Internal Report Y-7, January 24, 1964, Yale University.

11. Courant, E. D., Internal Report IA-3, EDC-43 (1961), Brookhaven National Laboratory.

12. Ohnuma, S., Technical Note S0-5, April 14, 1964, Accelerator Design Study, Yale University.

13. Wheeler, G. W., and Ludlam, T. W., Minutes of the Conference on Proton Linear Accelerators at Yale University, October 1963, p. 29.

NUMERICAL STUDY OF PARTICLE DYNAMICS IN A HIGH-ENERGY PROTON LINEAR ACCELERATOR*

M. Jakobson** and W. M. Visscher
Los Alamos Scientific Laboratory, University of California
Los Alamos, New Mexico

I. Introduction

We report here on the current status of a beam-dynamical calculation which has been evolving at Los Alamos for nearly a year. This paper should be considered as an addendum to and partial summary of a Los Alamos internal memo[1] which was written at the end of April. That report is considerably more complete and detailed than this one; we shall emphasize here the improvements and extensions which have been made since then.

At that time, most of our calculations had been made for a fictitious accelerator with plane symmetry, although some had utilized cylindrical symmetry in the accelerator sections with the beam constrained to move in only one of the transverse planes. Plane symmetry exaggerates the transverse defocusing and radial-phase coupling by a factor of two over the cylindrical case; it was therefore thought that conclusions valid for the plane problem would be pessimistic ones to apply to the cylindrical case. Our subsequent experience with the latter has borne this out.

The principal advance which has been made since our earlier report is the incorporation into the computer code of the other transverse dimension enabling us to calculate the real three-dimensional orbits of the protons as contrasted to 2 or 2-1/2 dimensions before. By 2-1/2 dimensions we mean three-dimensional fields with orbits constrained to two dimensions. We now take proper account of such things as x-y interaction and the effects of random rotations of the quads about the longitudinal axis. The addition of the third dimension has, unfortunately, nearly doubled the running time on the computer, but machine time has not been a serious problem as yet.

Another change which has been made is in the part of the code which designs the accelerator sections. Instead of designing them with a constant rf gradient, as before, we now design them with a constant power

*Work performed under the auspices of the U. S. Atomic Energy Commission.

**Permanent address: Department of Physics, Montana State University, Missoula, Montana.

consumption, for an obvious practical reason. The number of cells per section is, as before, a constant.

II. Method

We give here only a very sketchy description of the method used in the calculation; the interested reader can find much more detail in reference 1.

The π-mode rf field effective in accelerating the beam is assumed to be only that standing wave made up of components which have phase velocities equal to $\pm$ the synchronous particle velocity, and the impulse received by each particle in crossing a cell is approximated by that received by a particle moving across the cell in a straight line parallel the axis at constant speed. We call this the impulse approximation. The justification for these procedures is discussed in reference 1, and seems to be quite solid for the proton energies with which we are concerned.

The longitudinal and radial impulses calculated in this way are

$$I_z = \frac{\pi E_0}{2\omega} I_0(\kappa r)\cos\varphi \qquad (1)$$

$$I_r = -\frac{\pi E_0}{2\omega} I_1(\kappa r)\sin\varphi ,$$

where I_0 and I_1 are Bessel functions of imaginary argument, E_0 is the maximum amplitude of the synchronous component of the rf field, $\kappa = \pi/L\gamma$, and φ is the phase of the proton entering the gap relative to the time at which the E field is a maximum. Our convention is to take the synchronous phase negative; thus Eqs. (1) predict a radial defocusing of the synchronous particle as is required by Earnshaw's theorem.

The acceleration received by each particle in each cell is computed by Eqs. (1), and the bunch is thus transported to the end of the section. At this point it enters a magnetic quadrupole lens system, which can be a singlet, doublet, or triplet. On the assumption that the transverse velocity is small compared to the longitudinal velocity, the x and v_x coordinates of a particle, on passing through a quad, are changed to

$$x' = \frac{v_x}{\Omega}\begin{matrix}\sin\\ \sinh\end{matrix}(\Omega t) + x\begin{matrix}\cos\\ \cosh\end{matrix}(\Omega t) \qquad (2)$$

$$v_x' = v_x\begin{matrix}\cos\\ \cosh\end{matrix}(\Omega t) \mp \Omega x\begin{matrix}\sin\\ \sinh\end{matrix}(\Omega t) ,$$

where t is the time spent in the quad, and the upper (lower) signs and symbols refer to a focusing (defocusing) magnet. Similar equations are obtained for y' and v_y', with the upper and lower signs and symbols interchanged. Ω is the natural transverse oscillation frequency of a particle passing through the magnet, and is given by

$$(\Omega/\omega)^2 = 3.22 \left(\frac{\lambda}{2\pi}\right)^2 \frac{v_z}{\gamma c} H' \text{ (kilogauss/cm)} \qquad (3)$$

for protons.

The bunch is transported through the quadrupoles by Eqs. (2), and allowed to drift through any drift spaces which may be present. Then the computer designs the next section and the process is repeated.

III. Calculations

Perhaps the most efficient way to explain the features of the code is to display the input parameters and the form of the output graphs. Figure 2 shows the input parameters for the current version of our 7094 Fortran code. This problem simulates an accelerator of 50 sections, each 40 cells long, separated by magnet systems of length equal to 4 cell lengths. The magnet systems can be singlet, doublet, or triplet; the 4 cell lengths include the internal drift spaces for the doublet and the triplet. As is illustrated in Fig. 1, this setup allows no space between the sections and the lens system for installation of plumbing or probes; we therefore have made provision for some extra drift space before the beginning of the magnet system. This extra drift space input also allows study of the effect of the necessary gap in the accelerator at the frequency transition point, and of a gap for a possible intermediate energy station.

The magnet systems have length proportional to β (line 1); but the quads themselves are, say 10 cm (line 5) long for the whole length of the machine. It takes two quads to make a doublet; four (10-20-10 cm) to make a triplet. This means that the effective strength of the lens increases with the energy if the quad strength stays constant. Line 5 and line 6 of Fig. 2 contain the rest of the focusing system parameters, contained in

$$H' = H_0' \, (1 + c\,E^n)/(1 + c\,E_0^n) \, . \qquad (4)$$

c in Eq. (4) is the "quad coefficient", the synchronous energy E is raised to the "quad exponent" n, and H_0' is the field gradient (in kG/cm) of the quads at the beginning of the machine. We have not made an exhaustive study of variations in c and n; what we have done, however, indicates that the optimum is near c = n = 0.

In the 7th line are two remaining parameters which complete the description of the focusing system. The orientation of the first quad encountered by the beam is specified by saying whether it is converging or diverging in x. The repeat length is the periodicity of the lens system. For example, a doublet system with 4 section repeat length would be, schematically,

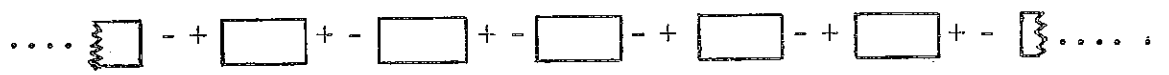

A repeat length between 6 and 12 sections seems best for triplets, and an infinite repeat length does well for doublets. Short repeat lengths give rise to unstable intervals in the stable range of quad strength.

More parameters to determine the geometry are in line 3 of Fig. 2. Synchronous input energy and design phase are self-explanatory. Phase shift and design beam load are numbers which describe the energy flow along the section, from cell to cell. We refer to reference 1 for discussion of them; here we only say that these and other effects which cause variation in phase velocity of the rf in time and position seem to cause no serious trouble. We have studied machines with constant cell length within a section, rather than phase velocity = "synchronous" particle velocity everywhere, which is what the code usually requires. Constant cell length has no noticeable deleterious effect for 40 cells per section; for much longer sections, however, it reduces the phase acceptance.

The hole radius has no effect on the fields, since we use only the lowest Fourier component; its only function is to provide criterion for deciding whether a given proton is still in the machine. We throw out particles when their radii exceed R_o, and only then. Particles often spill out of the phase-energy bucket and stay in the machine to the end due to the action of the quads. Our results indicate, in fact, that the rf can be turned off in a couple of sections near the start, resulting in the loss of the entire beam from the bucket, but the entire beam will be transported to the target. Also, the rf can be turned off entirely beginning at any point and the beam will coast out, or a few sections can be run with reversed rf and all subsequent ones with rf off. In this latter case a 600 MeV beam, say, can be made to come out at the 800 MeV end of the machine with the microstructure wholly debunched and a spread of 20 MeV. The drift length is shorter if a higher energy spread is allowable, and vice versa. Thus a variable energy machine could be designed with a maximum energy of 800 MeV (no debunching) and a completely debunched beam available from 700 MeV on down. Reference 1 contains a more quantitative discussion of this point.

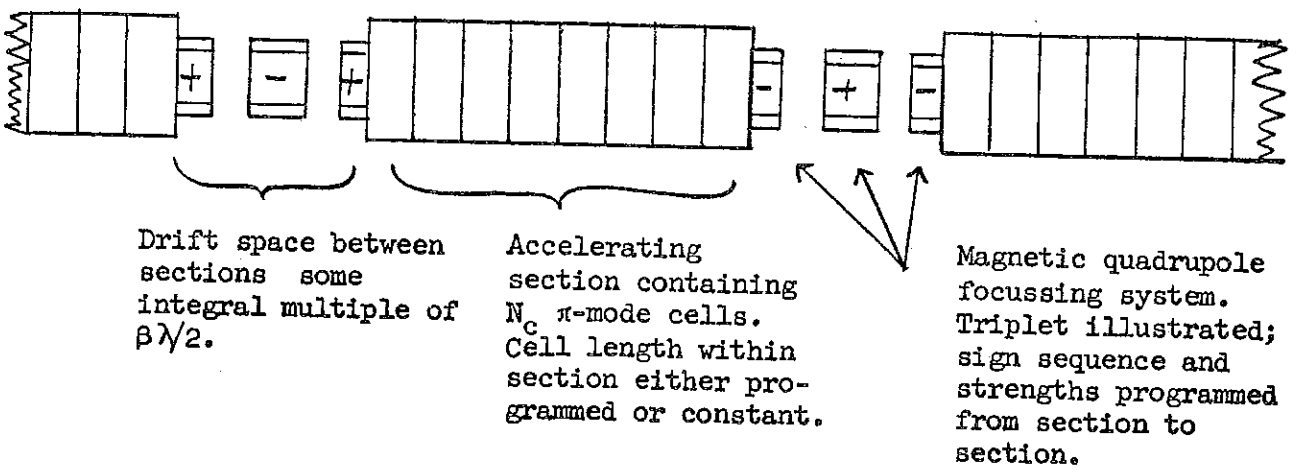

Figure 1. Schematic diagram of accelerator structure.

50 SECTIONS 40 CELLS PER SECTION 200 PROTONS IN BUNCH MAGNET SYSTEMS 4 CELLS LONG

DRIFT SPACE OF LENGTH 2 CELL LENGTHS AFTER THE 100TH SECTION REPEATED EVERY 1TH SECTION

INPUT ENERGY= 1.765E 02 DESIGN PHASE= -3.000E 01 PHASE SHIFT= 0. DESIGN BEAM LOAD= -0.

HOLE RADIUS= 2.000E-02 SECTION POWER= 5.000E-01 RANDOM START AT 1.900E 01

INITIAL QUAD GRADIENT= 3.000E 00 QUAD LENGTH= 1.000E-01 FREE SPACE WAVELENGTH= 3.750E-01

QUAD COEFFICIENT= -0. QUAD EXPONENT= -0

TRIPLET LENS SYSTEMS FIRST QUAD DIVERGING IN X 12 SECTION REPEAT LENGTH

SECTIONWISE AMPLITUDE ERROR= -0. CELLWISE AMPLITUDE ERROR= -0. SECTIONWISE PHASE ERROR= -0.

QUAD FIELD ERROR= -0. QUAD DISPLACEMENT= 10.000E-04 SECTION TWIST= -0. QUAD ROTATION= -0.

RF AMPLITUDE MULTIPLIED BY 0. FOR 0 SECTIONS STARTING WITH NUMBER 100

ENERGY LIMITS 1.765E 02, 1.765E 02 PHASE LIMITS -6.000E 01, 3.000E 01

X LIMITS -2.000E-02, 2.000E-02 Y LIMITS -2.000E-02, 2.000E-02

VR LIMITS -4.000E-03, 2.000E-03 VTH LIMITS -0, , -0.

Figure 2. Input Parameters for Computer Code.

Section power (megawatts) is in the input because rf gradient isn't. The sections are designed to consume a given amount of power with a 20 mA proton current and a ZT^2 given by an empirical formula for the cloverleaf structure (Knapp, LASL)

$$ZT^2 = 65\,\beta/(\beta + 0.76)\ \mathrm{M\Omega/m}\,. \tag{5}$$

We chose 1/2 Megawatt as the section power because the power supplies envisioned at LASL will deliver $\sim$ 1 Megawatt and splitting between two sections is feasible and will give sections of reasonable lengths and rf gradient; namely, 40 cells (4 meters up to 6 meters at 800 MeV) and 1.35 at 175 down to 1.20 MV/m synchronous particle energy gain at 800 MeV. The code designs each section with a synchronous phase velocity and converges on a given section power iteratively.

Random start has nothing to do with the machine or beam dynamics; it merely tells where to start reading the random number table. Random numbers are used for generating the seven "standard" kinds of random errors (uniformly distributed) listed in lines 8 and 9 (we have studied the effects of a number of other errors, besides those listed here), and also for generating the proton bunch. The bunch parameters are those in the last 3 lines of Fig. 2. It is characterized by upper and lower energy limits, phase limits, x and y, v_r and v_θ limits. All the particle coordinates but phase are chosen by the random number generator.

IV. Results

Our code should be able to given an answer to the question, "Are doublets or triplets better at focusing the beam in the high-energy linac?" The answer, we think, is that triplets are. Triplets give an acceptance zone in transverse phase space about 50% bigger than doublets in the example shown on Fig. 3. π milliradian-cm corresponds to the area of the small rectangle; we see therefore that either doublets or triplets are easily capable of accepting the transverse output thought to emanate from the drift tube section. Random errors of 1 mm in displacement of the lens system parallel to the axis cut the acceptance area by about 30% for each case, Radial beam confinement as reflected by the rms radii for the bunch seems about the same for triplets as for doublets; this is shown for triplets on the bottom curve on Fig. 4. Our tentative conclusion is that on the basis of simplicity and lower cost, doublets are preferable, unless doublet tilt or independent quad alignment tolerances prove to be excessively stringent, or very large transverse acceptance turns out to be necessary.

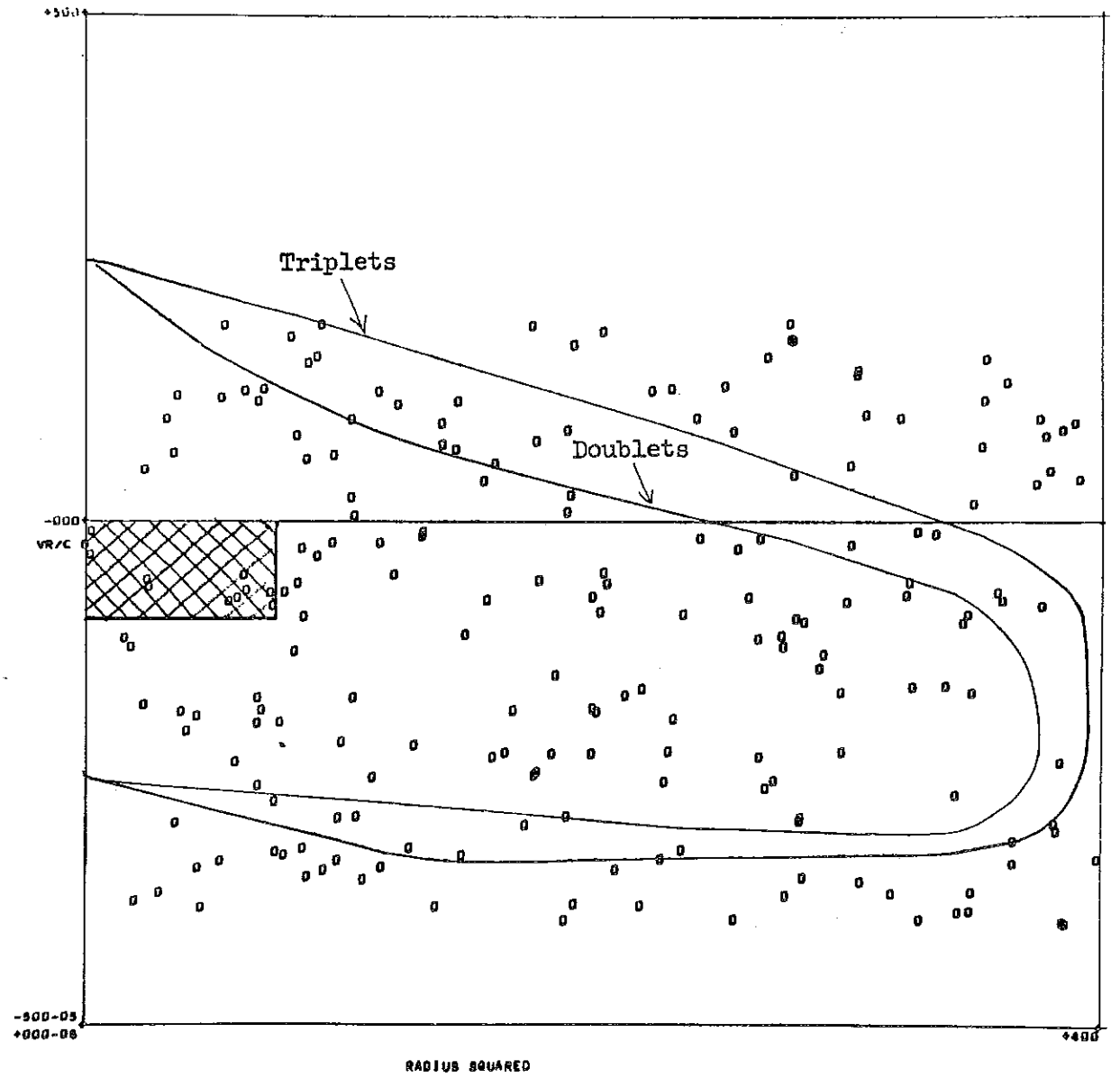

Fig. 3: Approximate acceptance envelopes in transverse sphase space for doublet and triplet focussing systems, both without errors. Crossbatched rectangle encloses π milliradian-centimeter beam area.

As an example of how the effect of a particular kind of error may be evaluated, we take a run for which the elements of the triplets are independently and randomly rotated about the longitudinal axis, up to a maximum angle of $\pm 0.5^{\circ}$. Figure 5 shows the transverse input, a rectangle in x, y space translated to r^2, v_r. Figures 6a, 6b, 6c are a series of phase-energy plots of the bunch as it progresses down the machine. Figure 7a, finally, is the summary plot, showing the rms radius and phase deviation from synchronous of the bunch, radius and phase of a particular particle, and the total number of surviving protons, all as a function of section number. Especially interesting here is the rms radius, which should be compared with Figs. 7b, 7c, which show the same for 0 and 1° quad rotation, respectively. See also Fig. 8, which is the summary graph for doublets with 1° quad rotations.

The effects of the other kinds of errors which we have studied (and are enumerated and discussed in reference 1) can be summarized by saying that no obviously impossible tolerances are imposed by beam dynamical requirements on the geometrical and electromagnetic parameters which we have varied. For example, sectionwise rf amplitude and phase tolerances are of the order of 2% and 2°. Tank axes can be a millimeter out of alignment (for 2 cm radius aperture), while the allowable spread in indiviudal quadrupole field gradients is about 1%. Bench alignment tolerances for the triplet lens systems are a few mils; we have not yet determined them for doublets.

LAPOSTOLLE: You mentioned the possibility of debunching the beam in the last sections, especially when you use your machine for a slightly lower energy. I think that for some experiments it might be interesting not to debunch but to use an rf structure, very short bunches. Would it be possible to keep the rf structure even at a lower energy.

VISSCHER: Yes, well it depends on what energy you want. It is not possible to get the rf structure out if we let it drift all the way from, let's say, 300 MeV, because then the energy spread in the bunch will itself be sufficient to debunch, I think.

WALKINSHAW: You could keep your rf on and change the respective phasing along the tanks if you recalibrate your phasing.

LAPOSTOLLE: That was my original question.

VISSCHER: Yes, but it wouldn't be something simple like just turning off the rf.

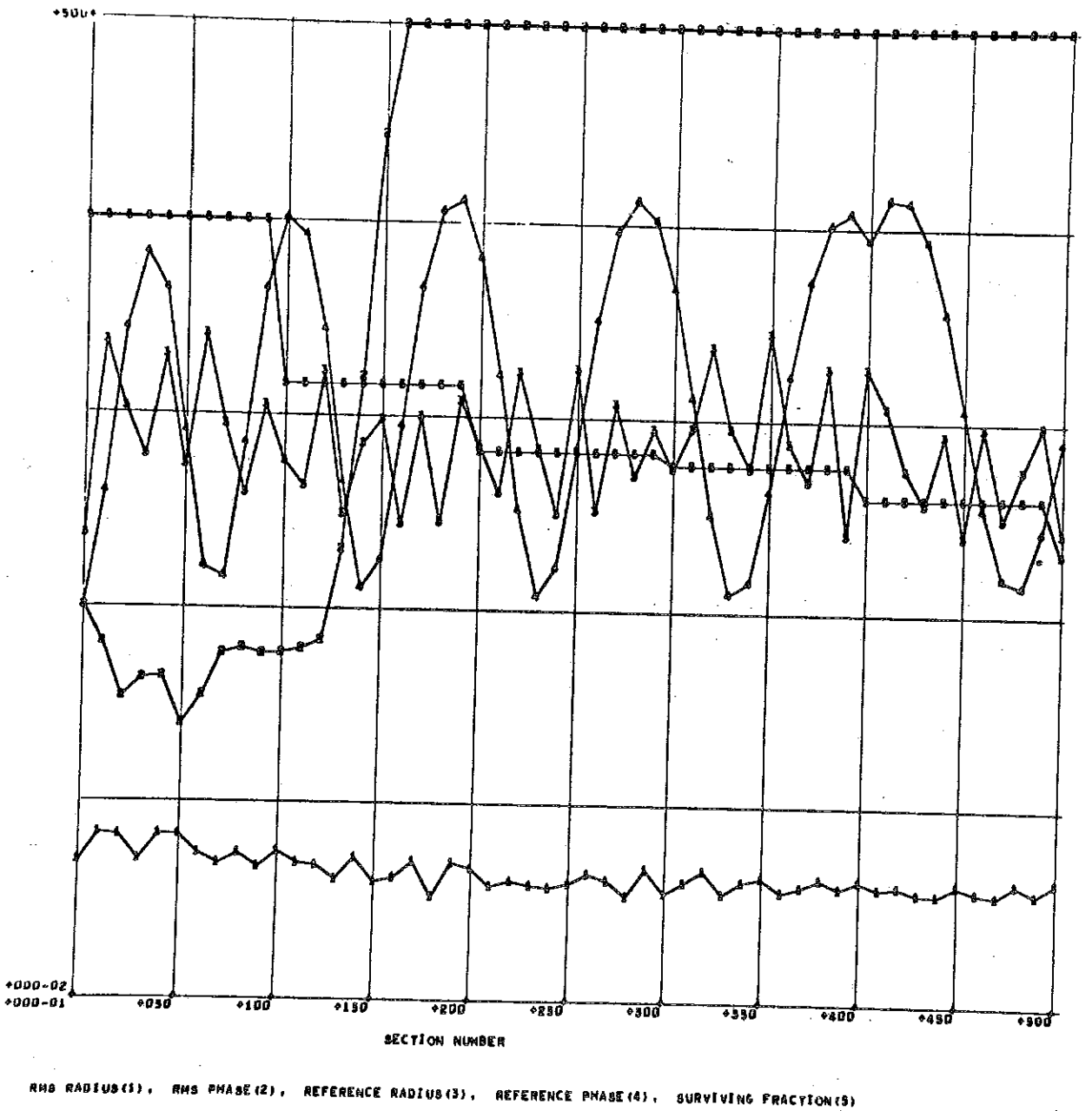

Fig. 4: Summary graph for triplet system. Particles are rejected for excessively large radius every 10 sections; the r.m.s. phase goes off scale because protons are lost from the phase bucket without blowing up radially. The "reference particle" is always that proton whose initial phase is smallest among the surviving particles. Quad displacement error for this run was 1 mm.

TENG: It would be possible only if the sections were short enough.

VISSCHER: Maybe it wouldn't be possible because the section length and the cell length wouldn't at all correspond with the beta of the particle that is drifting through.

WALKINSHAW: I don't think that matters.

TENG: Well it doesn't matter if it is short enough, but are they?

VISSCHER: In order for an accelerator section to be of any use in retaining the bunch structure, the number of cells in the section has to be less than about

$$N < \frac{\gamma(\gamma - 1)(\gamma + 1)}{4\,\Delta\gamma} ,$$

where $\Delta\gamma$ is the difference (mass units) between the synchronous energy and the beam energy. Thus, for example, in order to use a 700 MeV section to retain rf structure in a 600 MeV beam, the section length would be limited to 27 cells. (Otherwise the phase change of the beam within the section will exceed 180°.) For an energy difference of 300 MeV, say, this restriction becomes impossibly stringent. The beam could be coasted out with a bunched structure by inserting special rf bunchers between sections, but I don't think the accelerating sections themselves could be used for this prupose.

WALKINSHAW: Could you give a figure for the growth in transverse phase space area (with misalignment errors) relative to the phase space area of the synchronous particle? That is the increase in the transverse phase space area when errors are introduced.

VISSCHER: We have not yet made extensive studies of the transverse motions in three dimensions, but from those we have done combined with some extrapolations from the two-dimensional runs, I would expect the transverse phase space area of the beam to increase by less than a factor of two from 200 to 800 MeV with reasonable errors in quad alignment and rotation and section tilt.

REFERENCES

1. Informal report, "A Numerical Study of Radial and Phase Stability in a High-Energy Proton Linear Accelerator," Los Alamos, 30 April 1964.

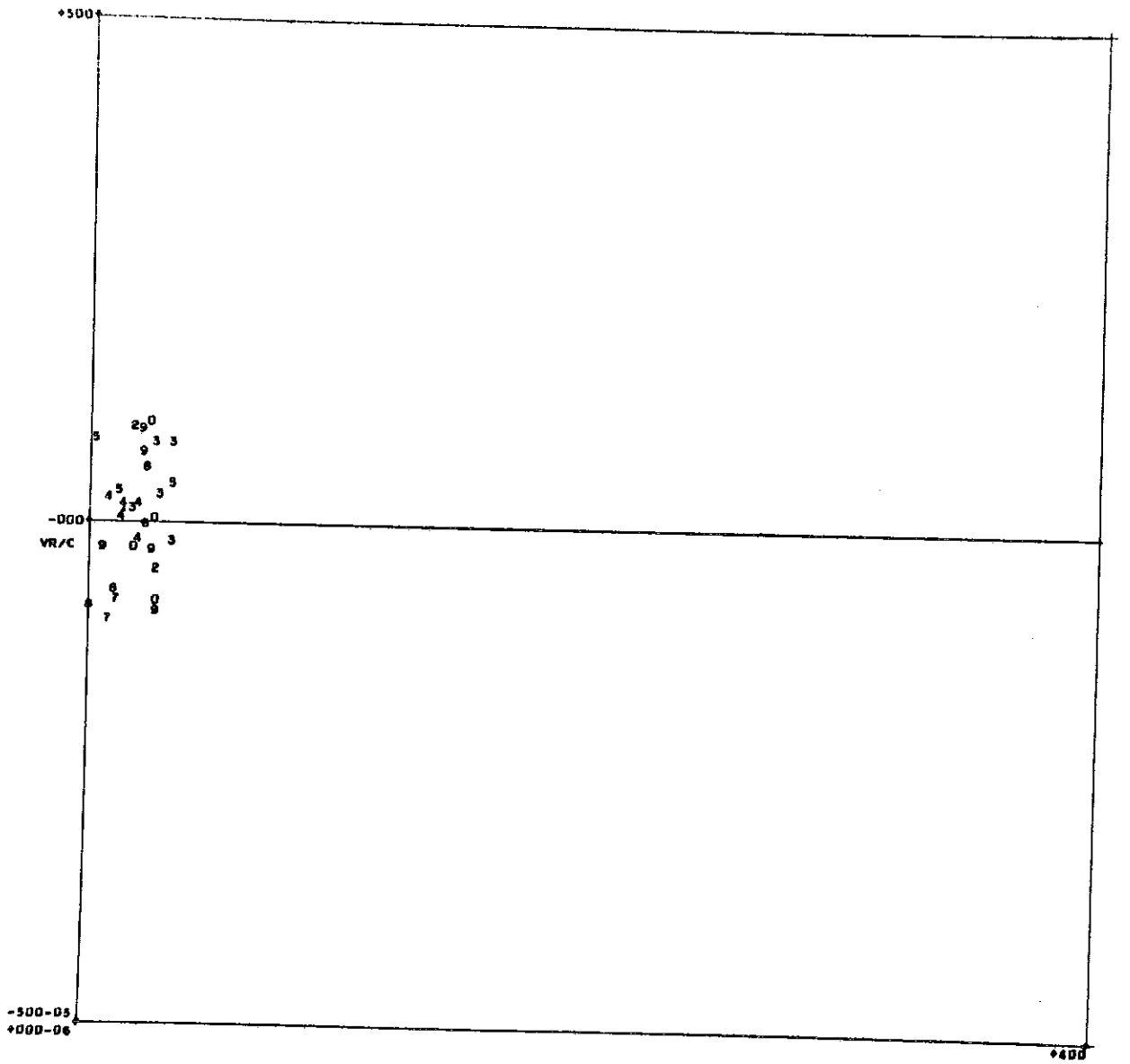

Fig. 5: Transverse input for quad rotation run. Area corresponds to 4 milliradian-cm. A plot symbol n means that $n/10 \leq v_\theta / v_{\theta\ \max} < (n+1)/10$.

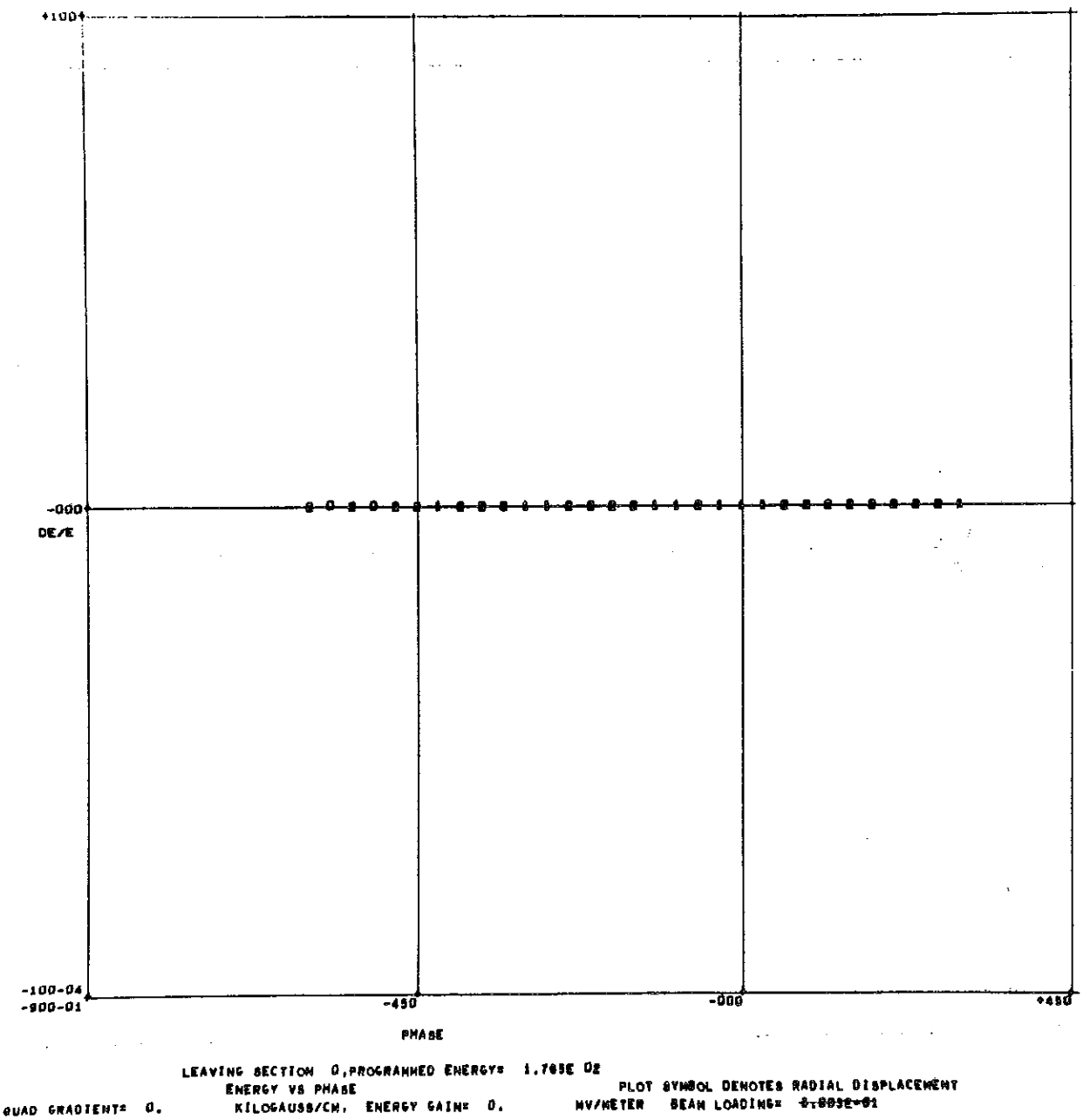

Fig. 6a: Phase-energy input for quad rotation run. Phase interval is 3 times synchronous phase; energy interval is zero, but the points will fill most of the range of the ordinate after the first section, since the phase oscillation wavelength is less than 3 sections for near-synchronous particles. A plot symbol n means the proton has $n/10 \leq r/R_0 < (n + 1)/10$.

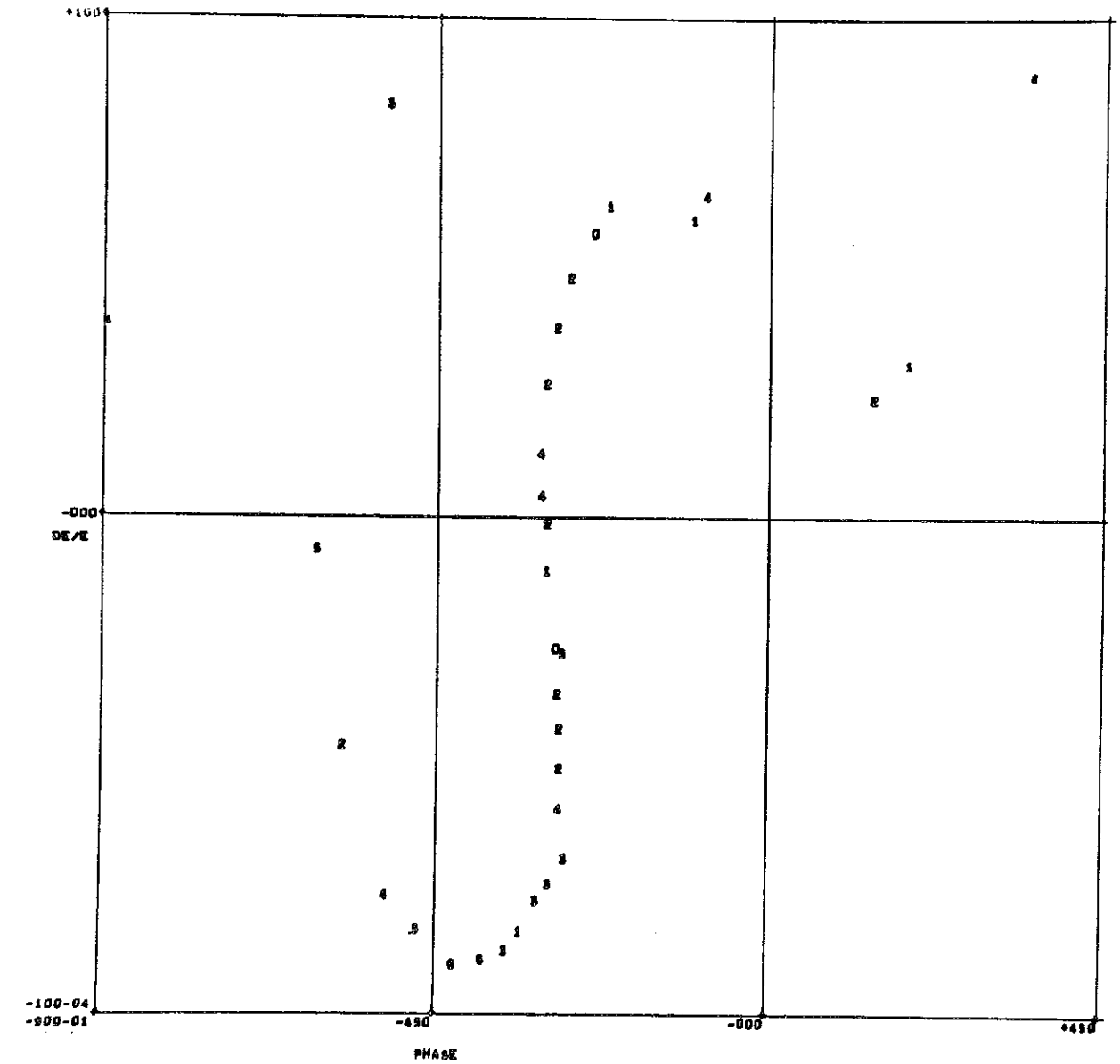

Fig. 6b: The same as Fig. 6a, but after 5 sections. The points would lie on a smooth curve were it not for the radial-phase interaction which causes the phase development to depend on the (initially random) transverse position. At this point the pattern has already rotated more than $1\frac{1}{4}$ times.

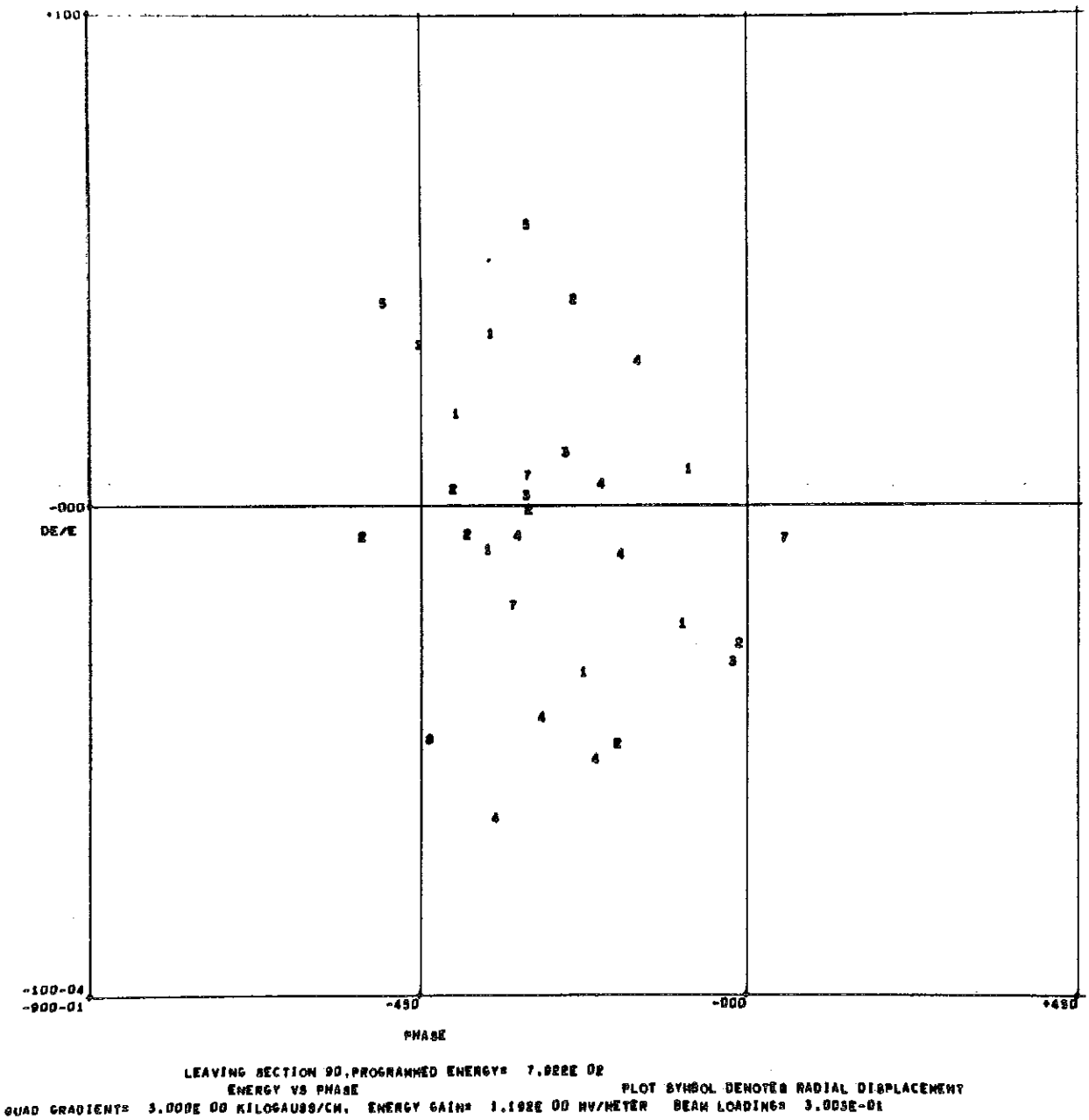

Fig. 6c: Same as Fig. 6b, but after 90 sections. Phase compression is noticeable; the wrapped-up line of the input is still recognizable.

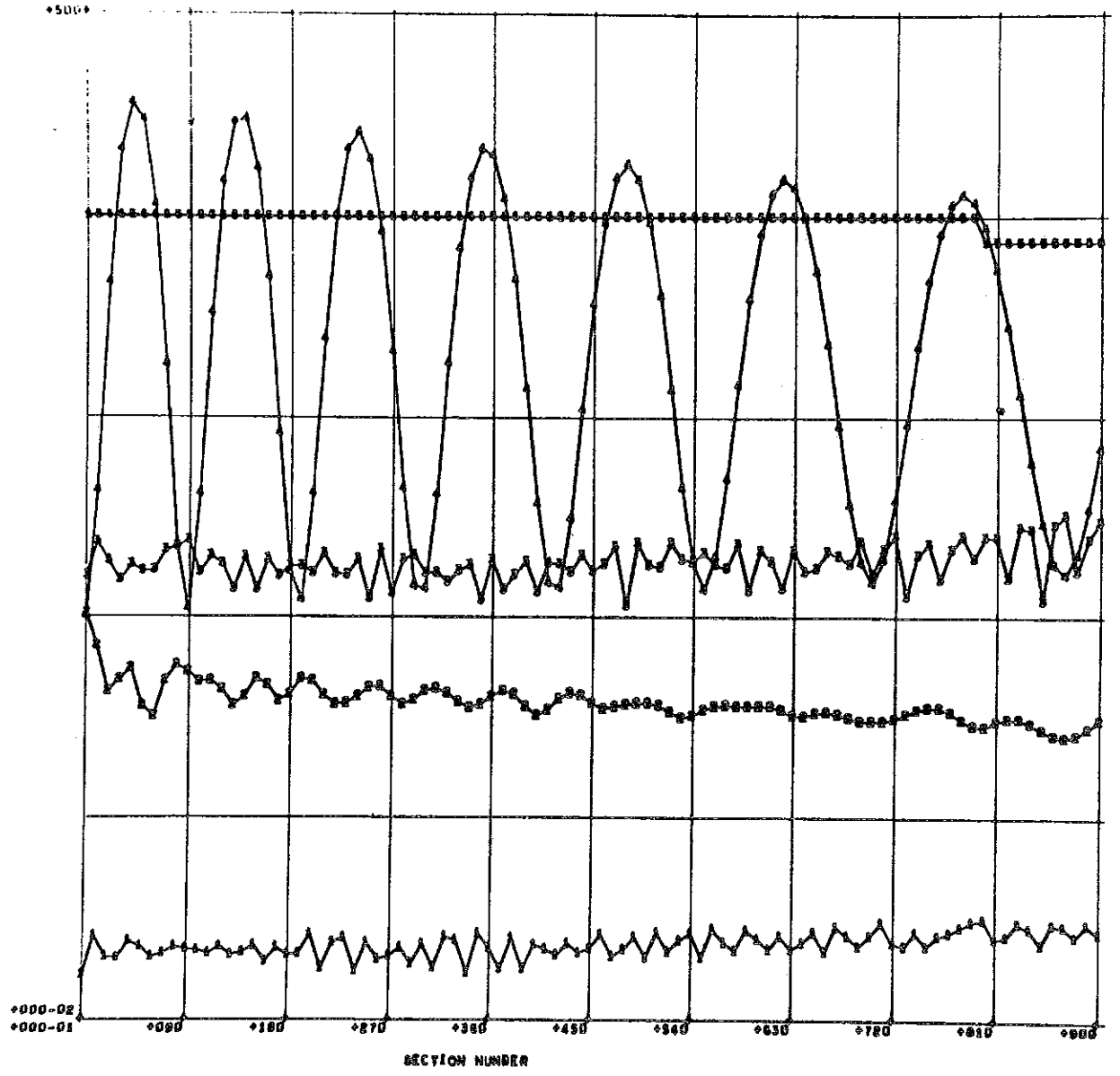

Fig. 7a: Summary plot for run with quad rotation errors of 0.5°. The r.m.s. radius shows a slight buildup, and a particle is lost radially at section 80.

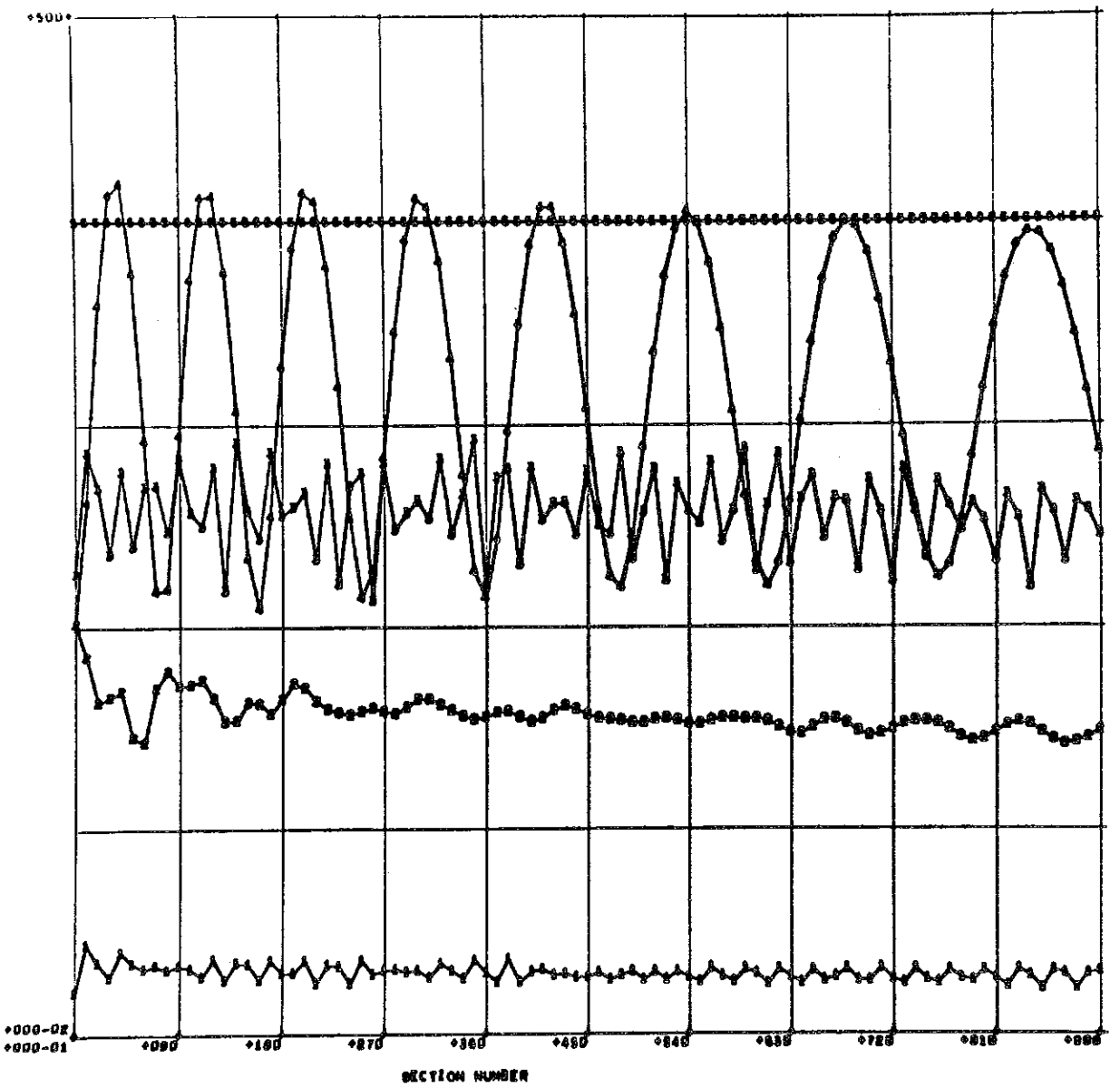

Fig. 7b: Same as Fig. 7a, but with no errors. R.M.S. radius is quite flat.

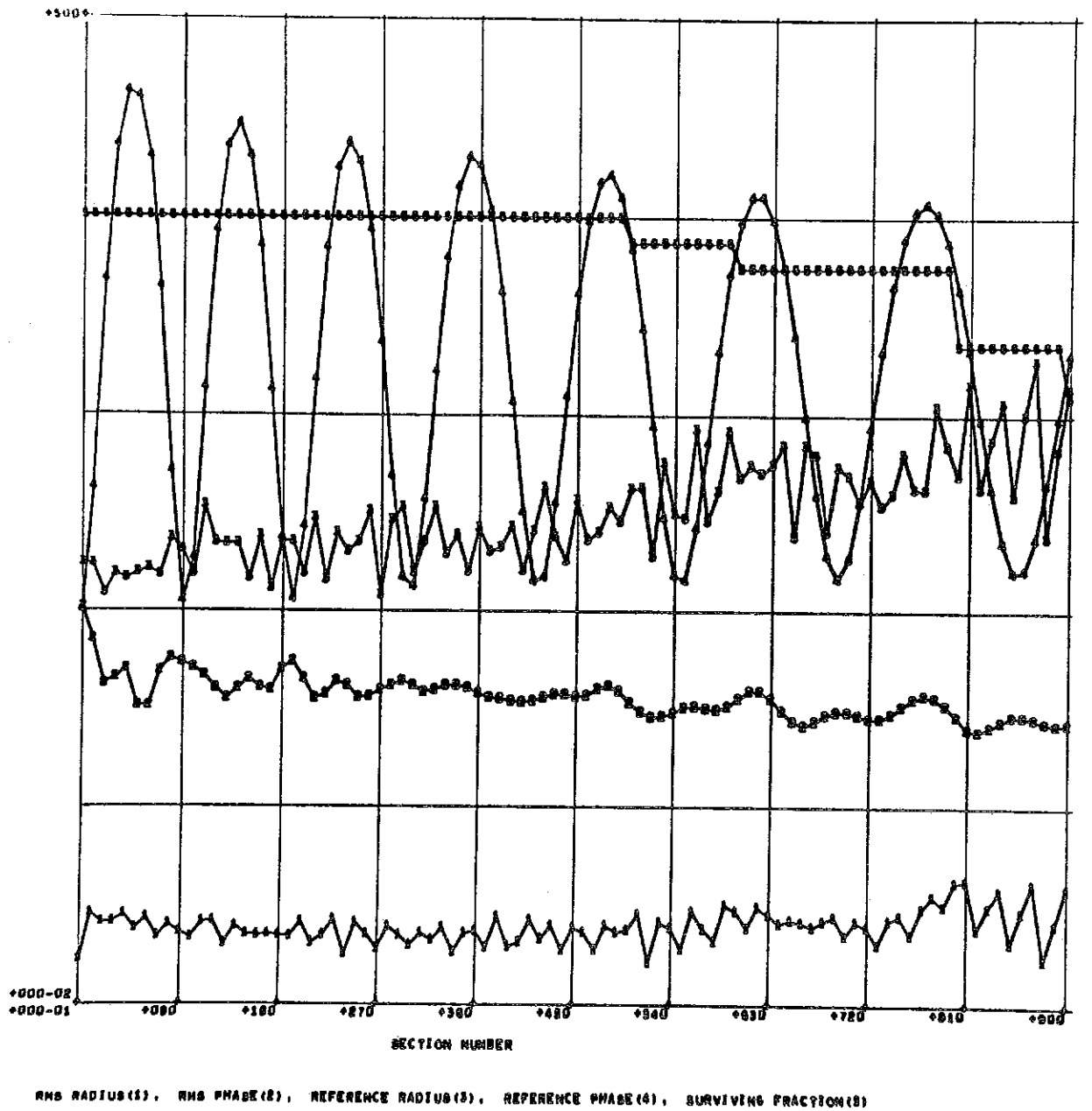

Fig. 7c: Same as Fig. 7a, but with 1° rather than 0.5° quad rotation errors.

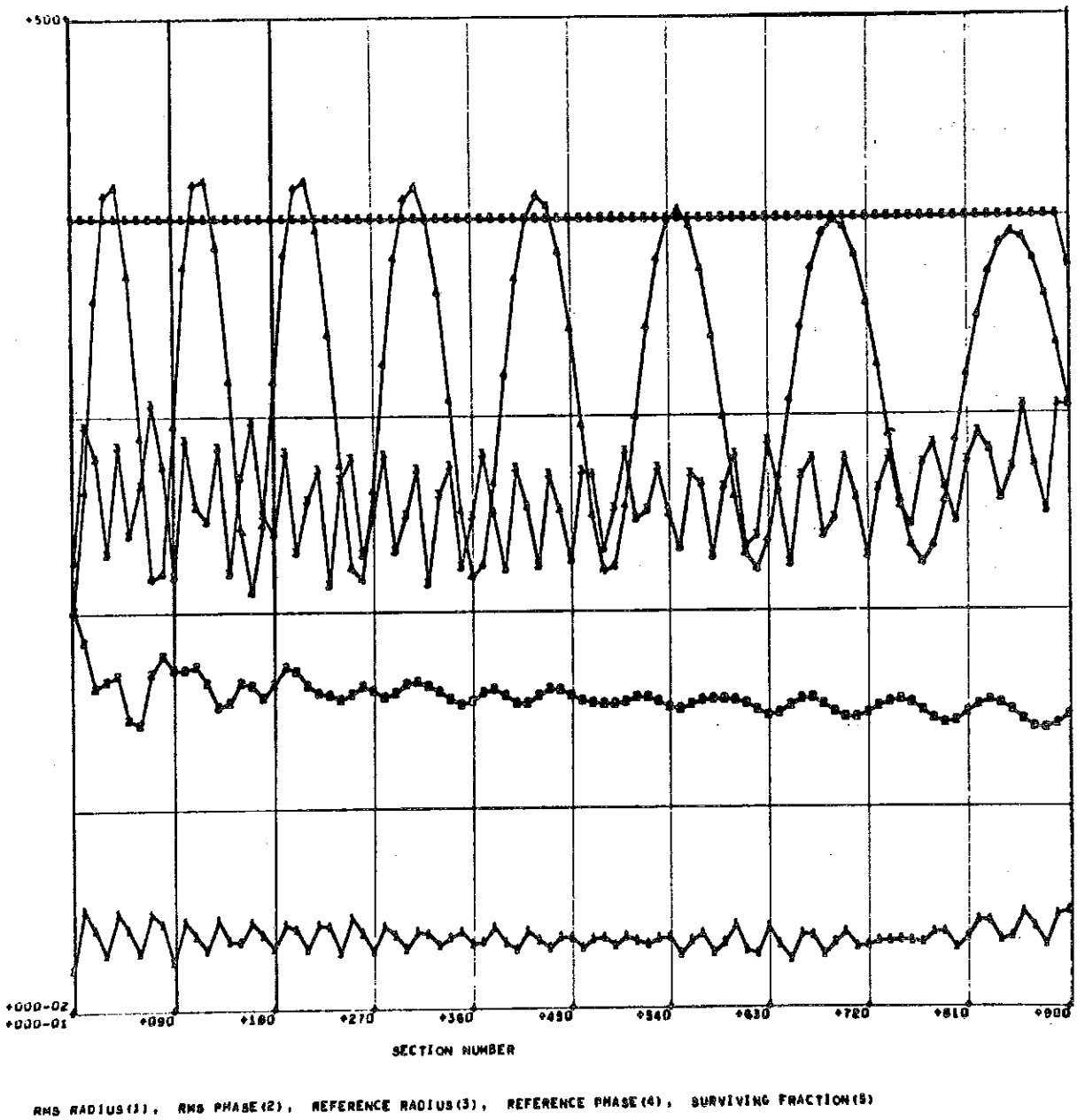

Fig. 8: Summary plot for doublets with quad rotation errors of 1^{o},

CONSTANT PHASE VELOCITY ACCELERATION SECTIONS IN A PROTON LINAC*

J. Parain
Centre D'Etudes Nucleaires De Saclay

For an accelerator with constant phase velocity acceleration sections, it is not possible to define a synchronous particle. One can however define a reference particle such that the motion of all particles might be related to this reference particle (1).

1 - Motion in one acceleration section

The equations of the motion in one acceleration section are:

$$\frac{dE}{ds} = e\,\xi\,\sin\varphi$$

$$\frac{d\varphi}{ds} = \frac{2\pi}{\lambda}\left(\frac{1}{\beta} - \frac{1}{\beta_r}\right)$$

where s is the direction of the motion, E the energy, ξ the electric field, φ the phase with respect to the accelerating field, λ the wavelength, β the relative velocity and β_r the phase velocity of the accelerating field in the section.

By writing $E - E_r = \Delta E$, the hamiltonian of the motion may be written

$$H = -\frac{\pi}{\lambda}\,\frac{E_o^2}{\left[E_r^2 - E_o^2\right]^{3/2}}\,\Delta E^2 + e\,\xi\cos\varphi$$

E_o is the rest energy of the particle.

---

* This work was started at the CERN.

A new variable energy may be defined by:

$$W = \frac{\Delta E}{e} A_o \quad \text{with} \quad A_o = \left[\frac{2\pi}{\xi \lambda \frac{Eo}{e} \beta_r^3 \gamma_r^3} \right]^{1/2}$$

The trajectories in the (W, φ) space will be the curves having for equation

$$\left(\frac{W}{2}\right)^2 + \sin^2 \frac{\varphi}{2} = ct$$

The length of an acceleration section is

$$L = \pm \frac{1}{\Omega_o} \int_{\alpha_o}^{\alpha_e} \frac{d\theta}{(1 - k^2 \sin^2 \theta)^{1/2}}$$

with $\Omega_o = \left[\frac{2\pi\xi}{\lambda \frac{Eo}{e} \beta_r^3 \gamma_r^3} \right]^{1/2}$ $k^2 = \left(\frac{W}{2}\right)^2 + \sin^2 \frac{\varphi}{2}$, $\sin\alpha = \frac{\sin \frac{\varphi}{2}}{k}$

This equation may be solved by introducing the $F(\alpha, k)$ elliptic integral of first kind. If $\phi = \Omega_o L$, one gets

$$\phi = \pm \left[F(\alpha_e, k) - F(\alpha_o, k) \right]$$

2 - The reference particle

The reference particle has for velocity the phase velocity in the middle of the section. At the beginning of the section, the initial conditions for this reference particle are $(\varphi_r, -W_r)$, the final conditions will be $(\varphi_r, +W_r)$. W will then increase by $2W_r$. . From W, φ diagram, two points may have this property, one of them will be stable, the other one unstable.

The phase of the reference particle is variable all the way through the section; in the middle of the section, the phase will have its maximum value φ_m ,

$$\text{with} \quad \sin \frac{\varphi_m}{2} = \left[\sin^2 \frac{\varphi_r}{2} + \left(\frac{W_r}{2} \right)^2 \right]^{1/2} .$$

One can compute the length of the acceleration section corresponding to the motion of the reference particle.

$$\phi = 2 \left[F \left(\frac{\pi}{2} , k_r \right) - F \left(\alpha_r , k_r \right) \right]$$

Figure No. 1 gives the curve $\phi = ct$ in the (W, φ) space. If the length of the section is small, the phase does not vary much, and the motion will be the same as in an accelerator with a synchronous particle, $\varphi_r \simeq \varphi_s$.

3 - Efficiency

For the reference particle, the energy increased in a section will be

$$2 \frac{\Delta E}{e} = \frac{2 W_r}{A_o}$$

If L is the length of the section, and ξ the electric field, the efficiency of the section may be written as

$$\eta = \frac{2 \frac{\Delta E}{e}}{\xi L}$$

Using reduced variables $\eta = \frac{2 W_r}{\phi}$

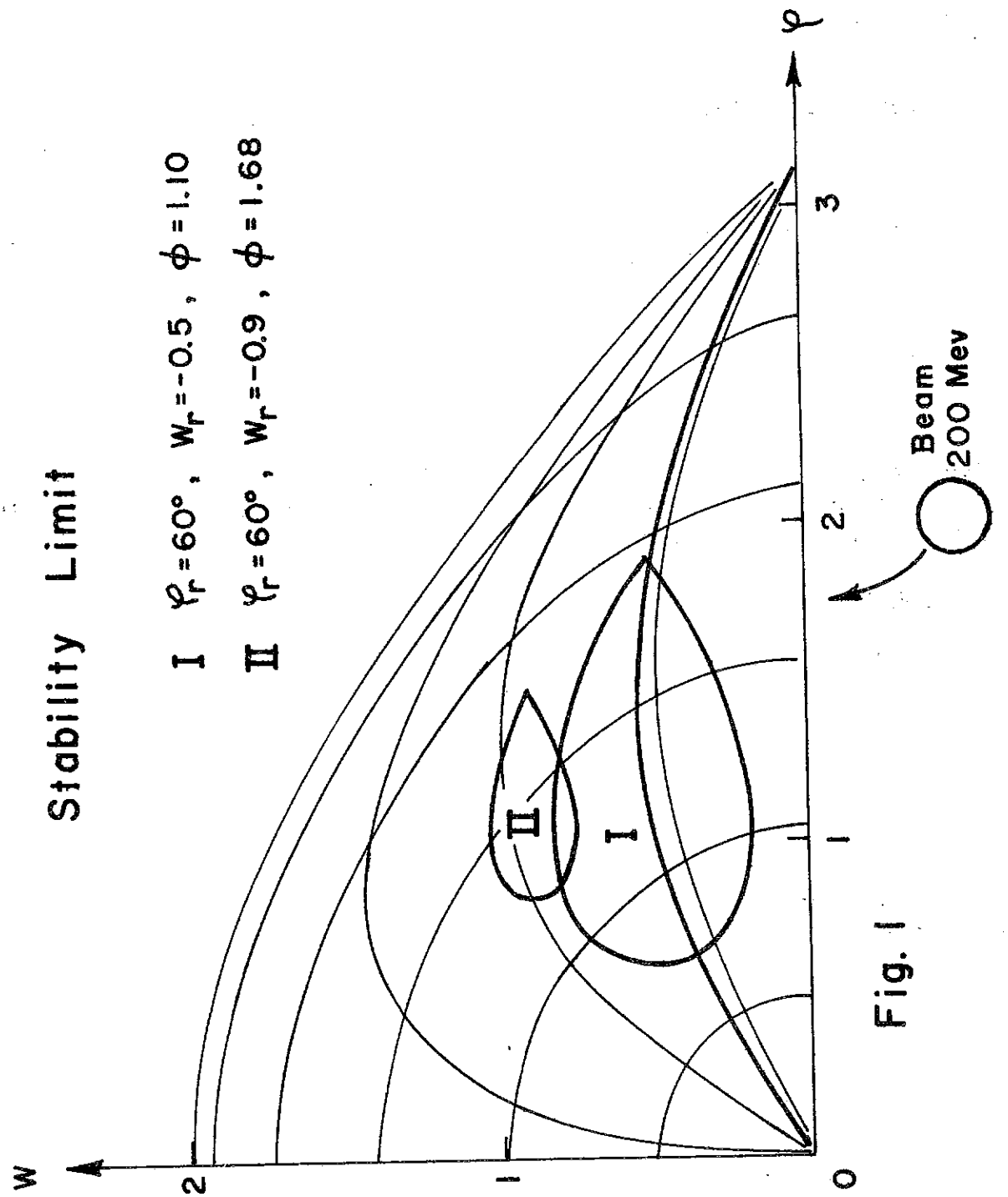
Stability Limit
I $\varphi_r = 60°$, $W_r = -0.5$, $\phi = 1.10$
II $\varphi_r = 60°$, $W_r = -0.9$, $\phi = 1.68$
W
2
1
0
1
2
3
φ
I
II
Beam
200 Mev

Fig. 1

Figure No. 2 gives the curves $\eta = ct$ in the (W, φ) space. For each value of ϕ, a maximum value of efficiency may be found such that

$$\eta_{max} = \frac{2\,(W_r)max}{\phi}$$

for smaller values of ϕ, $\eta_{max} = 1$, for $\phi = 2$, $\eta_{max} = 0.99$ but η_{max} decreases rapidly for $\phi > 2$.

4 - Motion of a particle around the reference particle

Let us now consider a particle with initial conditions (φ_1, W_1). Since this particle will travel the same length in the linac, one may compute the conditions at the end of the section.

$$F(\alpha_2, k) = 2F\left(\frac{\pi}{2}, k\right) - F(\alpha_1, k) - \phi$$

with $\sin \alpha_i = \dfrac{\sin \dfrac{\varphi_i}{2}}{k}$ and $k^2 = \sin^2 \dfrac{\varphi_i}{2} + \left(\dfrac{W_i}{2}\right)^2$

This expression gives φ_2 and W_2, that is the position of the particle at the end of the section. When entering the next acceleration section, the particle has the same phase, but the phase velocity of the new section is different, so that

$$(\varphi_1)_{j+1} = (\varphi_2)_j \text{ and } (W_1)_{j+1} = (W_2)_j - 2W_r .$$

The j indices are for the conditions in the j^{th} section. In all of this, no consideration has been given to the adiabatic evolution.

5 - Stability Area

If one computes the position of one particle at the end of each section by using the relation in Section 4, one can find that the consecutive positions of the particle are plotted on a curve in the (W, φ) space.

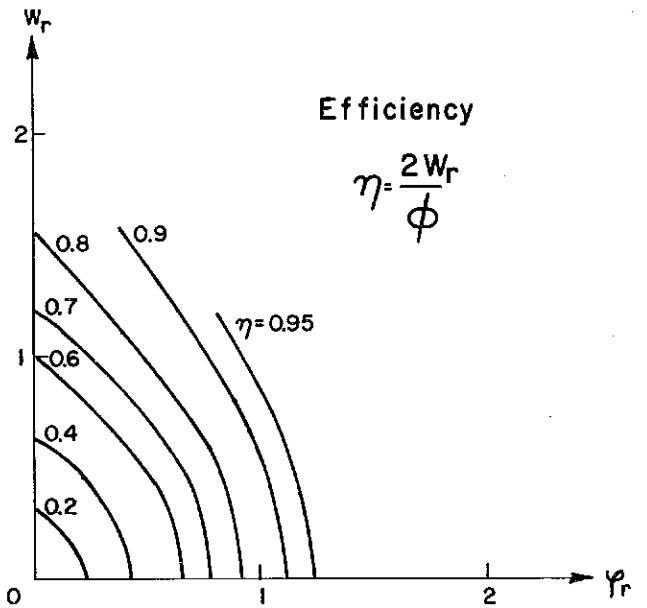
W_r
Efficiency
$\eta = \frac{2W_r}{\phi}$
2
1
0
0.8
0.9
0.7
$\eta = 0.95$
0.6
0.4
0.2
1
2
φ_r

Fig. 2

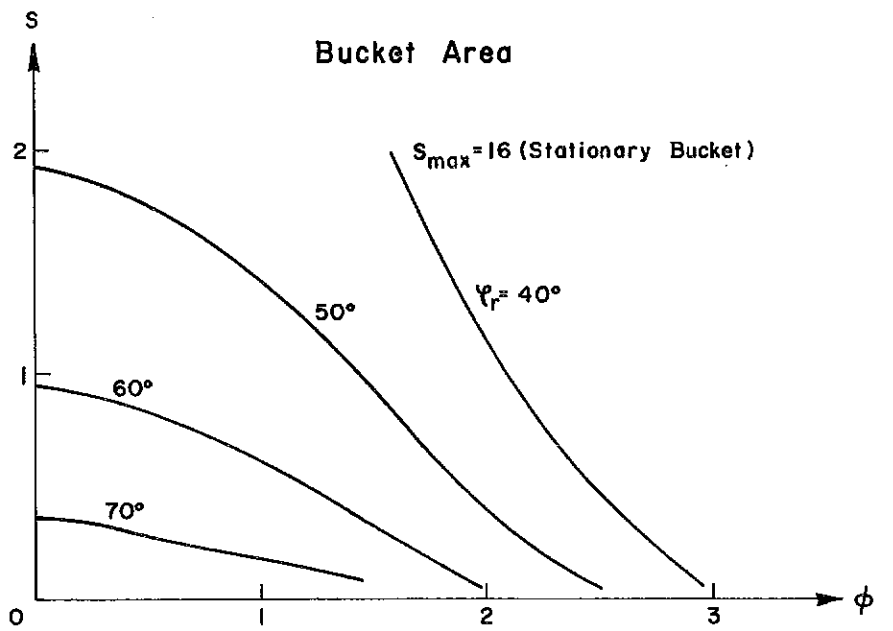
S
Bucket Area
$S_{max} = 16$ (Stationary Bucket)
2
1
0
50°
$\varphi_r = 40°$
60°
70°
1
2
3
ϕ

Fig. 3

For a small ϕ, one finds the curve of limit stability that is well known for an accelerator with synchronous particle. For greater ϕ, but ϕ still smaller than two, the curves have the same shape, the limit stability curves still go through the unstable point. Figure No. 1 shows the stability area for two values of ϕ.

For ϕ greater than two, that is for a number of synchrotron oscillations per section $\nu = \phi/2\pi$ of the order of 0.3 the motion is more complicated. For small amplitudes, the consecutive positions of the particle do not shape an ellipse centered on the stable point anymore. For larger amplitudes, the particle may become unstable after a few runs around the stable point. This case has not been thoroughly studied, since it is out of the limits of application.

The curves in Figure No. 3 give the surface of the limit stability curves versus ϕ for different values of φ_r. For ϕ smaller than two, it can be seen that the surface is the same as in accelerator with a synchronous particle the phase of which being such that $\eta = \sin \varphi_s$. For ϕ greater than two, the surfaces are smaller than it could be found from this approximation.

6 - Application

We shall now study a 200 MeV beam in a proton linac. For parameters defined in reference (2) that is $\xi = 2 \times 10^6$ V/m, $\lambda = 0.75$ m and an acceleration section length of 6 m, one finds $\phi = 1.4$. One still has to make choice of a reference phase such that all the particles might be contained inside the stability area. The 200 MeV beam has, in the $(\Delta E, \varphi)$ phase space, an area of 75.6×10^3 V.rd. In order to get a simpler image, one might admit that the adapted beam is a circle in the (W, φ) space, in that case

$$\Delta\varphi = \frac{A_0 S(\Delta E, \Delta\varphi)}{\Delta W}, \quad \text{Hence} \quad \Delta\varphi \simeq 0.1 \text{ rd.}$$

The Figure No. 1 gives the cross section of the beam. For $\varphi_r = 60^\circ$, the stability limit area is still 10 times greater than the beam area. This might be necessary to take care of phase and amplitude errors of electric field. The value of ϕ decreases for increasing energies, it is then possible either to keep constant the length of the section and to increase the efficiency or to increase the section length by increasing the number of identical sections, for example. The following table gives the length L and its corresponding value of ϕ, as a function of energy.

Energy BeV	L m	ϕ
0.2	6	1.42
0.4	6	0.80
0.4	12	1.60
1.0	12	0.66
1.0	24	1.32
2.0	24	0.63
2.0	48	1.25
3.0	48	0,78

These lengths still fit the quadrupole doublet radial focusing requirements. One might think of starting with a 50 MeV beam and 3 m long sections, ξ being 2 10^6 V/m and ξ = 1.5 m, ϕ would then still be = 1.5.

7 - Conclusion

It is possible to use constant phase velocity acceleration sections in a linac if the number of synchrotron oscillations per section is smaller than 0.3. With this condition, it is possible to obtain a large enough area of stability and an efficiency of about 0.9 for a proton linac of energy between 200 MeV and 3 BeV.

References

(1) SMITH,L. - Stepped phase velocity linacs
Conference on linear accelerators for high energies.
Brookhaven August 1962

(2) SHERSBY-HARVIE,R. B. R. - Tentative proposal for a 3 Gev Linac injector - CERN AR/Int. SG/63-18 - 24th October 1963

FOCUSING OF AN ALVAREZ LINAC BY USE OF MAGNETIC QUADRUPOLES ORIENTED AT 45°

D. T. Tran
CSF - Compagnie générale de télégraphie Sans Fil
Centre De Physique Electronique Et Corpusculaire
Domaine de Corbeville ORSAY (S. &. O.)

(Presented by M. G. Guilbaud)

Introduction

Strong focusing as used currently in Proton Linacs is made by quadrupoles in the N. S. N. S. or N. N. S. S. arrangement.

According to some authors (1), (2), (3), the acceptance of the system can be increased if the axis of the successive quadrupoles are oriented some angle, different from 90°. We have tried to analyze the situation when successive quadrupoles are at a 45° angle one from next.

We have taken the quadrupoles to be thin lenses, and assumed that the 'rf'. defocusing is also that of a cylindrical thin lens, located at the middle of the gap.

Stability

Fig. 1 shows the equivalent mesh, starting at the middle of an R. F. gap. d and 2g are the respective convergence and divergence of the quadrupoles and rf. gap. R represents the rotation of the lens.

---

(1) Krienen, F. CERN - SC. 57-28 (1957).

(2) Morpurgo, M. CERN - SC. 141 Bis (1957).

(3) Septier, A. Advances in Electronics and Electron Physics. Academic Press - Vol. XIV - 1961.

The transfer matrix of vector

$$(1) \qquad \vec{V} = \begin{pmatrix} x \\ y \\ x' \\ y' \end{pmatrix}$$

is, for a diverging lens,

$$(2) \quad [d] = \begin{pmatrix} 1 & 0 & 0 & 0 \\ 0 & 1 & 0 & 0 \\ d & 0 & 1 & 0 \\ 0 & -d & 0 & 1 \end{pmatrix} = \begin{pmatrix} [1] & [0] \\ D & [1] \end{pmatrix}$$

where

$$(3) \quad D = d \begin{bmatrix} 1 & 0 \\ 0 & -1 \end{bmatrix} = d\,\pi \quad , \text{ where } \quad \pi^2 = [1] \quad .$$

For an accelerating gap:

$$(4) \quad [g] = \begin{bmatrix} 1 & 0 & 0 & 0 \\ 0 & 1 & 0 & 0 \\ 2g & 0 & 1 & 0 \\ 0 & +2g & 0 & 1 \end{bmatrix} = \begin{bmatrix} [1] & [0] \\ 2G & [1] \end{bmatrix}$$

where

$$G = g \, [1]$$

since the rf . is defocusing both in the x and y directions.

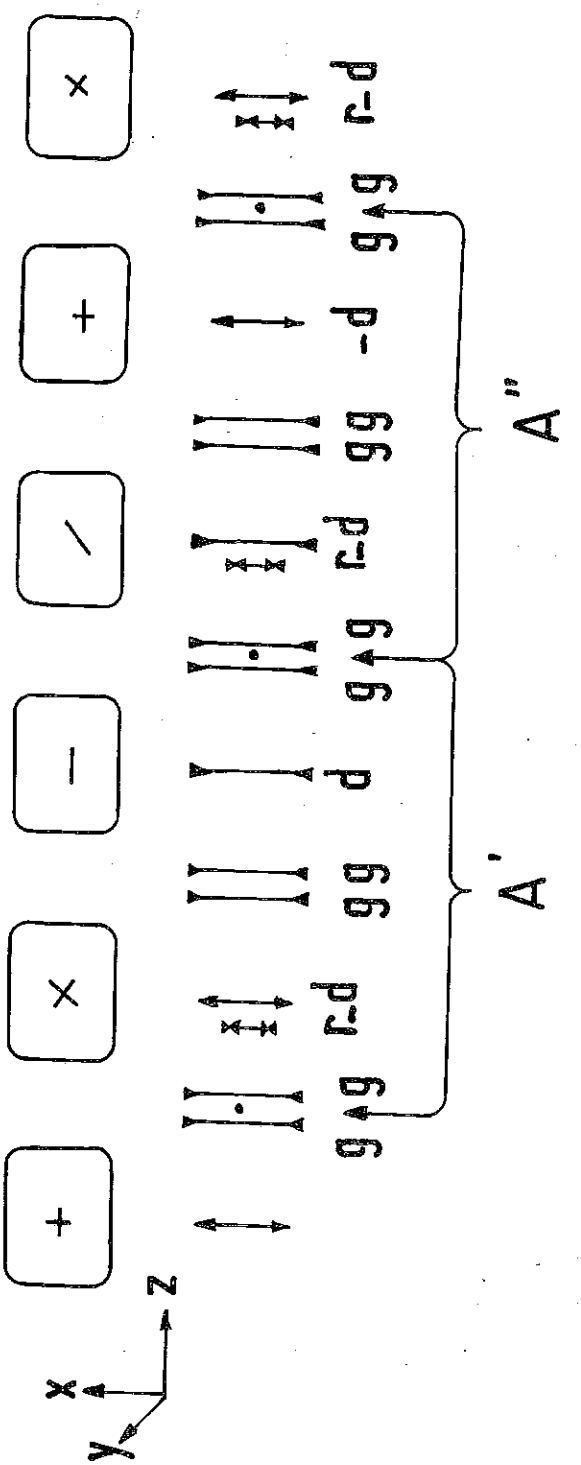

Fig 1 DISPOSITION SCHEMATIQUE

The zero field gap is represented by

$$(5)\quad [\ell] = \begin{pmatrix} 1 & 0 & \ell & 0 \\ 0 & 1 & 0 & \ell \\ 0 & 0 & 1 & 0 \\ 0 & 0 & 0 & 1 \end{pmatrix} = \begin{pmatrix} [1] & L \\ [0] & [1] \end{pmatrix}$$

where

$$(6)\quad L = \begin{pmatrix} \ell & 0 \\ 0 & \ell \end{pmatrix} = \begin{pmatrix} 1 & 0 \\ 0 & 1 \end{pmatrix}$$

if half a cell length is taken as the unit length.

The rotation comes to:

$$(7)\quad R = \begin{pmatrix} \cos\alpha & \sin\alpha & 0 & 0 \\ -\sin\alpha & \cos\alpha & 0 & 0 \\ 0 & 0 & \cos\alpha & \sin\alpha \\ 0 & 0 & -\sin\alpha & \cos\alpha \end{pmatrix}$$

In our case

$$(8)\quad R = \frac{1}{\sqrt{2}} \begin{pmatrix} 1 & 1 & 0 & 0 \\ -1 & 1 & 0 & 0 \\ 0 & 0 & 1 & 1 \\ 0 & 0 & -1 & 1 \end{pmatrix}$$

we write this

$$(9)\qquad R = \begin{pmatrix} \sqrt{J} & [0] \\ [0] & \sqrt{J} \end{pmatrix}$$

where

$$(10)\qquad \sqrt{J} = \frac{1}{\sqrt{2}} \begin{pmatrix} 1 & 1 \\ -1 & 1 \end{pmatrix}$$

Let us note that

$$(11)\qquad J = \left(\sqrt{J}\right)^2 = \begin{pmatrix} 0 & 1 \\ -1 & 0 \end{pmatrix} \quad \text{and } J^2 = -\begin{pmatrix} 1 & 0 \\ 0 & 1 \end{pmatrix} = -[1]$$

If A' and A'' are the transfer matrices of the mesh halves, the matrix is

$$A = A'' \circ A'.$$

where

$$A' = \begin{pmatrix} [1] & [0] \\ G & [1] \end{pmatrix}\begin{pmatrix} [1] & [1] \\ [0] & [1] \end{pmatrix}\begin{pmatrix} [1] & [0] \\ D & [1] \end{pmatrix}\begin{pmatrix} [1] & [1] \\ [0] & [1] \end{pmatrix}\begin{pmatrix} [1] & [0] \\ 2G & [1] \end{pmatrix}\begin{pmatrix} [1] & [1] \\ [0] & [1] \end{pmatrix}\begin{pmatrix} [1] & [0] \\ -D & [1] \end{pmatrix}$$

(12)

$$\begin{pmatrix} \sqrt{J} & [0] \\ [0] & \sqrt{J} \end{pmatrix}\begin{pmatrix} [1] & [1] \\ [0] & [1] \end{pmatrix}\begin{pmatrix} [1] & [0] \\ G & [1] \end{pmatrix}$$

A'' is obtained from A' by changing the sign of d.

This notation allows us to multiply 4 x 4 matrices as if they were 2 x 2.

Let us note also that since matrices $\sqrt{J}$, $\left[1\right]$ and G are commutative, we can write,

$$A'(90^{o}) = A'(0^{o}) \cdot \sqrt{J} \tag{13}$$

$$A(90^{o}) = A''(0^{o}) \cdot \sqrt{J} \cdot A'(0^{o}) \cdot \sqrt{J}. \tag{14}$$

So,

$$A(0^{o}) = \begin{pmatrix} (a^2 - b^2 + c\,\delta)\left[1\right] & 2c\,(a\left[1\right] + b\,\pi) \\ 2\,\delta\,(a\left[1\right] - b\,\pi) & (a^2 - b^2 + c\,\delta)\left[1\right] \end{pmatrix} \tag{15}$$

$$A\left(\frac{\pi}{4}\right) = \left(\begin{array}{c|c} (a^2 + c\,\delta)\,J - b^2\left[1\right] - ab\,\pi + ab\,\pi J & c(2a\,J + b(\pi + \pi J)) \\ \hline \delta(2a\,J - b\,(\pi + \pi J) & (a^2 + c\,\delta)\,J - b^2\left[1\right] - ab\,\pi + ab\,\pi\,J \end{array}\right) \tag{16}$$

If

$$\vec{V} = \begin{pmatrix} x \\ x' \\ y \\ y' \end{pmatrix} \tag{17}$$

we can write matrices:

(18)

$a^2 - b^2 + c\delta$	$2c(a+b)$	0	0
$2\delta(a-b)$	$a^2 - b^2 + c\delta$	0	0
0	0	$a^2 - b^2 + c\delta$	$2c(a-b)$
0	0	$2\delta(a+b)$	$a^2 - b^2 + c\delta$

$\mathcal{A}(90^\circ) =$

(19)

$-b(a+b)$	bc	$a(a+b) + c\delta$	$c(2a+b)$
$-\delta b$	$+b(a-b)$	$\delta(2a-b)$	$a(a-b) + c\delta$
$-(a(a-b) + c\delta)$	$-c(2a-b)$	$b(a-b)$	$-bc$
$-\delta(2a+b)$	$-\left[a(a+b) + c\delta\right]$	δb	$-b(a+b)$

where

(20)
$$\begin{cases} a = 1 + 8g - 2d^2 + 8g^2 - 4d^2 g - 2g^2 d^2 \\ b = 2d(g+1) \\ c = 4 + 8g - 2d^2 - 2g d^2 \\ \delta = 4g + 12g^2 - 2d^2 - 6g d^2 + 8g^3 - 3g^2 d^2 - 2g^3 d^2. \end{cases}$$

In the classical focusing arrangement, x and y motions are uncoupled, and have the same trace:

(20 bis) $$Tx = Ty = 2\,(a^2 - b^2 + c\,\delta\,)$$

And the stability condition is:

(21) $$\left|\, 2\,(a^2 - b^2) \;-\; 1 \,\right| \;<\; 1$$

In our case, the characteristic equation is:

(22) $$\Delta(\lambda I - \mathcal{A}(90^\circ)) \;=\; 0$$

And this gives

(23) $$\lambda^4 + 4\,b^2\,(\,\lambda^3 + \lambda\,) + \left[4\,(2\,a^2 - b^2)^2 - 16a^2 + 2\right]\,\lambda^2 + 1 = 0.$$

It is a 4th degree reciprocal equation, the roots of which are two inverse groups:

(24) $$\lambda_1\,,\quad \lambda_1^{-1}\quad ;\quad \lambda_2\,,\quad \lambda_2^{-1}$$

If we write:

(25) $$\lambda_1 = e^{i\mu_1}$$

$$\lambda_2 = e^{i\mu_2}$$

we get

(26) $$\text{Cos}\;\mu_1 = -\,b^2 + 2\,\sqrt{a^2\,(1 + b^2 - a^2)}$$

$$\text{Cos}\;\mu_2 = -\,b^2 - 2\,\sqrt{a^2\,(1 + b^2 - a^2)}$$

The stability conditions write then:

(27)
$$\boxed{\begin{aligned} 1 - b^2 &> 0 \\ 1 + b^2 - a^2 &\geq 0 \\ 4\,a^2\,(1 + b^2 - a^2) &< (1 - b^2)^2 \end{aligned}}$$

Relations (21) and (27) allow to draw the curves of fig. 2. The stability region of classical case is between curves 1 and 2, whereas for our case, it is between 1 and 4. It is much narrower.

From the point of view of stability, our arrangement is disadvantageous.

Acceptance

Let us consider the case when the four eigen-values λ_k are different (in the classical case, they make two identical couples).

Let

(28)
$$\vec{V_i} = \begin{pmatrix} X_i \\ X'_i \\ Y_i \\ Y'_i \end{pmatrix}$$

be the i^{th} eigen-vector.

A trajectory can be expressed as

(29)
$$\vec{v} = \begin{pmatrix} x \\ x' \\ y \\ y' \end{pmatrix} = \sum_i A_i \vec{V_i} \qquad i = 1, 2, 3, 4$$

when A_i depend only on the initial conditions:

$$(30)\quad \begin{cases} A_1 = \dfrac{W(xy;2)}{W(1;2)} & A_2 = A_1^* = \dfrac{W(xy;1)}{W(1;2)} \\ A_3 = \dfrac{W(xy;4)}{W(3;4)} & A_4 = A_3^* = \dfrac{W(xy;3)}{W(3;4)} \end{cases}$$

where

$$(31)\quad \begin{cases} W(xy;i) = \begin{vmatrix} x & X \\ x' & X'_i \end{vmatrix} + \begin{vmatrix} y & Y_i \\ y' & Y'_i \end{vmatrix} = \vec{v}\ S\ \vec{V}_i \\ W(i;j) = \begin{vmatrix} X_i & X_j \\ X'_i & X'_j \end{vmatrix} + \begin{vmatrix} Y_i & Y_j \\ Y'_i & Y'_j \end{vmatrix} = \vec{V}_i\ S\ \vec{V}_j \end{cases}$$

are the classical Wronskians, and

$$(32)\quad S = \begin{pmatrix} 0 & -1 & 0 & 0 \\ 1 & 0 & 0 & 0 \\ 0 & 0 & 0 & -1 \\ 0 & 0 & 1 & 0 \end{pmatrix}$$

this yields

$$(33)\quad \begin{cases} x = A_1 X_1 + A_1^* X_1^* + A_3 X_3 + A_3^* X_3^* \\ y = A_1 Y_1 + A_1^* Y_1^* + A_3 Y_3 + A_3^* Y_3^* \end{cases}$$

or

$$(34)\quad \begin{cases} |x|_{max} = 2\ \text{Max}\ \left(|A_1|\ |X_1| + |A_3|\ |X_3| \right) \\ |y|_{max} = 2\ \text{Max}\ \left(|A_1|\ |Y_1| + |A_3|\ |Y_3| \right) \end{cases}$$

The eigen-values X_i and Y_i are determined as follows: let x_1 , x_2 , x_3 , x_4 , and y_1 , y_2 , y_3 , y_4 be four different particular solutions, which can be determined from adequate initial conditions and by using the matrix of mesh $\mathcal{Q}(a_{ij})$.

We can write:

$$(35)\quad \begin{cases} X_i = \sum_j \sigma_{ij}\, x_j \\ X'_i = \sum_j \sigma_{ij}\, x'_j \\ Y_i = \sum_j \sigma_{ij}\, y_j \\ Y'_i = \sum_j \sigma_{ij}\, y'_j \end{cases}$$

Which yields, if

x_{10} = 1	$x_{20} = 0$	$x_{30} = 0$	$x_{40} = 0$
x'_{10} = 0	$x'_{20} = 1$	$x'_{30} = 0$	$x'_{40} = 0$
y_{10} = 0	$y_{20} = 0$	$y_{30} = 1$	$y_{40} = 0$
y'_{10} = 0	$y'_{20} = 0$	$y'_{30} = 0$	$y'_{40} = 1$

and since

$$\begin{bmatrix} X_i \\ Y_i \end{bmatrix}_{out} = \lambda_i \begin{bmatrix} X_i \\ Y_i \end{bmatrix}_{in}$$

four homogeneous equations:

$$(36) \qquad \left(\mathcal{A}(a_{ij}) - \lambda_i I \right) \begin{pmatrix} \sigma_{i1} \\ \sigma_{i2} \\ \sigma_{i3} \\ \sigma_{i4} \end{pmatrix} = 0 \qquad i = 1, 2, 3, 4.$$

This gives the characteristic equation (23) and coefficients σ_{ij}. So, from (34), we can determine the maximum amplitude of a trajectory corresponding to given initial conditions. Inversely, since the problem is linear, one can determine, at each point of the mesh, the bounding surface of initial conditions which yields trajectories which do not deviate from the axis by more than the hole radius. The volume bounded by this hyper-surface is the system acceptance. According to Liouville's theorem, this volume deforms but is of a constant value. As the motion is Hamiltonian, and, due to the symmetry of the system, this volume is an hyperellipsoid.

Results

We shall consider points A, B, C, and D on fig. 2. A, B, C are stable both in the classical arrangement and in our arrangement. D is stable only in the classical one. D is close to the line of maximum acceptance of the classical system, A is close to the line of maximum acceptance of ours.

To make the comparison, we have drawn the intersection of the hyper-volume with the phase planes (x , x') and (y , y'). These are ellipses (fig. 3, 4, 5, 6, 7, 8), the area of which is the acceptance of the system in said phase plane. We have chosen that the particles do not deviate from the axis by more than 10 mm.

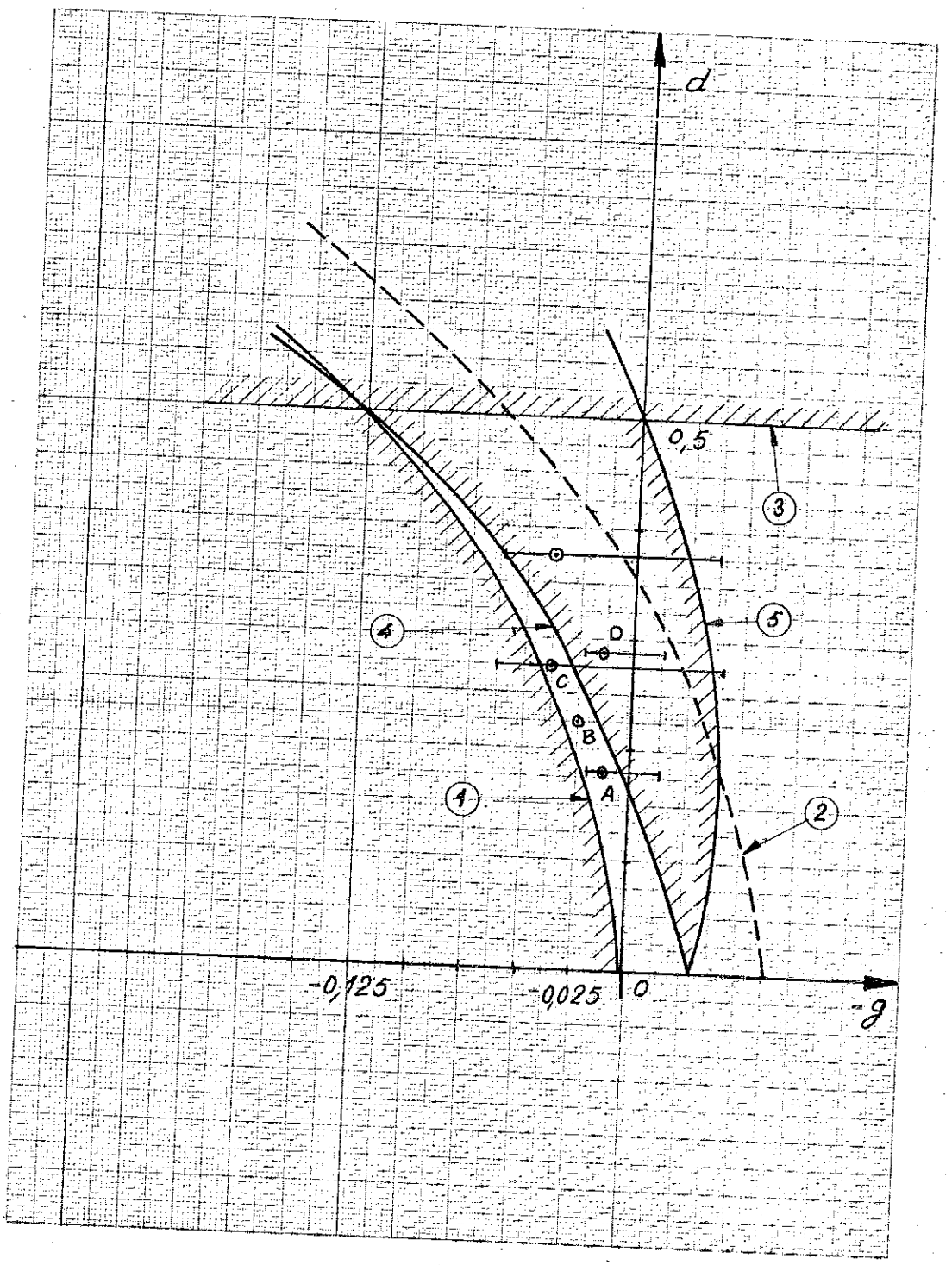

411 404-64

STABILITY DIAGRAMM

Fig. 2

INT 2011

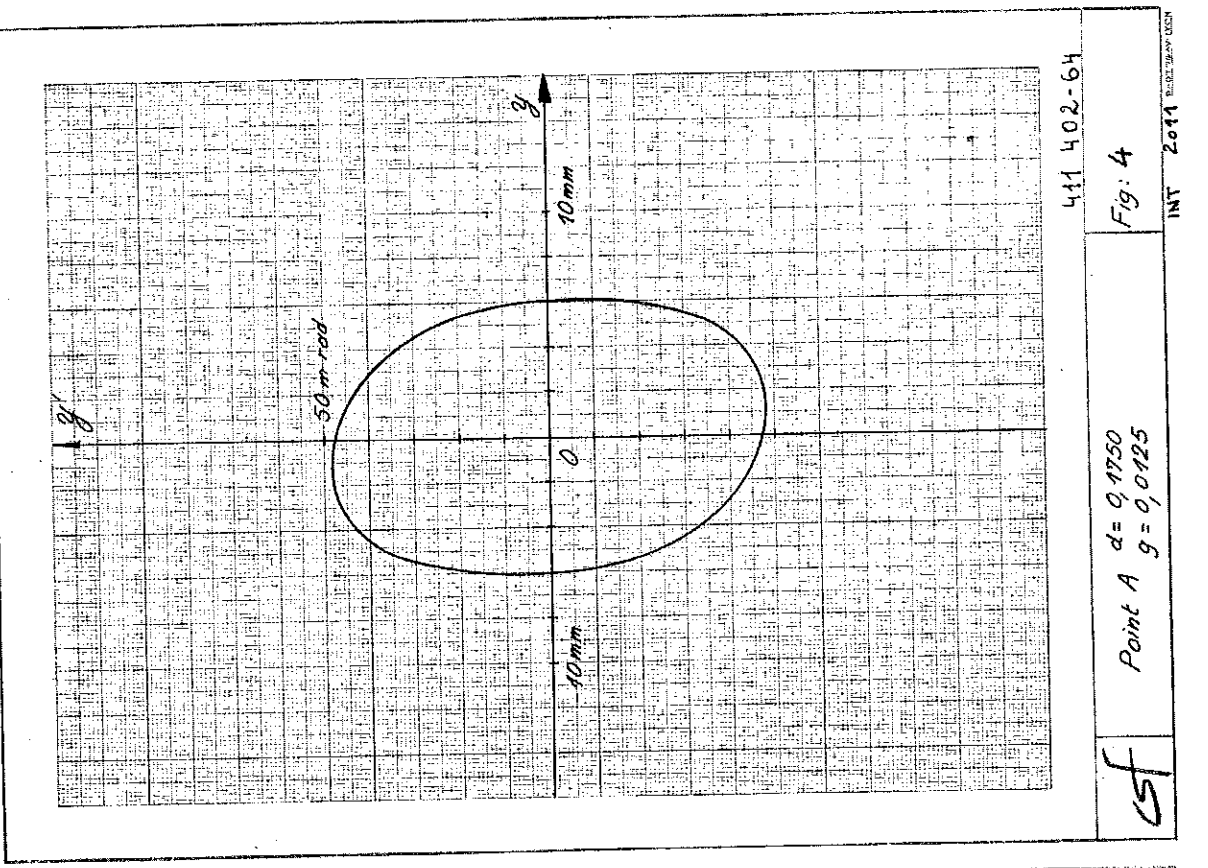
411 402-64
Point A d= 0,1750
g= 0,0125
Fig. 4
INT 2011
10 mm
0
-10 mm
50 µ rad

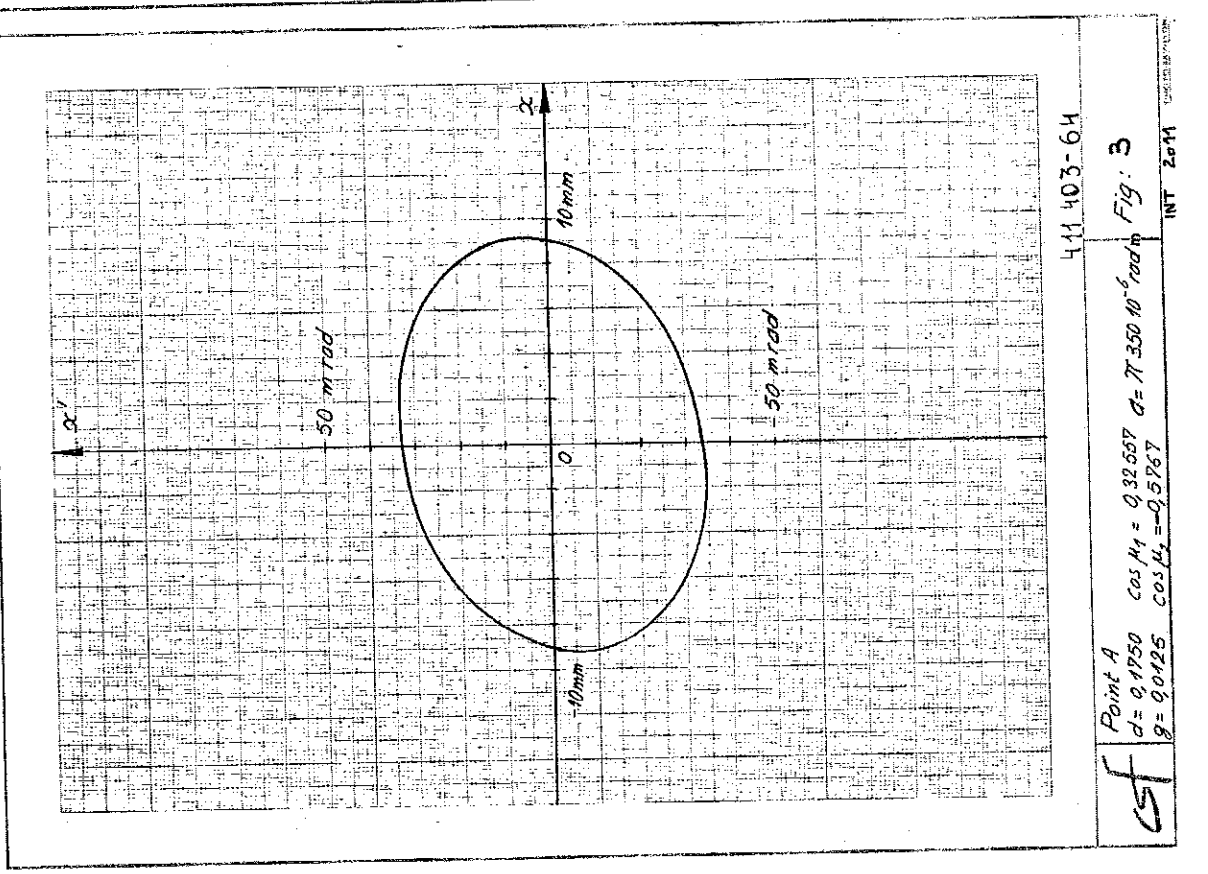
411 403-64
Point A
d= 0,1750 cos μ1 = 0,32557 α= 17,350 10⁻⁶ rad/m
g= 0,0125 cos μ2 = -0,5767
Fig: 3
INT 2011
10mm
0
-10mm
50 µ rad
-50 µ rad

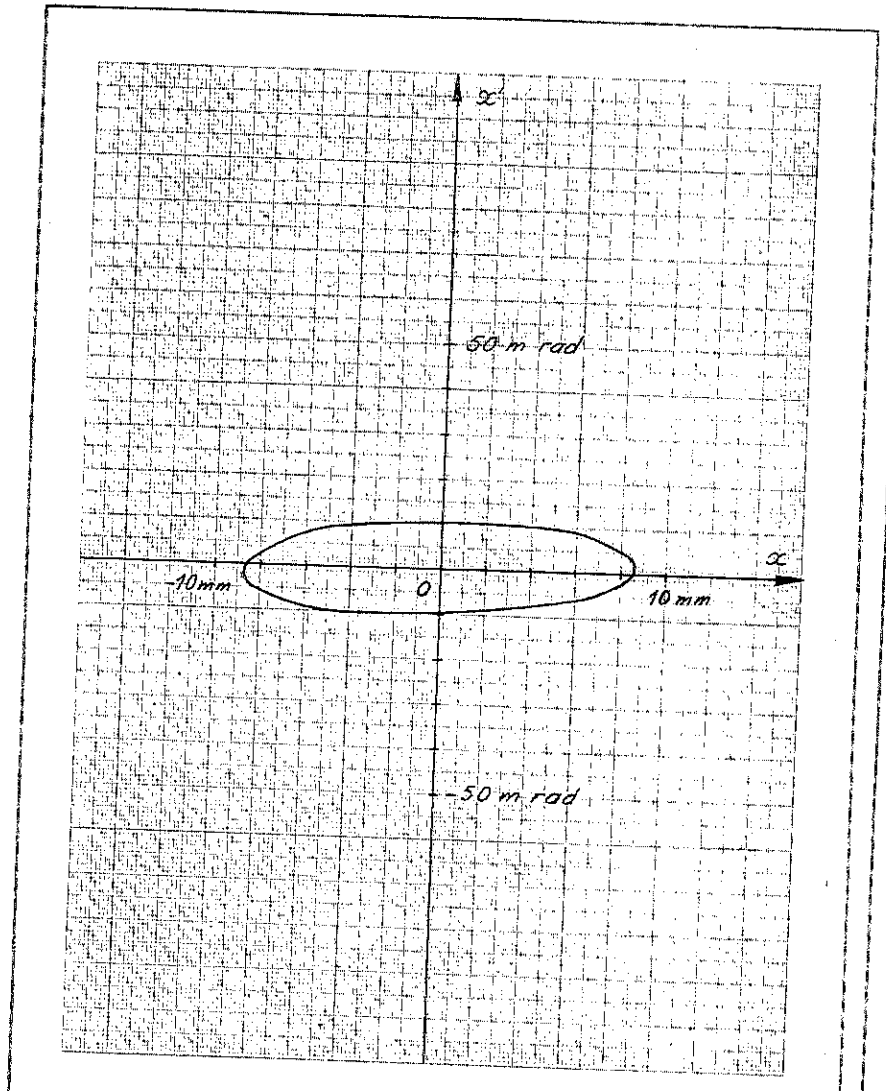

411 406-64

Point B
d=0,2250
g=0,0250
Demi trace
cos μ1 = -0,045754
cos μ2 = -0,37975
α=87π 10⁻⁶ rad m
Fig: 5

INT 2011

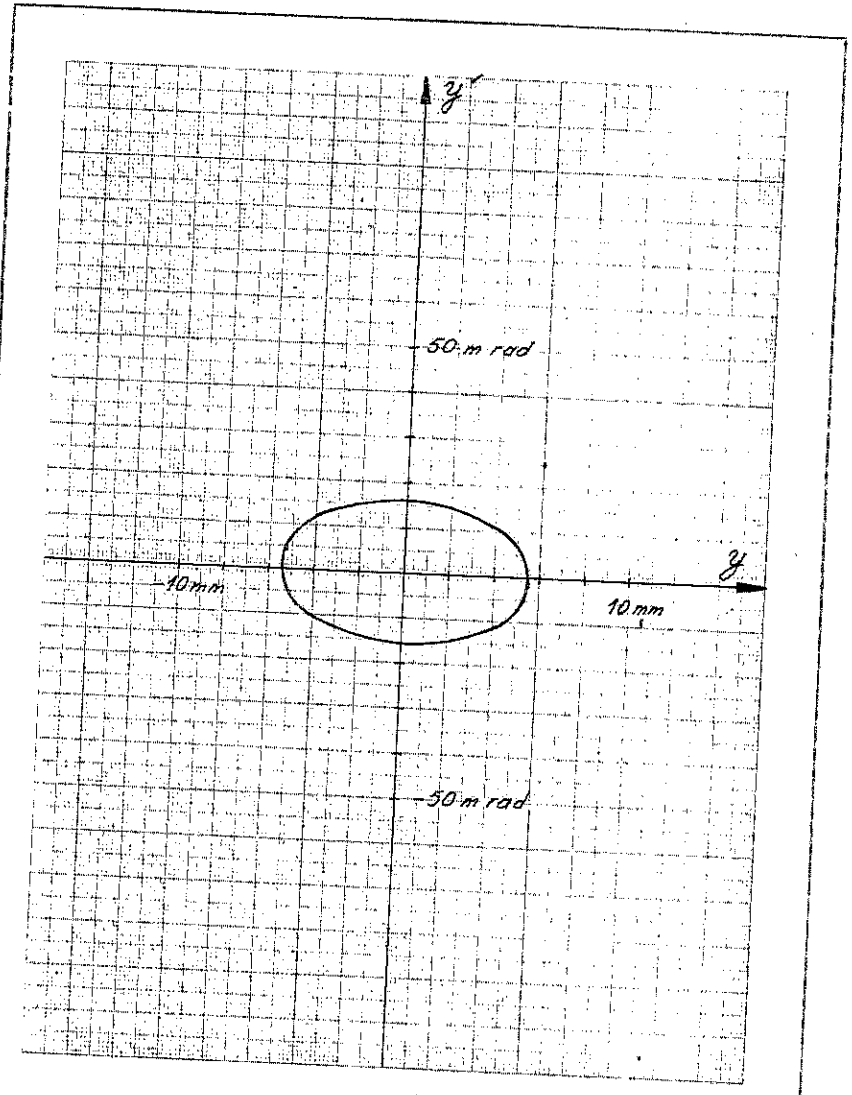

411 407-64

Point B

Fig: 6

INT 2011

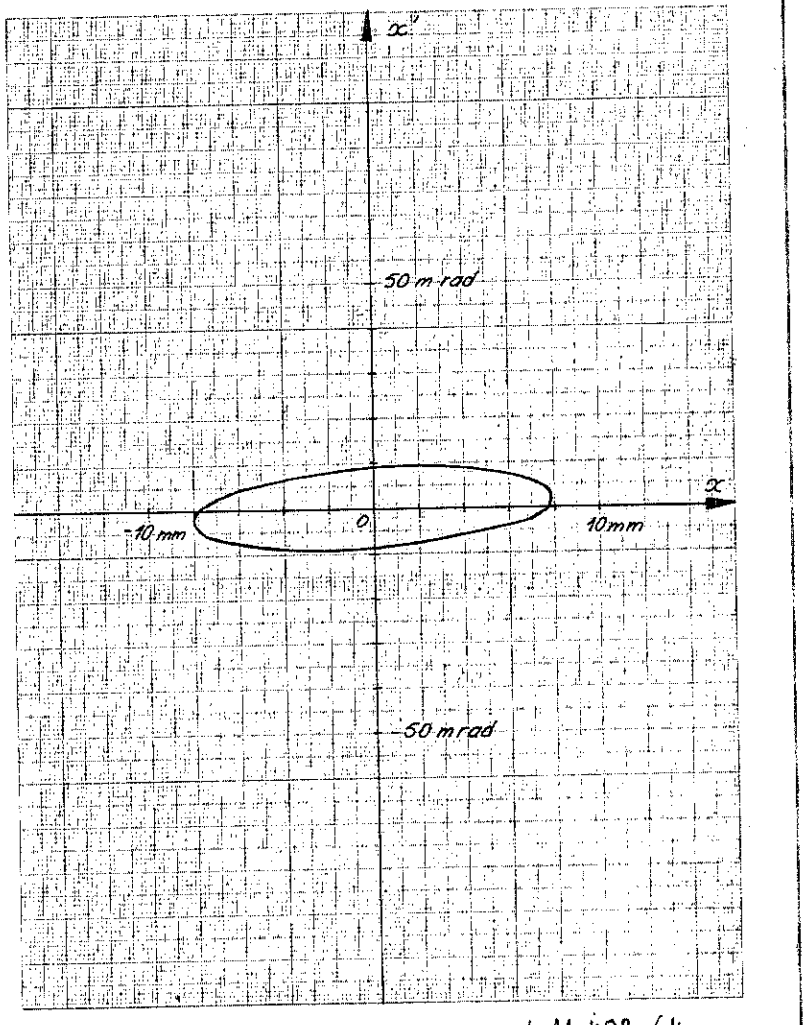

411 408-64

Point C	Demi trace		
d = 0,2950	cos μ1 = -0,13774	α = 72π·10⁻⁶ rad/m	Fig: 7
g = 0,0375	cos μ2 = -0,51349		

INT 2011

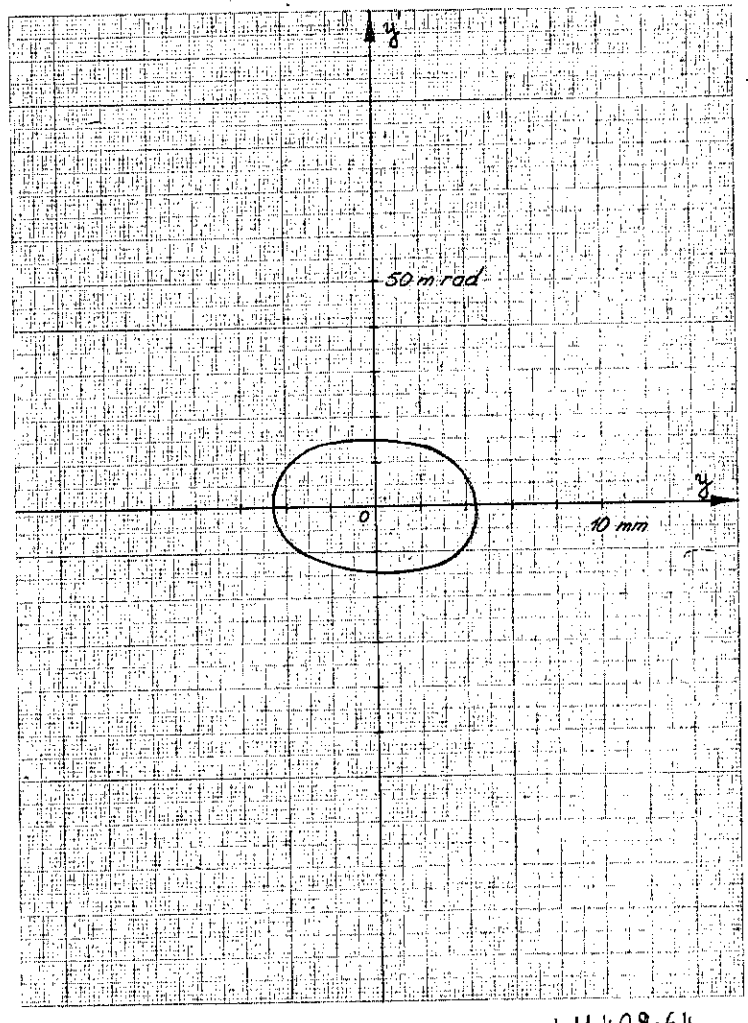

411 409-64

	Point C	Fig.8

INT 2011

From (19), one obtains, for the classical case:

$$\cos \mu = 2 (a^2 - b^2) - 1$$

$$\beta = \frac{2c (a + b)}{\sin \mu} = \frac{c (a + b)}{\sqrt{(a^2 - b^2) \left[1 - (a^2 - b^2) \right]}}$$

Since we have chosen that the mesh starts where β is maximum,

$$A_c = \frac{\pi a_o^2}{\beta \frac{L}{2}} = \frac{2 \pi a_o^2 \sqrt{(a^2 - b^2) \left[1 - (a^2 - b^2) \right]}}{L c (a + b)}$$

In the table, we compare results obtained, by use of an IBM 7090 computer of Saclay, for a classical arrangement Ac, and the helicoidal arrangement A_H.

Table I(*)

Point A	Point B	Point C	Point D
Energie: 3, 5 MeV	Energie: 0, 9 MeV	Energie: 0, 750 MeV	Energie: 2 MeV
d = 0, 1750	d = 0, 2250	d = 0, 2750	d = 0, 2880
g = 0, 0125	g = 0, 0250	g = 0, 0375	g = 0, 0175
$A_c = 59 \pi 10^{-6}$ rad m	$A_c = 39, 4 \pi 10^{-6}$ rad m	$A_c = 46, 5 \pi 10^{-6}$ rad m	$A_c = 140 \pi 10^{-6}$ rad m
$A_H = 350 \pi 10^{-6}$ rad m	$A_H = 87 \pi 10^{-6}$ rad m	$A_H = 72 \pi 10^{-6}$ rad m	

(*). These results correspond to an electric field of 1, 75 MV/m, and a synchronous phase of - 30°.

To make a better comparison, we should evaluate, in both cases, the volume of the hyperellipsoid. In the classical case, where the x and y motions are uncoupled, it is equal to the product of the acceptances in the two principal planes (x , x') and (y, y'), whereas in the case of any orthogonal sections, this volume is the upper limit of the products of the acceptances for any two planes. This means that the acceptances listed in Table I are lower than the acceptance of the system.

Conclusion

It can be seen that the proposed system leads to an acceptance gain of 2, 4 for a quadrupole strength reduced by 1, 6. fig. 2.

If one were to operate at the same points of the diagram in the two cases, the acceptance gain would be 6 at point A, 2, 2 at point B and 1, 55 at point C. This could be expected since A, B and C are relatively closer to the stability limit in the classifical arrangement than in the helicoidal one.

The disadvantage of the proposed helicoidal system is the reduced stability region. To make a thorough evaluation, account should be taken of the phase oscillations. Fig. 2 shows a rough evaluation of the effect of these phase oscillations. It is smaller for higher energies.

BLEWETT: It seemed to me that this 45° rotation is just a step in the direction of a continuous rotation which could be solvable analytically. Have you looked at that?

GUILBAUD: We have looked; we have wondered about taking other angles and we were afraid of the complication of it, but there might be a continuous analytical formulation of the problem.

SYMON: Kerst has looked at something like this where you have a continuous twist in connection with the design of a probe for plasmas. One interesting thing, if you have continuous twist, is that you no longer have alternating gradient equations but you can transform to a twisting coordinate system and reduce the equations to equations with constant coefficients.

GUILBAUD: That's interesting; has that work been published?

SYMON: I don't think so as yet, but it probably will be.

WALKINSHAW: John Bell did a similar transformation many years ago. That was published. It had exactly the same equations.

TENG: When you compare the acceptances, are you comparing the acceptances for the classical case and this case at the same point?

GUILBAUD: Yes, at the entrance.

TENG: The point A, for instance, is rather close to the edge of the stability band for the classical case. I am wondering if you move the point A to the middle of the classical stability band, how will they compare?

LAPOSTOLLE: You cannot go into the middle of the classical band because here it is unstable.

TENG: It's unstable for this case but not for the classical case.

GUILBAUD: No, the acceptance was computed in both cases for the same point. But on Fig. 7 we can compare points A and D. D is in the middle of the classical case, and then for 2 MeV the acceptance was 140 π 10^{-6} radian meters, and A for 3.5 MeV was 59 in the classical case. Now in our case, it was 350, so you see it is still better than D, but only by a factor of 2.2 but for weaker quadrupole strengths.

LAPOSTOLLE: Well, I might add something. I think that all these figures of acceptance are lower values in fact, since the product of any two normal cross sections is always lower than the hypervolume.

GLUCKSTERN: Is the classical case to which you compared a north-south north-south or a north-north south-south?

GUILBAUD: North-north south-south.

LAPOSTOLLE: Let me say that in principle, what you gain in acceptance, you may have to pay for by tighter tolerances.

APPLICATION OF CALCULATED FIELDS TO THE STUDY OF PARTICLE DYNAMICS

D. A. Swenson
Midwestern Universities Research Association

We have used a computer program by the name of PARMILA to study certain aspects of the phase and radial motion of particles in linear accelerators. Until recently, we have used expressions for the transit time factor and the radial impulse at the gap, which were derived from the simplest approximation of the field in the gap, that is, a field which is uniform across the geometrical length of the gap, and zero in the drift tube bore.

We have a great deal of information available to us on the actual distribution of fields in the entire linac cell in the form of output from our MESSYMESH program. It is possible to reduce these calculated field distributions to a few coefficients which reflect more precisely the effect of these fields on the particle motion.

I should say that this work was done primarily by Fred Mills and Don Young at a time when I was absent from the laboratory. More recently, I have gone over this work, and I have incorporated it into the PARMILA program.

Let $\mathcal{E}(r, z, t)$ be the electric field vector at radius r, longitudinal position z, and time t. The fields through which the particles travel, that is the fields near the axis of the linac, can be expressed in terms of the axial component of the electric field on the axis, $\mathcal{E}_z(0, z, t)$. At this point we take the time dependence to be sinusoidal and we define $E_z(z)$ so that

$$\mathcal{E}_z(0, z, t) = E_z(z) \cos(\omega t + \phi) .$$

It is instructive to compare the actual field distribution $E_z(z)$ with the simple uniform distributions of field. Figures 1, 2, 3, and 4 facilitate this comparison for typical linac geometries at 50, 100, 150, and 200 MeV. Both curves in each figure are scaled so that

$\frac{1}{L}\int_0^L E_z(z)\,dz$ is unity.

Maxwell's equation, in gaussian units, for cylindrical coordinates in a charge-free space, with the further restriction that $B_r = B_z = E_\theta = 0$, yield the following set of nontrivial equations.

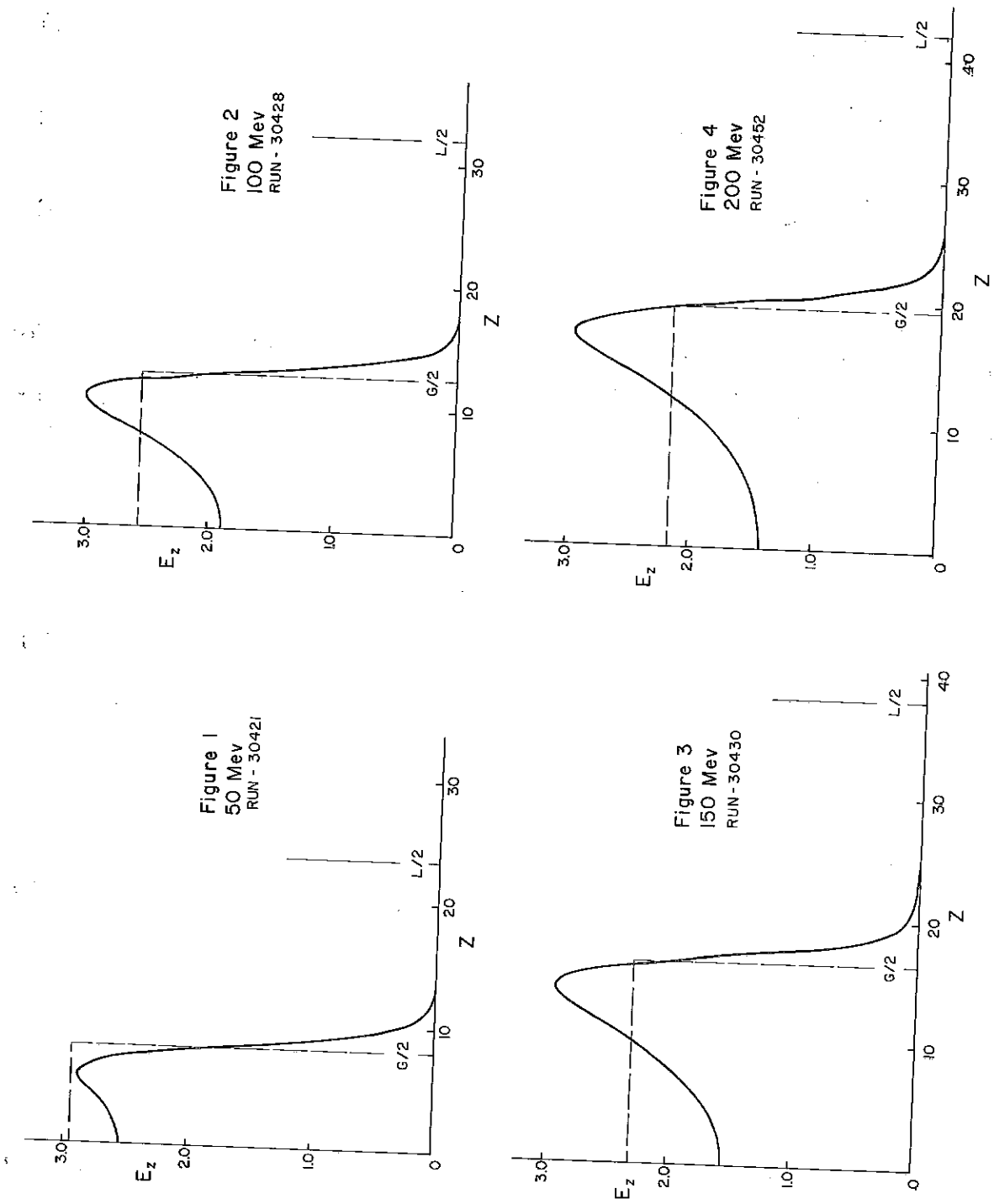
Figure 1
50 Mev
RUN - 30421
Figure 2
100 Mev
RUN - 30428
Figure 3
150 Mev
RUN - 30430
Figure 4
200 Mev
RUN - 30452
E_z
Z
G/2
L/2
0
1.0
2.0
3.0
10
20
30
40

$$\frac{\partial E_r}{\partial z} - \frac{\partial E_z}{\partial r} = -\frac{1}{c}\frac{\partial B_\theta}{\partial t} \tag{1}$$

$$\frac{1}{r}\frac{\partial}{\partial r}(r\,E_r) + \frac{\partial E_z}{\partial z} = 0 \tag{2}$$

$$-\frac{\partial B_\theta}{\partial z} = \frac{1}{c}\frac{\partial E_r}{\partial t} \tag{3}$$

$$\frac{1}{r}\frac{\partial (r\,B_\theta)}{\partial r} = \frac{1}{c}\frac{\partial E_z}{\partial t} \quad . \tag{4}$$

We now assume that we know the fields on the axis of the linac [i.e., $\mathcal{E}_z(0,z,t)$], and we attempt to get a satisfactory expression for the fields off the axis in terms of $\mathcal{E}_z(0,z,t)$. We employ an iterative procedure to get the n^{th} order field in terms of the $n-1^{st}$ order solution. This procedure yields the following expressions for $\mathcal{E}_z(r,z,t)$, $\mathcal{E}_r(r,z,t)$ and $B_\theta(r,z,t)$.

$$\mathcal{E}_z(r,z,t) = \mathcal{E}_z(0,z,t) - \frac{r^2}{4}\left(\frac{\partial^2 \mathcal{E}_z(0,z,t)}{\partial z^2} - \frac{1}{c^2}\frac{\partial^2 \mathcal{E}_z(0,z,t)}{\partial t^2}\right) + \text{terms in } r^4 \text{ and higher} \tag{5}$$

$$\mathcal{E}_r(r,z,t) = -\frac{r}{2}\frac{\partial \mathcal{E}_z(0,z,t)}{\partial z} + \frac{r^3}{16}\frac{\partial}{\partial z}\left(\frac{\partial^2 \mathcal{E}_z(0,z,t)}{\partial z^2} - \frac{1}{c^2}\frac{\partial^2 \mathcal{E}_z(0,z,t)}{\partial t^2}\right) + \text{terms in } r^5 \text{ and higher} \tag{6}$$

$$B_\theta(r,z,t) = \frac{r}{2c}\frac{\partial \mathcal{E}_z(0,z,t)}{\partial t} - \frac{r^3}{16\,c}\frac{\partial}{\partial t}\left(\frac{\partial^2 \mathcal{E}_z(0,z,t)}{\partial z^2} - \frac{1}{c^2}\frac{\partial^2 \mathcal{E}_z(0,z,t)}{\partial t^2}\right) + \text{terms in } r^5 \text{ and higher} \; . \tag{7}$$

We now proceed to use these fields to evaluate the energy gain and the radial impulse imparted to a particle on traversing a particular linac cell.

The energy gain ΔE is

$$\Delta E = \int_{\text{path}} \vec{\mathcal{E}} \cdot \vec{ds} = \int_{\text{path}} (\mathcal{E}_z \, dz + \mathcal{E}_r \, dr)$$

which can be written, with the fields above, as

$$\Delta E = \mathcal{E}_z (0, z, t) \, dz - \frac{r^2}{4} \int \left(\frac{\partial^2 \mathcal{E}_z (0, z, t)}{\partial z^2} - \frac{1}{c^2} \frac{\partial^2 \mathcal{E}_z (0, z, t)}{\partial t^2} \right) dz - \int \frac{r}{2} \frac{\partial \mathcal{E}_z (0, z, t)}{\partial z} \, dr \, . \qquad (8)$$

Before evaluating these integrals, we make a few definitions. We define the cavity length L and the average axial electric field E_o by

$$\int_{\text{cell}} dz = L$$

and

$$\int E_z (z) \, dz = E_o \, L \, .$$

We define the origin of z by requiring

$$\int E_z (z) \sin \frac{2 \pi z}{L} \, dz = 0 \, .$$

We define the transit time T by the relation

$$\int E_z (z) \cos \frac{2 \pi z}{L} \, dz = E_o \, L \, T$$

and we define an S factor by

$$\int z\, E_z\,(z) \sin \frac{2\pi z}{L}\, dz = E_o\, L^2\, S\,.$$

I will outline the evaluation of the first integral on the right-hand side of Eq. (8) to illuminate the meaning of the terms α and S.

$$\int \mathcal{E}_z\,(0, z, t)\, dz = \int E_z\,(z) \cos(\omega t + \phi)\, dz$$

where $t = \frac{z}{V}$. Let $\frac{1}{V} = \frac{1}{V_s}(1 + \alpha)$, where V_s is the velocity of the synchronous particle. Noting that $\omega t = \frac{2\pi z}{L}(1 + \alpha)$, we write

$$\int \mathcal{E}_z\,(0, z, t)\, dz = \int E_z\,(z) \cos\left(\frac{2\pi z}{L} + \phi + \frac{2\pi z\alpha}{L}\right) dz$$

$$= \int E_z\,(z) \left[\cos\left(\frac{2\pi z}{L} + \phi\right) \cos\frac{2\pi z\alpha}{L} - \sin\left(\frac{2\pi z}{L} + \phi\right) \sin\frac{2\pi z\alpha}{L}\right] dz$$

$$= \int E_z\,(z) \left[\left(\cos\frac{2\pi z}{L} \cos\phi - \sin\frac{2\pi z}{L} \sin\phi\right) - \right.$$

$$\left. - \frac{2\pi z\alpha}{L}\left(\sin\frac{2\pi z}{L} \cos\phi + \cos\frac{2\pi z}{L} \sin\phi\right)\right] dz$$

where we have let $\cos\frac{2\pi z\alpha}{L} = 1$ and $\sin\frac{2\pi z\alpha}{L} = \frac{2\pi z\alpha}{L}$.

For a symmetric gap where $E_z\,(z)$ is an even function of z, two of the four terms in the latter expression integrate to zero, and we are left with

$$\int \mathcal{E}_z\,(0, z, t)\, dz = E_o\, L\,(T - 2\pi\alpha S) \cos\phi\,.$$

The factor $(T - 2\pi\alpha S)$ can be interpreted as a transit time factor for particles whose velocity is different from the synchronous velocity (i.e., for $\alpha \neq 0$).

When we evaluate the other two integrals on the right-hand side of Eq. (8), the expression for the energy gain for one linac cell is

$$\Delta E = E_o L \left\{ \left(1 + \frac{\pi^2 r^2}{\lambda^2 \beta^2 \gamma^2}\right) (T - 2\pi \propto S) \cos \phi - \frac{r r' \pi}{\beta \lambda} T \sin \phi \right\}. \tag{9}$$

To evaluate the radial impulse imparted to the particle on crossing a gap, we write

$$\Delta p_r = \int_{\text{path}} |\vec{F}_r| \, dt = \int_{\text{path}} e \left(\mathcal{E}_r - \frac{V B_\theta}{c} \right) dt . \tag{10}$$

Using the expression for the fields given in Eqs. (6) and (7), and eliminating third and higher orders in the variable r, we find the expression for $\Delta r'$ to be

$$\Delta r' = - \frac{e\pi}{m_o c^2 \lambda} \frac{E_o L}{\beta^3 \gamma^3} r \sin \phi \, (T - 2\pi \propto S) \tag{11}$$

where $\Delta r' = \dfrac{\Delta p_r}{m_o c \beta \gamma}$.

It is of interest now to compared the factor $T_a - 2\pi \propto S_a$ with the transit time function for a uniform field distribution. The analytic expression for the transit time factor for uniform field distribution perturbed by a bore hole of radius "a",

$$T_u = \frac{\sin \frac{\pi G}{\beta \lambda}}{\frac{\pi G}{\beta \lambda}} \frac{I_o \left(\frac{2\pi r}{\gamma_s L} \right)}{I_o \left(\frac{2\pi a}{\gamma_s L} \right)},$$

can be expressed as

$$(T_u - 2\pi \propto S_u) \, I_o \left(\frac{2\pi r}{\gamma_s L} \right) \tag{12}$$

where

$$T_u = \frac{\sin \frac{\pi G}{L}}{\frac{\pi G}{L}} \qquad \frac{1}{I_o\left(\frac{2\pi a}{\gamma_s L}\right)}$$

and

$$S_u = \frac{1}{2\pi I_o\left(\frac{2\pi a}{\gamma_s L}\right)} \left(\frac{\sin \frac{\pi G}{L}}{\frac{\pi G}{L}} - \cos \frac{\pi G}{L} \right)$$

and α has the same meaning as above.

First of all, we note that the radial dependence of Eq. (12) is the same as that of the first term in Eq. (9). Secondly, it is of interest to compare the T_a and S_a obtained from the actual field distribution with the T_u and S_u derived from the uniform field distribution. A comparison is given in the Table I for some typical linac geometries ranging in energy from 2 to 200 MeV.

TABLE I

MESSYMESH Run Number	Energy (MeV)	L cm	G cm	A cm	T_a	S_a	T_u	S_u
25003	2.16	10	2.5	1	0.7354	0.0727	0.8198	0.0280
30243	18.21	29	10	1	0.7726	0.0663	0.8066	0.0546
30421	49.80	47	16	1.5	0.7775	0.0655	0.8126	0.0535
30428	97.73	64	25	1.5	0.7101	0.0839	0.7641	0.0682
30430	148.05	76	33	2	0.6262	0.1055	0.7139	0.0811
30452	195.41	84	39	2	0.5636	0.1183	0.6786	0.0902

From the Table I, one can see that the T_a is from 5 to 16% lower than T_u, and that S_a is 20 to 30% higher than S_u with exception of the 2 MeV results in which S_a is 150% higher than S_u. The actual field distributions, shown in Figs. 1 through 4, were obtained from the last four MESSYMESH runs presented in Table I.

I have made some exploratory runs to determine the transverse acceptance and the phase acceptance for an eight-tank 200 MeV linac. A brief description of the linac is given in Table II. It is described in more detail in MURA Technical Note 472 by Young and Austin. The results of

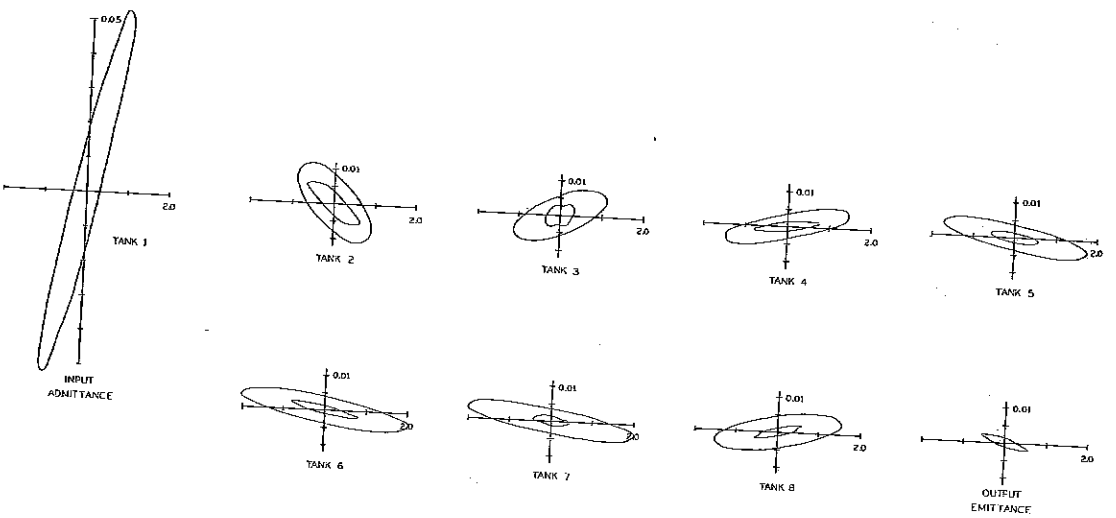

Figure 5 TRANSVERSE PHASE SPACE PLOTS

OUTER CURVE ADMITTANCE OF TANK N

INNER CURVE EMITTANCE OF LINAC THROUGH TANK N-1

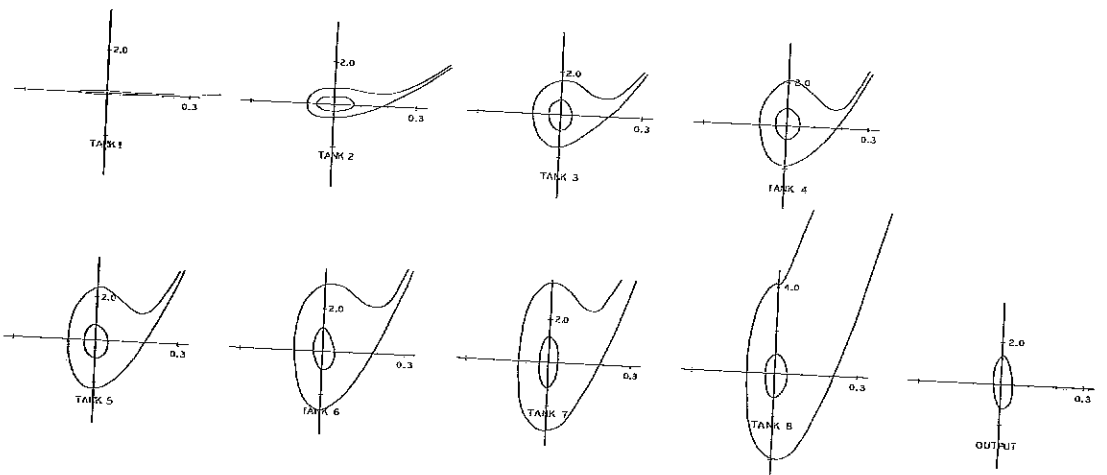

Figure 6 PHASE ACCEPTANCE PLOTS

OUTER CURVE ACCEPTANCE OF TANK N

INNER CURVE PHASE PLOT OF LINAC ACCEPTANCE TRANSFORMED THROUGH TANK N-1

these investigations, which I think are self-explanatory, are shown in Figs. 5, 6, 7, and 8.

TABLE II

Tank No.	1	2	3	4	5	6	7	8
Energy (MeV)	15	46	75	102	128	153	177	200
E_o (MeV/m)	2.0	2.8	2.8	2.7	2.6	2.5	2.4	2.3
Length (m)	9.4	14.8	14.4	15.4	16.3	17.1	17.6	18.5
Power Actual (MW)	2.25	4.95	4.92	4.82	4.96	4.96	4.95	4.79
Total Length				123.5 m				
Total Power				36.6 MW				

WALKINSHAW: If you ignore the change in velocity of the particle across a gap and do the analysis as you have done, then you can show that the correct formula is $E_o L$ times that next term in the brackets I_o of some factor of r, then the transit time factor and then cos ϕ . I don't understand where the term in $\propto S$ comes in unless you are assuming that the particle velocity was changing as it crossed the gap.

SWENSON: The factor $(T - 2\pi \propto S)$ is effectively a transit time factor for particles of energy E near the synchronous energy E_s. T is the transit time factor for the synchronous particle. The parameter $\propto$ is defined in the text, but is a function of $(E - E_s)$. $\propto$ is zero for $E = E_s$.

MILLS: Let me make some comments about this work. About four years ago when we became interested in linacs we began looking mostly for means for computational studies. Our starting point was the report by Panofsky published in 1953. You can see that these formulae are extensions of those in his report.

WALKINSHAW: There is in fact a paradox in some of his formulas.

MILLS: Your specific question about the second term can be answered the following way: In Panofsky's work, only the part of the fields that are traveling with the particle are included. This work includes all the other harmonics in the gap also. About two years ago, Phil Morton began his more complete treatment of the problem which many of you have seen.

WALKINSHAW: I think you will find that Panofsky now would accept that this formula is wrong.

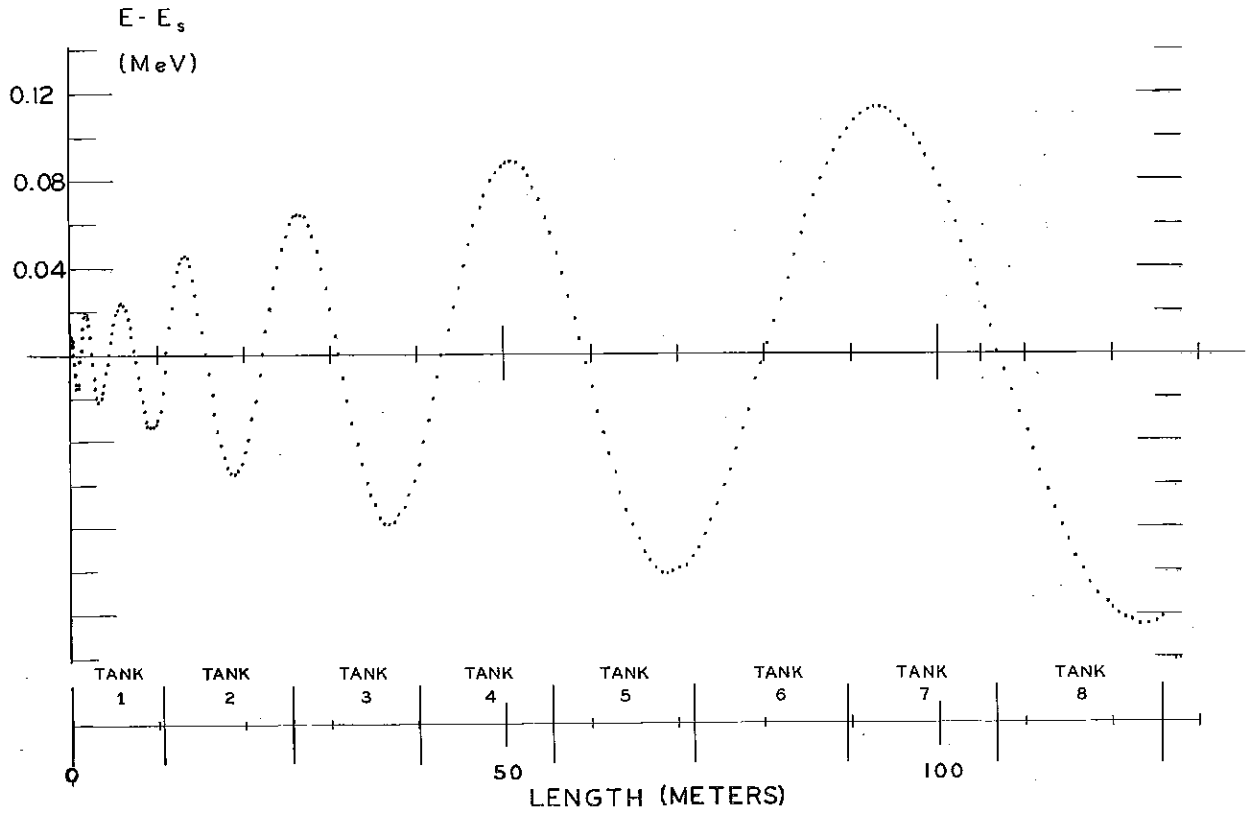

Figure 7 ENERGY OSCILLATION

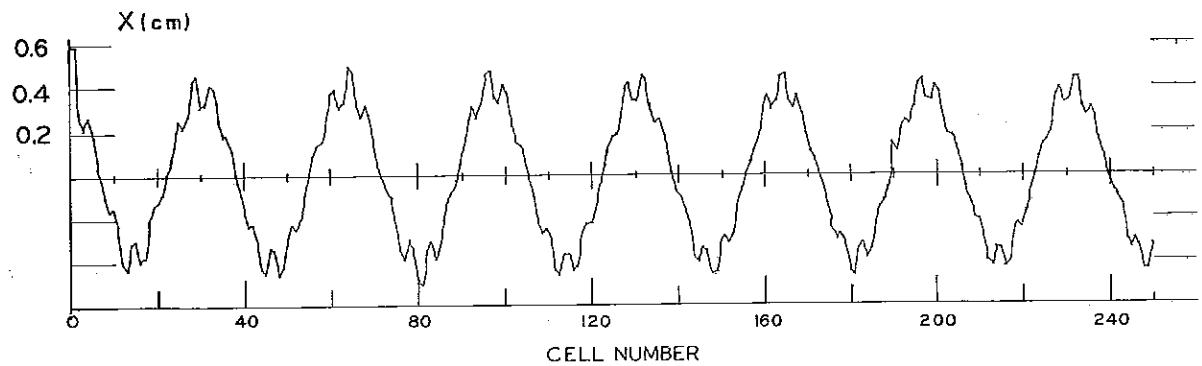

Figure 8 TRANSVERSE OSCILLATION

MILLS: I am not sure which one you mean.

WALKINSHAW: Well, I think that in calculating his transit time factor he put in a term which was dependent on the velocity. This is probably all right when you consider one gap, but when you change this into a differential equation, and consider the phase oscillations of the particle, you find that the phase damping is different from that in a harmonic traveling wave case. This is very curious because you are saying that the harmonic terms are causing some kind of extra phase damping. We wondered once if this was caused by some curious alternating gradient. Then we carried out the gap approximations, and discovered that there are indeed other second-order terms which cancel out the first one, and you come back to the simple approximation.

MILLS: The primary motivation here is the investigation of coupling between the axial and transverse motions. This is only intended to be an expansion in the next leading terms. There is another separate question which I think is related to what you said and that was the following: How adiabatic is the motion? This is a question which was investigated separately by Young and reported in 1961. Indeed the phase motion is not adiabatic in the low energy part of the linac.

WALKINSHAW: I think that the correct answer is the one that you get when you take the harmonic component only. We are quite sure of this. We spent a long time on this and corresponded with Panofsky. He agreed that there was this curious effect. It is quite complicated. What Panofsky was doing here was to integrate across one gap. You have to change this into the differential equation. If you do this by matrix techniques keeping in all higher order terms, including velocity variation, you find the modification to all the terms will cancel exactly the term you have on the board. The explanation that you are tempted to look for is that the higher harmonics, in some curious way, are causing some coherent effect on the linac. This is what started us off; we couldn't really see why this should be so. I think you will find that if you do this properly the harmonic term will in fact give you as accurate an answer as you want.

MILLS: I believe this is done properly in Morton's thesis. I did check to see the nature of the next order term and in fact when one totals up all the harmonics, just those present in this term are there.

OHNUMA: What kind of γ and β do you use? The γ and β are changing continuously across the gap.

SWENSON: We neglect the change of velocity across the gap and use for γ and β some sort of mean value.

OHNUMA: Another question. As I mentioned when I talked, this kind of effect or this kind of calculation might be important when energy is, say, below 50 MeV. But then I seriously doubt, aside from the academic question, in a practical design what the real importance of this kind of calculation would be. This is a point which is not completely clear, because there are all kinds of factors coming into the beam dynamics. Unless the effect is very serious, I do not see the particular importance in an exact point-by-point integration.

GLUCKSTERN: With regard to the point that Bill Walkinshaw made, I think there is another motivation for trying to include some velocity dependence in the formula. I agree with you in what you say in that, if the particle is trapped, then the only thing that can matter is the wave component which is traveling with the velocity of the particle. But an additional quantity of interest, if particles escape longitudinally, is the place where they strike the bore or the irises and cause radioactivity. To answer this question, I think one has to worry about the other wave components. If a particle escapes from a fish, if it is near the border, it will act as if it is stable for quite a way. And not until it gets far enough away so that all the waves average to zero can you take it as not having a change in energy.

WALKINSHAW: Well, I think if you truly analyze your performance, the higher order harmonics are traveling at such a vastly different phase velocity from the particle itself that the effect averages very quickly.

GLUCKSTERN: That is as long as the particle is traveling with the bunch.

WALKINSHAW: Oh, I see. You are saying you may trap them in some of the others.

GLUCKSTERN: No, I was referring to the fundamental wave component only, but for a particle traveling with almost the right velocity. When a particle escapes from a bucket, until it gets to a position where it does not oscillate very much, I think that the effects of the other waves will have to be taken into account.

WALKINSHAW: (Continuation of earlier discussion.) This paradox is a very interesting and amusing one really, because when we saw that the phase damping is different from the harmonic traveling wave case, we started to look for a physical explanation, and you can find one. The reason is this: if you look at the energy gained going across the gap, it will depend on the time it takes across the gap. Now if the particle is making phase oscillations, this means that it is taking different times during its phase oscillation. Part of the time it is going faster across

the gap, in which case it gains more energy, and then when it spins through half its oscillation, it gains less and you feel that you have some kind of integrated effect that could cause an increase in the rate of damping. Now that appears to be an explanation, but is the wrong explanation.

SYMON: I do not understand how two different approximations can give two different rates of damping because you can calculate the damping independently of any approximation just from the fact that the area on an energy time plot is rigorously constant independent of any approximations. That means that if the formula gives you a value which disagrees with that, it must be incorrect.

WALKINSHAW: I agree. That is where we started. We got two different rates of damping according to two approximations and then we tried to find out which one is correct and we decided it was the harmonic traveling wave approximation.

SYMON: But you can decide which one is correct by which one gives you the correct area in the end?

WALKINSHAW: Yes, quite so.

FEATHERSTONE: Regarding Dr. Ohnuma's question as to the value of this sort of calculation, I am sort of on the outside here, but looking at the figures over there, for ΔE, the difference between the flat and actual case amounts to more than 10%, which for the person who has to run these things means more than 20% in rf power. I think this is quite significant.

SWENSON: I believe Dr. Ohnuma questioned the significance of the velocity dependent term rather than the term which gives 10% effect which you mentioned. That really results from a better calculation of the transit time factor based on the actual fields in the gap.

BEAM DYNAMICS CALCULATIONS FOR ALVAREZ-TYPE LINEAR ACCELERATORS*

Marvin Rich
Los Alamos Scientific Laboratory, University of California
Los Alamos, New Mexico

I. Introduction

Detailed beam dynamics studies for Alvarez-type linear accelerators have generally been done on high speed computers using impulse-type approximations to simulate the particle acceleration within a gap or direct numerical integrations of the equations of motion. In this summary we would like to describe a procedure for studying such beam dynamics which retains most of the accuracy of the numerical integration without an excessive loss of computational speed as compared to the impulse approximation method. In addition, the results of some calculations for the proposed LASL meson factory will be presented.

Briefly, the procedure which has been used consists of assuming that the axial electric field within a gap between drift tubes is spatially constant and zero within the drift tubes. (A more general axial field could be used but with added complications.) This is as opposed to the more usual procedure of using the principal harmonic of the axial field within the gap. Using Maxwell's equations and the axial field form, the off-axis electric and magnetic fields can be obtained as a power series in the radial coordinate, r. This has been done through terms in r^3. In addition, one obtains radial and longitudinal impulsive terms which a particle will experience on entering or leaving a gap. Using the electromagnetic fields obtained in this way, an approximate solution to the relativistic equations of motion for a particle within a gap has been constructed. The impulses at the extremities of the gap are, of course, easily treated.

Comparisons of accelerator calculations using the approximate solutions mentioned above and an accurate numerical integration of the particle equations of motion have been made. Agreement to about four significant figures in energy and phase (absolute phase, not phase relative to the accelerator design particle) was found after passage of particles through 250 gaps. Similar comparisons using an impulse approximation treatment with the same accelerator design were noticeably poorer, particularly with respect to the final phase.

*Work performed under the auspices of the U. S. Atomic Energy Commission.

II. Method of Calculation

Only an outline of the computational procedure will be given. This may be divided into three parts:

(a) the form for the electromagnetic fields within a gap;
(b) the approximate solution of the particle equations of motion;
(c) the beam dynamics code.

A. The Gap Fields

For the purpose of the calculation it is assumed that the z-component of the electric field has the following spatial form on the axis, $r = 0$:

$$\begin{aligned} E_z(0,z) &= 0 && -L/2 \le z < -g/2 \\ &= E_0 f(z) && -g/2 \le z \le g/2 \\ &= 0 && g/2 < z \le L/2 \end{aligned} \tag{1}$$

where L is the distance between drift tube centers as illustrated in Fig. 1 and g is the gap length. The field may be thought of as periodic with period L and its time dependence is taken as $\cos \omega t$.

Using the knowledge of the E_z field at $r = 0$ and Maxwell's equations, the off-axis fields in the gap may be obtained as a power series in r, the first few terms of which give

$$\left.\begin{aligned} E_z(r,z,t) &= E_0 F(r,z) \cos \omega t \\ E_r(r,z,t) &= -E_0 G(r,z) \cos \omega t \\ B_\theta(r,z,t) &= -E_0 Q(r,z) \sin \omega t \end{aligned}\right\} \quad -g/2 \le z \le g/2 \tag{2}$$

where

$$\begin{aligned} F(r,z) &= f(z) + \frac{1}{4} r^2 S(z) \\ G(r,z) &= \frac{1}{2} r \left[\delta(z + g/2) f(z) - \delta(z - g/2) f(z) + \frac{df}{dz}\right] \\ &\quad + \frac{1}{16} r^3 \frac{dS(z)}{dz} \\ Q(r,z) &= \frac{1}{2} r \frac{\omega}{c^2} f(z) + \frac{1}{16} r^3 \frac{\omega}{c^2} S(z) \end{aligned} \tag{3}$$

and

$$S(z) = -\frac{\omega^2}{c^2} f(z) - \frac{d}{dz}\left[\delta(z + g/2) f(z) - \delta(z - g/2) f(z)\right] .$$

If the δ-functions are treated as slightly smeared δ-functions, representing the fall off of the fields within the drift tube hole, and it is assumed that a particle does not change its position or velocity appreciably over the fall-off region, then these terms merely contribute an impulse to a particle on entering and leaving a gap. The approximate effect of this impulse is given below in Eq. (7). Neglecting the impulse producing terms, the fields within a gap are

$$\left.\begin{aligned} E_z &= E_0 f(z)\left[1 - \frac{1}{4}\frac{\omega^2}{c^2} r^2\right] \cos \omega t \\ E_r &= -E_0 \frac{df(z)}{dz}\left[\frac{1}{2} r - \frac{1}{16}\frac{\omega^2}{c^2} r^3\right] \cos \omega t \\ B_\theta &= -E_0 \frac{\omega}{c^2} f(z)\left[\frac{1}{2} r - \frac{1}{16}\frac{\omega^2}{c^2} r^3\right] \sin \omega t \end{aligned}\right\} \quad -g/2 < z < g/2 . \quad (4)$$

In the following, $f(z)$ has been taken equal to unity, giving $E_r = 0$ within the gap.

B. Approximate Solution of the Equations of Motion

In Cartesian coordinates, the relativistic equations of motion for a particle moving in an electromagnetic field of the sort given in Eq. (3) are

$$\left.\begin{aligned} \frac{du_1}{dt} &= \frac{e}{m}\left[E_r - v_3 B_\theta\right]\frac{x_1}{r} \\ \frac{du_2}{dr} &= \frac{e}{m}\left[E_r - v_3 B_\theta\right]\frac{x_2}{r} \\ \frac{du_3}{dt} &= \frac{e}{m}\left[E_z + (v_1 x_1 + v_2 x_2) B_\theta / r\right] \end{aligned}\right\} \quad (5)$$

$$\frac{dx_i}{dt} = u_i/\gamma = v_i \qquad i = 1, 2, 3 \quad (6)$$

where indices 1, 2, and 3 correspond to the x, y, and z directions, respectively, $r = \sqrt{x_1^2 + x_2^2}$, and $\gamma = \sqrt{1 + \vec{u}^2/c^2}$. From Eqs. (2), (3), and (5) it can be shown that the change in u_i due to the impulse occurring on entering a gap is approximately

$$\Delta u_1 = -\frac{e}{m} E_0 f(-g/2) x_1 \left(\frac{1}{2} - \frac{1}{16}\frac{\omega^2}{u_3^2} r^2\right)\frac{\gamma}{u_3} \cos \omega t$$

$$\Delta u_2 = -\frac{e}{m} E_0 f(-g/2) x_2 \left(\frac{1}{2} - \frac{1}{16}\frac{\omega^2}{u_3^2} r^2\right)\frac{\gamma}{u_3} \cos \omega t \qquad (7)$$

$$\Delta u_3 = -\frac{e}{m} E_0 f(-g/2)\frac{\gamma}{u_3}\left(\frac{1}{4} r^2 \omega \gamma / u_3 \sin \omega t + \frac{1}{16}\frac{\omega^2}{c^2} r^2 \frac{u_1 x_1 + u_2 x_2}{u_3} \cos \omega t\right)$$

where the coordinates, u components, and time are those corresponding to the arrival at the gap. Similar equations with opposite signs apply on leaving the gap.

A relatively accurate approximate solution of the equations of motion across the gap can be obtained by assuming that the components of velocity may be written in the form

$$v_i(t) = v_0^{(i)} + v_1^{(i)} t + f^{(i)}\left[\cos(\omega t + \psi_0) - \cos \psi_0\right] + g^{(i)}\left[\sin(\omega t + \psi_0) - \sin \psi_0\right] \qquad (8)$$

where ψ_0 is the phase of the cavity field when the particle enters the gap and the z-coordinate and time at the beginning of the gap are taken as $z = 0$ and $t = 0$. Equation (8) is actually part of a more general ansatz that can be made for the velocity. The coordinates are then approximately

$$x_i(t) = x_0^{(i)} + \left[v_0^{(i)} - f^{(i)} \cos \psi_0 - g^{(i)} \sin \psi_0\right] t + \frac{1}{\omega} f^{(i)}\left[\sin(\omega t + \psi_0) - \sin \psi_0\right] - \frac{1}{\omega} g^{(i)}\left[\cos(\omega t + \psi_0) - \cos \psi_0\right]. \qquad (9)$$

If the coordinates and velocities given in Eqs. (8) and (9) are inserted into Eq. (5) for the u_i, using the previously described fields with $f(z) = 1$, the u_i can be obtained upon integration. These values of u_i and the relation $v_i = u_i/\sqrt{1 + \vec{u}^2/c^2}$ may then be used to identify the coefficients $v_1^{(i)}$, $f^{(i)}$, and $g^{(i)}$. When small terms are neglected, one obtains

$$
\begin{aligned}
v_1^{(i)} &= \left[u_1^{(i)} - v_0^{(i)} \vec{v}_0 \cdot \vec{u}_1 / c^2 \right] / \gamma_0 \qquad i = 1, 2, 3 \\
f^{(1,2)} &= a^{(1,2)} / \gamma_0 \\
f^{(3)} &= - v_0^{(3)} \vec{v}_0 \cdot \vec{a} / (\gamma_0 c^2) \\
g^{(1,2)} &= - v_0^{(1,2)} \vec{v}_0 \cdot \vec{b} / (\gamma_0 c^2) \\
g^{(3)} &= b^{(3)} / \gamma_0 - v_0^{(3)} \vec{v}_0 \cdot \vec{b} / (\gamma_0 c^2)
\end{aligned}
\tag{10}
$$

where

$$
\gamma_0 = 1 / \sqrt{1 - \vec{v}_0^{\,2} / c^2} \quad , \quad \text{and}
$$

$$
u_1^{(i)} = - \frac{e}{m} E_0 \frac{\cos \omega_0}{c^2} \left\{ \left(\frac{1}{2} - \frac{1}{16} \frac{\omega^2}{c^2} r^2 \right) v_0^{(i)} - \frac{1}{8} v_0^{(3)} x_0^{(i)} \frac{\omega^2}{c^2} \sum_{k=1}^{2} x_0^{(k)} v_0^{(k)} \right\}
$$

$$
a^{(i)} = - \frac{e}{m} E_0 \frac{v_0^{(2)}}{c^2} x_0^{(i)} \left(\frac{1}{2} - \frac{1}{16} \frac{\omega^2}{c^2} r_0^2 \right) \qquad i = 1, 2
$$

$$
b^{(i)} = \frac{e}{m} E_0 \frac{v_0^{(3)}}{\omega c^2} v_0^{(i)} \left(\frac{1}{2} - \frac{1}{16} \frac{\omega^2}{c^2} r_0^2 \right)
$$

$$
u_1^{(3)} = - \frac{e}{m} E_0 \frac{\sin \psi_0}{c^2} \left\{ \frac{\omega}{2} \sum_{k=1}^{2} x_0^{(k)} v_0^{(k)} - \left(\frac{1}{2} - \frac{1}{16} \frac{\omega^2}{c^2} r_0^2 \right) \sum_{k=1}^{2} v_0^{(k)2} \right\} \tag{11}
$$

$$
a^{(3)} = 0
$$

$$
b^{(3)} = \frac{e}{m} E_0 \frac{1}{\omega} \left(1 - \frac{1}{4} \frac{\omega^2}{c^2} r_0^2 \right) .
$$

In the limit of pure phase motion one has

$$
u_3 = u_0^{(3)} + \frac{e}{m} E_0 \frac{1}{\omega} \left[\sin (\omega t + \psi_0) - \sin \psi_0 \right]
$$

$$
v_3 = v_0^{(3)} + \frac{e}{m} E_0 \frac{1}{\omega \gamma_0^3} \left[\sin (\omega t + \psi_0) - \sin \psi_0 \right] \tag{12}
$$

$$
x_3 = x_0^{(3)} + \left[v_0^{(3)} - \frac{e}{m} E_0 \frac{1}{\omega \gamma_0^3} \sin \psi_0 \right] t - \frac{e}{m} E_0 \frac{1}{\omega^2 \gamma_0^3} \left[\cos (\omega t + \psi_0) - \cos \psi_0 \right] .
$$

C. The Beam Dynamics Code

The beam dynamics code which has been written using the above results is essentially the same as most such codes. However, the method for specification of the accelerator geometry is perhaps somewhat different from what is usual and should be described. Here, input values of stable phases and the g/L sequences for each tank are used to define an entering and an exiting phase of the "stable particle" in any gap, say gap n, by

$$\psi_{in}(n) = \psi_{stable} - \pi(g/L)_n$$

$$\psi_{out}(n) = \psi_{stable} + \pi(g/L)_n \ .$$

Starting at the end of the $(n-1)^{th}$ gap with longitudinal velocity v_{n-1}, the length of the $(n-1)^{th}$ drift tube is taken as

$$d_{n-1} = \left(\psi_{in}(n) - \psi_{out}(n-1) + 2\pi \right) \cdot v_{n-1}/\omega \ .$$

The length of the n^{th} gap and the velocity v_n at the end of this gap are obtained from Eq. (12), where the time to be used is $t = (\psi_{in}(n) - \psi_{out}(n))/\omega$ since the field was assumed to have phase $\psi_{in}(n)$ when the particle entered the gap and phase $\psi_{out}(n)$ when it left. If ϵ_0 is the energy gain per meter in the tank containing gap n, the constant E_0 appearing in Eq. (12) is

$$E_0(n) = 2\pi\epsilon_0 / \left[\sin\psi_{out}(n) - \sin\psi_{in}(n) \right] .$$

When the geometry of the accelerator has been determined, particles with varying initial energy, phase, and off-axis position and velocity can be carried through the structure using Eqs. (8) through (11). The time required to cross a gap is first obtained by iterating the $z \equiv x_3$-coordinate equation in the form

$$t_{k+1} = \left\{ g + \frac{f^{(3)}}{\omega} \left[\sin(\omega t_k + \psi_0) - \sin\psi_0 \right] - \frac{g^{(3)}}{\omega} \left[\cos(\omega t_k + \psi_0) - \cos\psi_0 \right] \right\} \times \left[v_0^{(3)} - f^{(3)} \cos\psi_0 - g^{(3)} \sin\psi_0 \right]^{-1}$$

using an initial guess of $t_0 = (\psi_{in} - \psi_{out})/\omega$. It has been found that two to three iterations are required for four-digit convergence. With this time interval, the remaining particle parameters are found by substitution into the remaining equations. Transit through quadrupole

magnets in drift tube sections is accomplished by the standard linear approximation.

The code also contains provisions for studying random errors in tank phase, tank or gap field amplitudes, drift tube and quadrupole misalignment, and quadrupole field magnitude.

III. Some Preliminary Results

Very little has been done as yet with regard to radial motion studies using the code described above. However, fairly extensive phase motion calculations have been made on a number of accelerator designs. In these, phase-energy acceptance "fishes" have been obtained with and without various types and combinations of random alignment and field errors, and output phase and energy spreads have been examined. A few examples of these results are given below for a geometry corresponding to the present design of the LASL meson factory. A definite statement about the effect of random errors will not be made since error studies for this geometry with many different sets of random inputs have not been completed.

Figure 2 shows a comparison of the phase and energy oscillations for a sample particle, using a numerical integration of the equations of motion (upper graph) and using Eqs. (12) (lower graph). The oscillatory solid lines give the phase motion and the dotted lines the energy deviations with respect to the stable particle. In Fig. 3 the acceptance fish for the design in Table I is shown (solid line) along with that when a particular set of random errors, specified in Table II, are introduced (dashed line). The effects of certain type errors, as tank-to-tank phase or field amplitude errors, have been found to have a more drastic effect on the acceptance region than when they are present as gap-to-gap errors. The remaining figures show the maximum phase and energy oscillation amplitudes of particles leaving the machine as a function of input phase and energy with and without the errors of Table II.

TABLE I

Specifications of the Drift Tube Portion of the LASL Linear Accelerator

Tank Number	1	2	3	4	5
Initial Energy	0.75	10.75	60.35	102.0	141.5
Final Energy	10.75	60.35	102.0	141.5	176.5
Stable Phase	- 26°	- 26°	- 26°	- 26°	- 26°
Energy gain/meter (MeV/m)	1.11	1.65	1.42	1.28	1.16
g/L Range	.2-.3	.19-.33	.35-.42	.40-.44	.43-.46
Drift Space (meters)	0.305	0.610	0.610	0.610	

TABLE II

Maximum Field and Alignment Errors for the Sample Problem

Axial Drift Tube Displacement Error	± 0.001 m
Field Error for Drift Tube Gaps	± 2%
Tank Field Error	± 2%
Tank Phase Error	± 1°

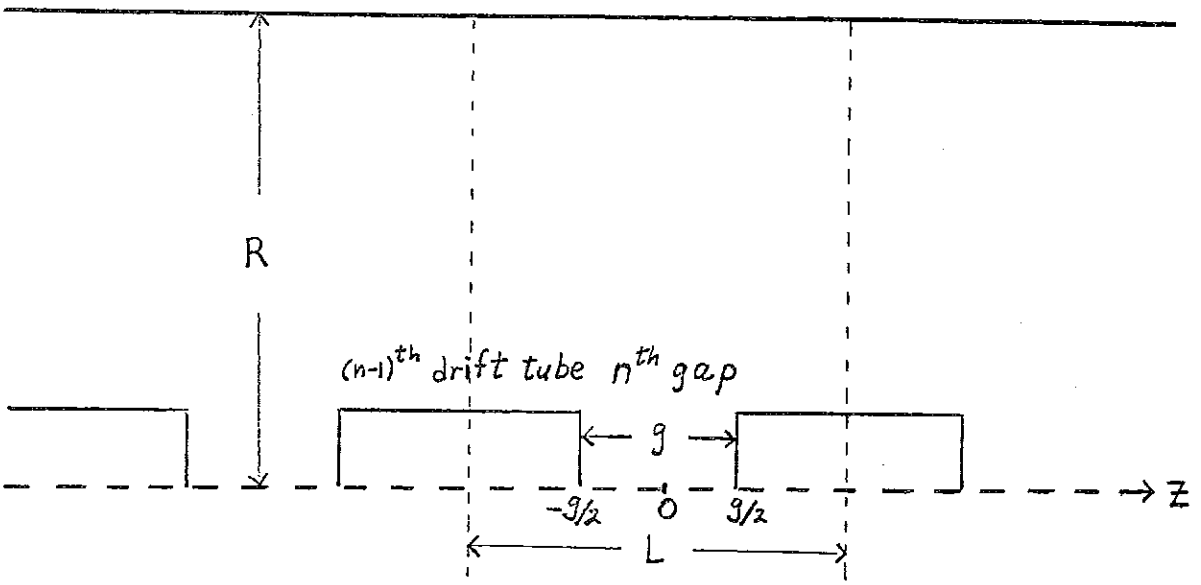

Figure 1: Schematic diagram of a drift tube section

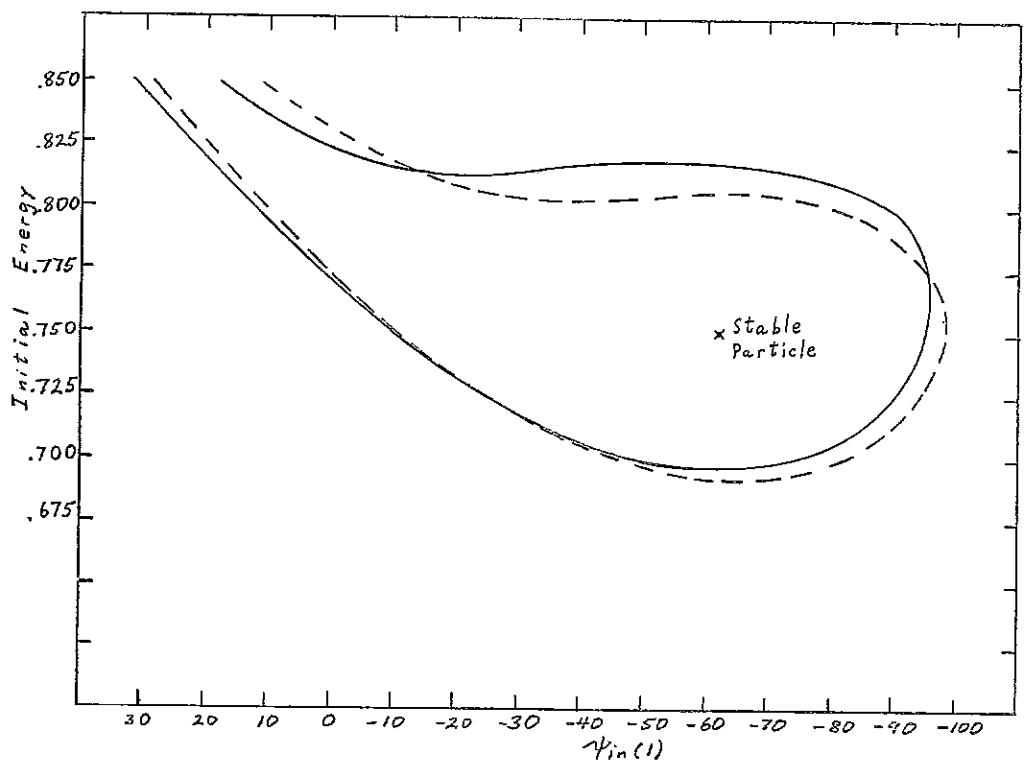

Figure 3: Phase-energy acceptance region for the accelerator geometry specified by Table I. The solid curve shows the acceptance when no errors are present and the dashed curve gives the acceptance for the errors of Table II.

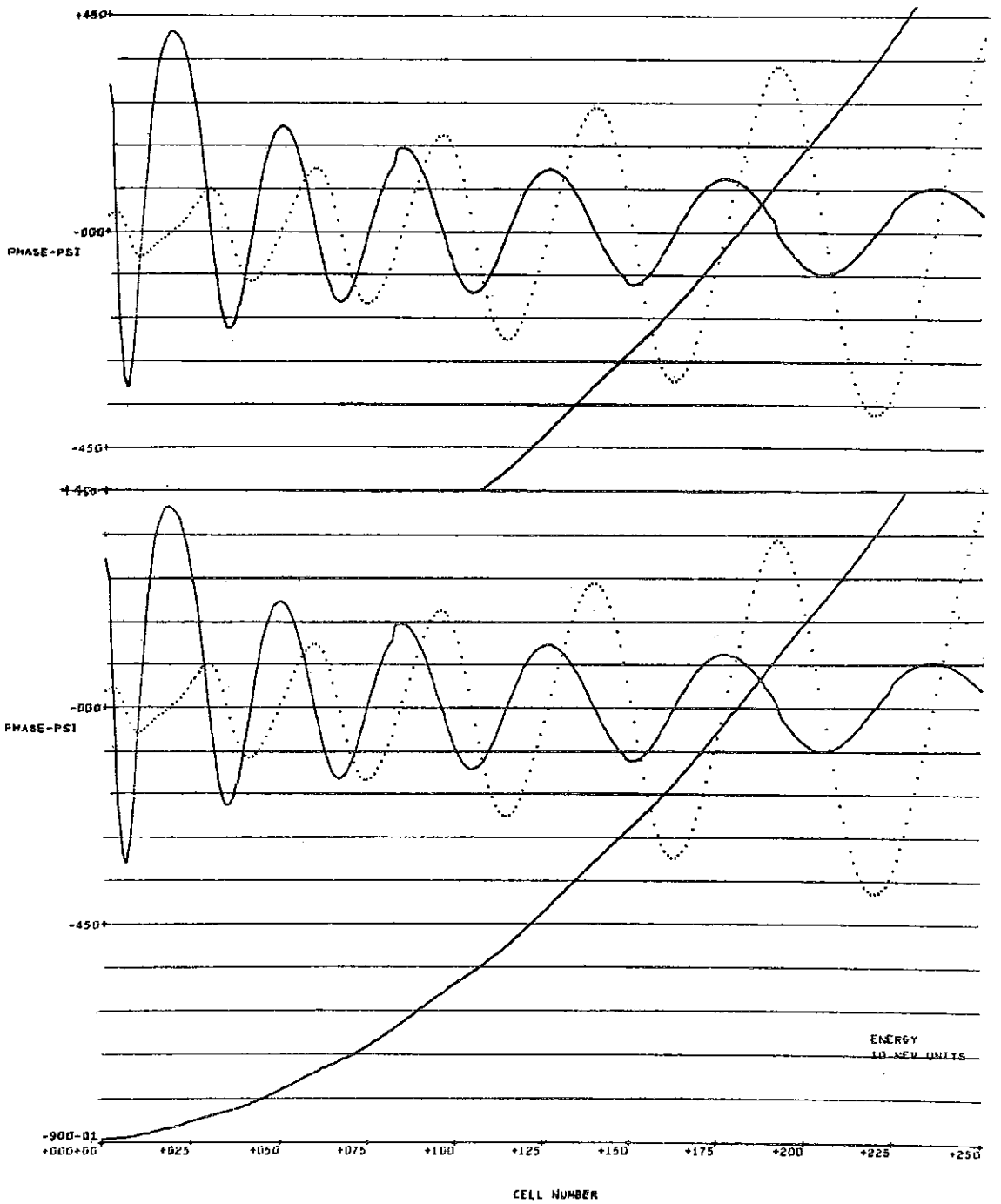

Figure 2: Comparison of phase and energy oscillations for a sample particle using a numerical integration of the particle equation of motion and using Equations (12).

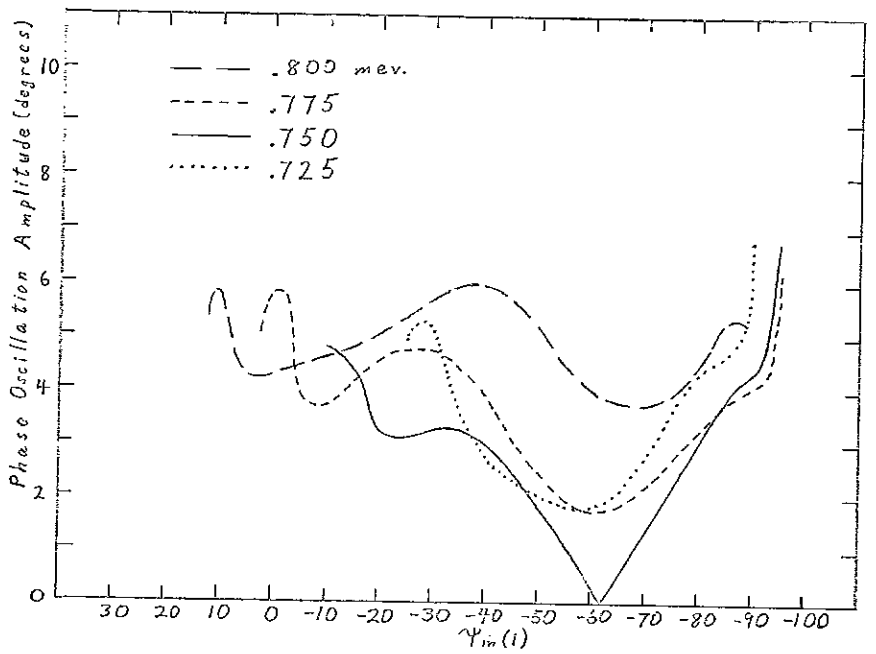

Figure 4: Final phase oscillation amplitude as a function of initial phase, $\psi_{in}(1)$, for various initial energies no errors are present.

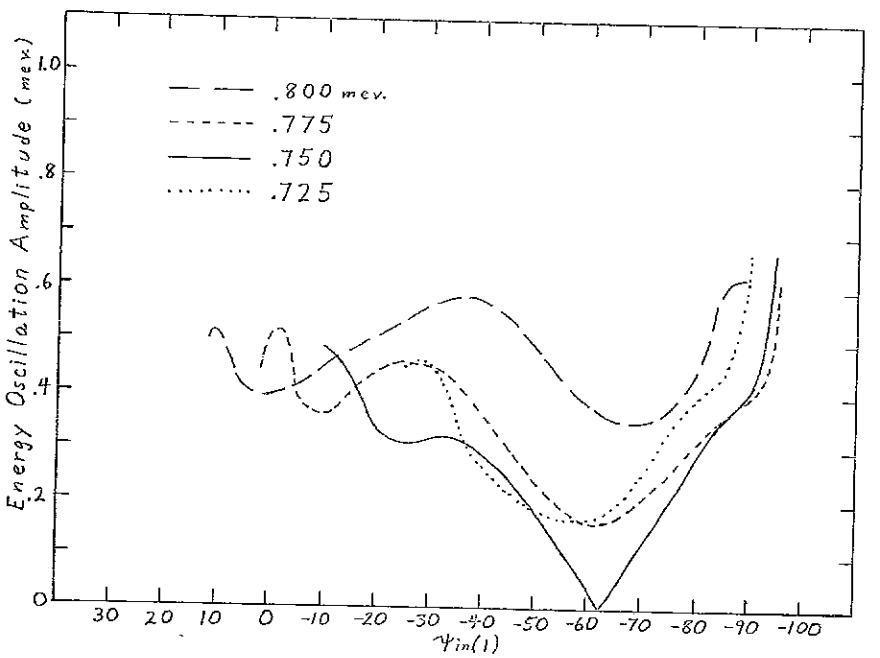

Figure 5: Final energy oscillation amplitude as a function of initial phase, $\psi_{in}(1)$, for various initial energies when no errors are present.

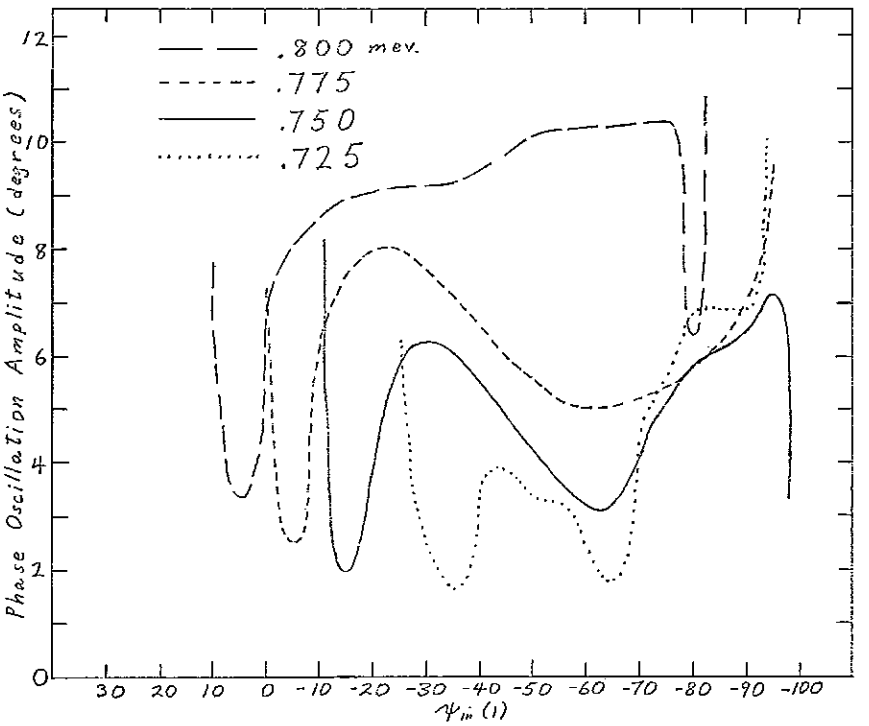

Figure 6: Final phase oscillation amplitude as a function of initial phase, $\psi_{in}(1)$, for various initial energies when the errors of Table II are present.

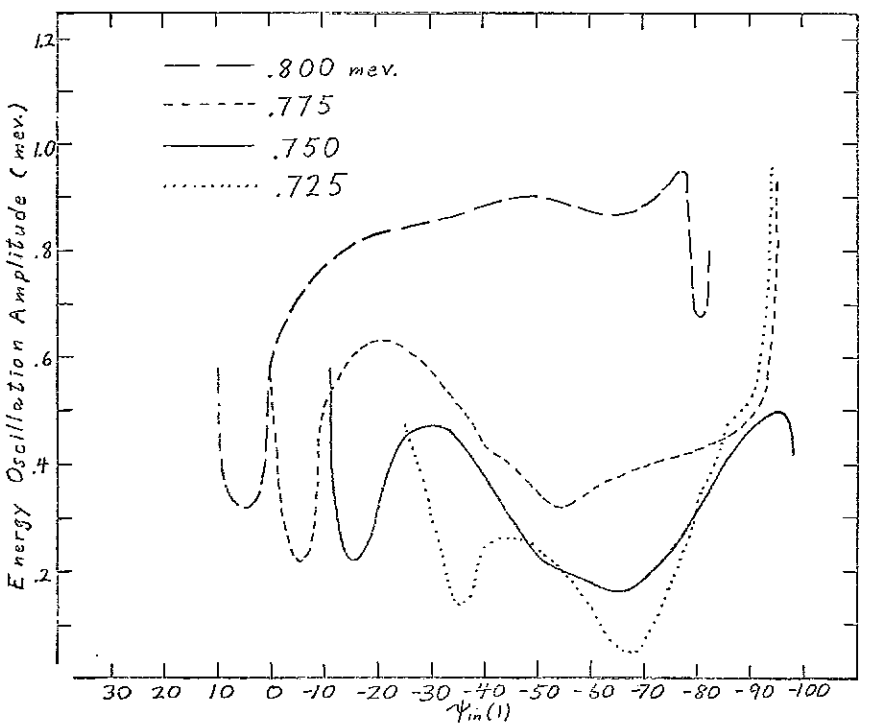

Figure 7: Final energy oscillation amplitude as a function of initial phase, $\psi_{in}(1)$, for various initial energies when the errors of Table II are present.

PERFORMANCE OF THE PS LINAC

C. S. Taylor
CERN

I. INTRODUCTION

With the exception of a recent increase of peak current to 75 mA the machine's characteristics remain much as reported at Dubna.[1] It has, however, revealed an appetite for deuterons.[2]

In these notes we shall mention briefly the minor changes which have taken place, describe some of the developments in the duoplasmatron and short column studies and in instrumentation, and conclude with some of the practical aspects of operation.

II. PREINJECTOR

1. RF Ion Source

Reductions in the height of the cathode protection brought increases in the source output current, with more than 300 mA observed in the laboratory. Further reductions however produced instability. A normal working current is 220 mA.

A miniature Faraday cup was used to scan the beam 30 mm from the source outlet and indicated a roughly triangular current density distribution.

2. Focusing and Beam Transport

The maximum current observed till now at the earth end of the column was 220 mA, but only 140 mA reached the input of the first tank.

The emittance "blow-up" factor of 2 to 3 in the lens and column is largely responsible for this loss, and is believed to be due in part to a time dependence. Recently we rearranged the column electrodes for greater acceleration at the source end with the object of reducing the lens strength required and hence of increasing the minimum particle velocity in the lens. This only reduced the 500 keV emittance by 10% for the same current.

It is believed that aperture limitation in the first triplet also contributes to the beam loss, and so the triplet diameter will shortly be in-

creased from 40 to 50 mm. The increase in peak current to 75 mA followed the widening of the second triplet aperture from 40 to 50 mm and the buncher aperture from 30 to 40 mm.

3. High Tension

New control circuits were installed towards the end of last year to permit:

(i) Automatic formation of the column, 0-500 kV in 3 hours, advisable after extended work on the column at atmospheric pressure.

(ii) Manual formation to 250 kV and automatic to 500 kV in 2 hours.

(iii) Fast automatic voltage rise 0-500 kV in 3 minutes.

Other items of interest are:

(a) An automatic restart circuit, which tries twice to reapply full H. T. after breakdowns and then shuts down the H. T. set. The breakdown rate averaged over 2-week runs varies between 1 and 3 per day.

(b) A multi-channel pen recorder for the continuous monitoring of voltage, column current and vacuum pressure simultaneously. A fourth channel is available for other parameters as required.

As a routine check on the state of the H. T. set, power factor is measured twice a month, and a precision measurement at the column divider resistor chain is made monthly in order to detect any incipient fault in this component. The present chain has been in operation for 2 years without trouble.

III. ADDITIONAL 500 KEV ELEMENTS

1. Harmonic Buncher

A second harmonic cavity has been added to the 200 Mc/s buncher cavity but awaits completion of the 400 Mc/s generator.

2. Chopper

An electrostatic deflector and power supply has been built to permit chopping of the 500 keV beam at the P.S. injection frequency (3 Mc/s) with variable mark to space ratio. This should relieve the linac rf system of charge which would lie between the synchrotron rf buckets and would be lost anyway. This will be installed and tested shortly.

IV. DUOPLASMATRON AND SHORT COLUMN DEVELOPMENTS

Following the plasma expansion cup developments in Leningrad, we have made some tests on different cup and extraction geometries. These were encouraging and the best beam for which we have complete figures was 450 mA at 100 kV in a phase volume of 0.59 cm mrad, giving a brightness of 130 mA cm^{-2} $sterad^{-1}$.

Assuming that high gradients are useful in controlling beam blow-up along the accelerating column, we have also been exploring the behaviour of different electrode materials in a re-entrant column arrangement. Use of a conventional column for these tests (13 - 40 kV sections)) enables us to put aside the air breakdown aspect of a short column for the time being while profiting from the range of potentials available for supplying intermediate electrodes.

The test setup consisted of the column within which two electrodes of the new material, carefully cleaned and polished, could be separated by a known gap. Cathode current, anode current, anode temperature, radiation level and voltage were monitored. The best materials were found to be low carbon stainless steel and titanium alloy as used for supersonic aircraft. At a pressure of 2×10^{-6} mm Hg provided by a mercury pump and liquid nitrogen baffle, we could hold 500 kV over a 10 cm gap.

Preparations are being made for testing the combination of duoplasmatron and high gradient gap in the laboratory. If successful, we plan to install it on the linac early in 1965.

V. INSTRUMENTATION

For emittance measurements the aperture-lens-aperture method is used where quick checks are required or where time dependence is suspected. Formerly it held another advantage in that it also yielded density distribution across the phase space, but the photographic emulsion method has now been developed to the point where the emulsion can be calibrated and made to supply contours as well as envelopes. These developments are described in references 3, 4.

The method was recently adopted for measurements of the first turn in the P.S., one wavelength downstream from the point of injection. A series of 24 exposures was made for different injection conditions, permitting estimates to be made of aberrations in the first P.S. wavelength, the acceptance of this section, and the matching achieved.

VI. OPERATION

1. Machine Reliability

The scheduled P.S. time which is lost due to linac faults remains at around 2% in spite of a fairly serious breakdown in May when 48 hours were lost in stripping down on FTH cavity and replacing the input loop which had flashed across at a metal-epoxy joint.

The FTH 470 tubes themselves have averaged 7000 hours, with one lasting for 11,000 hours.

2. Machine Stability

The pulse-to-pulse stability remains good but the P.S. is rather sensitive to mains voltage variations. The linac contribution to this seems to come from the modulators which are at present not regulating very efficiently.

There are certain major items of equipment which one expects to run without much attention, for example, the mercury vacuum pumps, the FTH cavities, the high-power phase shifters and power dividers, and the refrigerator compressors. After five years' running, however, we are finding that the pumps take longer to pull a tank down, and that breakdown occurs occasionally in the phase shifters and power dividers, provoking flash-over elsewhere in the rf system and reducing the range of adjustment, making the whole chain more critical of adjustment. We have also had the complete failure of an FTH cavity already mentioned, and recently the failure of a compressor.

We are therefore turning our attention to the overhaul of these items, one by one; this has involved for the mercury pumps the construction of a separate ventilated lab for cleaning and speed measurements on a dummy tank.

3. Setting-Up

The present rhythm of P.S. operation allows us from Sunday through Tuesday twice a month for maintenance and repairs, source

changes and measurements, with machine start-up on Wednesday. In the absence of faults it is sufficient to take standard values for source, rf and focusing, and trim around these values by successive approximation, progressing along the machine. The final criteria are intensity and pulse shape at the point of injection into the synchrotron, and 50 MeV emittance and energy spread. The emittance at 500 keV is also measured as a routine procedure.

4. Running

When the beam is handed over to the P.S. Main Control Room for injection, certain controls are also transferred and the linac control position is abandoned. A linac operator remains "on call" for fault repairs and readjustment, but otherwise works normally within reach of a telephone in his laboratory or office during the day, or sleeps in the operators' dormitory at night.

The controls transferred include the bending magnets, triplets and the vertical steering coils in the inflector region, variable apertures and the tank levels. The transfer of tank level controls and indications is questionable in principle, but the retouching of tank levels by the M.C.R. operators seems justified with the present stability of the modulators.

VAN STEENBERGEN: When you saw an increase of current, did you see increase in emittance?

TAYLOR: It didn't make a great deal of difference; the 50 MeV emittance is always around about 3 cm milliradians and it did not change very much.

HUBBARD: These standard operating values that you use to start up after shutdown, are they a set of values that do not change over a long period of time or are they just the ones you used when you turned it off before?

TAYLOR: Actually, by the control position we have a little piece of paper with them all marked down; this has been around for a year or so, and it is still the one we use.

WROE: You mentioned right at the beginning that you had reduced the height of the cathode shield. Could you say how much you reduced it by and what difference it made?

TAYLOR: I can't give you the exact figures, but it was the order of 1 or 2 mm. This pushed us up to the 300 mA from the source. We had been previously in the 200's.

WROE: We tried it at one time and it did not make any difference.

BLEWETT: Do you have any evidence of x-ray emission?

TAYLOR: No.

NORDBY: I was wondering about the 3 Mc chopper. Do you have any information on its operation?

TAYLOR: It is a couple of parallel plates with about 10 kV across them. We haven't used it yet. We had some trouble getting sufficient power in the driver stage.

NORDBY: Also on that photograph method, do you have any trouble with the surface building up potential and giving you erroneous readings?

TAYLOR: No.

OHNUMA: You mentioned about the routine measurement of the beam shape in the transverse direction. To what extent can you use the results of those measurements for adjusting the focusing system between the preinjector and the linac?

TAYLOR: It is almost entirely an empirical type adjustment. We do it rather as a check on the performance of the preinjector.

OHNUMA: Is it something you could probably control by, say, on-line computers or anything like that?

TAYLOR: We have got for the normal method at 50 MeV this arrangement of the slit, lens and a slit. This defines in the phase plane of the first slit a strip like this, which is swung around through 90° by the lens and drift system to the second slit where we further limit to a small rectangle in the phase plane. Now what we have done recently is to make up a new set of slits from which we can take digital information, with the object of feeding this to a computer eventually.

VAN STEENBERGEN: Have you noticed at those high currents any beam intensity modulations? Have you noticed with the duoplasmatron source, any plasma boundary instabilities?

TAYLOR: No, not yet.

VAN STEENBERGEN: At the high currents, with the duoplasmatron source, one finds that the beam extracted from the ion source shows hash or intensity variations. Does this exist with the rf source?

TAYLOR: Apparently not. The pulse shapes are always very clean. In the early days we found in the synchrotron a 60 Mc component and it looked as though it was beating between the rf frequency of the source, which is 140 Mc, and the tank which is 200 Mc. But as far as hash is concerned, we have not observed any problem.

NORDBY: We found some hash in the Argonne duoplasmatron source and we got rid of it by putting a small capacitor on the extractor supply.

FEATHERSTONE: I wonder if you know approximately what proportion of the beam current you quoted from the source is protons?

TAYLOR: Yes, it is between 90 and 95%.

FEATHERSTONE: Excellent. Also, have you a feeling as to the kind of electron current that flows up the column to produce unwanted x rays at the top? In other words, if this is the actual proton or positive current going down the column, the person who designs the bouncer to maintain stability on your Cockroft-Walton system has to contend with the electron loading as well. And I haven't seen figures quoted on what this amount is on typical installations.

TAYLOR: We said a little in the Dubna report. We've got a fairly big capacitor across the generator. And I gave some results, I believe typically 4 kV drop during the pulse. Measurements over a long period show that normally we have about equal electron and proton currents, occasionally rising to electron currents twice the proton current.

VAN STEENBERGEN: I would like to add to this question of Featherstone's. At High Voltage Engineering they mentioned that they normally take a factor of 2 into account. If you take 100 mA proton beam down one way, you count on a 100 mA of electrons the other way. May I ask at the same time, with the duoplasmatron source and the expanded plasma, are there any figures existent yet on proton percentages?

ANSWER: No.

VAN STEENBERGEN: One might worry here that the proton percentage might be drastically down from the conventional duoplasmatron source.

GUILBAUD: Could I offer a comment that we made such a duoplasmatron in our laboratory with expanded cup and at 40 kV we measured about 300 mA but these were protons. We had a magnetic focusing which took only protons on the target. I think I remember the proton percentage was estimated to be somewhere around 75%, but I am not sure.

WADDELL: The other day when you were talking about the machine, you described there that the phase between the first and the third cavities was zero and that the second cavity turned out to have a phase difference. You indicated at that time that you got a sharper beam, less spread at the end, and I was wondering if you were tuned for maximum current, whether you arrived at a similar condition without looking for the sharper energy spread.

ANSWER: The current in fact is determined by the level of Tank one and the focusing and matching, and thereafter it stays pretty well constant through the machine. You have to move the tank level a long way to drop the current and by then you would have a completely unacceptable beam.

QUESTION: The other day you indicated that the second tank had a different phase than the others and that at that time you got better energy spread operating in that mode. Is this reflected in the overall current acceptance?

TAYLOR: If you put the tanks in phase, you get about the same sort of current, but worse energy spread.

FEATHERSTONE: I am also interested in your high voltage experiment at 500 kV. When you say you were holding this across 10 cm, would it represent a voltage reached after a succession of conditioning sparks had been permitted to occur, or would this system be something that just never sparked at all?

TAYLOR: This is something which you form watching the sparking. You bring the voltage up gently, and reach a level where you get a low frequency of sparking.

FEATHERSTONE: So the sparking rate essentially drops off exponentially and after a time it becomes a negligible matter.

TAYLOR: Yes.

MORGAN: I believe you mentioned that you had about 220 mA of current out of the source and about 200 mA at the 500 kV level. Do you have any idea what happens to this 20 mA difference?

TAYLOR: We've got 300 mA maximum coming from the source and 220 mA maximum at the bottom of the column, and we think that the difference is scraped off by the aperture limitation at the end of the column. We have our first focusing triplet actually integral with the first accelerating electrode of the column.

MORGAN: I believe you extracted the high current at 28 kV; have you tried extracting it at higher gradients or higher potential levels?

TAYLOR: Yes, but that is about the limit of stable operation.

HUBBARD: I would like to ask Van Steenbergen about the electron drain number he quoted from High Voltage Engineering. Is that with one of their new inclined gradient columns or is that with the old-fashioned kind?

VAN STEENBERGEN: I couldn't tell.

REFERENCES

1. C. S. Taylor. "High Current Performance of the CERN PS Linac" (Presented at the 1963 Dubna Conference). Available as CERN internal report MPS/Int. LIN 63-9.

2. Th. Sluyters. "A Theoretical and Experimental Comparison of Proton and Deuteron Acceleration in the CERN Linear Accelerator (C. L. A.)," CERN 64-22.

3. Th. Sluyters. "Radial Beam Studies Using an Emulsion Technique Applied to the CERN Linear Accelerator." Nuc. Instr. & Meth. 26, 999 (1964).

4. C. Bovet and M. Regler. "Etalonnage d'emulsions pour les mesures d'emittance." MPS/Int. LIN 64-2.

PERFORMANCE OF THE PLA

J. M. Dickson
Rutherford High Energy Laboratory

Availability

The PLA has been operating 24 hours per day since January, 1962 on a schedule of 10 days for operation and 4 days for maintenance and for the setting up of experiments. In late summer of each year there has been a shutdown of one to two months for major modifications, repairs and installations. The percentage of this scheduled operating time which has been lost by machine faults has decreased from 30% in 1962 to 12.5% in 1964 (January to June). During the 12 months, July, 1963 to June, 1964, the total number of hours available to the experimenters was 4638 hours and the total number of hours scheduled for operation was 5424; an availability of 85.5%. Figure 1 shows the monthly availability figures since the start of regular operation in April, 1960.

Faults

Analysis of the fault log of the machine shows that the lost time was due to rf amplifiers (grounded grid triodes) (15%), modulators (20%), accelerating structure (15%), polarized source (10%), coaxial lines (7%) and miscellaneous small items.

The grounded grid triodes, which are continuously pumped valves manufactured by AERE Harwell and tested and serviced by the PLA group, operate for a total of about 30,000 valve-hours per year.

The faults which cause loss of time are water leaks (in the grid), damage to some silvered mica condensers in the cathode assembly, broken rf windows, anode-to-grid sparking, and broken cathodes. Grid water leaks are normally caused by the accumulation of deposits in the fine bore stainless steel tubes of the grid. Control of the water conductivity to less than 10 μmho and filtering by scintered stainless steel filters has not eliminated the trouble. The mica condenser forms part of the cathode/grid resonant circuit, and carries about 90 amp rf. Spark erosion of the silver reduces the capacity, puts the cavity off tune and reduces the gain of the valve. Mica life is about 6000 hours. Six to ten valve changes per year are due to the above faults.

Modulator faults are often minor faults now and have become less frequent since the main switch valves were changed from ignitrons to deuterium thyratrons (CV 3336). The basic circuit of the modulators is

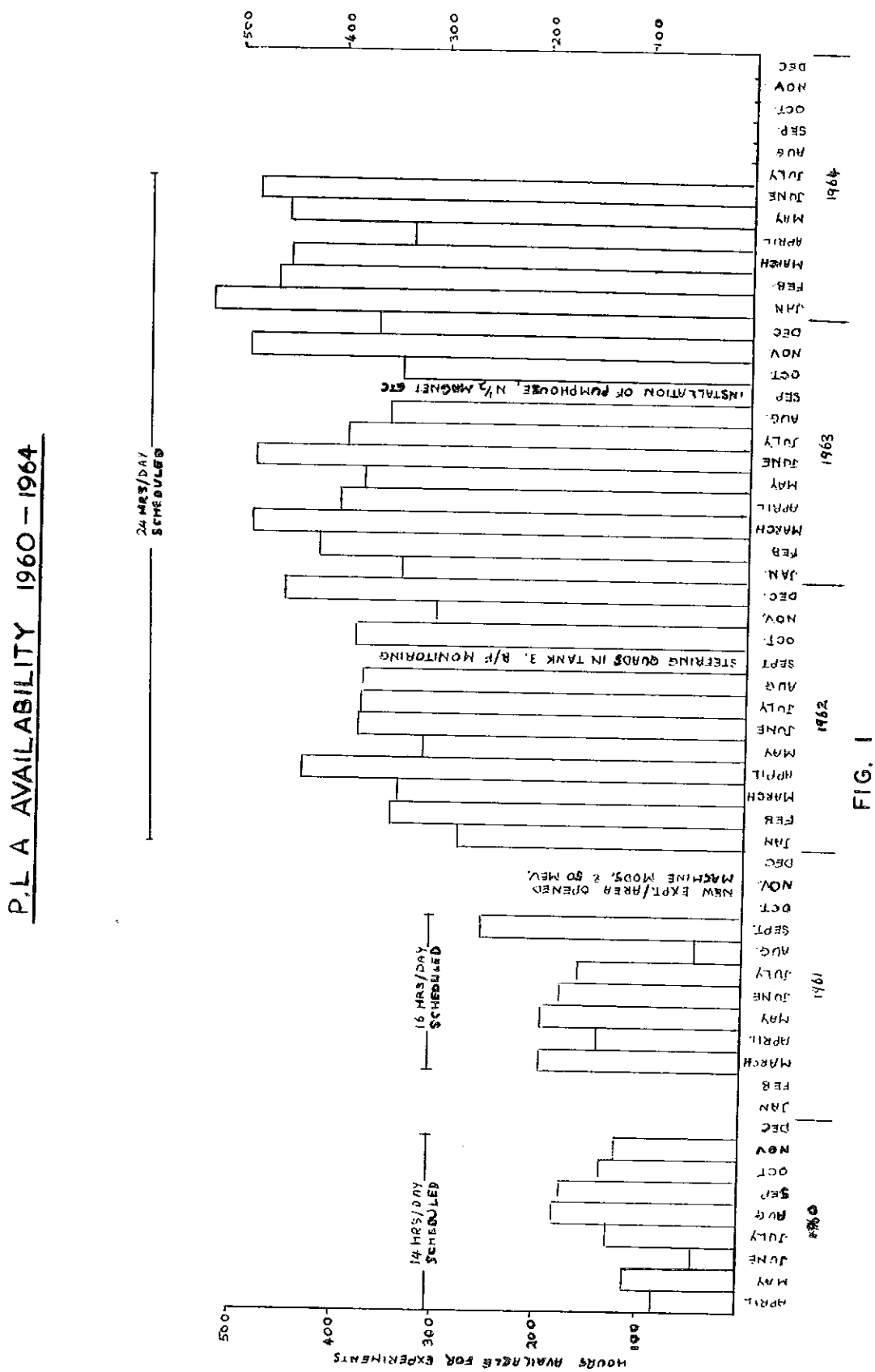
P.L.A AVAILABILITY 1960 – 1964
HOURS AVAILABLE FOR EXPERIMENTS
500
400
300
200
100
14 HRS/DAY SCHEDULED
16 HRS/DAY SCHEDULED
24 HRS/DAY SCHEDULED
NEW EXPT/AREA OPENED MACHINE MODS, £ 80 MEV.
STEERING GUARDS IN TANK 3. B/P MONITORING
INSTALLATION OF PUMPHOUSE, N½ MAGNET ETC
1960
1961
1962
1963
1964
APRIL
MAY
JUNE
JULY
AUG
SEP
OCT
NOV
DEC
JAN
FEB
MARCH
APRIL
MAY
JUNE
JULY
AUG
SEPT
OCT
NOV
DEC
JAN
FEB
MARCH
APRIL
MAY
JUNE
JULY
AUG
SEP
OCT
NOV
DEC
JAN
FEB
MARCH
APRIL
MAY
JUNE
JULY
AUG
SEP
OCT
NOV
DEC

FIG. 1

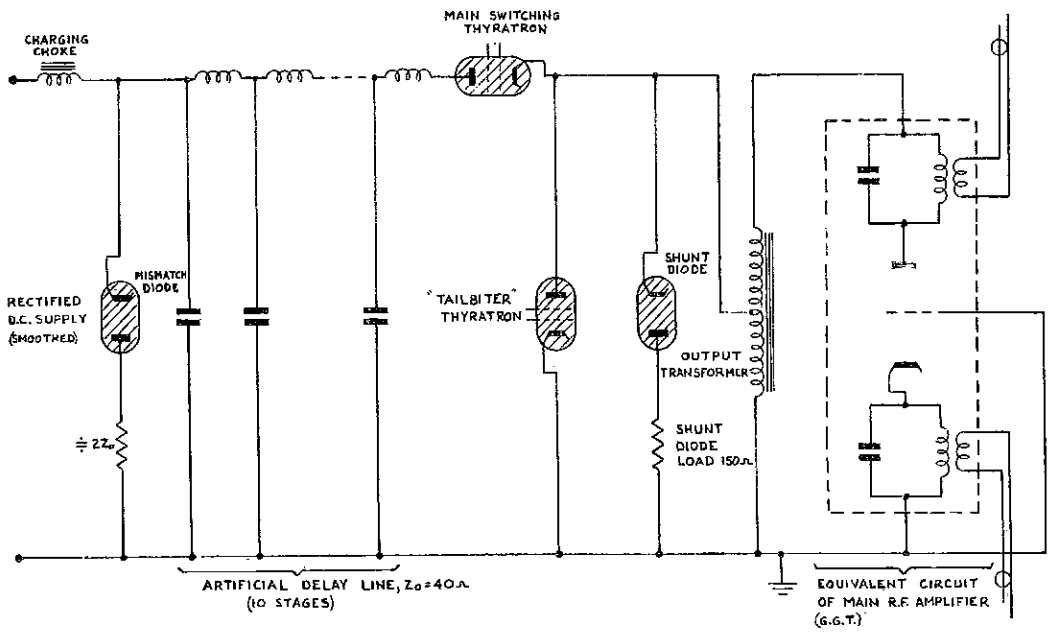

BASIC CIRCUIT OF PLA MODULATOR
FIG. 2

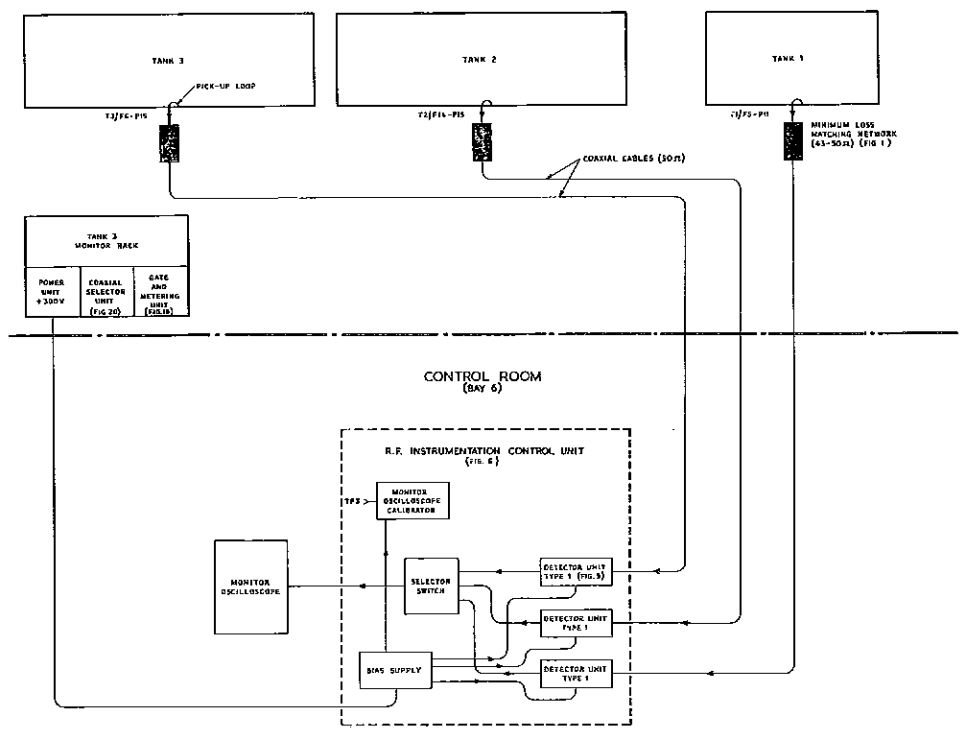

FIG. 3 BLOCK SCHEMATIC DIAGRAM OF ACCURATE R.F. LEVEL MONITOR

shown in Fig. 2. Protection against high impedance mismatch conditions of the modulator load is provided by the "tail-biter" thyratron which is triggered near the end of each modulator pulse. A negative voltage swing on the delay line results and the mismatch diode (a deuterium triggered diode) fires. Subsequently the main switch tube and tail biter are extinquished by the reflected wave. Low impedance mismatches are absorbed by the mismatch diode. The CV 3336 thyratrons have run well, one for over 10,000 hours without a fault. Some have had partial heater failures and some have had gas pressure trouble. These faults have caused very little lost time and are mostly due to preproduction difficulties with the valve and are being cured.

Lost time on the accelerating structure has been due to some water leaks in the drift tube and liner cooling circuits. These have all been "repaired" by pumping a weak solution of resin varnish through the faulty circuit.

Coaxial line faults are nearly always due to fractures in soft soldered joints or to accidental damage to joints during assembly. Peak powers of over 1 Mw (2% duty cycle) cannot be reliably carried by 50 ohm coaxial lines of 3" OD. The use of 4-1/2" and 6" lines and copper plating of all surfaces has improved the reliability very significantly. For further descriptions of the faults, see NIRL R/55 and R/60.

RF Monitoring

The basic requirement here is to obtain for each tank a measure of the rf accelerating field, the phase and the "tilt." Rf amplitudes are measured by loops in the cavity walls which transmit an rf signal to the control room to a matched and biased diode detector (Fig. 3). The bias voltage ($\sim$ 7 V) to give a 0.2 V residual pulse is read off the dial of a helipot. The accuracy of the measurement is $\pm$ 0.1% and the long term stability is about 0.2%. A measurement of the tilt of a cavity is obtained from several loops along the cavity; the calibration of each loop must be obtained by comparison with a perturbation measurement of the tilt. This comparison has only been completed for tank 1, where a perturbation measurement was performed recently. This showed that, for the same position of the tilt tuners, the tilt had changed greatly over the past four years. The tilt can now be checked from time to time to look for long term changes in the cavity. The tanks are individually servo tuned to maintain the cavity phase in a constant relation to the phase of the input power. The intertank phase is controlled manually and is monitored by a phase bridge with thermocouple detectors and a meter indication (Fig. 4). This system can detect small phase changes ($\sim 0.1^{\circ}$), but it is sensitive to changes in the shape of the rf pulses in the tanks,

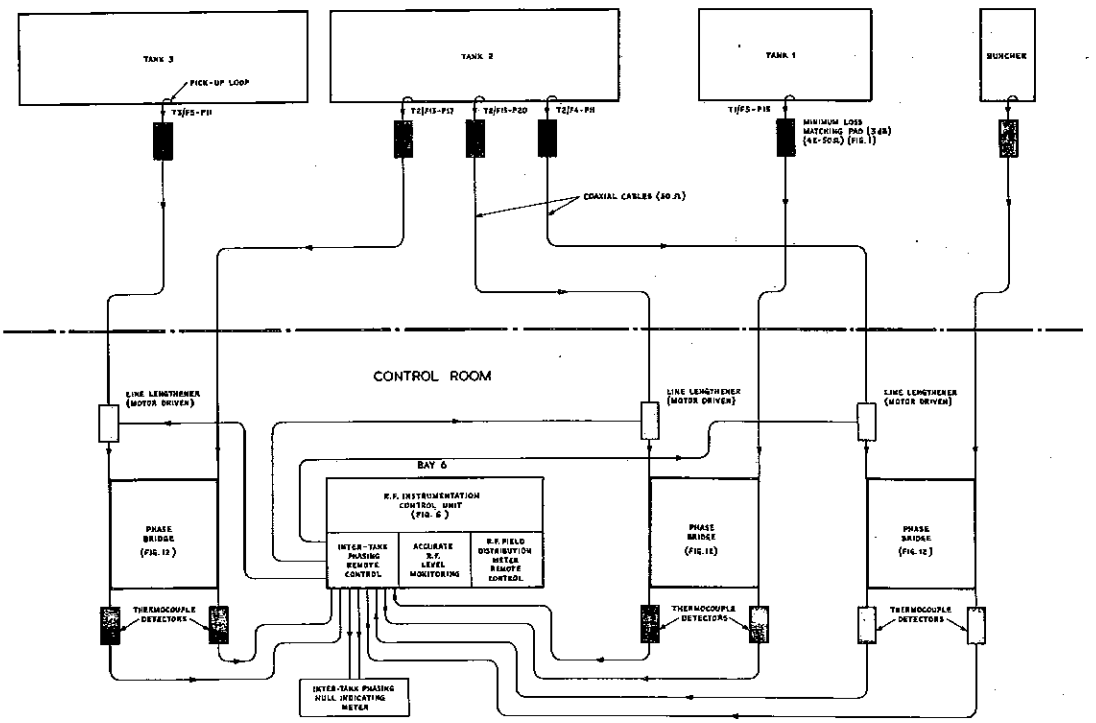

FIG. 4 BLOCK SCHEMATIC DIAGRAM OF INTER-TANK PHASE MONITORING SYSTEM

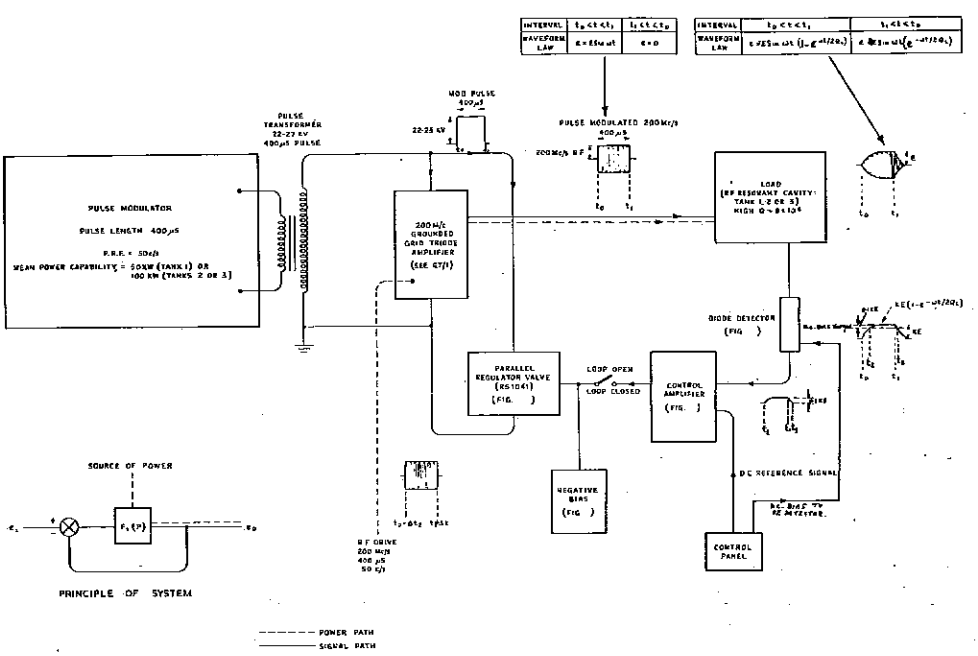

PRINCIPLE OF SYSTEM

SIMPLIFIED BLOCK SCHEMATIC DIAGRAM OF CAVITY R.F. FIELD STABILISER

FIG. 5

in particular to the build-up rate, which can be affected by changes of amplifier valves or their associated coaxial line components. It is hoped that by using diode detectors that better long term stability can be achieved.

RF Stabilization

It is important for many experimenters on the PLA that the output beam energy of the machine should remain constant over long periods and that it should be constant throughout each beam pulse. Slow acting stabilization of the rf could satisfy the first requirement, but the second is more demanding. The rf field stabilizer shown in the block diagram, Fig. 5, produces a nearly flat-topped rf pulse; variation along the pulse is about 0.1% and $\pm$ 5% changes in field can be corrected by a factor of 50. Variation of the modulator mains or H.T. voltages produces a variation in the length of the flat top of the stabilized pulse. This is particularly noticeable, when the Nimrod magnet is being pulsed at full power, but it is not embarrassing operationally.

Beam Energy Monitor

Beam energy measurements by the time of flight method, by momentum and by range measurement have all been used to observe the dependence of beam energy on machine parameters. The range measurement method has the advantage of requiring relatively simple appartus and in the arrangement used it imposes only one restriction on the beam, that it should have a peak current of 10^{-6} to 10^{-9} A. The beam energy monitor is located about 6 feet from the end of tank 3 and can be moved in an out of the beam by remote control.

Figure 6 shows the principal parts of the device. Ion chambers A and B form a differential ion chamber with a common collector which is connected to a vibrating reed electrometer. The thin degrader is equivalent in thickness to two standard deviations of the nearly Gaussian range distribution. The relative thicknesses of A and B is such that the larger number of protons passing through A is compensated by the greater ionization loss per proton in B, to produce equal currents in A and B when the mean range of the protons is coincident with the center of the thin degrader. The thick degrader is removed for measurements at 30 MeV. The variable wedge degrader is motor driven and arranged to give a digital read-out of its position. The ion current as a function of the wedge position (results for a prototype with a dial reading only) is shown in Fig. 7. The zero cross-over point can be repeatedly found to be better than the equivalent of $\pm$ 10 keV for 30 and 50 MeV beams; its position is insensitive to changes in the ion chamber voltages under the recommended operating conditions.

This energy monitor needs to be calibrated at one energy near 50 MeV and one near 30 MeV. The incremental energy calibration can be obtained from range energy tables and the mechanical movement of the wedge degrader; it has also been checked against time of flight energy measurements. The monitor measures the mean energy of the beam and it is insensitive to the energy spectrum provided it is not too wide (less than 1 MeV). The most important advantages of this instrument is that it is always available for measuring the beam energy, whatever experiment is scheduled and its calibration remains unchanged since it depends only on one measurement of degrader thickness.

Beam Loss in Tanks 2 and 3

When the PLA was first operated, there was practically 100% transmission of beam current from the end of tank 1 (10 MeV) to the output of tank 3 (50 MeV). Recent measurements showed that the transmission had deteriorated to about 60%. Part of this loss was found to be due to a fault in the quadrupole current wiring in tank 2 which had increased the current in one of the quadrupoles by 40%. When this fault was cleared, the transmission increased to about 75%. Further measurements of quadrupole currents showed that there was a rms deviation from a $1/\beta$ quadrupole gradient law of 7%, which would produce an rms increase in beam spot size of 3 mm radius. This fault alone would not account for the beam loss, but it is also known that the mechanical alignment of the quadrupoles is not perfect and this will cause a radial oscillation of the beam, which now appears to be sufficient to cause the beam to be intercepted by the drift tubes. After a run at 1 μA mean beam current for a few hours, radioactivity of the drift tubes can be detected by a γ-ray monitor outside the vacuum envelope. Two peaks, at approximately a half-wave radial oscillation interval, are found, one of 2 mr/hr near the output end of tank 2 and one of 10 mr/hr in tank 3.

The majority of the neutron radiation, measured outside the shielding walls of the machine, is due to this beam loss, since the irradiated material here is copper, while all beam degraders, collimators and beam stoppers in the experimental areas are carbon. Experiments on the relative neutron yields from various materials are planned, which will give useful data for the control of radiation from machines of around 50 MeV.

SHAYLOR: I was interested to see that you are using a simple shunt type modulator to regulate rf amplitudes. Are you happy that just regulating the drive in the way you are doing keeps the whole of one tank flat to 0.1%? Don't you think that you may be regulating the rf level at the point where the detector is, but not elsewhere in the tank?

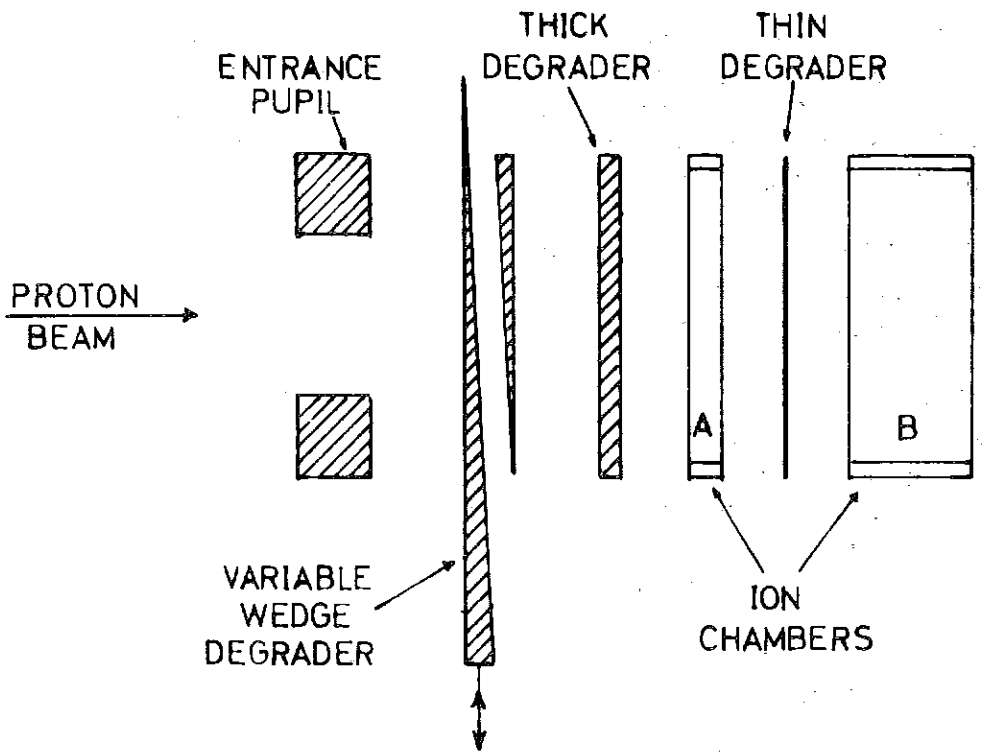

Fig. 6 Layout of Beam Energy Monitor.

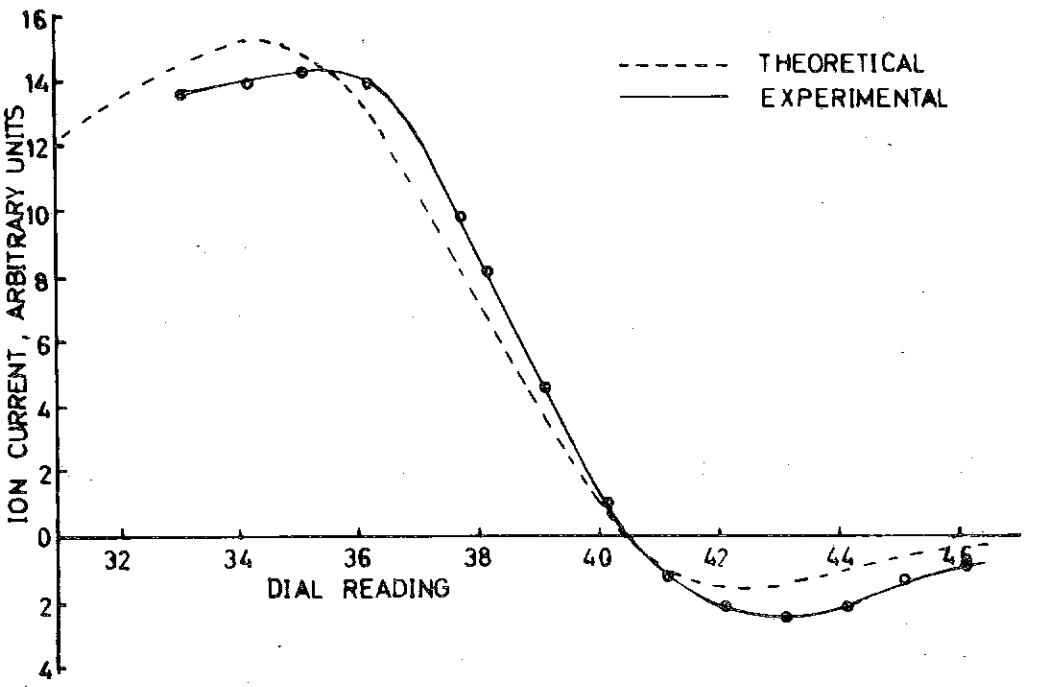

Fig. 7. Response Curve of Beam Energy Monitor.

DICKSON: I haven't seen any trouble like this, no. I have not looked at this very carefully, but we have got some evidence on this because the pickup for the stabilizer is at one part of the tank (I think in the middle), and the pickup for some other monitoring is in another part of the tank. They both flatten together.

SLUYTERS: We have done also at CERN these radiation measurements along the tank, but we have not found these bumps. Everything was very equal all along the tanks.

PRIEST: You have a nice servo mechanism there which keeps the pulse flat. I would like to know more about what it tells you. I think you are talking about the last part of the pulse after the beam is injected into the machine. And this corresponds with what Taylor was talking about. Have you got a measure of the extra amount of power that you have to put in when the beam is turned on?

DICKSON: Very little in our case. We are only running with at the most a peak current of around 200 μA. Beam loading doesn't worry us.

TENG: Do you have any experience similar to CERN that you can reduce the energy spread by detuning the phase of the second tank.

DICKSON: Can we leave that till Carne gives his paper? We have not measured the absolute phase between tanks.

HUBBARD: Can you not affect beam loss as you have indicated by adjusting the quadrupole magnet strengths?

DICKSON: I hope we can. We have not tried this yet. The adjustment is not so easy since the adjusting resistors are in boxes right underneath the tanks and there are a whole lot of things built in front of them all the way along. It is a slow and tedious business, but it probably has been done by now, since there was a shutdown last week. I hope that it has been fixed.

PERRY: Do you contribute any significance to the second peak?

DICKSON: No.

FEATHERSTONE: I was interested in your experience on blocking the water passageway within one of your vacuum tubes. This is an experience we share in our resnatrons. In our case, it turned out to be largely copper compounds which apparently had been removed from other parts of the system, and we are now undertaking a program of deoxygenating

and filtering and hope to prevent recurrences of this sort. We have also been trying to go to a higher purity of water. Are these the measures that seem appropriate in view of your experience? First of all, was it copper that plugged up the passages in your case?

DICKSON: There is some copper in the water circuits. We used not to have very much but in the last three months it has been building up. We don't know why but we had this blockage of the grid tubes before that. One of the main components is silica in this blockage. I think there are all sorts of other components.

QUESTION: What was the conductivity of the water.

DICKSON: 10 micromhos.

BEAM ENERGY MEASUREMENTS ON THE RUTHERFORD LABORATORY P. L. A.

K. Batchelor, A. Carne, J. M. Dickson, D. J. Warner
Rutherford High Energy Laboratory

I. Introduction

The results to be described are from measurements made using the time-of-flight method described previously,[1] and are a continuation of the work reported at other accelerator conferences.[2,3] As a result of recent observations some of the work reported previously needs some qualification. In particular, the 10 MeV and 30 MeV spectra have previously been affected by the residual power in Tanks 2 and 3 which results from the drive power feeding through the grounded grid triode amplifiers into these cavities even though the E. H. T. is removed from the amplifiers. Also early comparison between theory and practice from the 10 MeV beam has been invalidated by the fact that the field law in Tank 1 was distorted from its original value, which was used in the computer program. These effects are discussed below.

II. Effect of Residual Power on the Beam

Figure 1 shows the layout of the rf system of the P. L. A., for reference. The effect on the 10 MeV beam of varying the amplitude of residual power in Tanks 2 and 3 respectively, with these tanks maintained at the correct resonant frequency, is shown in Figs. 2a and 2b. The level of residual power was varied by means of the variable attenuators Att 2, Att 3 in the power dividing network. The effect of varying phase was found by setting the attenuators at their normal operating values, and detuning each tank in turn. The resulting spectra are shown in Figs. 2c and 2d for detuning of Tank 2 and Tank 3 respectively. It can be seen that the residual power affects the spectrum shape and position quite considerably. For normal settings of attenuators and frequency tuners the residual voltages were 6.4% of operating value in Tank 2, and 8.8% in Tank 3 (see Fig. 2). An amplitude reduction by a factor 0.7 (to give 'half power point' amplitude) produced a doubling of the beam energy spread at FWHH, and a small shift of mean energy $\sim$50 keV by each tank. A detuning of $\pm$ (f/2 Q) $\equiv \pm 45^{\circ}$ (to give the same reduction in amplitude, but now plus a phase shift) produced a change in beam energy spread at FWHH by a factor 3 ($+45^{\circ}$), 0.6 (-45°) by Tank 2, and 3 ($+45^{\circ}$), 0.5 (-45°) by Tank 3, and a shift of mean energy of + 20 keV ($+45^{\circ}$) by Tank 2, and - 40 keV ($+45^{\circ}$), - 120 keV (-45°) by Tank 3.

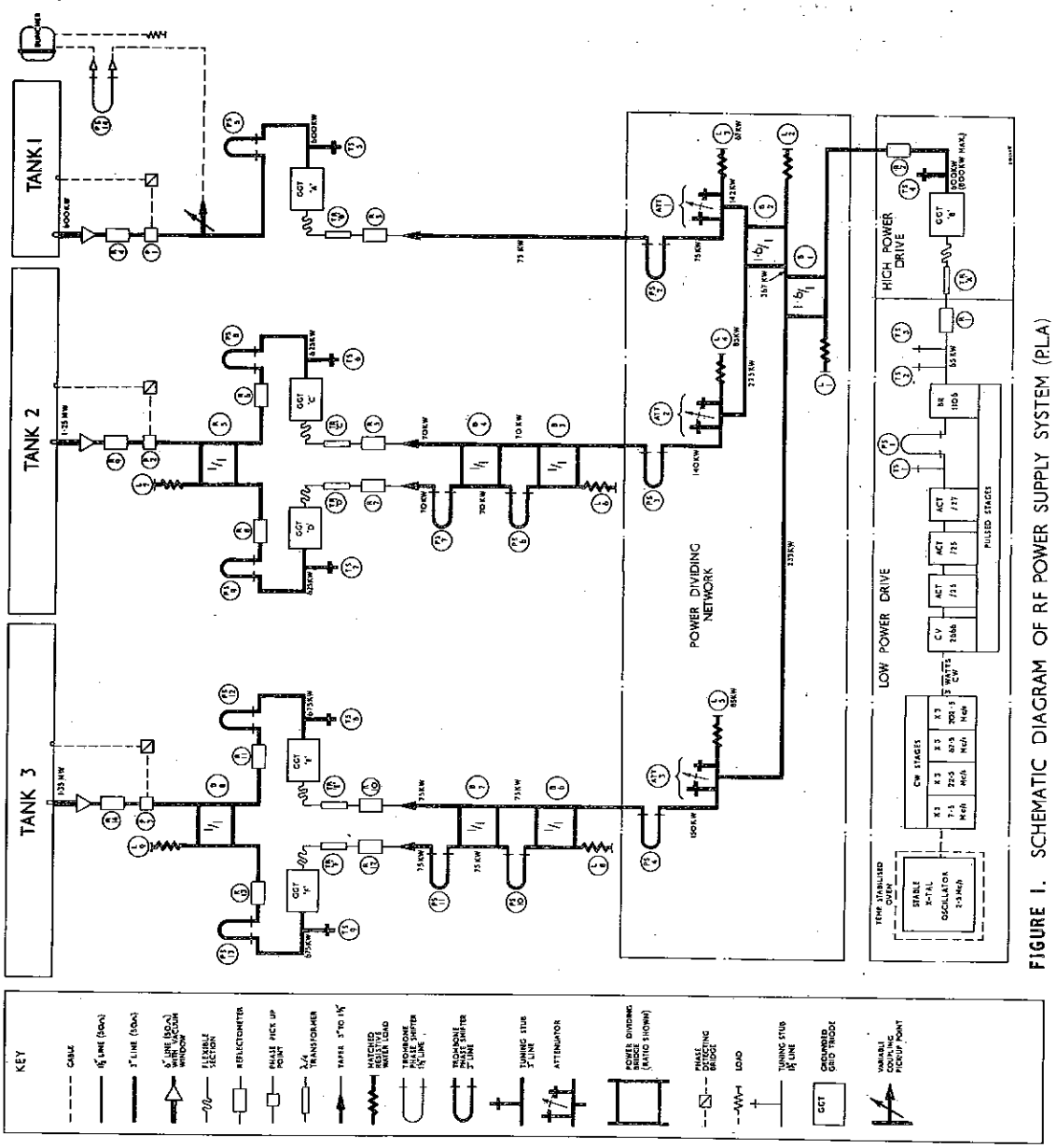

FIGURE 1. SCHEMATIC DIAGRAM OF RF POWER SUPPLY SYSTEM (PLA)

Figures 3a and 3b show the effect of residual power in Tank 3 on the the 30 MeV beam. For normal settings of the attenuator and frequency tuner of Tank 3, the residual voltage was 10% of operating value. An amplitude reduction by 0.7 produced little or no effect on the 30 MeV beam energy spread, but a shift of 120 keV. Detuning by $\pm 45^{o}$ produced marginal changes in energy spread, and a shift of mean energy - 350 keV ($+ 45^{o}$) and + 50 keV ($- 45^{o}$).

It is now normal operating procedure to reduce the residual power to a minimum in nonoperating cavities, this being achieved by detuning the tanks and insertion of maximum attenuation in the drive lines to the grounded grid triodes.

III. Measurements on Tank 1

Due to the discovery of the effect of residual power on the spectra it was decided that some of the early work on the 10 MeV beam should be repeated to try to improve the agreement between theory and practice which, at this energy, had not been good. Figure 4 shows some typical spectra for different injection energies and rf field levels, the tilt tuners being set at their assumed "flat field" setting (tilt 50-50). Computed spectra and phase acceptance did not agree well with measured values. Also the transparency of the tank was down by a factor 5 on its original value. It was therefore decided to remeasure the axial field in Tank 1 to see if this could be the cause of the disagreement. The field law measured for "tilt 50-50" is plotted in Fig. 5 and is compared with the field law measured when the cavity field was set up seven years ago (i.e., the field law used for computer calculations). It can be seen that gross distortion of the field has occurred, probably due to a change of dimensions caused by temperature cycling and periodic dismantling over the past seven years.

The actual measured field law has been used in the computer program to give comparison with some of the measured data of Fig. 4, and the computed spectra are given in Fig. 6. The experimental spectra of Fig. 4 do not show the same fine structure as the computed spectra, due to "smoothing out" by jitter in rf level and phase, and injection energy. But, with this proviso, comparison of corresponding spectra (A, B, C, etc.) now shows quite good agreement.

The field law has been restored to the proper value shown in Fig. 5. The transparency of Tank 1 has returned to its original value (i.e. 1/50). Results for the new field setting are not yet available.

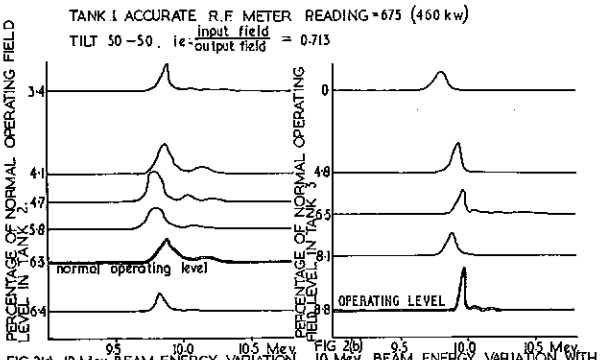

FIG 2(a) 10 Mev BEAM ENERGY VARIATION WITH RESIDUAL R.F LEVEL IN TANK 2.

FIG 2(b) 10 Mev BEAM ENERGY VARIATION WITH RESIDUAL R.F LEVEL IN TANK 3.

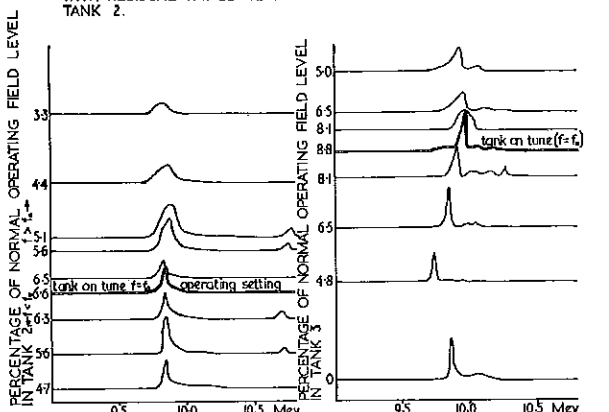

FIG 2(c) 10 Mev BEAM ENERGY AS A FUNCTION OF TUNER SETTING FOR TANK 2.

FIG 2(d) 10 Mev BEAM ENERGY AS A FUNCTION OF TUNER SETTING FOR TANK 3.

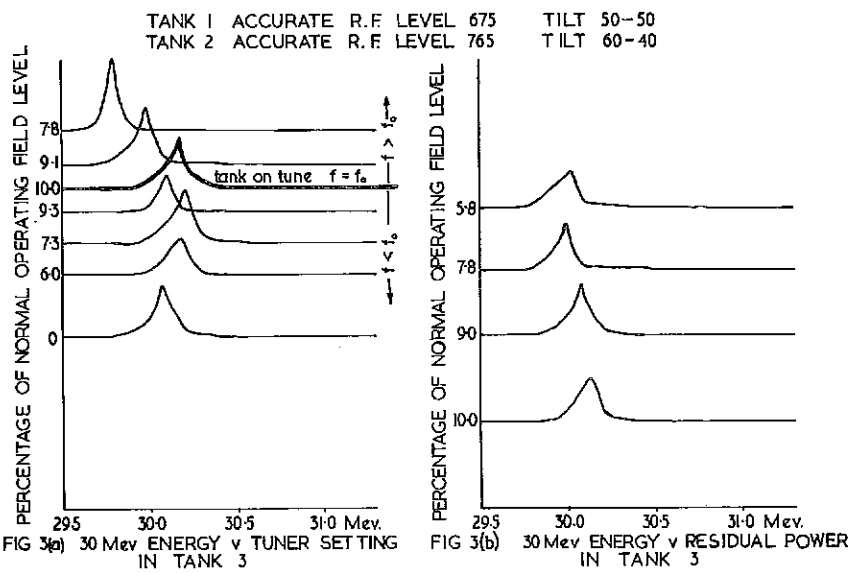

FIG 3(a) 30 Mev ENERGY v TUNER SETTING IN TANK 3

FIG 3(b) 30 Mev ENERGY v RESIDUAL POWER IN TANK 3

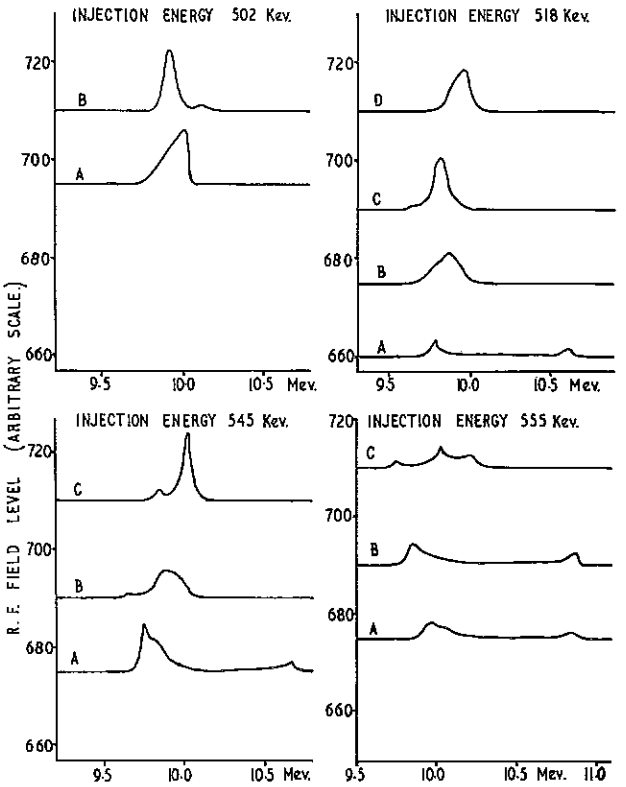

FIG 4. 10 Mev. ENERGY AS A FUNCTION OF R.F LEVEL IN TANK 1 AND VARIOUS INJECTION ENERGIES.

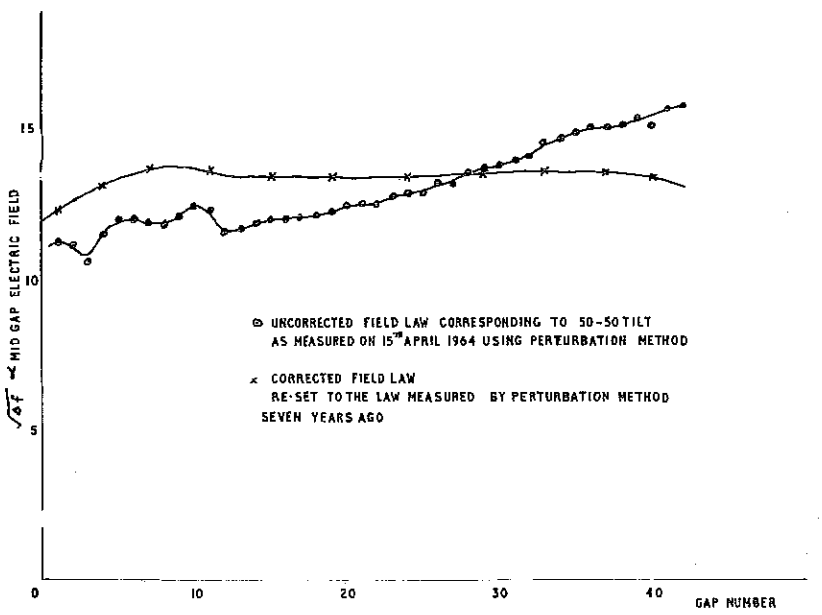

FIG 5. AXIAL FIELD LAWS FOR TANK 1 (BEFORE AND AFTER CORRECTION)

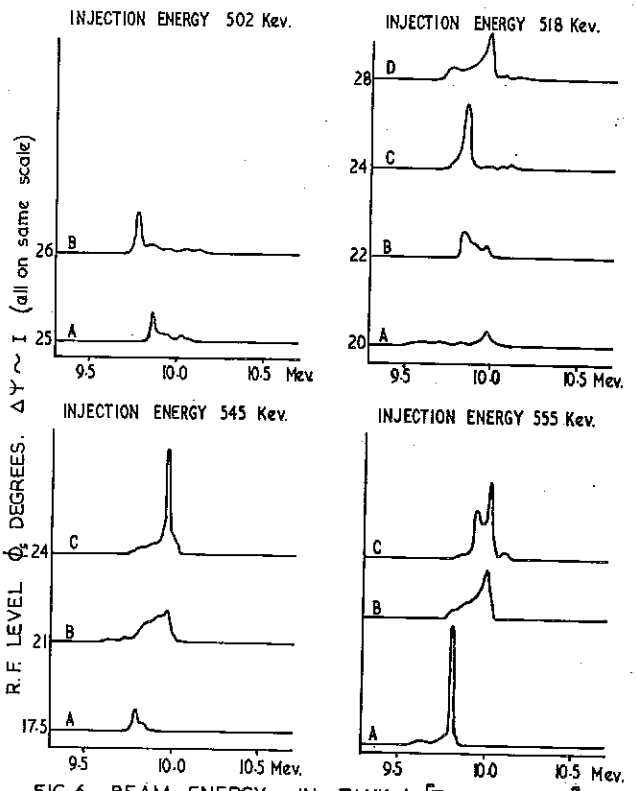

FIG 6. BEAM ENERGY IN TANK 1 [THEORETICAL]

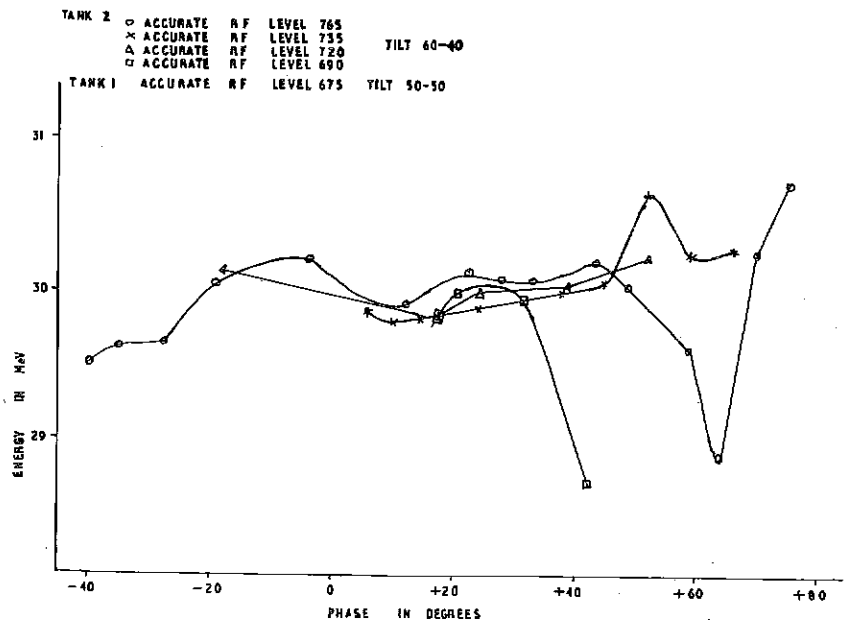

FIG 7 30 MeV ENERGY V INPUT PHASE

IV. Setting of Tanks 2 and 3

Before correcting the field law for Tank 1 measurements on the 30 MeV and 50 MeV beams were made to determine good operating levels of Tanks 2 and 3 for minimum energy spread in the beam. For the 30 MeV beam it is possible to run Tank 2 at an rf field level which gives an integral number of phase oscillation half wavelengths along the tank, and hence a flat energy vs. input phase region for the linear phase oscillation range of $\phi_s \pm 15^o$. Additionally it is required that the beam energy spectrum should be narrow. Figure 7 shows the variation of output energy with input phase: in particular, the rf level 735 is nearest to the required condition. The effect of input phase on output energy for the chosen rf level in Tank 2 (735) is plotted in Fig. 8, showing a roughly constant energy over the phase range, with little change in energy spread.

In Tank 3 it is not desirable to operate at a level corresponding to an integral number of phase oscillation half wavelengths, since the $\lambda\phi/2$ level is too near threshold for acceleration, and the 2 $\lambda\phi/2$ level is such that sparking would occur in the tank. Thus Tank 2 is operated at a different level (765) to give nearly integral number of phase oscillation half wavelengths between the input of Tank 2 and the output of Tank 3. The resulting 30 MeV spectra as a function of input phase to Tank 2 are shown in Fig. 9; the 50 MeV spectra versus input phase to Tank 3 is shown in Fig. 10. Finally Fig. 11 shows the energy spectra as a function of rf level in Tank 3.

V. Tank Tolerances

From the above results it is possible to make estimates of the stability of the output beam in terms of mean energy and energy spread as functions of machine parameters. Also use has been made of the Beam Energy Monitor described by Hanna and Hodges[4] to complete some of the results not determined by time-of-flight methods. This monitor, which utilizes a combination of degrading wedges for range determination, and a split ion chamber as a detector system, is very useful for determining mean energy, and can measure shifts of the order of 5 keV. A set of measurements with this monitor takes only a few minutes compared with several hours by time-of-flight methods. In the future the energy monitor will be used as a survey instrument to determine machine conditions worthy of further investigation by the longer method.

The following tables summarize the effect of injection energies, rf field levels and intertank phases on the output energies of the P. L. A., for the settings specified in Section IV.

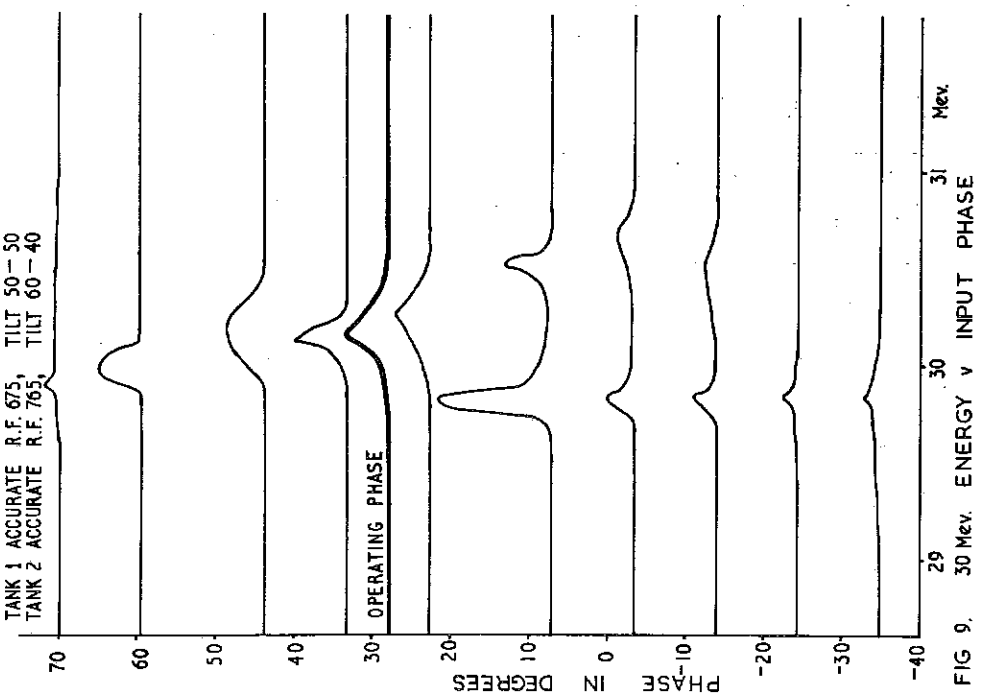

FIG 9. 30 Mev. ENERGY v INPUT PHASE

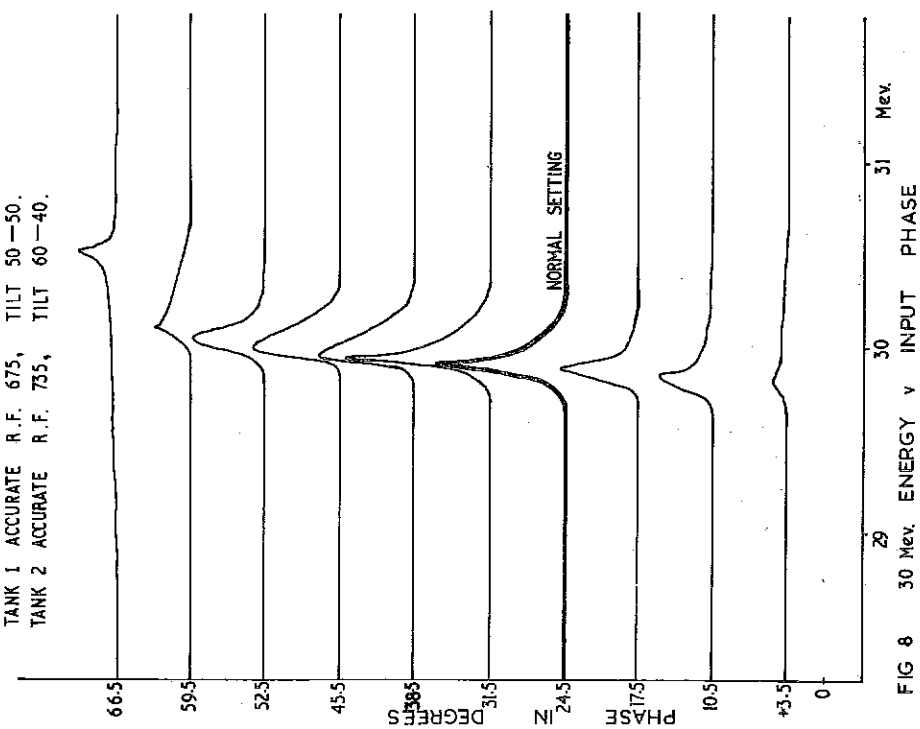

FIG 8 30 Mev. ENERGY v INPUT PHASE

Tolerances on Various Machine Parameters Affecting the Output Energies of the P.L.A.

(a) Injection Energy

Change of Injection Energy		Output Energy MeV	Change in Mean Energy keV	Measured by
%	kV			
		10	Not measured yet	
		30	Not measured yet	
+1	+5	50	-12 (-0.024%)	B.E.M.
-1	-5	50	+12 (+0.024)	

(b) RF Levels

Change in RF %		Acc. RF	Output Energy MeV	Change in Mean Energy keV	Measured by
Tank 1	+1	+5.5	10	-30 (-0.3%)	T.o.F.
	-1	-5.5	10	+30 (+0.3%)	
	+1	+5.5	30	-25 (-0.08%)	T.o.F.
	-1	-5.5	30	+25 (+0.08%)	
			50		
			50	Not yet measured	
Tank 2	+1	+8	30	+80 (+0.27%)	B.E.M.
	-1	-8	30	-80 (-0.27%)	
			50	Not yet measured	
Tank 3	+1	+9	50	0	B.E.M.
	-1	-9	50	-50 (-0.1%)	

(c) Intertank Phases

	Change in Intertank Phase. Degrees	Output Energy MeV	Change in Mean Energy keV	Measured by
Tanks 1/2	1^{o}	30	24 (0.08%)	B.E.M.
	1^{o}	50	18 (0.036%)	T.o.F.
Tanks 2/3	1^{o}	50	45 (0.09%)	

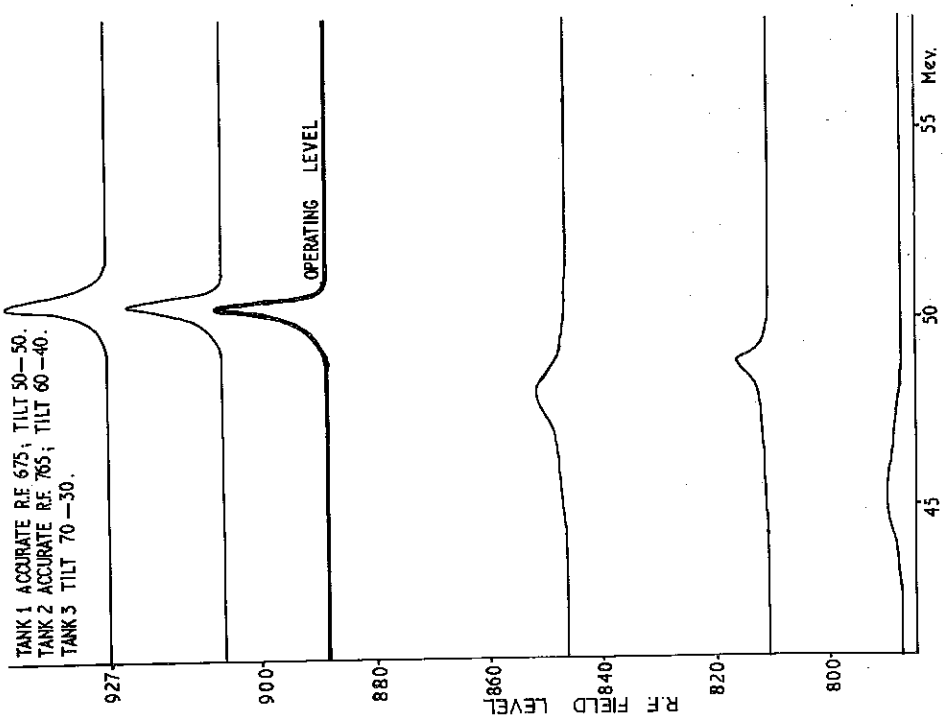

FIG 10.

FIG 11. 50 Mev ENERGY AS A FUNCTION OF R.F. LEVEL IN TANK 3

Conclusions

The change of energy and energy spread in a beam drifted through a cavity containing some residual rf power has been shown to be such as to cause concern if a precise output spectrum is required.

Agreement between computation and experiment at 10 MeV has been improved, after finding the actual field law in Tank 1. This field law has now been set to its correct value, and it is intended to check the field laws in Tanks 2 and 3 in the near future.

The settings and tolerances given for the P. L. A. represent the state of the art at the present time. Detailed work is continuing, by the use of the Beam Energy Monitor and time-of-flight apparatus, to determine more closely the optimum operating conditions.

Acknowledgements

The authors wish to acknowledge the help of Messrs. A. P. Banford, D. H. Carpenter, E. M. Mott, and S. Webb during these measurements, and members of the P. L. A. Operating Staff.

TENG: Do you understand all these?

CARNE: Well, certainly the agreement between axial motion computations and the experiment is quite good. This is particularly true in the case of tanks two and three, where we have used a large signal calculation, that is, a 32 step-by-step integration per cell. The agreement in tank one is now quite good and we think we can improve the situation. We think in terms of phase oscillation wavelengths, and the picture ties up fairly well.

TENG: The shifts you are talking about are very large, 50 kV in 50 MeV.

CARNE: Sure that's alarming, but these figures in fact agree with equations given by Lloyd Smith some time ago in LS-3. These give quite tight tolerances.

WHEELER: When you change the level in a cavity by say 1%, did you change the phase between the cavities to compensate for the change in the position of the bucket?

CARNE: No.

LAPOSTOLLE: When you spoke about the inference of residual field in tanks two and three on measurements done at 10 MeV, do you think that even the field induced by the beam could affect such measurements?

CARNE: There could be some effect, but as John Dickson said earlier, we have a peak current of the order of 200 μA, so that fields induced by the beam are of the order of a factor 1000 down on the residual fields in the cavities, where there are still a few kilowatts of rf power.

TAYLOR: I will just mention that we have had exactly the same effect. Unless we drop the field to zero, we find that the measurements are turned about all over the place and we have a high current too.

REFERENCES

1. An Accurate Determination of the P. L. A. Beam Energy by a Time of Flight by C. J. Batty and D. J. Warner. NIRL/R/9.

2. Accurate Energy Measurements on a 50 MeV P. L. A. report submitted to 1963 Accelerator Conference in Dubna U. S. S. R. (Also P. L. A. Acc/Phys. 18).

3. Beam Observations in the P. L. A. by K. Batchelor, A. Carne, J. Dickson and D. J. Warner. Report on 1962 Conference on Linear Accelerators for High Energies at Brookhaven National Laboratory. BNL 6511.

4. A Beam Energy Monitor by R. C. Hanna and T. A. Hodges. P. L. A. Progress Report 1963 NIRL/R/50.

ZGS INJECTOR OBSERVATIONS

Philip V. Livdahl
Argonne National Laboratory

In considering the design of multicavity, high current linacs, the effects of beam loading on the cavity gradient are matters of greater concern as the beam currents become increasingly large. Presented in this discussion will be observations of these effects made on the ZGS, 50 MeV injector. Also some comments will be made on observations of group velocity and cavity phase acceptance.

Beam Loading

The 50 MeV beam from the ZGS injector is bent into the synchrotron through a 107° achromatic magnet system. At the center of the second bending magnet of the system there is a focus at the same point where the energy dispersion is greatest.[1] Therefore, by arranging to have a narrow (0.010") vertical slit (i.e., a slit which confines the beam to a vertical line) which can be positioned at any point in the transverse plane across the center of this magnet, it is possible to make analysis of the distribution of energies in the beam. The dispersion at this position is $\frac{\Delta E}{E} = 4.6\%$ per inch. Since the absolute value of the fields in the magnets have not been precisely determined, only relative observations can be made.

In using this slit for orbit measurements in the synchrotron under conditions of limited energy spread in the injected beam, it had been noted that there was a distinct variation of energy with time during the pulse under conditions of large beam loading as shown in Fig. 1.

This observation led to investigation of the variation of the mean energy and energy spread with rf gradient in the cavity. Figure 2 is a typical energy distribution as determined by sweeping the slit under a given set of conditions. The results of these measurements of the energy distributions at various rf levels are shown in Fig. 3.

By observation of the high energy and low energy extremes of the distriubtions (see Fig. 1) measured at each rf level, one can observe the variation of total energy spread with cavity gradient. This variation is shown in Fig. 4.

The operating conditions of the entire linac system were maintained constant while taking the data represented in Figs. 3 and 4; that is, there were no changes of preaccelerator conditions or focusing magnets made to

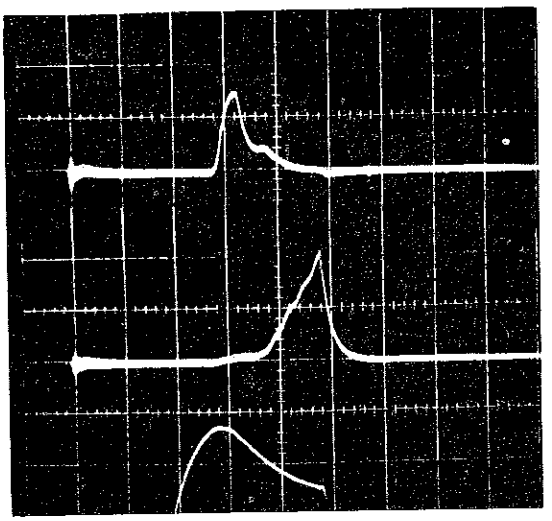

Beam pulse through slit on High Energy side of energy distribution.

Beam pulse through slit on Low Energy side of energy distribution.

Expanded rf pulse under heavy beam loading condition. 2% of rf gradient/cm, 100 μ sec/cm.

Fig. 1 Time Variation of Beam Energy Under Condition of Large Beam Loading

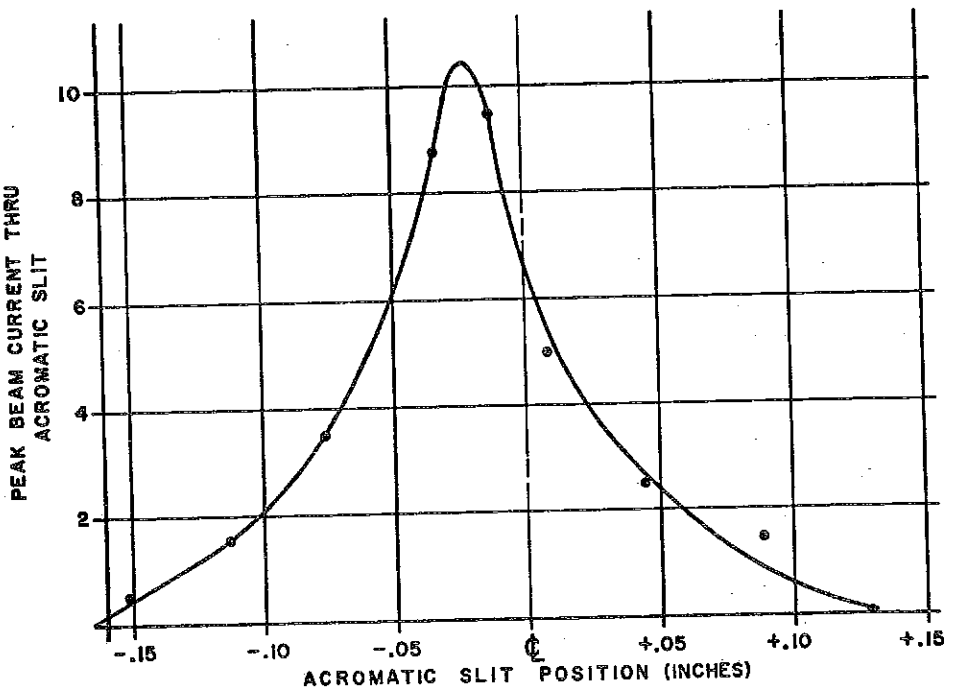

FIGURE 2 – ENERGY DISTRIBUTION AS OBSERVED BY SWEEPING ACROMATIC SLIT

adjust the injection matching conditions at the various rf levels. However, the cavity rf level was adjusted for each measurement so that there was no beam loading present.

We do not as yet understand the reasons that the mean energy and energy spread vary as observed, but will continue experiments to determine the reasons for this behavior.

Beam Loading Compensation

The ZGS injector rf system[2,3] was designed with a series, hard tube modulator for regulation of the plate voltage to the output stage of the driven amplifier. This provides a means for delivering a variable amount of power to the linac cavity during the rf pulse for cavity voltage stabilization and beam loading compensation.

Ideally, the compensation is provided by a feedback system which regulates the power amplifier output for a constant rf cavity voltage through a closed loop servo system. Unfortunately, the servo loop of this system must include the final amplifier stage of the rf system and the characteristics of this stage are variable depending on tuning of the rf circuits. For this reason, the servo loop on the ZGS injector, as of this time, has been closed only under test conditions and not under operating conditions where its effects could be evaluated. This is not to imply that there is anything impossible about the task of establishing closed loop operation but rather that the tuning conditions of the power amplifier and the matching power amplifier to the cavity must be established as fixed conditions for the closed loop system to be satisfactory. This condition is being approached but has not yet been reached on the ZGS injector.

Beam loading is now compensated by an open loop system shown in the block diagram of Fig. 5. The operation of this open loop system is shown in the scope pictures of Figs. 6.1 through 6.8.

Measurements of pulse compensation voltages required for a cavity envelope which is flat during the time of the beam pulse with 50 mA of 50 MeV beam indicate that this should be within the capability of the system when such beam currents become available from the ZGS preinjector.

Questions had been raised from time to time of the ability of the beam loading compensation system to correct all parts of the cavity properly for beam loading. Figure 7.1 shows the cavity envelope near the low energy end, center and high energy end of the cavity under condition of heavy beam loading and Fig. 7.2 shows the same output loops under operation with the open loop correction of Fig. 5. These scope pictures

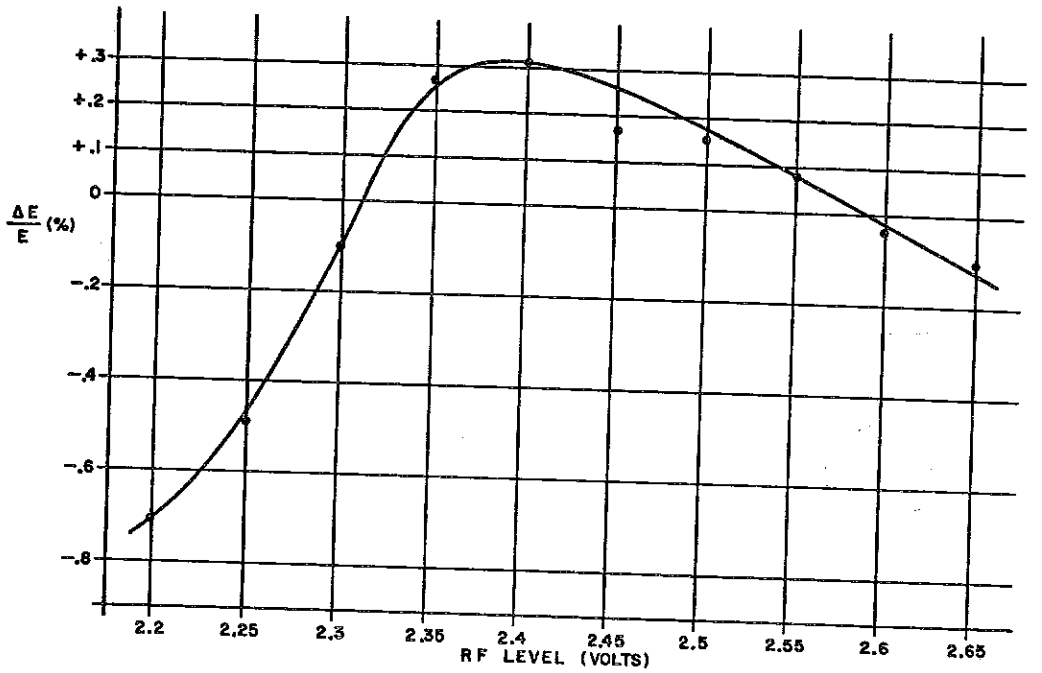

FIGURE 3 – VARIATION OF MEAN ENERGY WITH RF GRADIENT

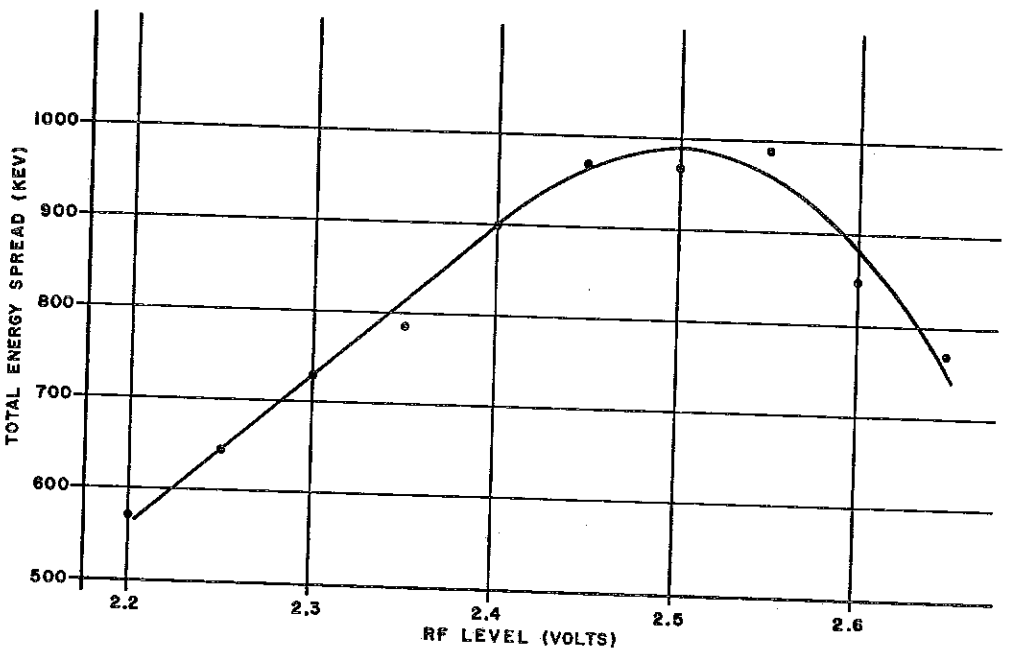

FIGURE 4 – VARIATION OF TOTAL ENERGY SPREAD WITH RF LEVEL

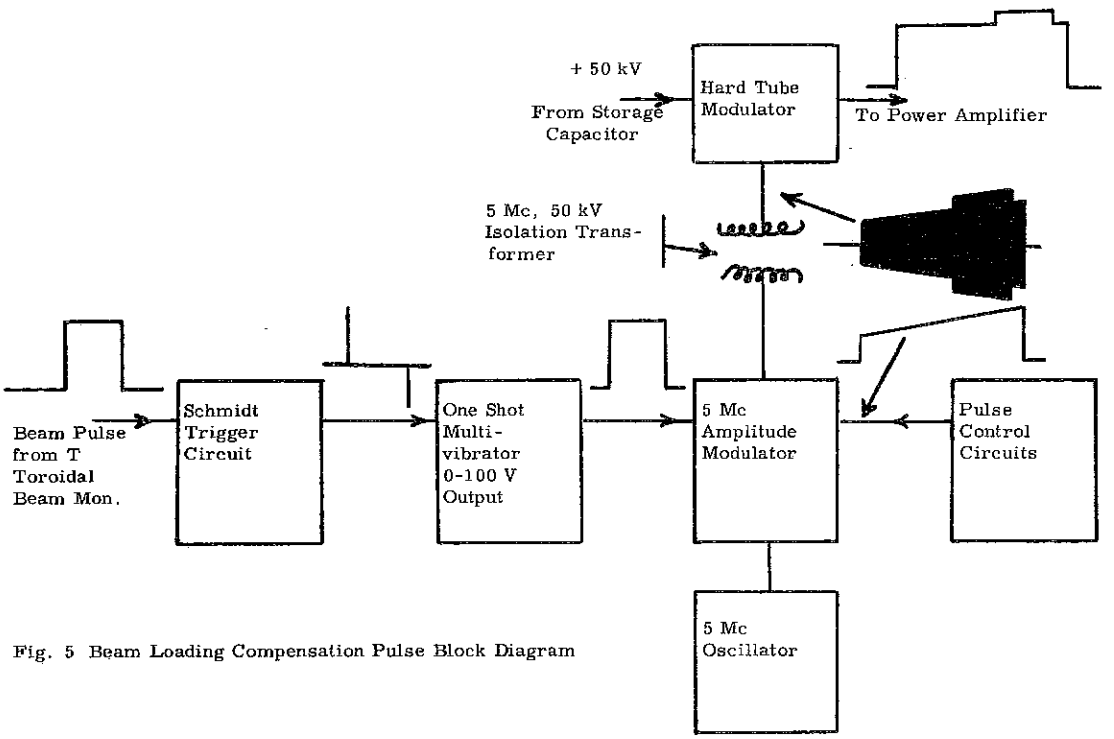

Fig. 5 Beam Loading Compensation Pulse Block Diagram

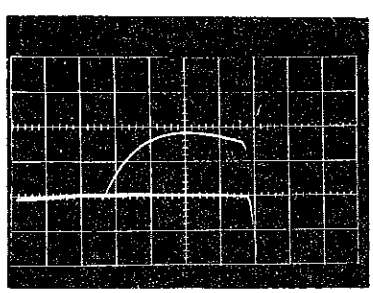

Fig. 6.1 No Beam through Cavity
No Compensation Pulse

Top Trace

Rectified cavity rf voltage.
.05 v/cm - zero suppressed.
(2.4 v is accel. gradient.)

Bottom Trace

Power amp. plate voltage.
10 kv/cm.
Sweep - 50 μ sec/cm.

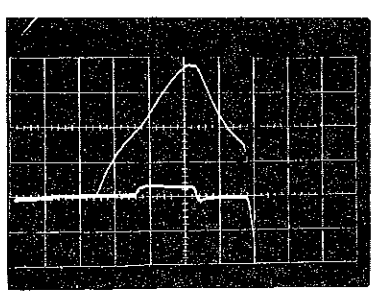

Fig. 6.2 No Beam through Cavity with
Compensation Pulse 3 kv

Top Trace

Rectified cavity rf voltage.
.05 v/cm - zero suppressed.
(2.4 v is accel. gradient.)

Bottom Trace

Power amp. plate voltage.
10 kv/cm.
Sweep - 50 μ sec/cm.

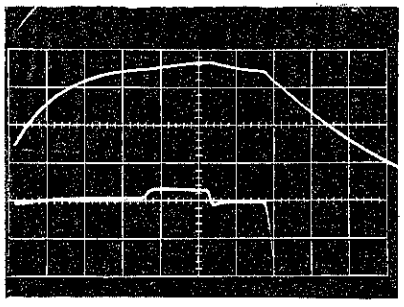

Top Trace

Rectified cavity rf without zero suppression.
1 v/cm.

Bottom Trace

Power amplifier plate voltage with 3 kv compensation.
10 kv/cm.
Sweep - 50 μ sec/cm.

Fig. 6.3 Same as 6.2, but without Expanded RF Scale

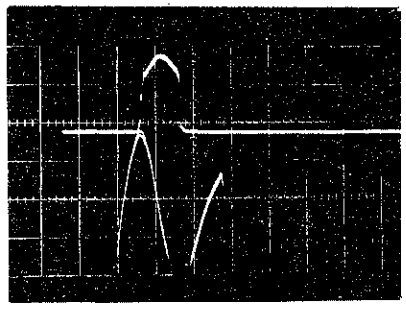

Top Trace

Beam pulse - 10 mA/cm.

Bottom Trace

Expanded rf voltage.
.05 v/cm.
Sweep - 100 μ sec/cm.

Fig. 6.5 Same as 6.4 with Expanded RF Voltage

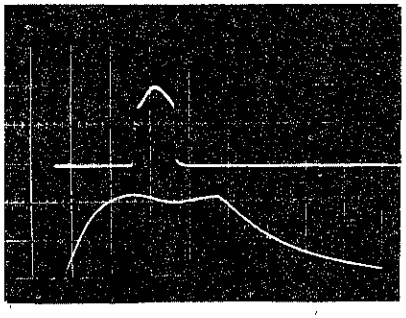

Top Trace

Beam pulse - 10 mA/cm.

Bottom Trace

Rectified cavity rf voltage.
1 v/cm.
Sweep - 100 μ sec/cm.

Fig. 6.4 20 mA Peak Beam Pulse RF Loading without Compensation

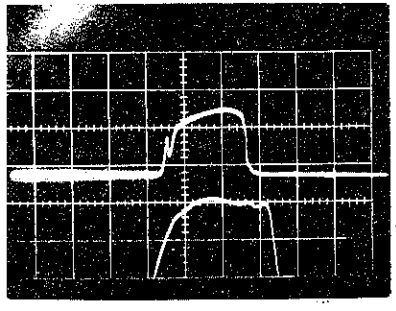

Top Trace

Beam pulse - 10 mA/cm.

Bottom Trace

Expanded rf voltage.
.05 v/cm.
Sweep - 50 μ sec/cm.

Fig. 6.6 Beam Pulse and Expanded RF Voltage with Compensation

(NOTE: Beam pulse shape changes from pictures 6.1 through 6.5, is not due to rf compensation but rather different injection conditions. 6.6 and subsequent pictures were taken on a different day.)

indicate that the cavity envelope is compensated everywhere, minor differences in the corrected waveform are due to the fact that they are not taken on the same pulse and there is some pulse-to-pulse variation when operating with the open loop system.

Group Velocity in the Linac Cavity

The group velocity, or rate of transfer of rf energy from the coupling loop to the extreme ends of the cavity, was observed in the following way. Using a dual beam scope, the output of the monitoring loops at the high and low energy ends of the cavity were compared at the time of initial cavity build-up with the rectified rf signal from an identical loop at the center of the cavity. (In this linac the rf feed loop is located at the center of the cavity.)

Figures 8.1 and 8.2 show the build-up of rf at the initial rise of the pulse. Figure 8.1 compares the center of the cavity (upper trace) with the low energy end. It is noted that the build-up of the field in the center of the cavity is very small until the rf energy has been propagated to the ends of the cavity where the initial build-up is much more rapid. The length of cavity between the two loops is 17.3 meters and the delay to start of build-up at the low energy loop is 9 μ seconds, giving a group velocity of 1.9 meters/ μ second.

No explanation for the apparent initial negative slope of the center loop has been found; changing detectors, cables, etc., has not shown the reason to lie in the detection equipment.

Figure 8.2 compares similar waveforms at the high energy end. The length of cavity between loops is 15.7 meters and the delay of build-up to the high energy loop is 3 μ seconds. This results in a group velocity in this end of the cavity of 5.2 meters/ μ second.

These observations raise the question of whether or not these numbers are characteristic of an unfilled cavity or if they do indeed remain the same in a cavity which is already excited. To observe this, the compensating pulse was applied to the power amplifier plate voltage after accelerating gradient in the cavity has been achieved and similar observations are then made of the changing rf level in the cavity due to the increased drive power. Figures 9.1 and 9.2 show the same loops as in Figs. 8.1 and 8.2 under excited cavity conditions using high gain, zero suppression plug-in units with delayed sweep.

These pictures indicate a delay of at most 2 μ seconds at the low energy end and about 1 μ second at the high energy end which would

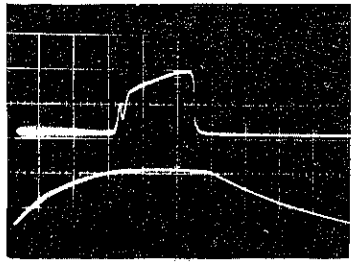

Top Trace

Beam pulse - 10 mA/cm.

Bottom Trace

Sweep - 50 μ sec/cm

Fig. 6.7. Same as 6.6, but without Expanded RF Waveform

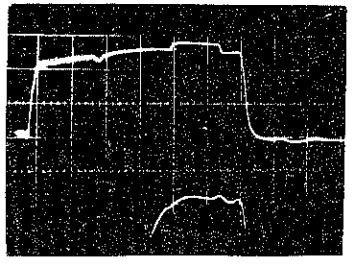

Top Trace

Power amplifier plate voltage with compensation pulse.
10 kv/cm.
Sweep - 50 μ sec/cm.

Bottom Trace

Rectified cavity rf voltage
.05 v/cm.

Fig. 6.8. RF Voltage Pulse and Plate Voltage Waveform with Compensation for Beam Loading

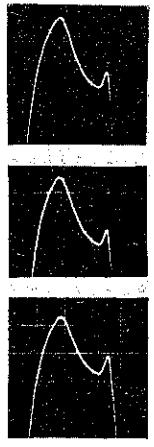

Low Energy End of cavity. Loop 9.2%/cm, 50 μ sec/cm.

Center of cavity. Loop 42, 2%/cm. 50 μ sec/cm.

High Energy End of cavity. Loop 58, 2%/cm, 50 μ sec/cm.

Fig. 7.1. RF Envelope at 3 Cavity Positions Under Heavy Beam Loading Conditions

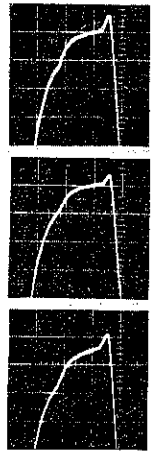

Low Energy End of cavity. Loop 9, 2%/cm, 50 μ sec/cm.

Center of cavity. Loop 42, 2%/cm, 50 μ sec/cm.

High Energy End of cavity. Loop 58, 2%/cm, 50 μ sec/cm.

Fig. 7.2. RF Envelope at 3 Cavity Positions With Open Loop Beam Loading Compensation

indicate group velocities which are greater by about a factor of 5 (8.6 meters/ μsecond) at the low energy end and 3 (15.7 meters/μ second) at the high energy end under the condition where the cavity is excited.

Linac Phase Acceptance

Phase acceptance measurements are made as the ratio of the peak beam current entering the bore of the first drift tube, as measured by a shielded toroid which measures only those particles which enter the bore of the first drift tube, to the peak beam current accelerated through the linac (as measured by either stopping the beam or by a toroid). The expected phased acceptance without buncher at the design synchronous phase angle and accelerating gradient is $\frac{3 \times 26^{o}}{360^{o}}$ or 22.6%. This phase acceptance, or transmission efficiency, is observed at an rf level of 2.35 volts (see Fig. 1) and the threshold for acceleration is 2.15 volts. Raising the rf level beyond 2.45 volts has not ever been observed to raise the transmission efficiency without buncher beyond 25%. One would expect it to continue to rise as the gradient is increased, provided appropriate compensation of quadrupole focusing fields were made. Efforts to achieve this have not been successful.

Measurements of phase acceptance as a function of preaccelerator injection energy have confirmed those measurements made at BNL.[4] Use of the first harmonic buncher has yielded transmission efficiencies as high at 65% (68% is the design expectation) but 55% to 60% is the usual day-to-day operating condition.

These phase acceptance measurements make no correction for proton percentage. In the ZGS system the two sets of triplet quadrupole matching lenses serve to separate such a large percentage of the molecular hydrogen and other heavy ions which are produced in the ion source that only a negligible amount of these ions are injected into the linac.

Conclusions

These observations show that very precise rf level control is necessary to meet the design requirements of a multicavity system to maintain the required injection energy as the beam progresses from section to section. In connection with the use of this particular linac as the injector for the ZGS, the data shows that by an appropriate programming of the rf level, it may be possible to use the changing energy characteristic to an advantage by providing an increasing injection energy with pulse length.

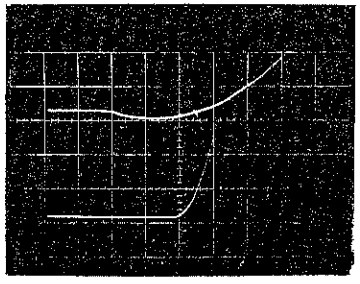

Top Trace

Loop 34 (center of cavity) time base 5 μ sec/cm.

Bottom Trace

Loop 1 (low energy end of cavity) time base 5 μ sec/cm.

Fig. 8.1 Initial Cavity Build Up at Center and Low Energy End of Cavity

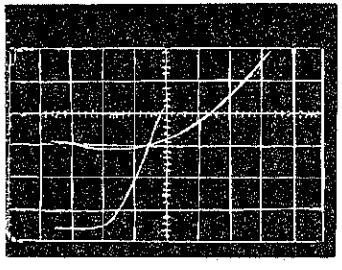

Top Trace

Loop 34 (center of cavity) time base 5 μ sec/cm.

Bottom Trace

Loop 64 (high energy end of cavity) time base 5 μ sec/cm.

Fig. 8.2 Initial Cavity Build Up at Center and High Energy End of Cavity

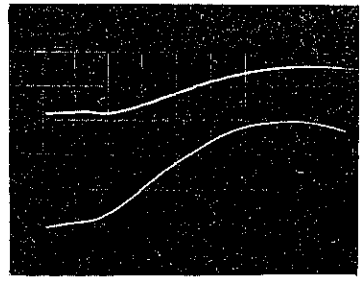

Top Trace

Loop 34 (center of cavity), 10 μ sec/cm.

Bottom Trace

Loop 1 (low energy end), 10 μ sec/cm.

Fig. 9.1 Change of Cavity RF Envelope Due to Spike on Power Amplifier Plate Voltage at Center and Low Energy End of Cavity

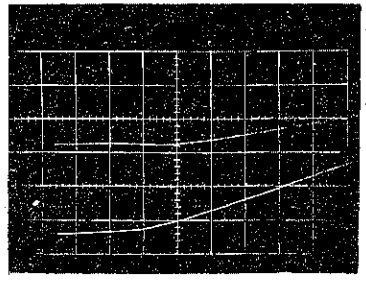

Top Trace

Loop 34 (center of cavity), 5 μ sec/cm.

Bottom Trace

Loop 64 (high energy), 5 μ sec/cm.

Fig. 9.2 As in Fig. 9.1 except comparing center and high energy end of the cavity.

Beam loading control with long pulse length at high beam current is certainly feasible but all of the engineering problems on our particular machine are not as yet solved.

SHAYLOR: I presume you are using a Tektronics 555 Scope for the double display work.

LIVDAHL: That is correct.

SHAYLOR: Until recently I was at Birmingham (England) and there we have very great difficulties with earth loops, due to certain peculiarities of our synchrotron. The 555 is particularly difficult to use in this respect since you can't selectively earth both signal inputs simultaneously unless you are using differential input amplifiers. So now one question is: Are you using differential input plug-ins? If not, what is the voltage you have at your probes so as to give us a feel for your pickup problems. Another question is, have you tried testing with the offending loop that goes negative short circuited, but still earthed in the normal way? I am looking for cross talk or trouble between the amplifiers. I am deeply suspicious of the negative-going curve, and if in fact the kick-off point is not where it starts to go negative but where it starts to go positive, then the time schedules of all these things are going to be significantly different.

LIVDAHL: In answer to your first question, differential plug-in units were not used. As a matter of fact, type Z, zero suppression plug-in units were used. I am not sure what type of units were used for the initial build-up.

CASTOR: They were the type Z used without the slide back.

LIVDAHL: In connection with the cabling to the loops, neither loop is grounded anywhere in the system. There is a teflon shield around the loop where it penetrates into the cavity so that there are no ac or grounding problems. It is a floating system all the way to the scope.

SHAYLOR: The type Z unit, the slide-back unit, has in fact a lot of hook diodes on its input, and I think that feeding a bit of the 200 Mc rf into it may produce some interesting effects.

ROWE: I would like to make a couple of remarks on this--an old user of Tektronics Scopes--I never noticed this particular difficulty with the type Z plug-in, but the CA plug-in has an obnoxious habit of ringing at very high frequency, far beyond the response of the scope proper. This seems

to be associated with the input attenuator and the first stage of the amplifier. And you can get some truly magnificent results under some condition; I was thinking along the same lines this gentleman was and I was wondering if maybe that might be the trouble. We got around some of these problems once by buying intentionally a poor scope.

LIVDAHL: Nevertheless, I believe that where you saw this negative-going trace was the point at which the pedestal was placed on the plate voltage waveform. For this reason I didn't worry about this because that was not what I was attempting to look at. The fact that the top trace came up at a delayed time relative to the lower trace and that we knew that this was synchronized within less than a microsecond with the pedestal on the waveform just did not seem like there was any reason to worry too much about the negative undershoot.

SHAYLOR: You were not trying to interpret anything from the point where the top trace rose above the base line?

LIVDAHL: That is correct. All of the numbers that I gave you were from this point to this point.

KEANE: I might have a different explanation on this same topic. I think I have seen the same thing and I think it is moding. We have scalloping on our waveform. I am going to talk about this next, but essentially because you have a variance from probe to probe, I feel it is not the scope itself but rather the existing modes in the tank.

PRIEST: If that is the case, what Shaylor suggested would prove it, would it not; if you short circuit the loop or rotate it so that it doesn't couple, this negative thing will disappear whether it is a mode or not, if it is an rf effect, it will disappear, but if it is some kind of an extraneous spurious effect, it won't disappear. At least it would be a check.

LEISS: We are probably pushing this a little bit too much. However, it is quite possible that it actually represents one of the things which we have calculated in the extreme transit behavior of the machine. This is the following. You probably have before your main pulse, for example through the grid drive, a small amount of rf in the cavity. Now when you turn the pulse on, you get some very interesting transients and phase oscillations. What you detect in your diode is the total field vector, which can have oscillations on it and these oscillations have actually been observed. I would suspect that this is actually a real phenomena that one can predict in the extreme transient behavior on this machine as you start filling it.

LIVDAHL: I just cannot believe this, Jim, because this is nothing but the rectified output of an rf envelope and this says that this loop has got to be taking power out of the cavity.

LEISS: Well, the point is that if you have a small amount of rf in there, which I suspect you do, because your grid drive is probably on before the plate voltage, then you have an offset zero and it really has not gone negative; it has just gone down closer to true zero.

LIVDAHL: Yes, the drive does come on about 10 microseconds before the plate pulse and I do not know that we have looked for this.

LEISS: There is another interesting example you can predict and which has been observed on a lot of machines. When you turn the rf off, instead of the detected rf signal going down it initially has a rise. This is again precisely the same thing. This is the phase oscillation that is induced when you make a sudden change in the rf level of the cavity.

JAMESON: I might comment on this last statement. We did some measurements on a cell iris-loaded structure in which we put in a square wave input and looked at the build-up with a sampling scope. We took the pictures and measured the 63% rise time, and these indicated that the structure filled from the back end first. We also saw the transient that you spoke of at pulse turn-off. This effect was greater the further away you got from the drive. Now, these measurements that we did were done at signal generator power levels and I have some reservations about the techniques as far as quantitative results are concerned. One thing was that we were coupling out more than we should have been with the measurement loops. However, the observed results were qualitatively exactly as predicted by the equivalent circuit theorem.

VAN STEENBERGEN: May I make one comment on the closing of the loop? Mr. Otis, together with John Keane, has worked on the rf stabilization loop at Brookhaven. So far he has succeeded in closing the loop and keeping a stable system for the cut-off frequencies up to 20 kc and loop gains up to 5. When he exceeded these limits of cut-off frequency and loop gain, he saw strong excitation of extramoding of the tank. We just could not work with a loop stabilization system which had a wider frequency band which means that if there were to be any corrections, they had to be of a very slow variety in our particularly long tank.

FEATHERSTONE: I think everybody here who is interested in rf systems would like a status report on life and performance of 7835's.

LIVDAHL: I knew that question would be asked, so I looked at the clock last week. At the present time our mode of operation is to start up at midnight on Wednesday night and run through the following Friday morning, a period of 25 shifts, with operation on the succeeding days as we need for maintenance, observation, development, etc. At this rate we build up a maximum of 500 hours per month, so we really do not have an awful lot of data on it yet. However, last November 21, we put a 7835 in the power amplifier; it has been in there since. The power amplifier has not been apart in that time and we have operated for 4,400 hours in that time and the tube had a little over a 100 hours on it before that. The other two tubes that we own have 2,000 and 2,200 hours on them. There is no reason to believe that any of the three tubes have changed characteristics in that time.

REFERENCES

1. Teng, L. C., "Achromatic Bending Magnet Systems", ANLAD 48, Argonne National Laboratory, April 8, 1958.

2. Abraham, J., et al., Operational Experience with the ZGS Injector, Argonne National Laboratory, July 9, 1963.

3. Livdahl, P. V., ZGS Injector Linac, Minutes of the Conference on Proton Linear Accelerators, Yale University, October 23, 1963, pp. 231-239.

4. Blewett, J. P., Phase Acceptance and Bunching in the AGS Linac, JPB-18, Brookhaven National Laboratory, March 27, 1963.

EXPERIMENTS ON RF FIELD PATTERNS IN THE BNL LINAC

J. T. Keane
Brookhaven National Laboratory

The major portion of this presentation will be concerned with the scallops observed on the rf probe patterns of the linac tank. Questions concerning this phenomena were brought up last year at Yale during Phil Livdahl's talk on the ZGS injector linac. It is contended that the cause of these scallops is due to excitation of higher order modal resonances. Figure 1 shows the scallops observed on the rf tank pattern. Note that this disturbance dies out as steady-state conditions are reached.

TANK VOLTAGE PATTERN WITH DISTORTION

TANK VOLTAGE PATTERN UN-DISTORTED

Figure 1

Before giving experimental proof of the cause of these scallops it seems appropriate to review the modes that can exist in a linac tank.

The wave types for a circular guide and their cutoff wavelengths are shown in Table I. It is seen that if as in a linac tank the diameter of the guide is adjusted for a cutoff frequency of 200 Mc in the TM_{01} mode (d = 1.15 meters), the TE_{11} mode is the only remaining mode above cutoff. As will be shown the frequency of resonance of the linac tank operating in the TE_{11} mode is 153 Mc. Since this is much lower than the excitation frequency of 200 Mc, this mode will provide little trouble.

Wave Type	Cutoff Wavelength	Cutoff Frequency if d = 1.15 m
TE_{11}	1.71 diameter (d)	153 Megacycles (Mc)
TM_{01}	1.31 d	200 Mc
TE_{01}	0.82 d	320 Mc
TE_{21}	1.03 d	255 Mc
TM_{11}	0.82 d	320 Mc

TABLE I. Modes in Circular Waveguides

NOTE: TM_{10} and TE_{10} modes impossible since zero tangential electric field at conducting walls requires 1 0.

For the TE_{11p} mode where p is the number of variations in the longitudinal direction the resonant wavelength is as shown below

$$\lambda = \frac{2}{\left[\left(\frac{p}{\ell}\right)^2 + \left(\frac{1}{1.706a}\right)^2\right]^{1/2}} \cong 2\,a\,(1.706) \text{ since } \ell \gg p$$

$$\therefore \lambda \cong 1.706\,d = 1.706\,(1.15) = 1.96 \text{ meters}$$

$\therefore$ all resonances = f $\cong$ 153 megacycles where ℓ = 33.5 meters, the length of present linac tank

a = radius of tank
d = diameter of tank .

Thus the majority of the TE_{11p} mode resonances for a long tank will be near 153 Mc.

The only remaining resonant modes needing consideration are the higher order TM_{01p} modes. Their resonant frequencies are given as follows.

$$\text{For } TM_{01p} = \frac{2}{\left[\left(\frac{p}{\ell}\right)^2 + \left(\frac{1}{1.306\,a}\right)^2\right]^{1/2}} \frac{1.5}{\left[1 + \left(\frac{0.75\,p}{33.5}\right)^2\right]^{1/2}}$$

where a = 0.575 meters
ℓ = 33.5 meters

$$\lambda \cong 1.5\left[1 - \left(\frac{0.75\,p}{\ell}\right)^2\right] = 1.5\left[1 - \left(\frac{0.75\,p}{33.5}\right)^2\right]$$

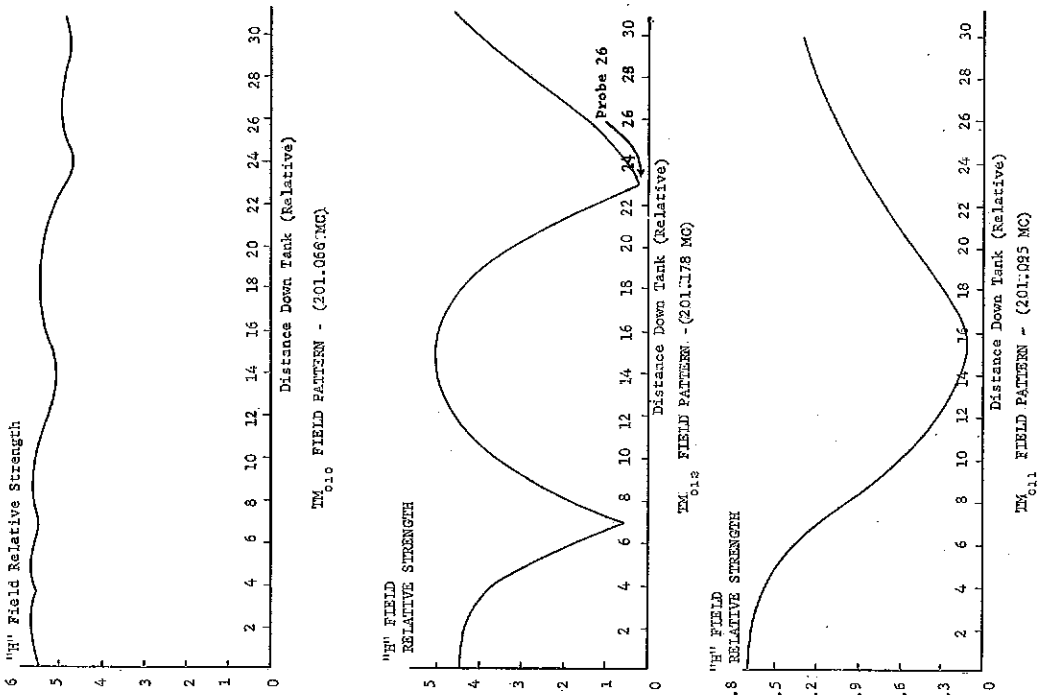
"H" Field Relative Strength
Distance Down Tank (Relative)
TM010 FIELD PATTERN - (201.066 MC)
"H" FIELD
RELATIVE STRENGTH
Probe 26
Distance Down Tank (Relative)
TM012 FIELD PATTERN - (201.178 MC)
"H" FIELD
RELATIVE STRENGTH
Distance Down Tank (Relative)
TM011 FIELD PATTERN - (201.095 MC)

FIG. 3

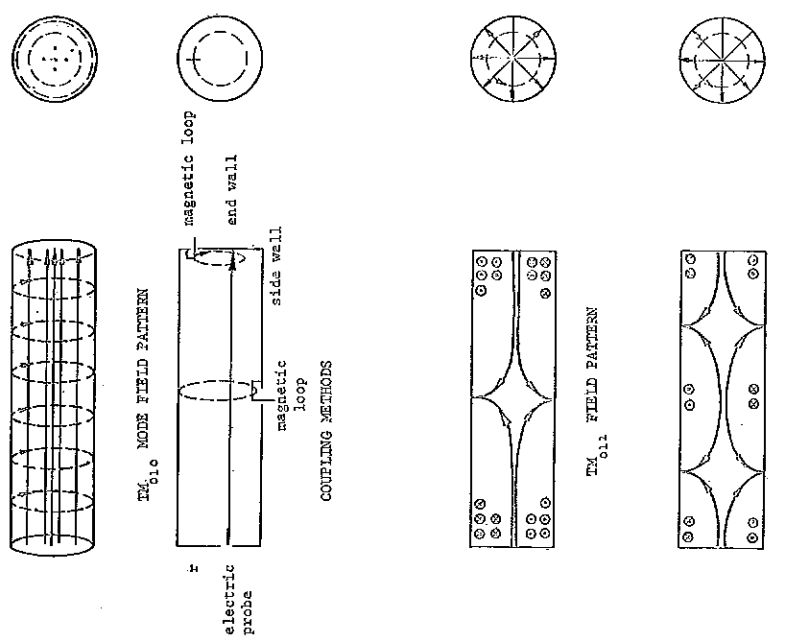
TM010 MODE FIELD PATTERN
magnetic loop
end wall
side wall
magnetic loop
electric probe
COUPLING METHODS
TM011 FIELD PATTERN
TM012 FIELD PATTERN

FIG. 2

Note: Resonant wavelength for higher order modes approach that of TM_{010} as ℓ increases.

$$\Delta f = f \frac{\Delta\lambda}{\lambda} = 200 \times 10^6 \left(\frac{0.75\,p}{33.5}\right)^2 \left(\frac{1}{1.5}\right)$$ where Δf is cycles above the resonant frequency of TM_{010} mode.

$$\underline{\Delta f = p^2 \ (66.2 \times 10^3) \text{ cycles}}$$

TM_{011}: $p = 1$ $\therefore \Delta f =$ 66 kilocycles (kc)
TM_{012}: $p = 2$ $\therefore \Delta f =$ 264 kc
TM_{013}: $p = 3$ $\therefore \Delta f =$ 6 megacycles (Mc)

It is thus seen that the TM_{011} and TM_{012} modes can be excited very readily in a linac structure. Of course, their strength will be highly dependent on the location of the coupling loop into the tank. If a single magnetic loop is used, its location can be unfavorable to either the TM_{012} mode or the TM_{011} mode but not both (see Fig. 2). Since BNL's loop provides magnetic coupling at a point centrally located along the tank length,

(a) weak coupling to the TM_{011} mode will result since this is a point of minimum "H" field for this mode;

(b) strong coupling to the TM_{012} mode will result since this is a point of maximum "H" field for this mode.

Having reviewed the possible modes that can exist in a linac tank we can get on with the results of modal studies on BNL's tank. The capability of a linac structure to support a TM_{011} and TM_{012} mode was vertified by changing the excitation frequency and looking for the characteristic modal configurations of the TM_{011} and TM_{012} waves along the length of the tank. These patterns were ascertained by use of 34 calibration loops located along the tank length. Essentially they measure the magnetic field strengths at the tank walls.

The results of the test are given in Table II below.

Mode	Frequency	Maximum Observed Field Strength Relative Reading	f	Calc. f
TM_{010}	201.066 Mc	5.7	0	0
TM_{011}	201.095 Mc	5	29 kc	66 kc
TM_{012}	201.178 Mc	1.65	112 kc	264 kc

TABLE II. Observed Modes in BNL Linac (see Fig. 2)

Since this linac is excited by a single magnetic loop centrally located, the results agree with theory. As was expected the field strength was strong for the TM_{012} mode but weak for the TM_{011} mode. It is noted, however, that the resonant frequencies of the TM_{011} and TM_{012} modes were closer to that of the TM_{010} mode than expected. This apparent deviation from theoretical findings is easily explained. The existence of varying length drift tubes and ball tuners should alter results expected from an unperturbed cylindrical guide analysis.

Figure 3 shows plots of the relative "H" field steady-state strength along the length of the tank for the normal TM_{010}, the TM_{012} and TM_{011} modes. Note that as expected the "H" field for the TM_{012} mode has a minimum at Probe 10 and Probe 26, also that the field strength of the TM_{011} mode is smaller than that of the other two.

Essentially the initial statement that the scallops on the rf patterns were due to moding is proved by the data just presented.

With the tank excited at its normal frequency the following observations were made.

1. At Probes 10 and 26 where the tangential magnetic field of the TM_{012} field pattern was minimum, the scalloping on the TM_{010} excited rf pattern was not present.

2. The relative magnitude of the scalloping on the TM_{010} rf pattern increased along the tank length in the same manner as the magnetic field intensity of the TM_{012} pattern.

3. The frequency of the scallops agreed closely to the difference frequency between the TM_{010} and TM_{012} resonances.

4. As the steady-state tank response to TM_{010} mode excitation is reached, the scalloping dies out.

From the above statements it is concluded that during the build-up time of the tank the TM_{012} resonant mode is excited. Due to two different frequency sources present the measuring loops detect a modulating signal whose frequency is equal to the difference frequency of the two sources ($TM_{010} + TM_{012}$).

It is well known that the Fourier power spectrum of an rf pulsed signal has frequency components around the center frequency. These frequency components serve as the source of the TM_{012} excitation during the build-up period and tend to die out once steady-state conditions are reached. Since BNL's method of coupling is favorable to the TM_{012} mode, the scallops are observed.

At this point we took a closer look at the probe patterns that did not have the noticeable scallops, namely Probes 10 and 26. It was noted that there was a slight modulation at 30 kc which indicated that the TM_{011} mode was also excited but to a much lesser extent than the TM_{012}.

Since this time, A. Otis of BNL has done work on an rf level stabilization loop. In his first attempts at closing a loop he had oscillations. Again the frequency of oscillation was the difference frequency of the (TM_{011} and TM_{012}) modes away from the TM_{010} mode.

Now that the existence of these modes has been verified, what does it mean? Certainly it will prove cumbersome to a closed loop system being controlled by a linac tank signal. Again since the tank is more susceptible to these undesired oscillations during transient periods, what effect will it have on beam compensation schemes? Both these modes have radial "E" field components that would prove detrimental to the beam. The big question which unfortunately I cannot answer is how strong can these defocusing fields be when 50 or 100 ma beams are passing through linac tanks? Hopefully they are weak enough to neglect. One way to lessen the effects of these resonances would be to keep the tank length down. Previously I showed a resonance equation that indicated that the frequency of these undesired oscillations moved further away from the TM_{010} mode resonance as tank length decreased. This would tend to decrease the power present in the side bands.

The scalloping just described is always present on BNL linac probes. We are blessed with another type of scalloping, however, that acts something like a phantom. It crops up suddenly and leaves just as suddenly. Fortunately it only stays for very short periods. The magnitude of these scallops are much larger than the ones just described. The scalloping frequency and distribution along the tank length indicates it is a TM_{011} modal excitation. Apparently it is caused by particles coming from the

Cockcroft-Walton generator. This is concluded by the fact that it can normally be eliminated by

1. Turning on beam chopper, or
2. Closing the valve at the linac tank entrance, or
3. Putting in a flag between the Cockcroft-Walton and linac tank.

We have done studies during one of its short stays recently and found that

1. It is independent of the buncher--the rf feedback loop from the tank was taken off and it still existed.

2. It is very sensitive to the Cockcroft-Walton voltage. It disappeared when the voltage is below 737 kV.

3. It is relatively insensitive to the linac tank rf power level. When the power is brought well below accelerating levels, it is unaffected--but if the level is brought above tank level, its magnitude starts to decline.

4. It is very sensitive to gas pressure. The tank is more prone to these scallops when the gas pressure is decreased.

Unfortunately this is as much as we know about these scallops and we will have to wait for its further reappearance before more data is accumulated.

DICKSON: On our closed loop stabilizer, I did not say that we had never seen scallops. We do see scallops at times but we can get rid of them and there seem to be two things that affect them. One is that if one tunes the tank so that it appears to be exactly on tune, I think this gives scalloping. If one tunes slightly off maximum, then the scalloping can be reduced to practically zero. The other thing that affects the scalloping is the length of coaxial line between the final amplifier and the tank. If one changes this line length, then the impedance presented to the tank by the amplifier changes and this has some effect on the scalloping as well. So we play with these two things and can get rid of the scalloping. We had not related the scalloping to the modes of the cavity in the way you have.

KEANE: We tried to move the resonant frequency of the higher modes. They are quite sensitive to ball tuners, etc. Anything in the line will tend to change the frequency to a greater extent than it changes the normal frequency.

TAYLOR: Can I just confuse the issue? When they are on tune, we see no scalloping and when we move off, we see a beating which corresponds to the beating between the drive frequency and the tank resonant frequency.

WADDELL: I would like to merely comment that this modal business, of course, was something that is seen in the original machine. That is, we have the original Alvarez accelerator and it differs from all the others that you are talking about in that it is a self-excited oscillator, and so during the tune-up procedure the operator has to essentially adjust the pre-exciters so that one is on the proper mode. It is possible to tune up the machine on the wrong mode and probably Earl White could speak on this, but what we do is instead of presenting a rectified waveform in the control room, we actually present the rf and then it is quite simple for the operator to look at this pattern and to simply tell what modes are being generated as the pre-exciter is being tuned.

KEANE: I would like to make one comment on this--these scallopings are very slight, small in amplitude; indeed if you detune, I can take my whole pattern and I have gigantic scallopings, but these scallopings do not attenuate. Essentially what I am saying is that these scallopings are more pronounced during the transient time and they die out once steady-state conditions are reached. Definitely if you detune, you get off frequency and you will get more violent scallopings.

JAMESON: Nagle and Knapp have pointed out the equivalent circuit theory that we are fond of at Los Alamos. I have extended this theory to a transient analysis, and I am going to talk about it tomorrow. It points out in a rigorous fashion how these scallops occur. It is the beating between the drive and the modes in the pass band, all of which are excited during transients. This beating dies out in the steady state. I have some runs also that show the behavior that you get when you drive off frequency where you get large transient bumps and then a settling back down to a steady state on which there are regular "scallops" produced by beating between the drive and the nearest mode frequency. It all comes out quite nicely in terms of the equivalent circuit theory.

BLEWETT: Something that bothers me about these higher order modes is the fact that,as John showed in his pictures, they all have radial components. Why aren't these shorted out by the drift tube stem? Our drift tube has got two stems at right angles to each other. I was wondering what sort of mode pattern you get if you had say four drift tube stems going out in all directions, or what these actual mode patterns look like in the present case.

KEANE: I will note one thing. The Q of the TM_{012} seemed to be much lower than that of the normal tank. The rise time looked to be in the order of 120 microseconds in the pattern.

LAMB: We did an experiment some years ago which is relevant to this problem. It was cleaner because there weren't any drift tubes--it was a cylindrical tank--it was resonant at around 200 Mc and into this tank we introduced the burst of electrons. The tank was surrounded by a solenoid and these electrons were just shot into the tank, and they had many Fourier components in their front. We did not detect any frequencies lower than the fundamental frequency, but we detected essentially every frequency from there on up and of course it varied where the probe was located as he pointed out. There were different ones in different places--TE's, TM's, and very high order modes. In order to suppress these modes so we could carry on with our experiments and see some electrical signal in this tank, we did the things that John just suggested. We tried to short certain modes out by putting conductors across the tank, and this would deQ this particular one, but the conductors would then look like an end wall to some other mode.

PERRY: I think there is no question that these modes do exist. In the tune-up stage of our machine we excited quite a number of these with a lock-on oscillator.

AUTOMATIC CONTROL AND STABILIZATION OF THE ORSAY LINAC

P. Brunet, L. Burnod and L. Lheritier
Ecole Normale Superieure - Orsay, France

Before speaking about automatic control, I would like to show briefly the present status of the Orsay linac. In this initial design the electron linac itself was built by the CSF Company. Since the end of 1961, the laboratory of the Orsay linac has the machine in charge for operating and improvements.

There are now four experimental areas (Fig. 1) available for physics experiments; one at 250 MeV in use since 1960, one at 500 MeV and one at 1 GeV in use since January, 1962, and the last one at 1.3 GeV is just finished now, including the deflecting system. Another experimental area is ready to receive the 500 MeV electron-positron storage ring, but the storage ring itself will be ready in 1965. The positrons will be extracted from a radiator located at the 700 MeV electron energy level and then accelerated from a few MeV to 250 MeV before injection. The electrons will be accelerated from another gun by the last part of the linac and injected in the ring at the same point as the positrons are.

We already accelerated a positron beam extracted at 200 MeV electron energy level. For a 700 MeV positron beam, the ratio of the positron intensity in 3% energy spread to the electron intensity on the target is 10^{-4}.

Now there is another proposal to extend the electron energy from 1.3 to 2.8 GeV, by doubling the length of the machine, and to increase the duty factor by a factor of 3, from 50 pps to 150 pps. In this case, the new part of the machine will be built at the front of the present linac, the shielding of the 1.3 GeV experimental area being sufficient for a 3 GeV beam.

Operating a multisection electron linac for physics experiments requires a high stability for both beam current and energy.

It is quite easy to obtain 50% of the beam current in a 1% energy spread, if the transient beam loading is compensated for by early injection or changing the modulator timing.

However, it is difficult to maintain these adjustments over a long period of time, and in addition, the setup time is long unless automatic controls are incorporated.

The influence of variations in the main machine parameters such as High Voltage, Frequency, Temperature, etc., are well known.

It is my intention here to speak only about some of the systems which have improved the Orsay accelerator and some systems which will be incorporated in the machine extension from 1.3 to 2.8 GeV.

I. Klystrons High Voltage

In the initial design, the klystrons and modulators were supplied from a single ac power supply controlled by an induction regulator with a stability of $\pm$ 1%. Such a long term stability may be sufficient if the operator can control the long term energy fluctuation. However, with a short term stability of the same magnitude, every fluctuation in the power lines is transmitted to the klystron high voltage resulting in beam energy variations of the same order. With a narrow energy spectrum and energy defining slits, excessive variations in the analyzed beam current result. Furthermore, for the induction regulator which was used, the response to the power lines transients is very slow, of the order of one second, which means that the short term stability was much worse than 1%.

In order to overcome this short term instability, we are now using a motor generator set with an ac voltage regulator of $\pm$ 1%. We now get a short term stability better than 0.1% due to the large inertia of the set. Such a system can keep approximately 2×10^{11} electrons/pulse within a 2% energy spread for several hours with current variations less than $\pm$ 5%. The long term stability can be further improved by controlling the alternator output not from the ac output voltage but rather from the charging voltage of the pulse-forming network. This means we can also adjust the klystrons high voltage by the inductor of the alternator.

II. Phasing

An automatic phasing system is already installed on five sections, or 300 MeV, of the present accelerator and it is yet working but it is under test too.

The rf phase of the section input signal is compared to the beam phase obtained from a low Q cavity excited by the beam (Fig. 2). The electronic length of the rf comparison circuit is set up so that a null on the phase detector is obtained for the optimum rf phase (Fig. 3). This optimum rf phase is determined by means of a beam energy measurement and fixed by a phase shifter. The phase detector is a magic T with two linear rf diodes (or one diode and a phase wobbling system). The two diode voltages are stretched to a dc voltage and compared in a

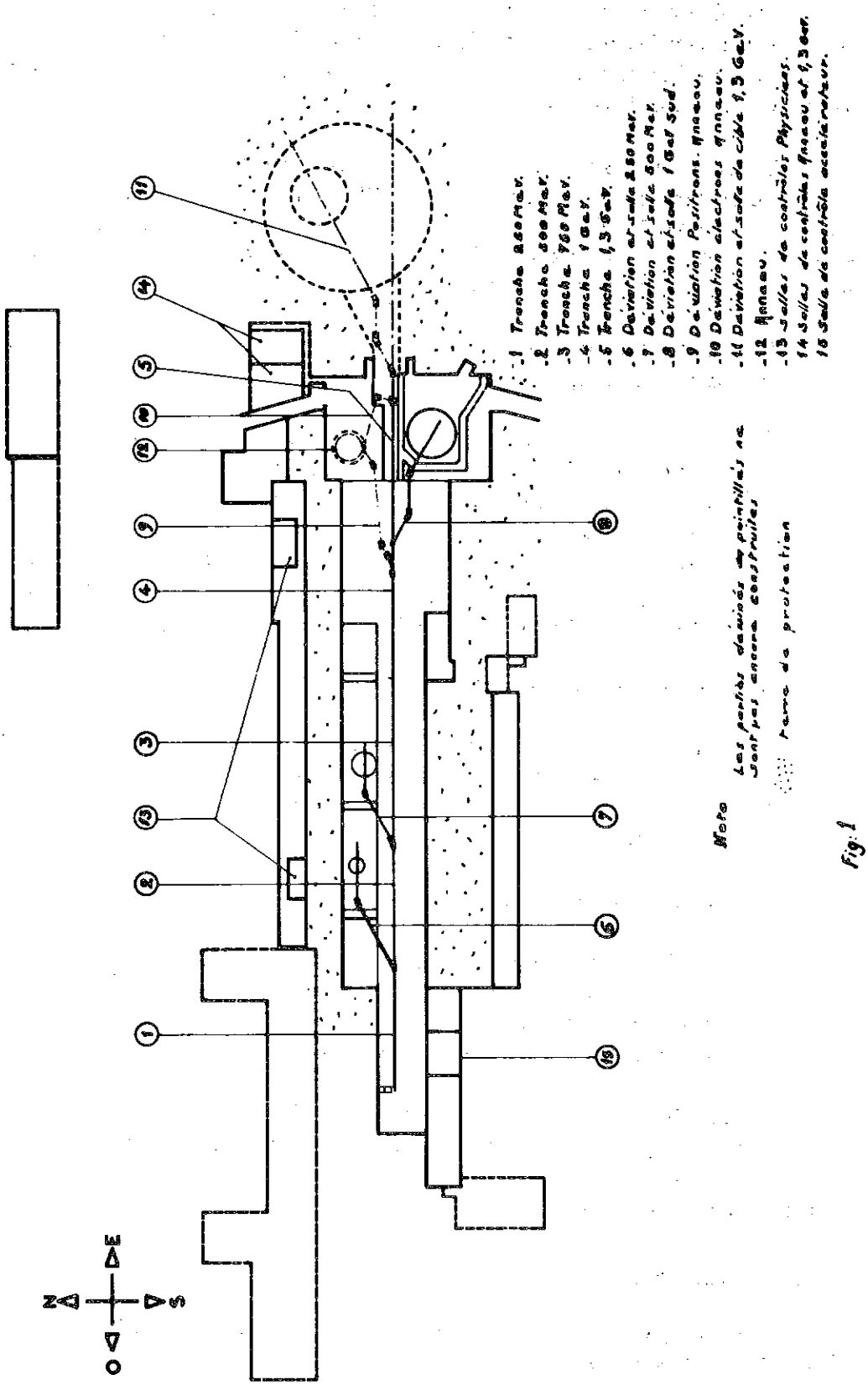
1 Tranche 850 Mev.
2 Tranche 600 Mev.
3 Tranche 750 Mev.
4 Tranche 1 Gev.
5 Tranche 1,3 Gev.
6 Déviation et salle 850 Mev.
7 Déviation et salle 600 Mev.
8 Déviation et salle 1 Gev Sud.
9 Déviation Positrons. Anneau.
10 Déviation électrons anneau.
11 Déviation et salle de câble 1,3 Gev.
12 Anneau.
13 Salles de contrôle Physiciens.
14 Salles de contrôle Anneau et 1,3 Gev.
15 Salle de contrôle accélérateur.
Les parties déjà réalisées ne sont pas encore construites
Mètre
Parc de protection
E
S
O

Fig. 1

differential dc amplifier which controls the phase of the rf klystron input. A transmission cavity in one arm of the rf comparison circuit, temperature locked to the section, compensates for small frequency and temperature variations.

With such a system we can control the phase within $\pm 3^{o}$ with a range of beam intensity from 20 to 80 mA and a 3 db klystron power range (10 to 20 MW). However, we do not know yet the behavior of the system over a long period of time, let us say for more than one month, without a new energy calibration.

It seems feasible that such a long term stability can be obtained with the following improvements.

(a) Increasing the phase stability of the rf comparison system by choosing rigid and short transmission lines.
(b) Broadening the range of operation to a 10 to 1 variation in the beam current and 6 db for the klystron power.
(c) Achieving a more simple and accurate phase calibration for example, by adjusting the set: Section + Cavity + Rf Comparison Circuit in a separate room set up for this purpose.

The disadvantages of the system are:

(a) A complete system is required yet for each section (cavities, rf comparison circuit, electronic).
(b) We must trust the phase stability of the rf phase comparison system.

The advantages are:

(a) It does not require a special accelerator triggering system nor sections with output couplers, i.e., it can be adapted on the present machine.
(b) It is a continuously operating system.

Assuming the rf driver frequency is stable, there are still two other control systems which must be incorporated if stable and reliable operation of the linac is to be obtained. These are temperature and beam position controls.

III. Temperature

The rf power level in each section is controlled by means of the klystron high voltage and is set to give the optimum performance of

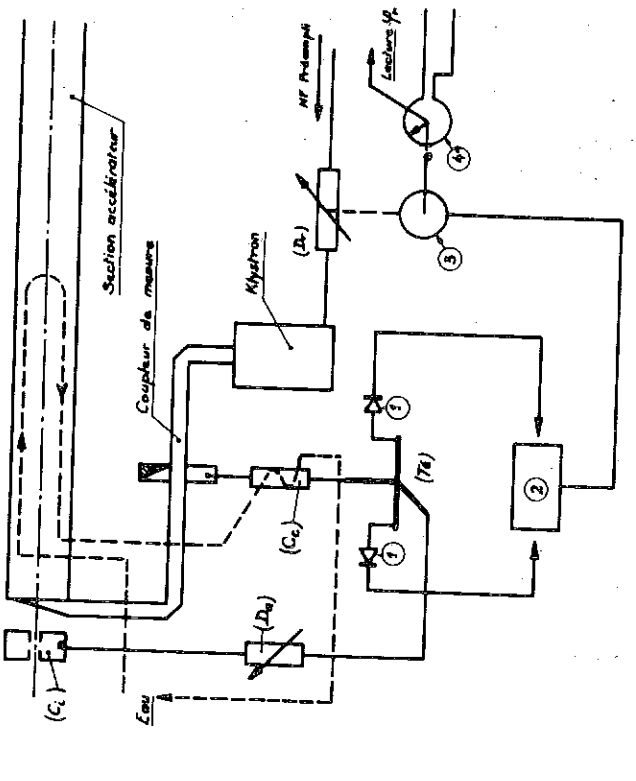

Réglage automatique des phases hyperfréquence
Schéma synoptique

Fig. 3

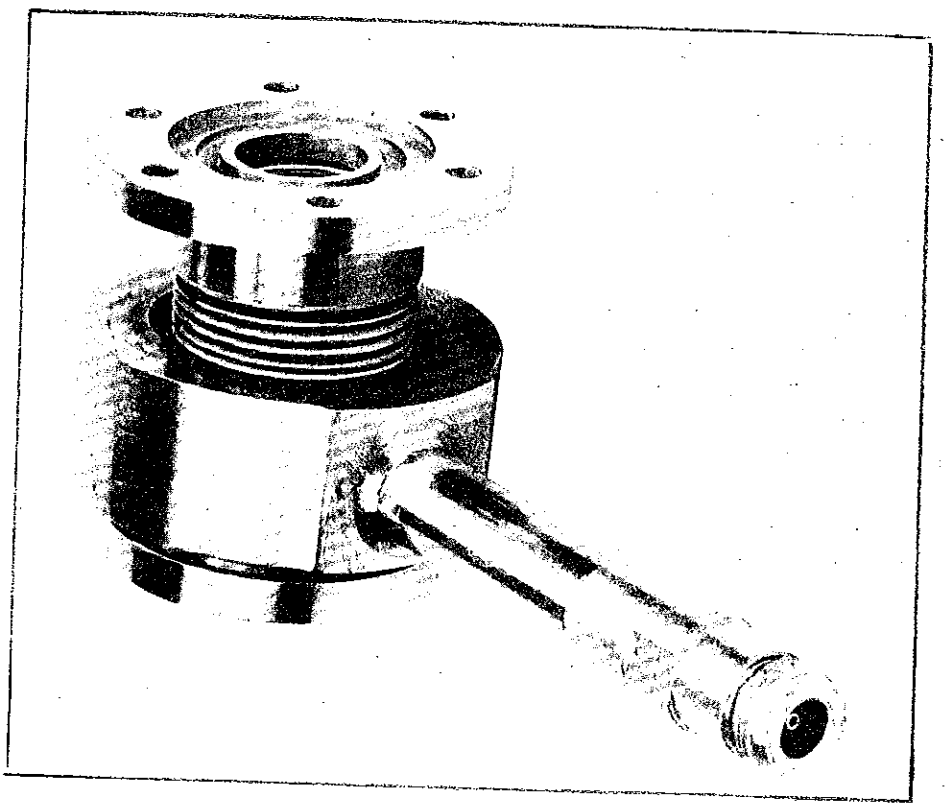

Fig. 2

section and klystron. Preliminary measurements on the heat transfer between the sections and the water indicated that the temperature gradient between the copper and water is not independent of the power. This means that the cooling of each section has to be independently adjusted. This can be achieved by controlling the rf phase between the input and output of the section.

This comparison can be seen to be extremely sensitive, since

$$\Delta\phi = \alpha\omega\tau \cdot \Delta\theta$$

where

α is the coefficient of linear expansion of copper
ω is 2π x frequency
τ is the filling time of the section
$\Delta\theta$ is the temperature change

For example, with

$\omega = 2\pi \times 3 \times 10^{9}$
$\tau = 10^{-6}$ seconds
$\alpha = 1.6 \times 10^{-5}$

$$\Delta\phi = 17 \text{ degrees/degree C.}$$

IV. Beam Position Control

For a high power beam, it is very important to keep the beam on the axis. A steering system which is really independent of energy and stray magnetic fields appears difficult to build. However, for a single beam operation it should be possible to use an error signal derived from a beam position monitor to control steering dipoles and keep the beam on axis; after phasing a given sector, the beam can be steered and the position monitored. This sequence of events is then carried out on each successive sector.

Despite the multiplicity of parameters affecting the beam dynamics, it should be possible to design in such a way an automatic beam steering system.

In this stage we still prefer to put local control loops, better than a central computer, and to increase the stability of the components.

In conclusion, at Orsay the present philosophy is always to manually control the accelerator with the exception of the automatic systems which I have described.

BLEWETT: Could you give an estimate of the ultimate that you could achieve in the control of phase?

BURNOD: With the electronics which we have now, because we use a mechanical phase shifter, we think that $\pm 3^{o}$ is a limit we cannot improve. If we use a ferrite phase shifter instead of a mechanical one, we can have a continuous variation of the phase and a better short-term stability, but of course using such a ferrite device we will lose in long-term stability due to the ferrite and its power supply.

JAMESON: What kind of short-term phase stability are you talking about?

BURNOD: Oh, the phase stability is now $\pm 3^{o}$ over several hours. There is no problem for the short-term stability using a mechanical phase shifter.

FEATHERSTONE: Must you control the temperature of the transmission lines which bring the phase information to your control devices?

BURNOD: It is not done yet, but we must do it.

PROGRESS IN HIGH INTENSITY ION SOURCE AND ACCELERATOR COLUMN DEVELOPMENT

A. van Steenbergen
Brookhaven National Laboratory

Recent work on ion sources has shown a gradual increase of proton beam intensities obtainable from preinjector systems. In general, together with an increase in beam intensity an increase of the beam emittance was observed. Up to the space-charge limit in the BNL AGS, this will become most likely the determining factor in AGS beam intensity. This will be especially so when multiple turn injection will be used at the AGS, which is scheduled to be completed during the next month.

Further, preinjector intensities for the proposed BNL 500 MeV linac injector will be of the order of 500 mA in order to obtain linac beam intensities of at least 100 mA.

Only recently have ion sources been developed capable of total beam outputs of this order of magnitude and being suitable at the same time for use in conjunction with particle accelerators because of emittance characteristics. For completeness sake a short enumeration of these sources follows:

1) PIG Ion Source. Here a plasma is obtained by means of a gas discharge in a simple two electrode structure. Secondary electron emission to sustain the discharge is obtained by means of ion impact on the cold cathodes. Electron oscillation between the two cathodes is maintained for high ionization efficiency by means of the anode-cathode electrical field and an axial magnetic field.

2) Rf Ion Source. An electrodeless ("magnetically" excited) discharge, by means of a radio-frequency field is obtained in a ceramic or pyrex source "pot." An extra electrode in the plasma chamber is used to establish a field in a ceramic channel for ion extraction from the plasma boundary located within the source pot.

3) Duoplasmatron Source. A hot cathode (emission layer coated cathode or a tungsten cathode) is used for the production of electrons for gas ionization in a three-electrode structure. With a conical geometry of the extra electrode between cathode and anode some plasma compression is obtained. Further compaction, between the extra electrode and the anode is accomplished by means of magnetic mirror fields around the

interspace of these electrodes. For higher output currents, a specially shaped aperture button makes it possible to obtain ion emission from a larger area than the source aperture opening (small plasma cup).

4) Lamb-Lofgren Source.* This source is a version of the "magnetic" ion source, i.e., a hot cathode discharge type source with plasma concentration by means of an axial magnetic field. Here, instead of a single aperture hole, a multiple of apertures is used to let the plasma expand in a large cylindrical plasma expansion cup. With the extraction field a concave plasma sheath is formed within the relatively large plasma expansion cup.

5) "Modified" Duoplasmatron Ion Source (Solnyshkov, et al). A large plasma expansion cup is attached to the basic duoplasmatron source and ion extraction takes place from a shaped plasma boundary sheath.

6) "Modified" PIG Source (Gabovich, et al). This is the basic PIG source with hot cathode and large plasma expansion cup.

In order to establish some criteria by which to compare these various ion sources, it is useful to define source brightness and related beam emittance again. The momentum normalized beam emittance, as related to the two-dimensional phase space projection is given by,

$$v = \beta\gamma \frac{\iint F(x, \alpha_x)\, dx\, d\alpha_x}{\pi} = \beta\gamma E$$

where v is the emittance invariant and $F(x, \alpha_x)$ represents the two-dimensional transverse phase space boundary for a proton beam, determined at a particular energy.

The source "brightness" may now be defined as:

$$B = \frac{I}{\pi^2 v^2},$$

---

*Ion extraction from a large plasma boundary and plasma boundary shaping ("plasma boundary focusing") by means of grids or extraction fields, as applied in the "modified" duoplasmatron source and "modified" PIG source were first incorporated in this particular ion source design.

which specifies the particles per unit time density in four-dimensional phase space, assuming a simplified E, t distribution.[1,2] This definition is identical to the statement that the source brightness is the particle flux (current density) per unit solid angle.

Referring now to the conventional duoplasmatron source, the rf source and the PIG source, these sources showed generally the behavior that the emittance increased linearly with the output beam current. This was observed at BNL for the PIG source and conventional duoplasmatron source and similarly at CERN for the rf source. This behavior is expressed as:

$$v = \frac{I}{\pi \delta}$$

and consequently,

$$B = \frac{\delta^2}{I} \quad ,$$

with δ a constant.*

It was rather disturbing to observe that the four-dimensional phase space density decreased with extraction of higher beam intensities from the ion source. Regarding this, it is useful to consider the optimum expected ion source emittance versus output beam intensity.

The minimum emittance is determined by the transverse velocity components existing at the plasma boundary from which beam extraction takes place. The magnitude of the transverse components is determined by the plasma temperature.

Taking the simplest case of a plane plasma boundary and homogeneous particle density filling of the plasma of N ions per unit volume, then for ion extraction from an area a^2 one finds for the emittance

$$v = \frac{2}{\pi} \beta \gamma \, a \, p_x/p_z = \frac{2 \beta \gamma \, a \, m_o \bar{v}_x}{\pi \beta \gamma \, m_o c} = \frac{2 \, a \, \bar{v}_x}{\pi c} \quad .$$

Using a simple cut-off of the Maxwell-Boltzmann momentum distribution and assuming plasma equilibrium, i.e., $T_i \cong T_e$, one finds[3]

---

*The brightness as defined here refers to four-dimensional phase space only, the time structure of the beam may change the δ and B values.

$$\bar{v}_x \leq \left(\frac{k\,T_i}{m_o}\right)^{1/2} .$$

Here $\bar{v}_x$ is the x component of the mean velocity of the ions near the plasma boundary.

Further, the total beam extracted from the plasma boundary for a space-charge limited beam may be obtained from the diffusion equation:

$$I = a^2\,Ne\,\bar{v}_z$$

or similarly

$$a = I^{1/2}\left[N^{1/2}\,e^{1/2}\left(\frac{k\,T_i}{m_o}\right)^{1/4}\right]^{-1} .$$

Actually, because of limitations in beam extraction due to space-charge effects, a more practical expression for a would be given by Langmuir's equation:

$$a = I^{1/2}\left[\frac{4\,\epsilon_o}{9}\,\frac{2\,e}{m_o}\,\frac{V_{extr.}^{3/2}}{g^2}\right]^{-1/2} .$$

Comparison of the two expressions indicates that a practical upper limit exists for N. For higher values of N and a given extraction field and geometry the plasma boundary takes on such a shape that unacceptable optical conditions result. Therefore, for any practical system, the maximum value of N may not be determined by the ion source capabilities only, but, especially with recent ion source developments, by limitations in $(V_{extr.}^{3/2}/g^2)$.

For the present argument the first expression for a will be used. Substitution of a and $\bar{v}_x$ yields:

$$v = \left(\frac{1}{\pi\,B_o^{1/2}}\right) I^{1/2}$$

with B_o a constant,

$$\left[\text{or } v = \frac{2\,a}{\pi}\left(\frac{k\,T_i}{m_o c^2}\right)^{1/2}\right]$$

and by definition $B = \frac{I}{\pi^2 v^2}$, therefore

$$B = B_o = \frac{N e c}{4\left(\frac{k T_i}{m_o c^2}\right)^{1/2}} .$$

Contrary to experimentally observed behavior, theoretically the source brightness would be independent of output current, as it should be.

The foregoing approach may be enforced by substituting some practical values for T and N in the expression for B_o. An expanded plasma from a pulsed high-intensity PIG source with hot cathode was studied by Gabovich et al.[4] Here, a plasma expansion system, similar to that used by A. I. Solnyshkov[5] for the duoplasmatron ion source, was used. Typical values for N and T in the expanded plasma are $10^{12}/cm^3$ and $10^5\ ^oK$, respectively. This substituted yiel ds for B_o:

$$B_o = 1.2 \times 10^{10} \frac{ma}{cm^2\text{-}rad^2} .$$

This value is indicated in Fig. 1. Also given here are values for B and v derived from Solnyshkov's results obtained with a modified duoplasmatron source. Through these points lines have been drawn in the log-log emittance current plot of "suggested" output current dependence of the modified duoplasmatron source. At the present time this is only supported by the assumption that with extraction from a relatively large plasma boundary area the theoretical expected current dependence of v and B may be approached.

The B_o value as calculated is of the same order of magnitude as the approximate B value obtained from Solnyshkov's experimental results.

The experimental observed behavior of v and B as a function of I for the conventional duoplasmatron source, rf source and PIG source is also given in this figure. Further the range of some recent results for v and B with the modified duoplasmatron source as obtained by B. Vosicki at CERN and L. Oleksiuk at BNL are also indicated. These results will be discussed in detail by L. Oleksiuk.

The foregoing approach suggests immediately that it is desirable to keep the plasma temperature low in order to obtain high B_o values and low v values. It also explains the reason for the encouraging results obtained with the sources with large plasma expansion.

419

$$V = \beta\gamma \frac{\text{Area } F(x, \alpha_x)}{\pi} = \beta\gamma E \; ; \; B = \frac{B(p_z^2)}{\beta^2\gamma^2} \; ; \text{ for } \delta \text{ definition, see text.}$$

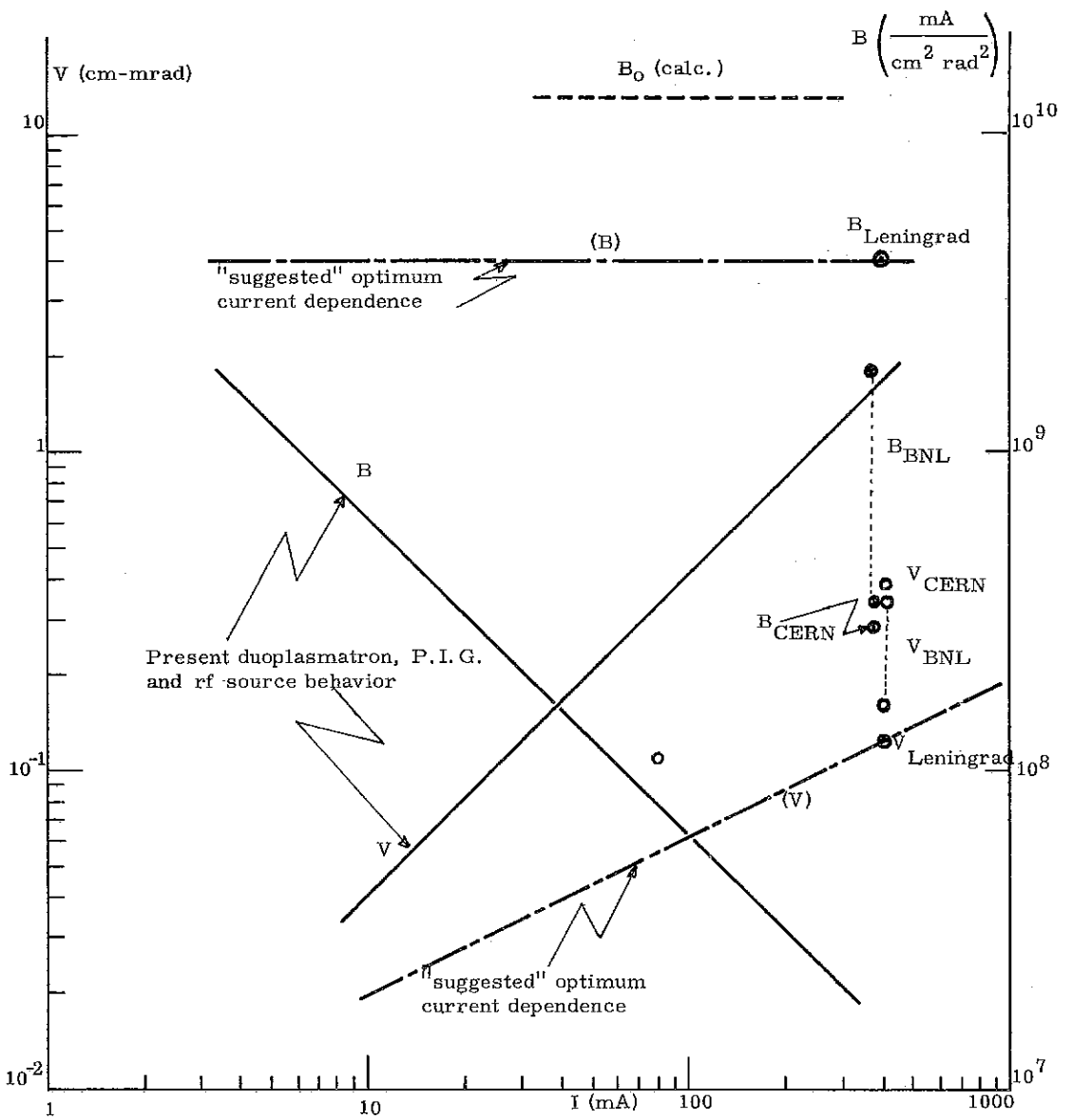

Fig. 1. ION SOURCE CHARACTERISTICS

It is evident that the ion sources using plasma expansion and plasma boundary focusing may substantially improve present ion source (PIG, rf and duoplasmatron) brightness figures. With these sources, beam intensities of the order of 500 mA are readily obtained. It is in a sense secondary how the expanded plasma is established, as long as the appropriate plasma temperature and density may be obtained. Therefore, in a first approach several of the above mentioned ion sources will be suitable. Some pertinent parameters of these sources have been collected from the literature and from BNL experience. These are given in Table I. The figures given are meant for comparison only and all values given should be considered to be approximate only. There should be no clear cut choice between the modified PIG souce, the Lamb-Lofgren "magnetic" source and the modified duoplasmatron source. However, with the duoplasmatron a high density primary plasma is obtained in a rather efficient way. This source is therefore more suitable to produce an expanded plasma without actually enlarging the ion source aperture to any appreciable extent, which should be avoided to the extent possible because of neutral gas flow into the acceleration column.

Some thought has been given to the most desirable shape of the plasma boundary in the modified duoplasmatron source. This is illustrated in an oversimplified way in Fig. 2. The possibility of positive aberration and also space-charge blow-up with a consequent equivalent negative aberration in the proton beam should be avoided to reduce effective phase space dilution. Presently, the first case illustrated, i.e., that of an essentially flat boundary is being considered as a desirable configuration together with a high gradient column approach as will be further detailed below.

In Fig. 2 is also indicated the possible reason for the experimentally observed emittance-current behavior in the conventional duoplasmatron source ($v = C_1 I$ instead of $v = C_2 I^{1/2}$ as expected). As illustrated the measured emittance would be

$$v \cong \beta\gamma a\alpha .$$

From elementary electron optics $\alpha = C_3 I^{1/2}$, further, Langmuir's equation gives $a = C_4 I^{1/2}$, consequently $v = I/\pi\delta$.

Even though the source brightness values obtained with the Solnyshkov source are promising one might say that developments are not so far advanced yet that one could speak of an operational source at present. Some problems are mentioned:

TABLE I

Evaluation of High Intensity Ion Sources					With large plasma expansion and plasma boundary focusing		
		P.I.G. Source	RF Source	Duo-plasma-tron Source	Lamb-Lofgren "Magnetic" Source	P.I.G Source With Hot Cathode	Modified Duoplasmatron Source
Reported maximum	units						
Ion currents: after single electrode acceleration	mA	150	350	1000	1000	1000	800
after C-W acceleration	mA	90	250	150	-	-	400
Ion source brightness: B* (for definition see text)	$\frac{A}{(m \cdot rad)^2}$	5.10^8	5.10^8	5.10^8	$\geq 5.10^7$	-	5.10^{10}
Expectation of approaching $B = B_o$ instead of $B = \delta^2/I$		neg.	neg.	neg.	pos.	pos.	pos.
Physical characteristics:							
beam energy spread	eV	< 10	10	< 1	-	-	-
typical maximum proton percent	%	50-80	60-90	60-90	95	-	-
Characteristics related to complexity of auxiliary equipment: gas consumption	Ncm^3/h	10-100	10-100	50	2000	1000	100-200
power input** / duty factor	kW	0.5-5	1-10	0.5-2	5-10	5	1-5
power for solenoids etc.	kW	1	0.5	0.5	10	1	0.5
cathode heating	kW	-	-	0.1-0.5	1	0.1-0.5	0.1-0.5
discharge current	A	1-5	-	10-40	100	40	20-100

*Because of the measured current dependence (or possible current dependence), the value given refers to the cited current after C-W acceleration.

**Related to source discharge current only.

a. With the large plasma boundary extraction use is made of plasma boundary focusing, i.e., the beam optics will depend on the boundary shape. This in turn depends sensitively on extraction field, its distribution and plasma density. Slight variations in source parameters are expected to affect beam optics substantially. In this connection also the nonuniform plasma density is a problem resulting in complex emittance patterns. For plasma boundary shaping a shaped grid might be used. This is shown in Fig. 3 together with a version of the modified duoplasmatron source. If a grid is used on the extraction electrode scattering of protons due to the fine structure of the local fields might prove to be causing effective dilution of phase space. This is presently being studied at BNL.

b. Plasma oscillations and boundary instabilities. With the conventional duoplasmatron source, beam intensity modulations with frequencies up to 30 Mc/s and even higher have been observed with the wide band frequency system of the AGS. At times, beam intensity modulations of nearly 75% have been observed, while under optimum conditions this was still of the order of 5% to 10%.

c. Further measurements are needed on proton percentage from an expanded, lower temperature, plasma with the Solnyshkov source.

With conventional Cockcroft-Walton acceleration columns the voltage gradients are such that a relatively large diameter column aperture is needed in order to be able to transfer of the order of 400 mA total beam. Also, with a larger diameter beam, problems connected with aberrations would be more serious.

An alternative is to try to improve the accelerator column gradient. Further, with the possibility of extracting beams from large plasma boundary diameters and actually also the desirability of doing so in connection with beam emittance and source brightness, it becomes attractive to consider again the "Pierce" approach of beam formation. In the small beam diameter case, an unpractical high voltage gradient is required to support the "rectilinear: beams; this because of the higher current densities involved, i.e., $\cong$ 1 A/cm^2. With current densities of the order of 0.1 A/cm^2 the required fields approach practical values again. Various text books on electron optics detail the "Pierce" approach. Here only the resulting formulas will be given:

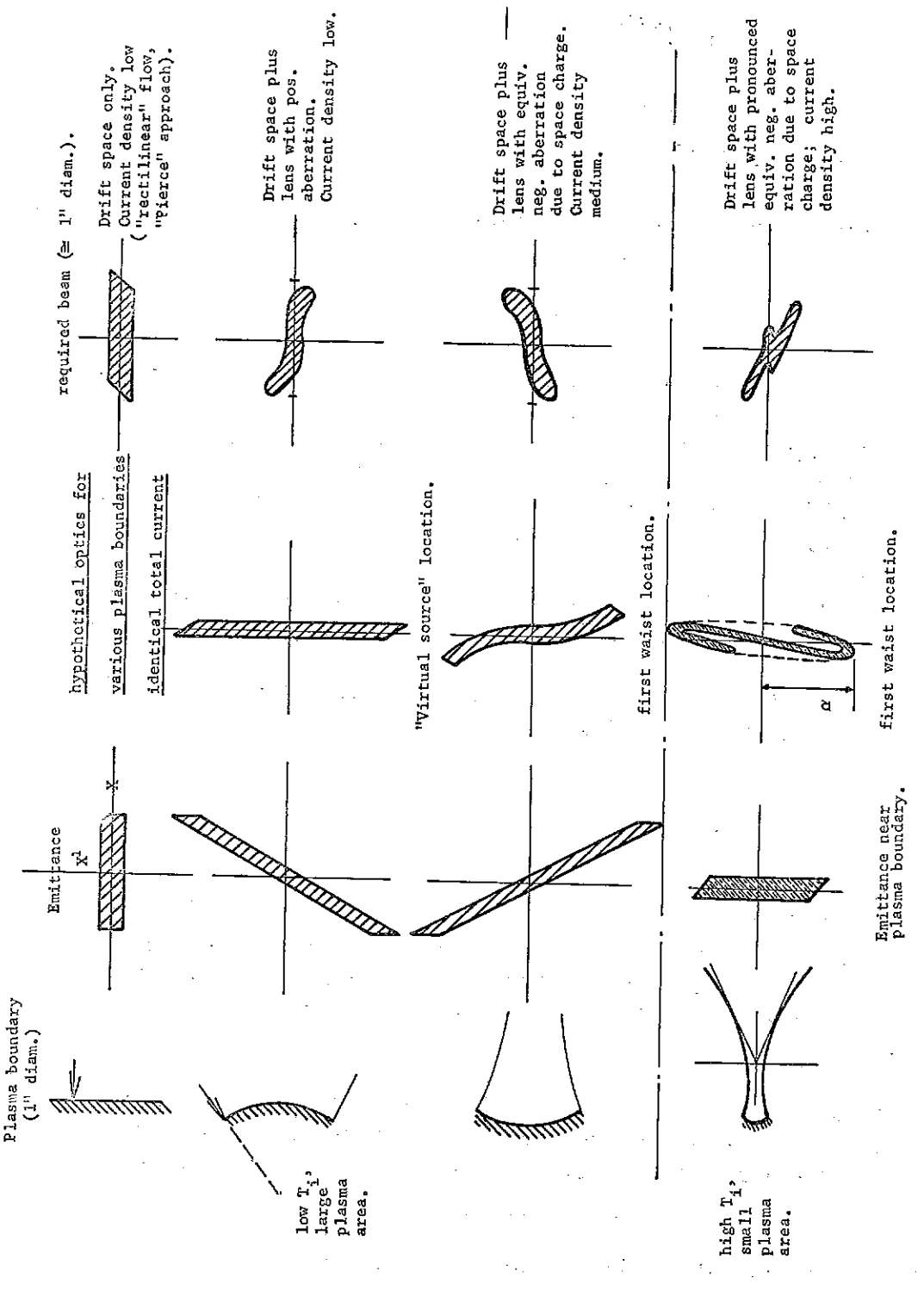
Plasma boundary (1" diam.)
Emittance
X'
X
low T_i, large plasma area.
high T_i, small plasma area.
Emittance near plasma boundary.
hypothetical optics for various plasma boundaries identical total current
required beam (≅ 1" diam.).
Drift space only. Current density low ("rectilinear" flow, "Pierce" approach).
Drift space plus lens with pos. aberration. Current density low.
"Virtual source" location.
Drift space plus lens with equiv. neg. aberration due to space charge. Current density medium.
first waist location.
Drift space plus lens with pronounced equiv. neg. aberration due to space charge; current density high.
α
first waist location.

Fig. 2

For a "rectilinear"* flow with cylindrical boundaries the axial potential distribution is given by

$$U_{z,o} = A_i Z^{4/3}$$

with

$$A_i = \left(\frac{m_p}{m_e}\right)^{1/3} A_e \quad \text{and} \quad A_e = 5.7 \quad 10^3 \quad j^{2/3} .$$

For a plasma boundary of 1 inch diameter and 500 mA total current one obtains $j_o = 0.1$ A/cm^2 and

$$U_{z,o} = 1.5 \quad 10^4 \quad Z^{4/3} .$$

The potential distribution outside the beam boundary has to match this distribution at the beam boundary. This has been obtained analytically and can be approached for practical electrode shapes with an electrolytic tank. The axial distribution together with the required fields as a function of axial location are given in Fig. 4. In this case the extraction electrode held at 50 kV is matched at the proper location and given the proper shape. Consequently 700 kV will be held across a gap of approximately 16.5 cm. The maximum axial field indicated is $\cong$ 50 kV/cm. Similarly some parameters for the spherical case, i.e., a beam cone cut out of the inner space between two spheres has been explored. Again a plasma boundary diameter of 1 inch and total beam of 500 mA have been assumed. The axial potential distribution is given by

$$I_{op} = 2.4 \quad 10^{-6} \quad \frac{\sin^2 \frac{\theta}{2}}{\alpha^2} \quad U_{z,o}^{3/2}$$

with $\alpha^2 = f\,(R/R_{\text{plasma boundary}})$, a known function. The results, matched again to the extraction electrode, are also shown in Fig. 4. The field has been limited to 10 MV/m, resulting in a slight deviation from the required potential distribution above 650 kV. This is not thought to be serious.

As a first approach the "rectilinear" beam with cylindrical beam boundaries have been considered. An electrode system enforcing the required potential distribution has been designed and at present, first

---

*This would constitute a beam emittance of zero value, which does not occur in practice. Nevertheless the approach is useful.

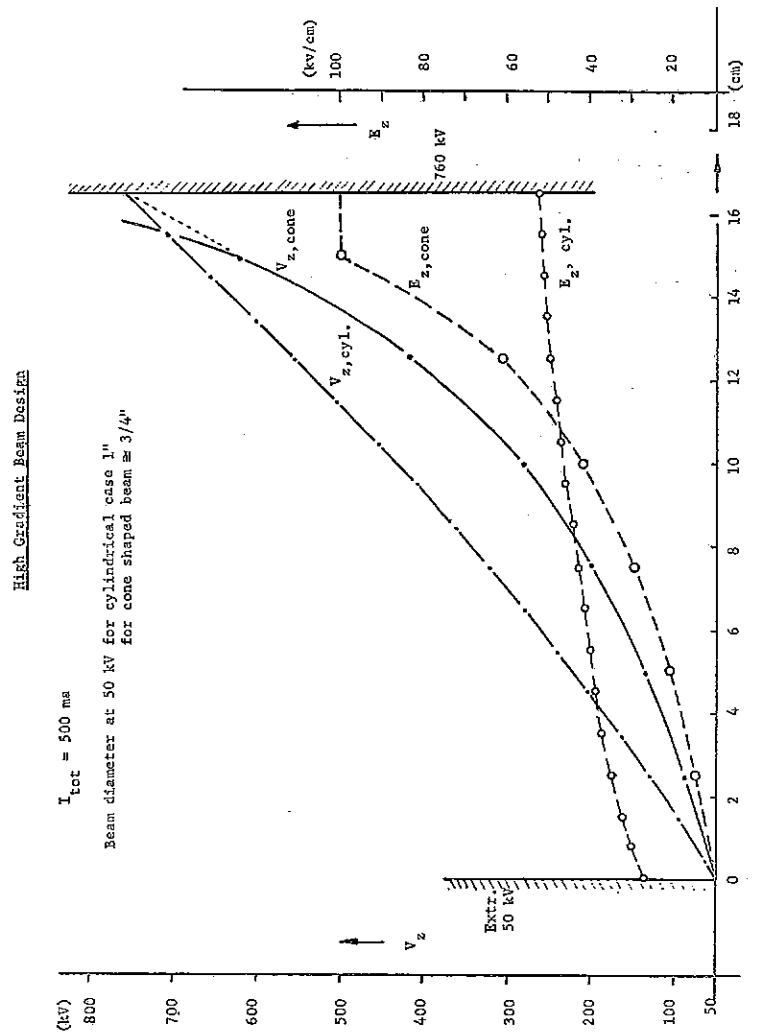

Fig. 4

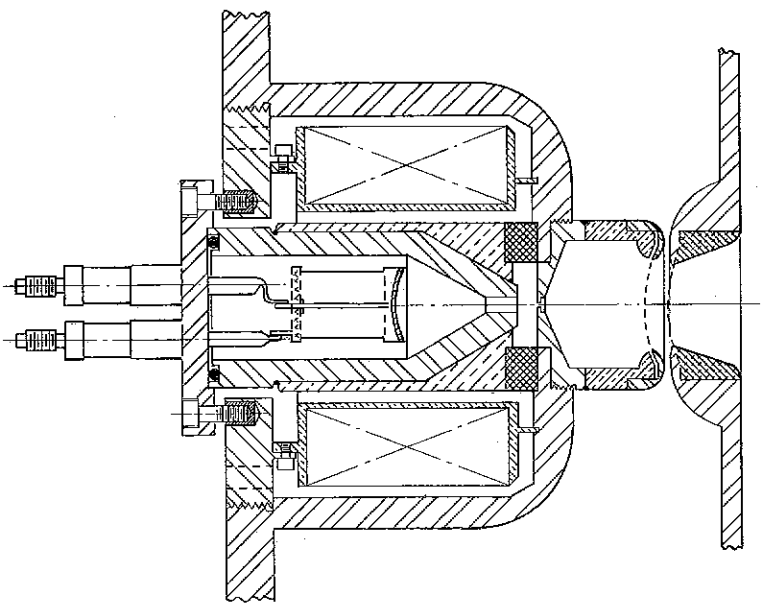

Fig. 3 Modified Duoplasmatron

approach equipotential measurements have been done with a semi-automatic equipotential plotter. An electrolytic tank of 30" x 24" and the plotter have been built by Mr. A. Soukas, who also did some of the measurements, an example of which is given in Fig. 5.

The finally synthesized electrode structure will be mounted in a high gradient large diameter column structure, as shown in Fig. 6. This is a double walled structure with the possibility of conditioned and cooled gas mixture flow in the interspace for cooling of the voltage dividing resistors and improved voltage rating. The total length of the column is about 40 inches for 750 kV. A test section is presently being built up to evaluate some of the design approaches in more detail. The over-all preinjector arrangement as envisaged at present is shown in Fig. 7.

LAPOSTOLLE: I would like to ask you two questions. First, what type of aberration do you consider due to space charge? Is that due to non-uniform density or to the potential drop inside the beam?

VAN STEENBERGEN: I have talked in terms of equivalent negative aberration, because the space-charge effects, even in a homogeneous beam with potential drop inside the beam, tend to distort the two-dimensional phase-space boundary in a sense opposite to that due to spherical aberration. I assume that boundary distortion due to space-charge in a nonhomogeneous beam would tend to be more serious and lead to more equivalent negative aberration.

LAPOSTOLLE: Now, I have the second question, which was about your high gradient column design where you try to have a field distribution which fits the space-charge law in some way. That of course only applies for a given current density.

VAN STEENBERGEN: The equipotential distribution at the boundary is correct for one value of current density only. Therefore, at present the preliminary design is for a particular total current, i.e., 500 mA only; it is not expected to suit typically a 50 mA total beam.

MORGAN: In your high gradient column design, did you worry about regions of electron oscillation in the stray field of the solenoid lens which is right beneath the column? We found this to be real critical in the design of our column.

VAN STEENBERGEN: We did not consider this yet.

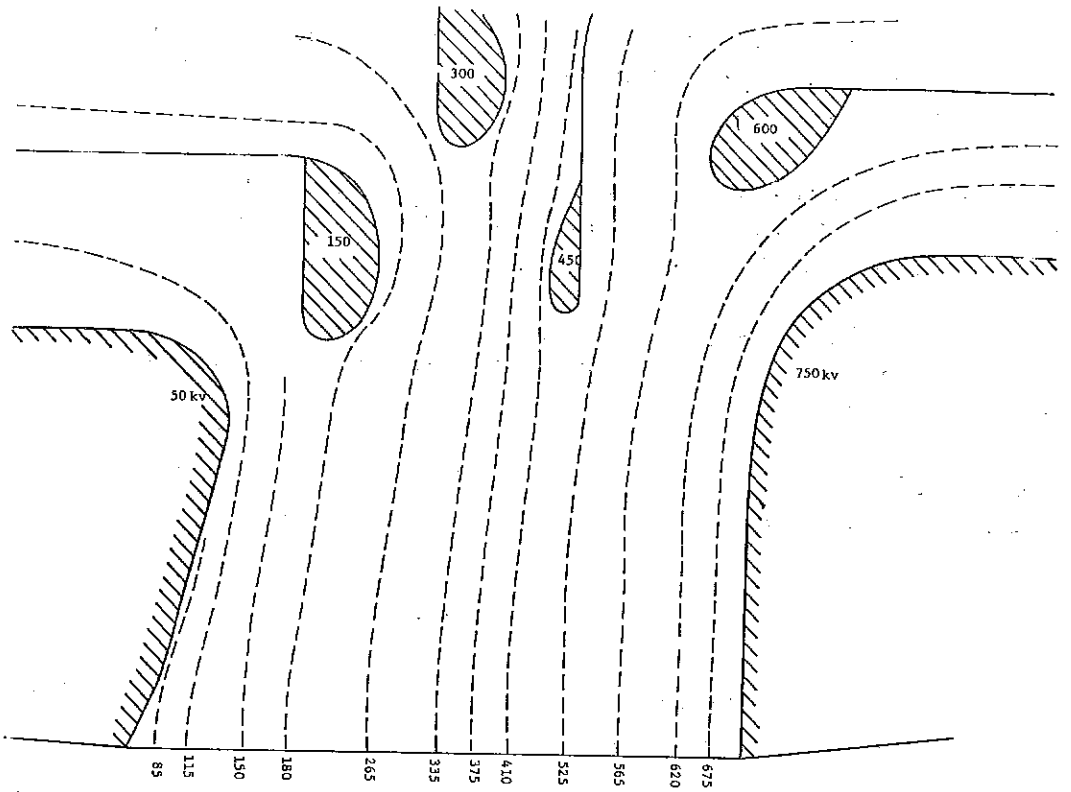

Fig. 5

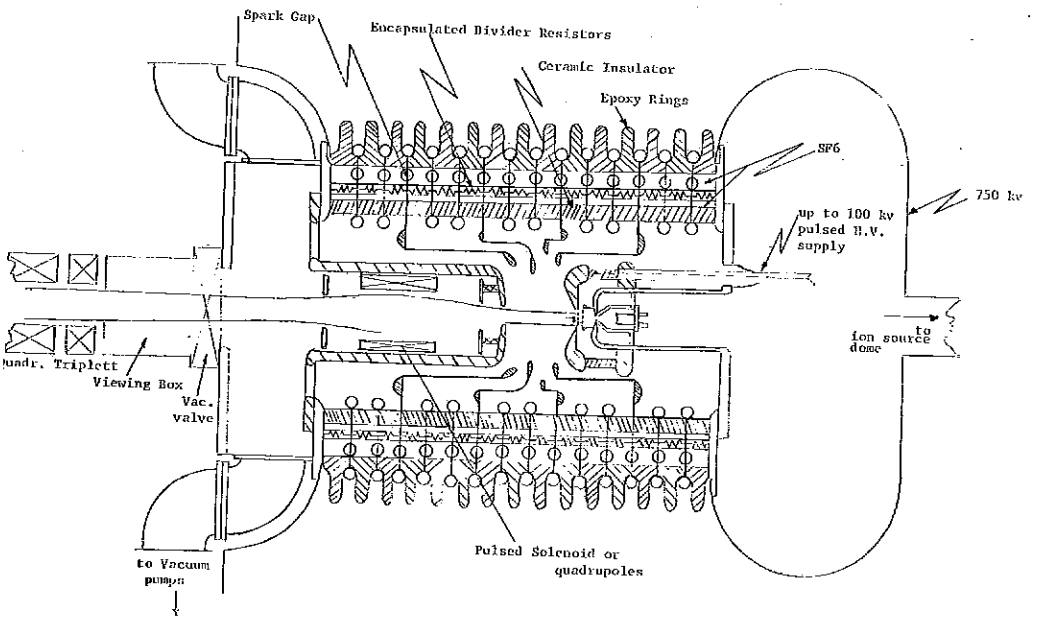

Fig. 7 High Gradient Accelerator Column Arrangement

TAYLOR: Have you plotted trajectories through on a computer? And if so, I want to ask you what sort of program you use and how you included the space charge?

VAN STEENBERGEN: We hope to start using the Kirstein program but have not done so yet. I recognize completely that the equipotential tank leads to a first approximation only.

WROE: Would you say a bit more about those ion temperatures you quoted? I notice you wrote down 10^5 ^{o}K and 10^{12} ions per cm^3. Is this a measured value?

VAN STEENBERGEN: This was a measured value by Gabovich with an expansion cup attached to a hot cathode P.I.G. source.

REFERENCES

1. A. van Steenbergen et. al. Proceedings of the International Conference on High Energy Accelerators, Dubna, August 1963.

2. A. van Steenbergen, BNL Internal Report, AADD-29, March 1964.

3. A. Guthrie and R. W. Wakerling, "The Characteristics of Electrical Discharges in Magnetic Fields", McGraw-Hill, May 1949.

4. M. D. Gabovich et al. Soviet Physics-Technical Physics, Vol. 6, March 1, 1961, p. 766.

5. A. I. Solnyshkov et al., Proceedings of the Conference on High Energy Accelerators, Dubna, August 1963.

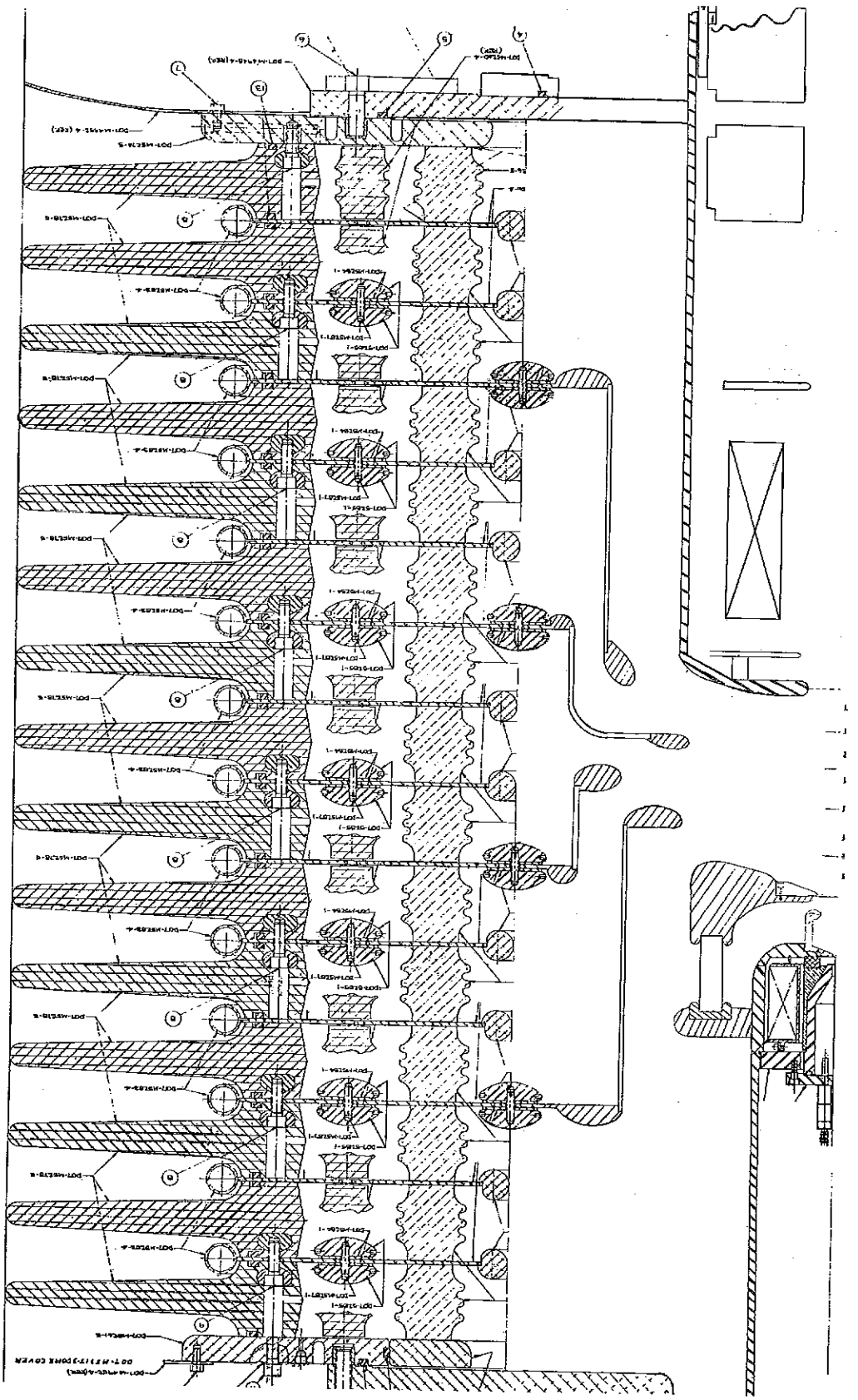

Fig. 6

RECENT DEVELOPMENTS IN RF PROTON SOURCES

H. Wroe
Rutherford High Energy Laboratory

1. Introduction

An rf ion source of the Schneider type[1] was originally developed for Nimrod, but it suffered severely from internal breakdown when delivering intense beams with a pulse length of 1 millisecond. The onset of breakdown marked the end of the useful life of the source which was often short and unpredictable. The breakdown problem was never solved in spite of intense effort and eventually the Schneider source was abandoned in favor of an arrangement similar to that described by Thonemann and Harrison.[2] This source has been reliable in operation on Nimrod and some of its characteristics are given below.

2. Description of Nimrod RF Source

The source is shown in Fig. 1. It is mounted on a mild steel base plate, 1, which carries the invar cathode, 2, on an accurate register. The source pot 7 is made from a piece of standard 1" bore QVF pyrex pipe line with one end sealed, and ground parallel to the lower end. The pot is mounted on the dural extraction plate, 4, which is insulated from the cathode by the pyrex ring, 6. A pyrex disc, 5, almost completely covers the top surface of the extraction plate so as to reduce the area of metal exposed to the plasma to a minimum. Extraction of ions is achieved by pulsing the extraction plate (and therefore the plasma also) to a positive potential. To prevent discharges between the source pot and rf coil, which is "earthy", the insulating envelope, 10, is pumped up with compressed air to about 30 lbs/in^2. This also prevents breakdown from the extraction plate to the base plate over the outside of the ring, 6, at high extraction voltage.

The rf circuit consists simply of a 50 Ω coaxial line stretcher and stub connected directly to the coil, as shown in Fig. 2. The lengths of the line stretcher and the short circuited stub shown in Fig. 2 are typical values. When a 50 Ω power meter is connected in place of the tuner and source, a maximum pulse power of 20 kW can be obtained. The frequency is 125 Mc/s.

Hydrogen is fed into the source through a hole in the base plate via a nickel leak.[3]

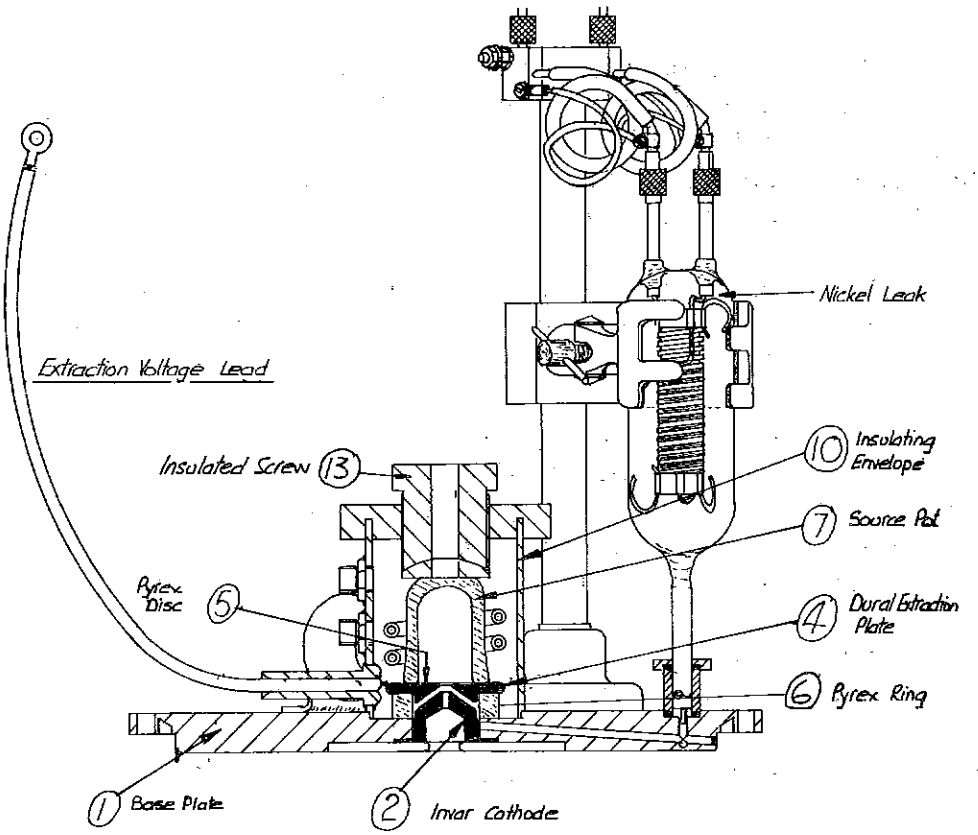

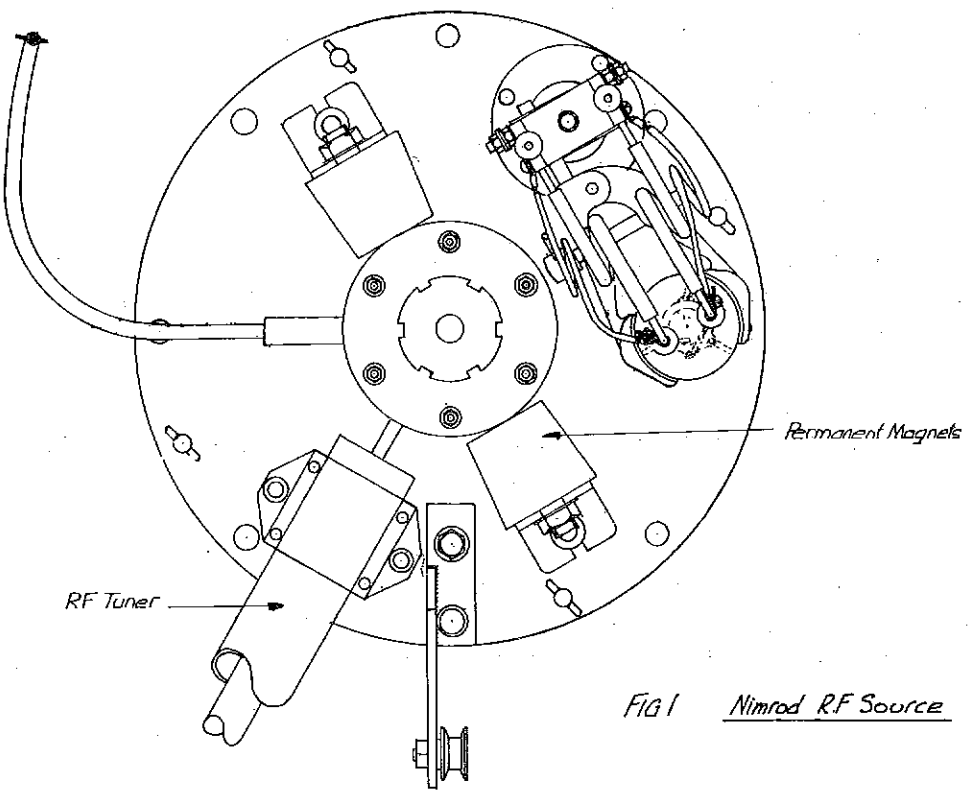

FIG 1 Nimrod R.F Source

The vacuum seals on the source itself are 1/32" diameter indium wire compressed to a thickness of 0.004". Considerable pressure is required and this is achieved by a strong insulated screw, 13, on top of the outer envelope. A pressure pad with a spherical upper surface takes up slight misalignment between the screw and source pot.

Two permanent magnets provide a roughly transverse magnetic field of about 50 gauss which greatly increases the ion density in the plasma, for a given rf power input.

The dimensions of the extraction gap used at present on Nimrod are shown in Fig. 3. Alignment of the extraction plate and cathode is critical. It will be seen that the insulating pyrex ring is well shielded from the beam and plasma and this is considered to be an important contribution to the high breakdown voltages achieved in operation.

Figure 4 is a photograph of a source assembly and Fig. 5 is a view of the source in position on the Nimrod preinjector.

3. Performance of the Source on a Laboratory Rig

3.1 Source Pressure

A special source pot was made up with a Pirani gauge head mounted on top. The variation of source pressure with the nickel leak current is shown in Fig. 6. The pressure readings are corrected for hydrogen. Normal operating pressure is about 10^{-2} Torr and the power consumption of the nickel leak at this level is 36 watts.

3.2 Output Current

A reliable current measuring device has been developed, which combines electrical and calorimetric methods, as shown in Fig. 7. The principle of the calorimeter is the same as that of Harrison.[4]

A collector cup, made in 2 mil copper foil to reduce its thermal capacity, is mounted on a double "stem" of copper strip 3/8" wide and 0.020 thick. A transverse magnetic field of about 200 gauss is applied to the cup, by permanent magnets, to suppress secondary electrons and a michrome wire heating coil is wound on it for calibration purposes. Thermistors are used for temperature measurement. Figure 8 shows a general view of the device. Both the calorimeter and the bridge circuit used to measure the resistance of the thermistors are well screened as shown in Fig. 10.

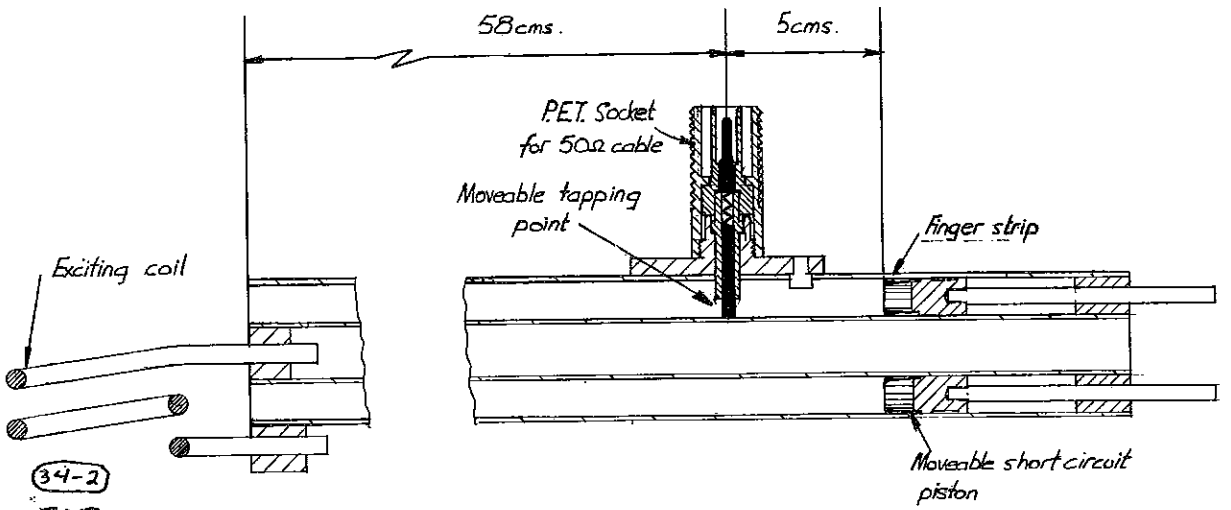

FIG. 2 R.F. Tuner

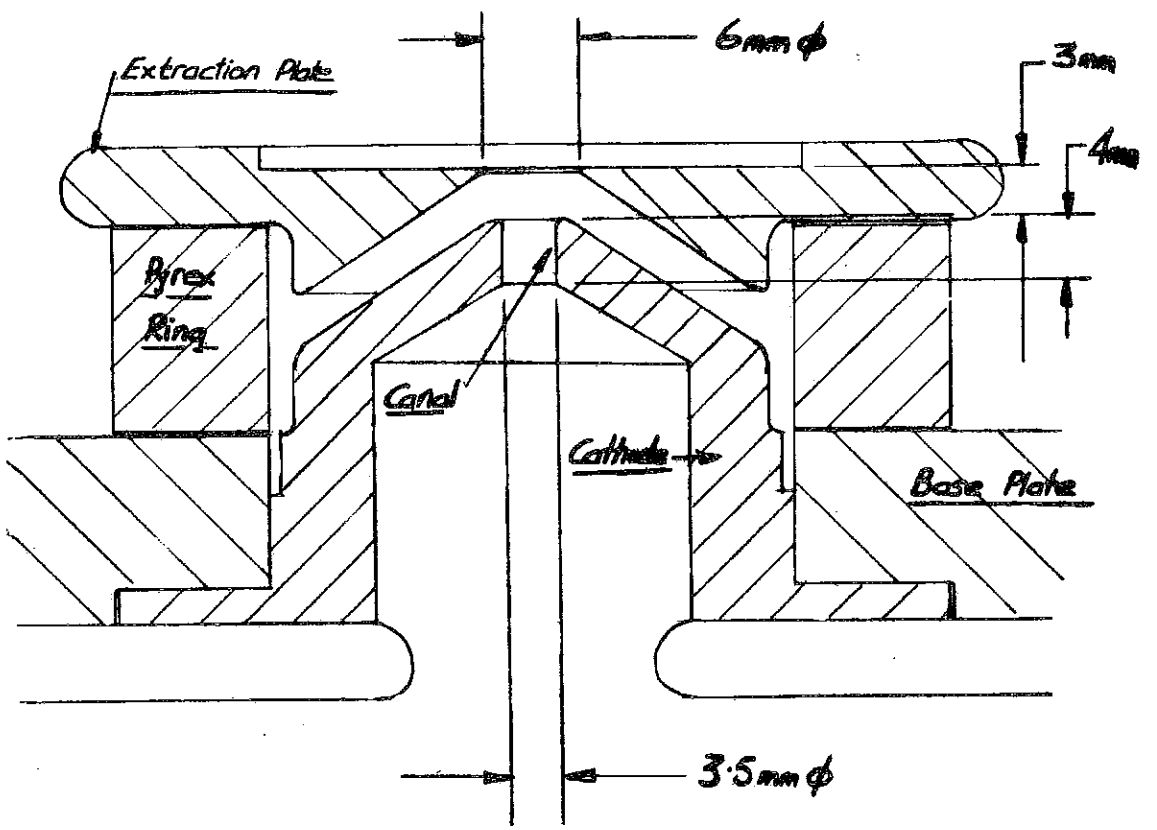

FIG. 3 Extraction Gap Dimensions

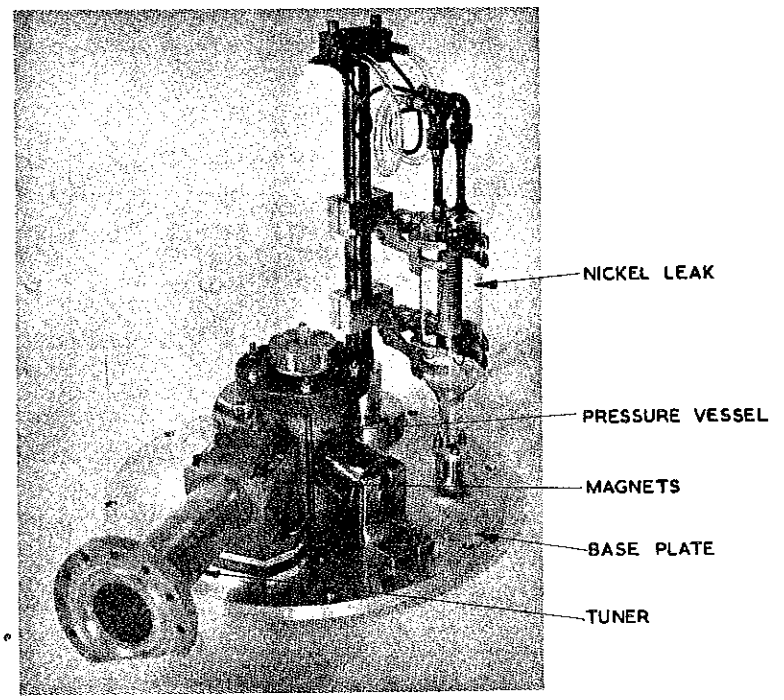

FIGURE 4 GENERAL VIEW OF SOURCE ASSEMBLY

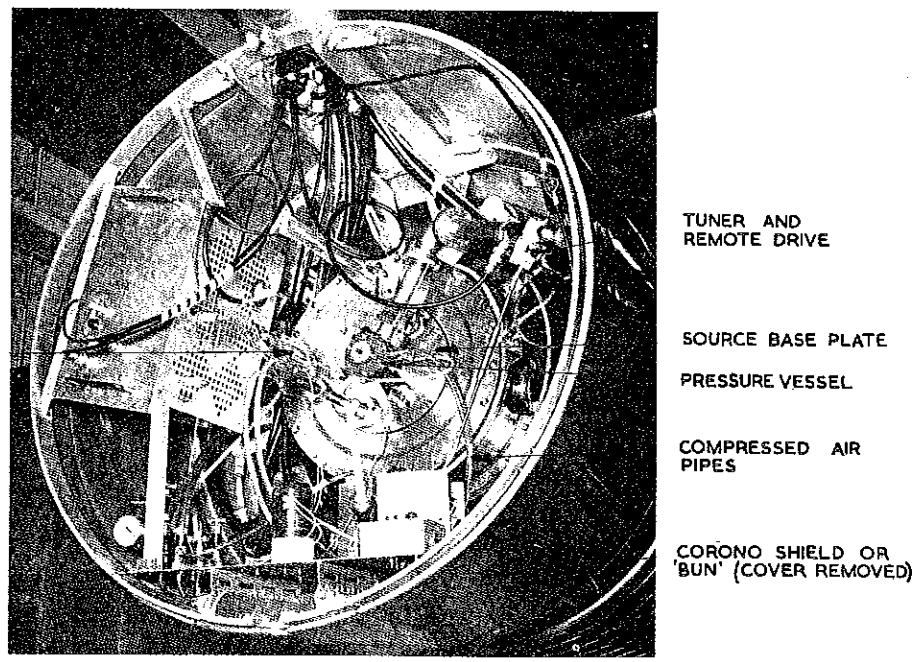

FIGURE 5 GENERAL VIEW OF SOURCE FITTED TO THE NIMROD PREINJECTOR

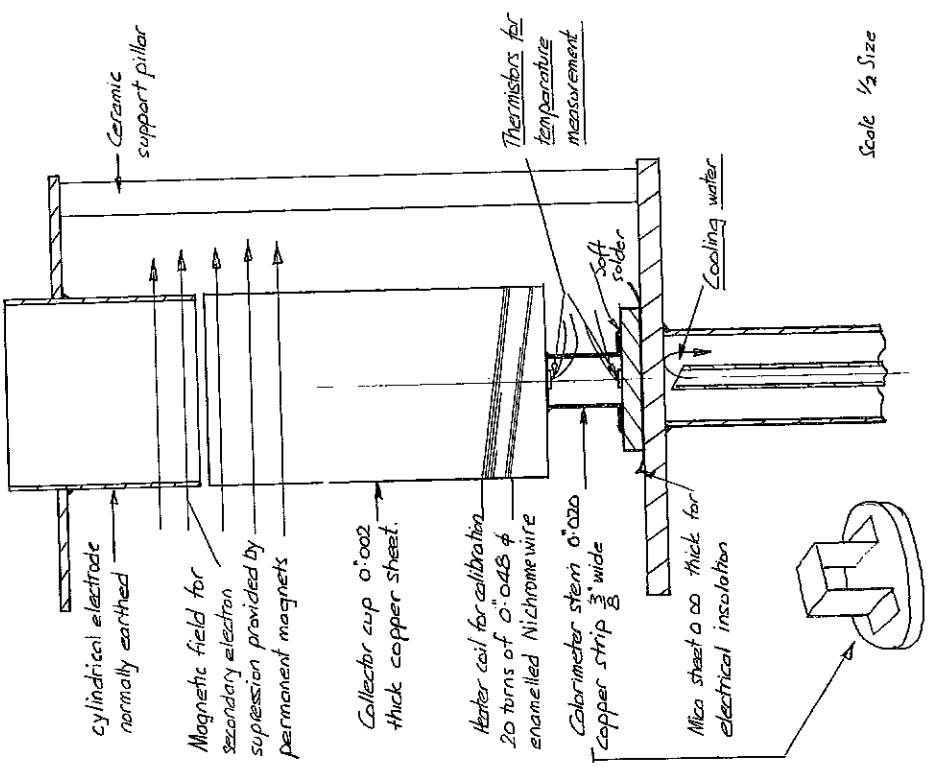

FIG. 7 Combined calorimeter & collector cup for beam current measurements.

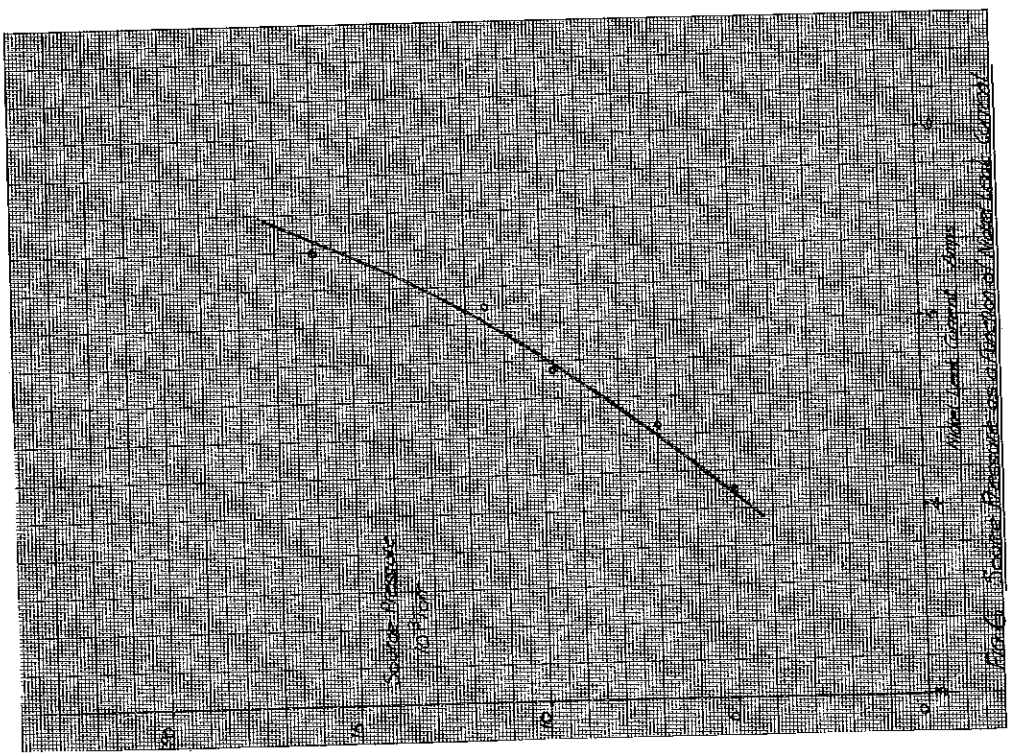

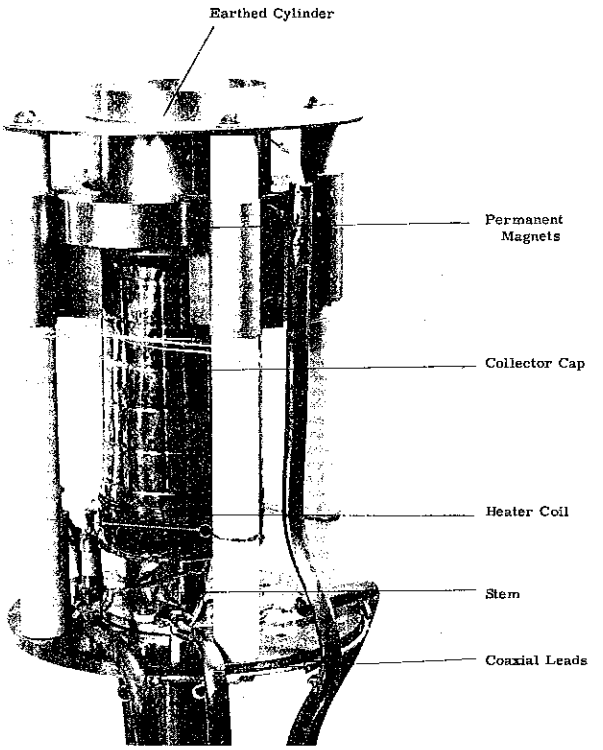

FIG 8 Current Measuring Device

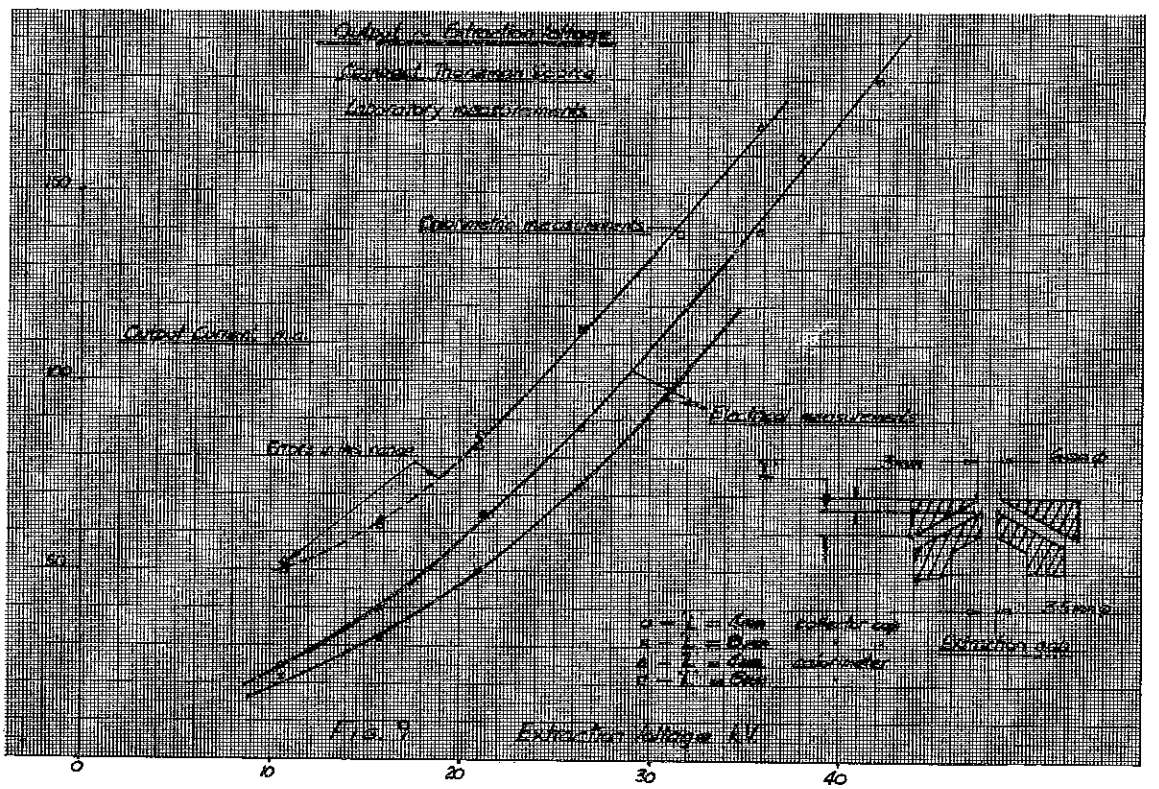

FIG 9

Curves of output current against extraction voltage for two different canal lengths are shown in Fig. 9. The rf power level was adjusted to give a maximum output current at each value of extraction voltage. The difference between the calorimetric and electrical measurements is probably due to the neutral content of the beam, i.e. the total ion current crossing the plasma boundary under given conditions is the same for each canal length but the number of charge exchange events occurring in the beam is greater for the longer canal. Thus the charged component of the beam is smaller for the longer canal. The dotted part of the calorimetric curve in Fig. 9 is in error due to direct pickup of rf power by the thermistors--this result was obtained before the screening arrangements were fitted.

3.3 Multiwire Target

Preliminary experiments have been carried out using a technique for rapid measurement of beam properties such as diameter, current density distribution or emittance. The device is a target consisting of 25 tungsten wires, 0.2 mm diameter, spaced 2 mm apart and insulated from each other, each wire being connected to a condenser. When exposed to a beam, the charge collected by each wire produces a proportional voltage on its condenser. The latter are then "scanned" by a mechanical commutator which discharges each in turn through a resistor. Thus, a series of spikes is produced, the height of each one proportional to the charge collected by the wire in the first place.

This is illustrated in Fig. 11 where the target was used to measure the diameter of the beam at various axial distances from the source. The target itself is shown in Fig. 12.

Permanent magnets are built into the target to provide a magnetic field for suppression of secondary electrons, but they are not very effective and there is evidence that the space charge in the beam is at least partially neutralized by secondary electrons. Thus the dotted curve in Fig. 11 is not a real beam profile. The four positions of the target probably gave rise to four different beams, though the source conditions were the same.

It is hoped to extend this technique to the measurement of emittance.

3.4 Source Emittance Measurements

Some measurements of emittance of the beam immediately below the source have been made using the slotted plate and copy paper method. [5]

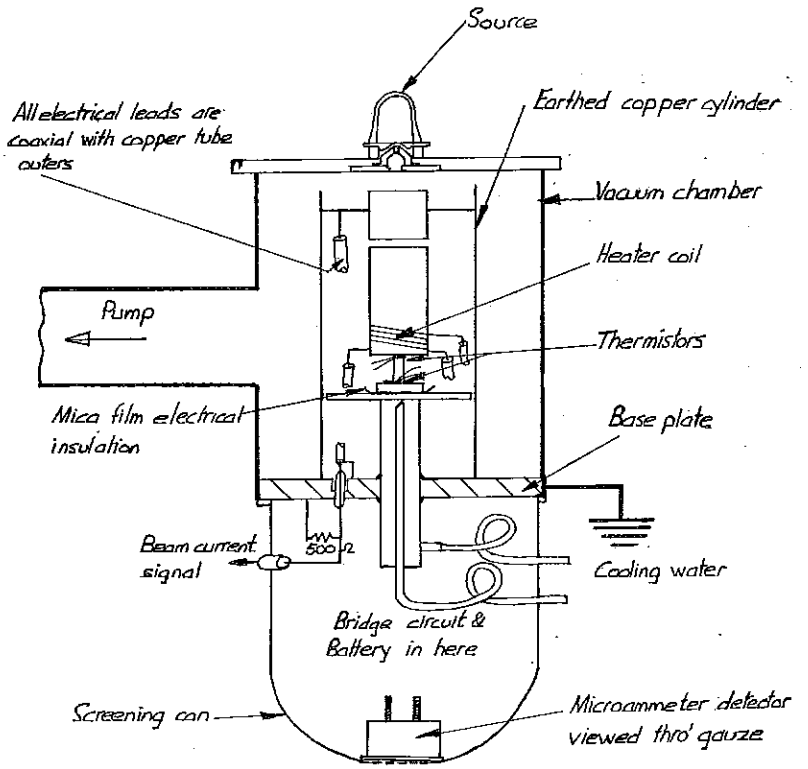

FIG 10 Screening arrangements for calorimeter

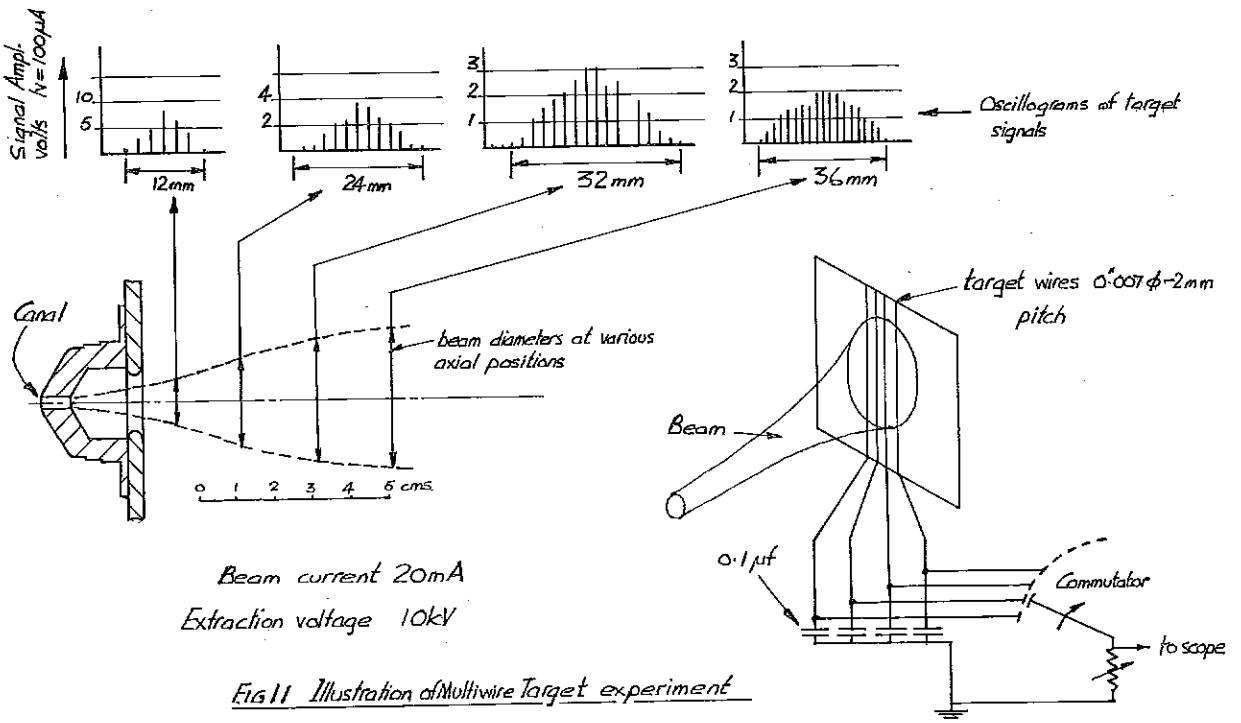

FIG 11 Illustration of Multiwire Target experiment

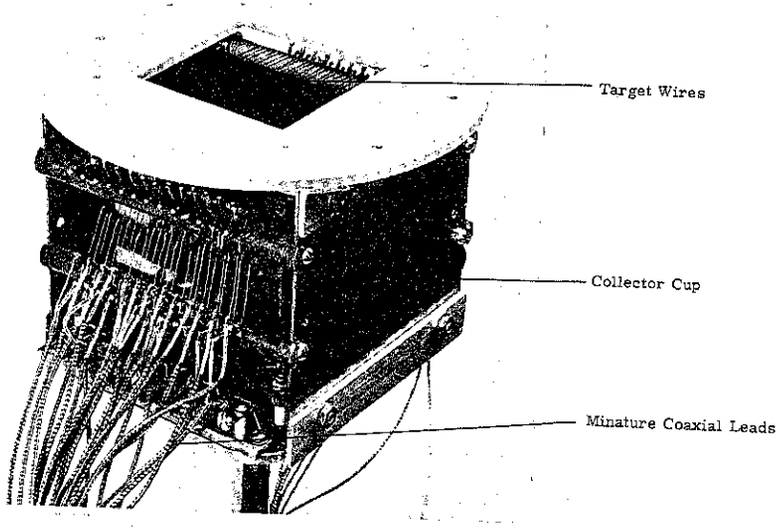

FIG 12 Multiwire Target

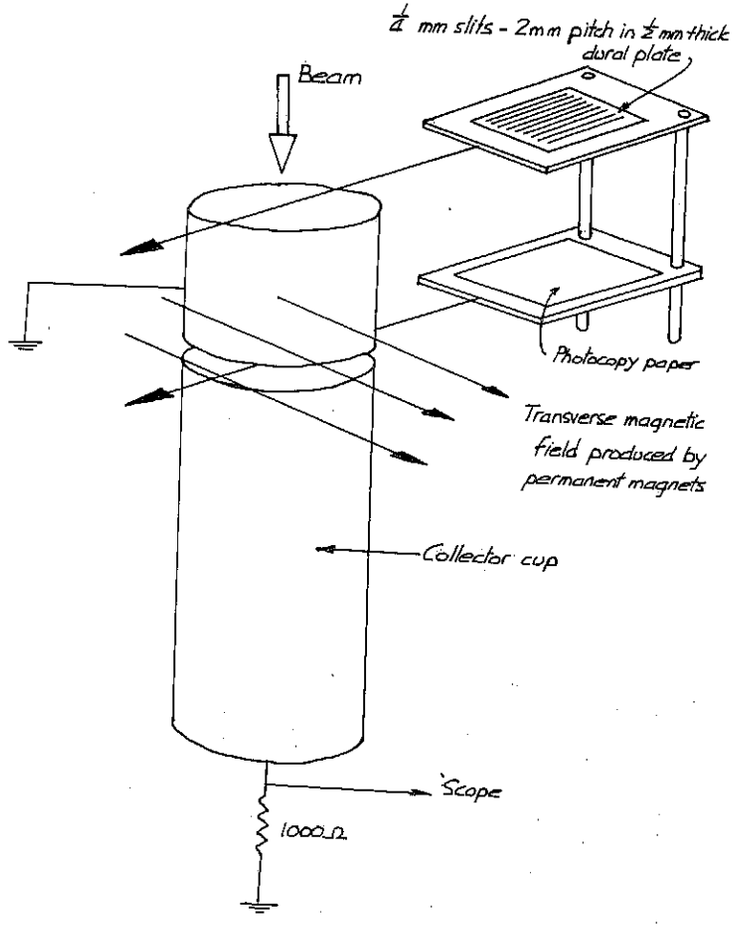

FIG 13 Emittance Measuring Device

The slits used were 1/4 mm wide, spaced 2 mm apart, in a 1/2 mm thick dural plate and they were built into a standard collector cup as shown in Fig. 13. The beam current was first measured with the plate and copy paper withdrawn, then they were pushed into the beam and the exposure made. A typical image is shown in Fig. 14 and preliminary plots of emittance are shown in Figs. 15 and 16. Both the area of the diagrams and the details of the images are closely similar to those obtained by Tallgren[5] with a Schneider type source. There seems to be a dense central region to each image which may well correspond to a large fraction of the beam.

Less dense markings, at larger values of divergence are often completely separated from the main "spectrum." The explanation of these effects is not yet clear, but they are not peculiar to the Schneider type source. They may well be common to all high intensity rf sources.

4. Source Performance on Nimrod

The source has proved reliable and consistent on Nimrod during a period of over a year. The present normal beam current is about 38 mA. At this level the useful life of the source is not yet known but a unit has been in service on Nimrod for four months of routine operation without detectable deterioration. The period of operation, to the time of writing, is about 1000 hours "beam-on" time.

The curve of output current against extraction voltage is shown in Fig. 17. The beam current was measured at 600 kV using the beam monitor system and the values shown were optimized at each value of extraction voltage.

Figure 18 shows an emittance diagram of a 40 mA beam which was obtained by using two 4-jaw apertures in the low energy drift space of the Nimrod injector as shown in Fig. 19. The apertures were set to 1 mm wide vertical slits. The diagram shows the distribution of current in phase space. There is evidence that the "side arms" on the diagram are due to the molecular ion component of the beam which was separated out by the quadrupole.

5. Future Developments

The present objective is to discover the upper limit of the performance of the source. Improved rf screening (with higher rf power inputs) is being incorporated and compressed sulphur hexafluoride is being substituted for compressed air so as to improve the external insulation. It is hoped to increase the extraction voltage to 50 kV.

BEAM CURRENT 100 ma. EXTRACTION VOLTAGE 20 KV.
0·5ms PULSE LENGTH. EXPOSURE 120 PULSES.

FIGURE 14 IMAGE PRODUCED ON PHOTO COPY PAPER DURING EMITTANCE MEASUREMENT

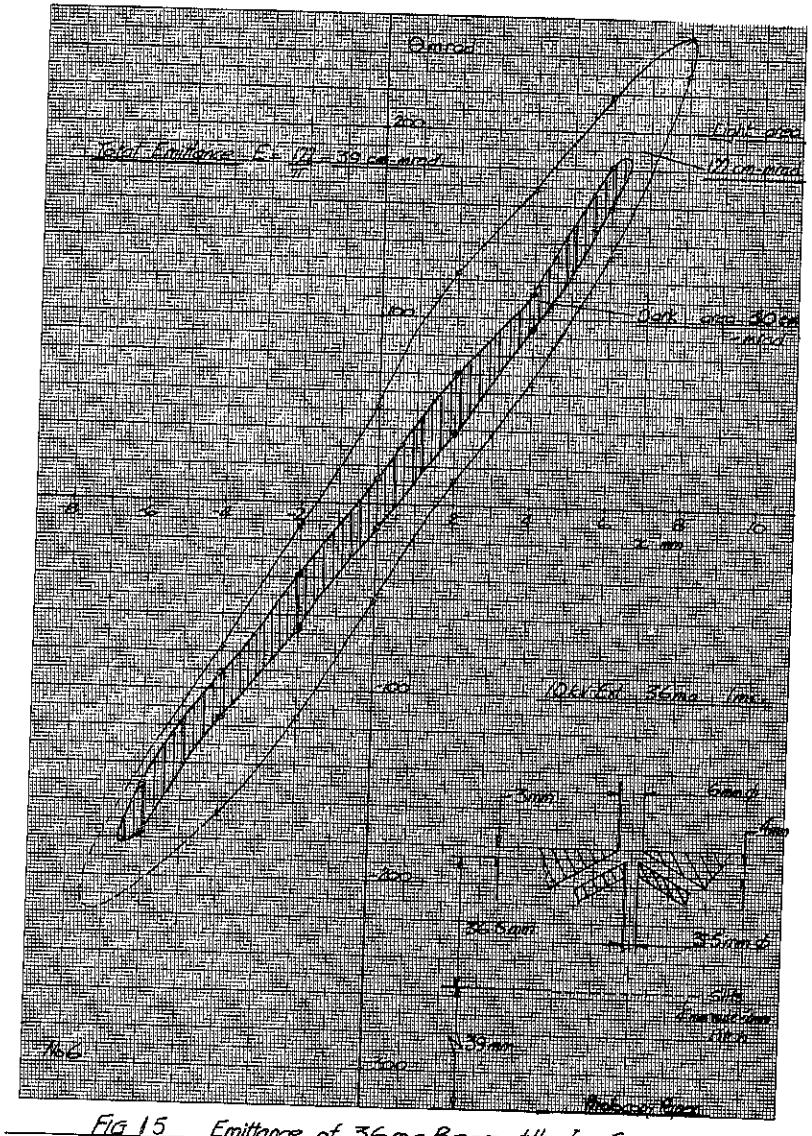

FIG 15 Emittance of 36 ma Beam at the Ion Source

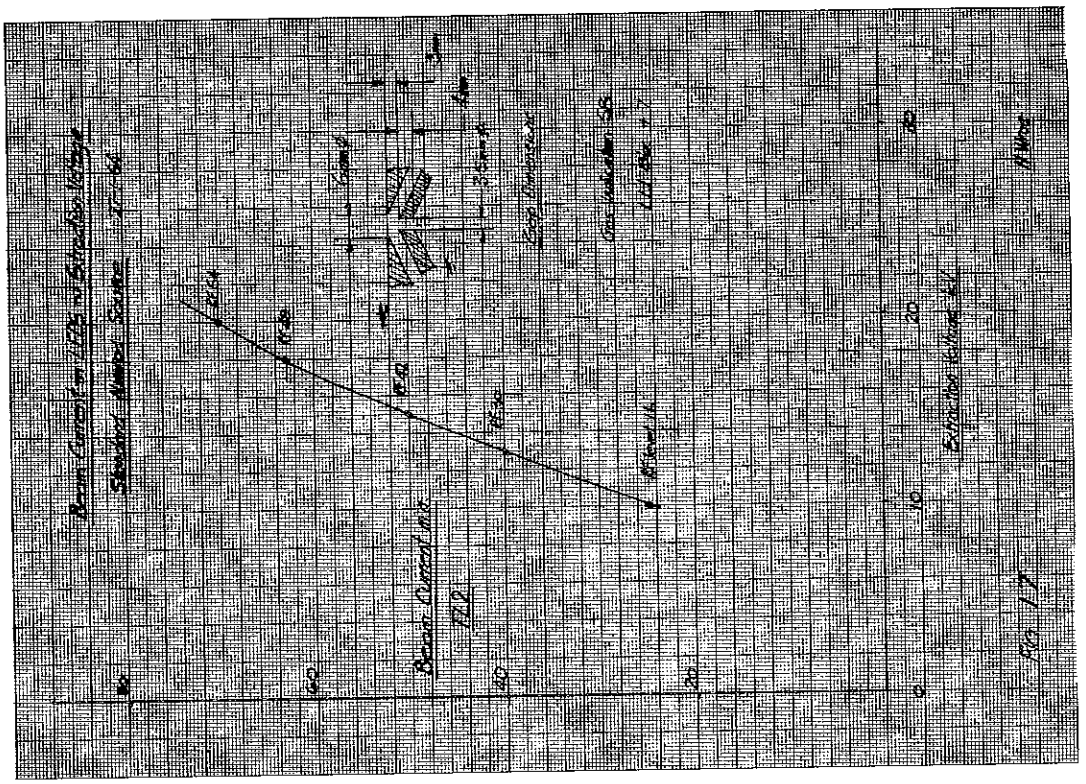

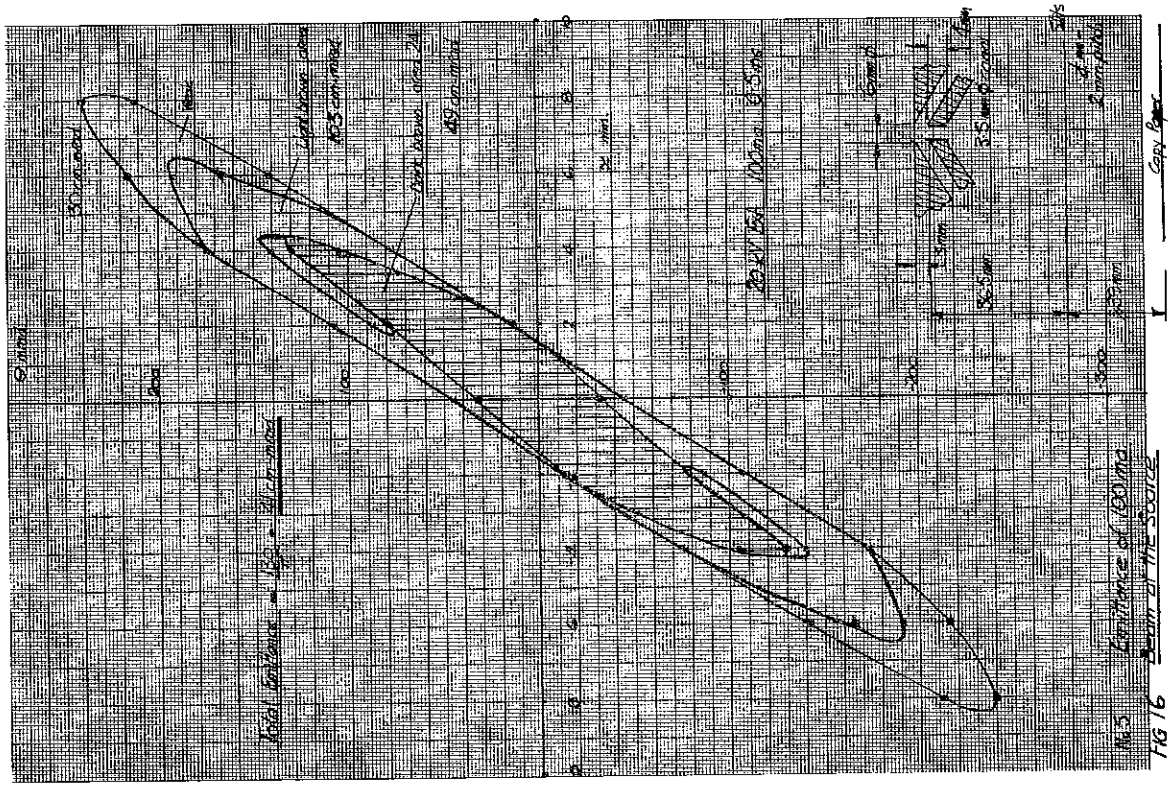

Fig 16

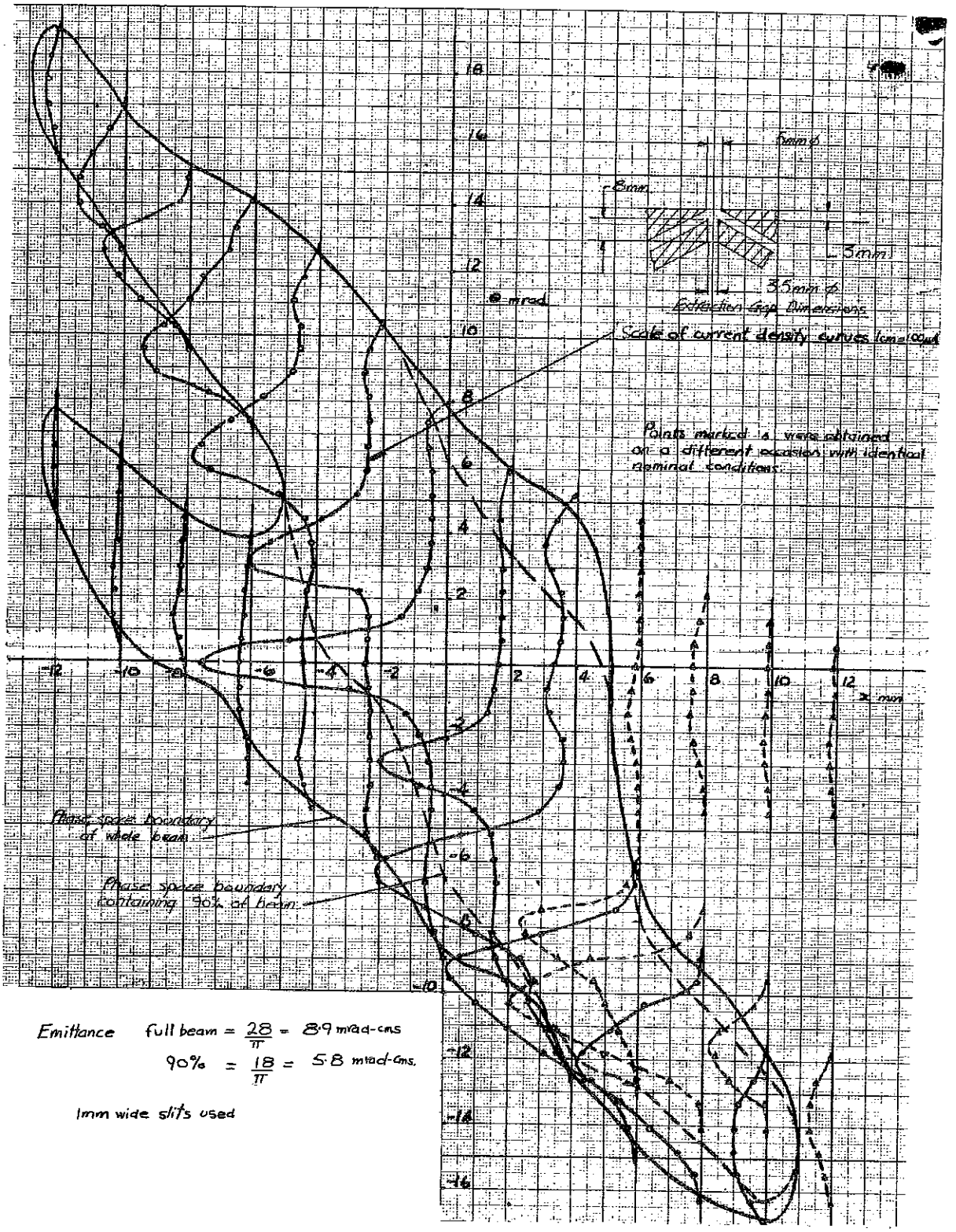

Fig 18 Emittance Diagram 40 mA Beam at 600 kV [Horiz Plane]

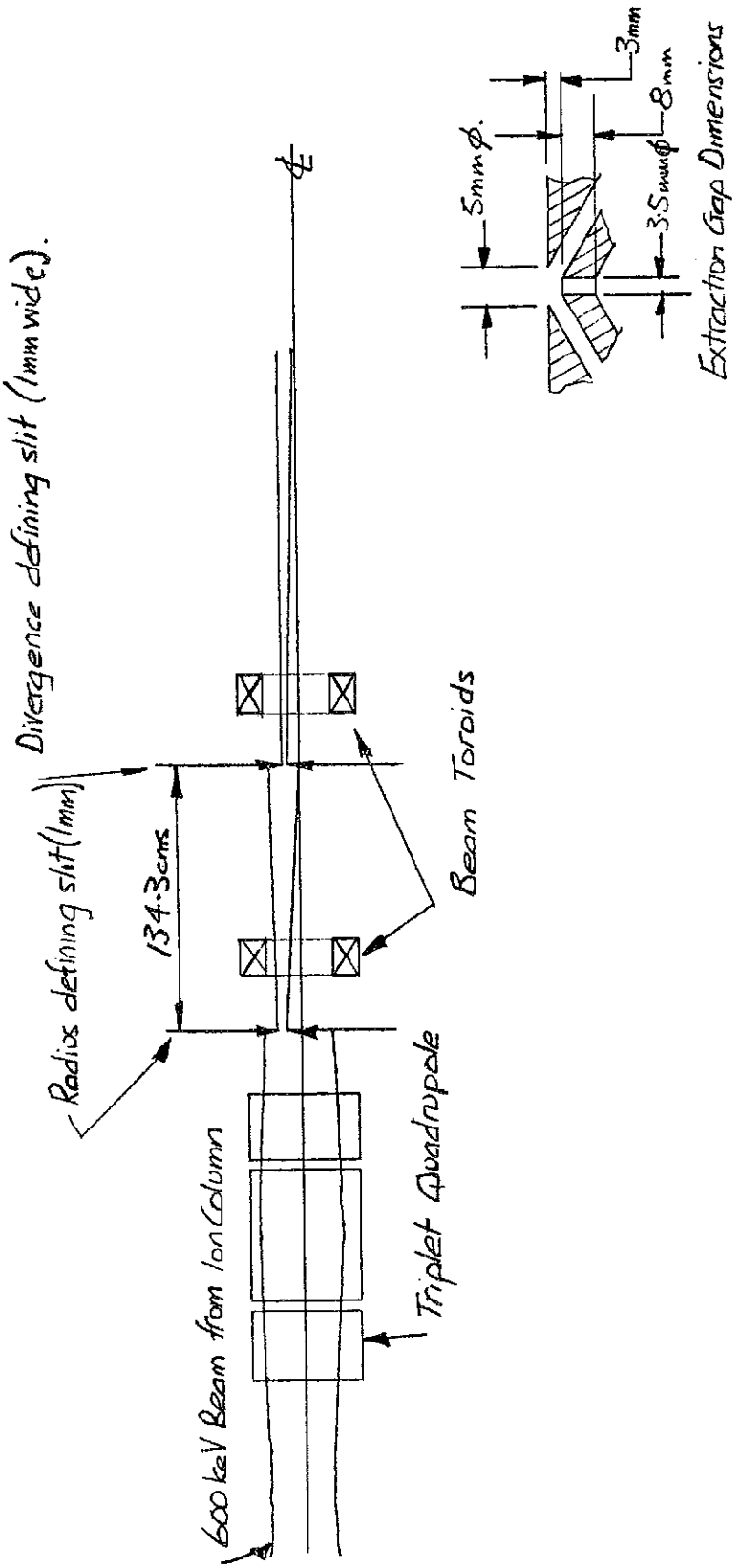

FIG. 19 Arrangement for Emittance Measurements at 600 kV

LAPOSTOLLE: I would like to make a comment and ask you a question about the various parts in the emittance diagrams you have shown or, in other terms, the existence of several beams. First, I would like to say that what you observed in the rf source exists in many sources; it is for instance the same in the PIG source. Now I would like to ask, what is your explanation?

WROE: Well, I haven't got one of course. There are so many things it could be. For instance, this technique gives you the integrated beam which strikes the film. You cannot distinguish any changes with time. Now we have evidence that changes of emittance occur during a pulse. If you examine waveforms of beam pulses through a set of emittance measuring slits, they are hardly ever square and flat topped, though the waveform of the whole beam is. It looks as if beam is shifting about in phase space.

LAPOSTOLLE: You then think that it might come from different parts of the pulse?

WROE: Yes. We are going to look at this sort of thing in more detail on the source itself. This measurement I have just told you about was done at 600 kV. I really cannot offer any serious explanation yet.

HUBBARD: With respect to this wire target you use for measuring emittance, how do you handle the secondary electrons from the wires?

WROE: What we intended to do is just put the magnetic field along the wires. There is a field on this present target, a weak magnetic field. It doesn't seem to do very much good. What we are thinking of now is to make a target in the form of a stack of thin plates with insulation between and a fairly strong magnetic field along the plates. If the field falls off rapidly enough as you move away from the target, then it will not affect the trajectories of the ions. The idea is to cause an electron liberated from a plate to be returned to that plate and not a nearby plate.

SHAYLOR: I wondered if you could do anything successful in that line by putting a potential on the wires you are not using adjacent to the wires you are using?

WROE: I do not like electrostatic means of suppression you see, and we have got experience of incredible things that secondary electrons seem able to do in a field of this sort. I don't like it at all.

SHAYLOR: But you are quite happy with magnetic techniques?

WROE: Yes.

VAN STEENBERGEN: You have measured only current distribution, not emittance?

WROE: That is right.

HUBBARD: You measured the current distribution after a slit?

WROE: The idea of the wire target was simply to substitute it for the photocopy paper, so that you have a series of slits and you get out of the wire target a series of profiles in a single pulse, which you can interpret in terms of divergence angle. That is the idea.

REFERENCES

1. The CERN Proton Synchrotron (2nd Part) Chapter V, Injection, CERN 60-26 (1960), p. 22.

2. P. C. Thonemann and E. R. Harrison. AERE Report No. GP/R 1190.

3. L. C. W. Hobbis and E. R. Harrison. Rev. Sci. Instr. 26, 303 (1955).

4. E. R. Harrison. Jour. Sci. Instr. 30, 242-244 (1957).

5. U. Tallgren. MPS/Int. LIN. 62-3, 1962.